



Anderson, Hilary Jane (2018) *Dynamic surfaces for mesenchymal stem cell self-renewal and differentiation*. PhD thesis.

<https://theses.gla.ac.uk/30641/>

Copyright and moral rights for this work are retained by the author

A copy can be downloaded for personal non-commercial research or study, without prior permission or charge

This work cannot be reproduced or quoted extensively from without first obtaining permission in writing from the author

The content must not be changed in any way or sold commercially in any format or medium without the formal permission of the author

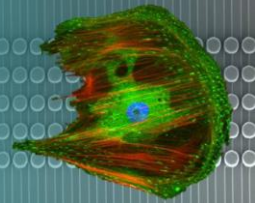
When referring to this work, full bibliographic details including the author, title, awarding institution and date of the thesis must be given

Enlighten: Theses

<https://theses.gla.ac.uk/>  
[research-enlighten@glasgow.ac.uk](mailto:research-enlighten@glasgow.ac.uk)



Centre for  
Cell Engineering



# Dynamic Surfaces for Mesenchymal Stem Cell Self-Renewal and Differentiation

**Hilary Jane Anderson**

BSc (Hons), MRes

Submitted in fulfilment of the requirements for the degree of Doctor of  
Philosophy (PhD)



University  
of Glasgow

Centre for Cell Engineering

Institute of Molecular, Cell and Systems Biology  
College of Medical, Veterinary and Life Sciences  
University of Glasgow

Glasgow

G12 8QQ

## **CONTENTS**

<b>ABSTRACT</b> .....	<b>VI</b>
<b>ACKNOWLEDGEMENT</b> .....	<b>VII</b>
<b>PUBLICATIONS</b> .....	<b>VIII</b>
SCIENTIFIC PUBLICATIONS .....	VIII
PUBLISHED WRITING .....	VIII
<b>GRANTS</b> .....	<b>VIII</b>
<b>AWARDS</b> .....	<b>VIII</b>
<b>PRESENTATIONS</b> .....	<b>IX</b>
ABBREVIATIONS.....	X
AMINO ACIDS.....	X
TERMS .....	XI
MEASUREMENTS .....	XV
<b>LIST OF TABLES</b> .....	<b>XVI</b>
<b>AUTHOR'S DECLARATION</b> .....	<b>XX</b>

### **1. INTRODUCTION: MESENCHYMAL STEM CELLS AND TISSUE ENGINEERING. 1**

<b>1.1 STEM CELLS</b> .....	<b>2</b>
1.1.1 EMBRYONIC STEM CELLS (ESCs) .....	3
1.1.2 INDUCED PLURIPOTENT STEM CELLS (IPSCS) .....	4
1.1.3 ADULT STEM CELLS .....	5
1.1.3.1 Mesenchymal Stem Cells .....	6
<b>1.2 THE NICHE</b> .....	<b>8</b>
<b>1.3 THE EXTRACELLULAR MATRIX</b> .....	<b>10</b>
<b>1.4 CELL ADHESION</b> .....	<b>11</b>
<b>1.5 BONE TISSUE ENGINEERING</b> .....	<b>15</b>
<b>1.6 MATERIALS FOR MSC TE</b> .....	<b>19</b>
1.6.1 TOPOGRAPHY .....	20
1.6.2 CHEMISTRY .....	22
1.6.3 STIFFNESS .....	23
<b>1.7 STIMULI RESPONSIVE MATERIALS</b> .....	<b>25</b>
1.7.1 LIGHT .....	25
1.7.2 TEMPERATURE .....	27
1.7.3 ENZYME RESPONSIVE .....	28
<b>1.8 PROJECT OBJECTIVES</b> .....	<b>29</b>
1.8.1 SOLID PHASE PEPTIDE SYNTHESIS (SPPS) .....	31
1.8.2 SPPS FOR CELL-SURFACE INTERACTIONS .....	34
<b>1.9 CONCLUSION</b> .....	<b>37</b>
<b>1.10 PROJECT AIMS</b> .....	<b>38</b>

<b>2. GENERAL METHODS.....</b>	<b>39</b>
2.1 SUPPLIER INFORMATION .....	40
2.2 SURFACE MODIFICATION .....	41
2.3 BUFFERS.....	44
2.3.1 PHOSPHATE BUFFERED SALINE (PBS).....	44
2.3.2 FIXATIVE.....	44
2.3.3 PERMEABILITY (PERM) BUFFER .....	44
2.3.4 PBS/BSA .....	44
2.3.5 TWEEN .....	44
2.4 MESENCHYMAL STEM CELL CULTURE .....	45
2.4.1 CELL CULTURE .....	45
2.4.2 EXPERIMENTAL SET UP .....	45
2.5 MMP ANALYSIS .....	45
2.5.1 ZYMOGRAPHY .....	45
2.5.2 ENZYME-LINKED IMMUNOSORBENT ASSAY (ELISA).....	46
2.5.3 HUMAN MMP ANTIBODY ARRAY .....	46
<b>3. DESIGN AND SYNTHESIS OF ENZYME RESPONSIVE DYNAMIC SURFACES....</b>	<b>48</b>
3.1 INTRODUCTION.....	49
3.1.1 MMPs .....	49
3.1.2 MMP PROTEIN STRUCTURE.....	52
3.1.3 ACTIVATION.....	53
3.1.4 REGULATION.....	55
3.1.5 MSCs AND MMPs .....	56
3.1.5.1 Migration .....	56
3.1.5.2 Differentiation .....	56
3.2 METHODS.....	58
3.2.1 SUPPLIER INFORMATION .....	58
3.2.2 SPPS .....	58
3.2.3 ZYMOGRAPHY .....	58
3.2.4 6-WEEK SUPERNATANT ANALYSIS .....	58
3.2.5 MMP ANTIBODY ARRAY .....	58
3.2.6 FLUORESCENT SPECTROSCOPY.....	58
3.2.7 WATER CONTACT ANGLE (WCA).....	59
3.2.8 TOF-SIMS FOR SEQUENCE ANALYSIS.....	60
3.2.9 MMP TREATMENT OF DIGE-D COVERSLEIPS .....	61
3.2.10 SUPERNATANT TREATMENT FOR TOF-SIMS.....	61
3.3 RESULTS.....	62
3.3.1 MSC SECRETION OF MMP.....	62

3.3.2	MMP SUBSTRATE PREFERENCE .....	66
3.3.3	DESIGN AND SYNTHESIS OF THE SURFACE .....	73
3.3.4	SURFACE CHARACTERISATION .....	73
3.3.4.1	Pre-treatment .....	73
3.3.4.2	Amino Acid Addition .....	75
3.3.4.3	DIGE-D Cleavage.....	81
3.3.4.4	Surface Response to Supernatant.....	83
<b>3.4</b>	<b>DISCUSSION.....</b>	<b>84</b>
<b>3.5</b>	<b>CONCLUSIONS.....</b>	<b>87</b>
<b><u>4.</u></b>	<b><u>BIOCOMPATIBILITY.....</u></b>	<b><u>88</u></b>
<b>4.1</b>	<b>INTRODUCTION.....</b>	<b>89</b>
<b>4.2</b>	<b>METHODS.....</b>	<b>92</b>
4.2.1	SUPPLIERS INFORMATION .....	92
4.2.1	CELL SEEDING .....	92
4.2.2	VIABILITY .....	92
4.2.3	IMMUNOHISTOCHEMISTRY .....	93
4.2.4	PROLIFERATION .....	94
4.2.5	MMP PROFILE .....	95
<b>4.3</b>	<b>RESULTS.....</b>	<b>96</b>
4.3.1	CELL VIABILITY.....	96
4.3.2	CELL ADHESION .....	103
4.3.3	PROLIFERATION .....	109
4.3.4	MMP RESPONSE TO THE SURFACE.....	112
4.3.4.1	Gelatinases.....	112
4.3.4.2	MMP Family Members .....	115
<b>4.4</b>	<b>DISCUSSION.....</b>	<b>117</b>
<b>4.5</b>	<b>CONCLUSION .....</b>	<b>120</b>
<b><u>5.</u></b>	<b><u>PHENOTYPE .....</u></b>	<b><u>121</u></b>
<b>5.1</b>	<b>INTRODUCTION.....</b>	<b>122</b>
5.1.1	OSTEOGENESIS AS A RESULT OF ADHESION .....	124
5.1.2	METABOLOMICS .....	125
5.1.3	AIMS .....	126
<b>5.2</b>	<b>METHODS.....</b>	<b>126</b>
5.2.1	SUPPLIER INFORMATION.....	126
5.2.2	ICW .....	126
5.2.3	VON KOSSA .....	127
5.2.4	QRT-PCR.....	127

5.2.5	METABOLOMIC ANALYSIS.....	128
<b>5.3</b>	<b>RESULTS.....</b>	<b>129</b>
5.3.1	SELF-RENEWAL .....	129
5.3.2	EARLY MARKERS OF OSTEOGENESIS .....	130
5.3.3	METABOLITE ANALYSIS, WEEK 3 .....	131
5.3.4	DIFFERENTIATION, WEEK 4 - 6 .....	134
5.3.5	SPONTANEOUS DIFFERENTIATION .....	138
<b>5.4</b>	<b>DISCUSSION.....</b>	<b>140</b>
<b>5.5</b>	<b>CONCLUSION .....</b>	<b>142</b>
<b>6.</b>	<b><u>DISCUSSION.....</u></b>	<b><u>143</u></b>
<b>6.1</b>	<b>INTRODUCTION.....</b>	<b>144</b>
<b>6.2</b>	<b>REGENERATIVE MEDICINE.....</b>	<b>145</b>
<b>6.3</b>	<b>THESIS DISCUSSION .....</b>	<b>147</b>
<b>6.4</b>	<b>LIMITATIONS .....</b>	<b>150</b>
<b>6.5</b>	<b>FUTURE WORK.....</b>	<b>151</b>
<b>6.6</b>	<b>CONCLUSION .....</b>	<b>152</b>
	<b><u>REFERENCES.....</u></b>	<b><u>153</u></b>

# Abstract

It is thought that stem cells hold promise for use in future therapeutics. One such application is tissue engineering (TE) which aims to repair or replace diseased or damaged organs *in vitro*. Successful applications of TE, where the tissue is replaced and is functional, could improve a patients' quality of life. Mesenchymal stem cells (MSCs) are a form of adult stem cell that are a precursor for fat, cartilage and bone cells. Bone is the second most transplanted tissue after blood therefore, enabling TE strategies through provision of high quality bone cells to facilitate bone repair would be beneficial. As MSCs are a precursor to bone, their use is attractive. Additionally, their proliferative potential and immunoregulatory properties make MSCs an ideal candidate cell for TE. MSCs require behavioural cues *in vitro* that direct phenotype in a targeted way. One method to direct stem cell behaviour is to utilise materials engineering. Static materials (examples include topography, chemistry and stiffness) have been employed but research has now moved towards stimuli responsive technologies to provide dual functionalities for culture and that emulate the properties of the stem cell niche.

It is the intention of the work described in this thesis to utilise an enzyme responsive technology to promote MSC self-renewal and stimulate MSC differentiation to bone. Using solid phase peptide synthesis (SPPS) a biomimetic enzyme responsive material was made with the sequence PEG-GPAG↓LRGD tethered to a glass coverslip. Due to enzyme action on the sequence, the PEG cap is removed to create on demand adhesion to the peptide RGD. Further, the surface is designed to be under the control of cell secreted enzymes, rather than in response to enzymes added in by the user.

The cell secreted enzymes that were investigated for this thesis were the matrix metalloproteases (MMPs). Here we confirm that the primary MMP secreted by MSCs was the gelatinase MMP-2 and a peptide sequence was designed to be cleaved by this MMP. It is known that redundancy can occur in MMP families and the role of MMP-9 was also investigated. The results show that MMP-9 is as efficient for surface cleavage, although cell supernatant concentration was 100-fold lower. MMP-2 concentration increased at week 3 specifically in response to peptides and so formed the original hypothesis that cleavage occurred at that time point. However, due to the potency of MMP-9 this may not be the case. Due to the limitations of manual synthesis and availability of materials, there was not enough evidence of MSC self-renewal. Further there was some indication of osteogenesis, specifically in response to the sequence at 4-6 weeks, however this is too long in culture to be therapeutically relevant. It may be better in the future to employ an enzyme responsive surface that can guarantee 100% efficiency of cleavage to ensure a synchronised population of end terminal cells.

## Acknowledgement

There are many people who I'd like to thank for their support during this study. I'd like to thank my supervisors Matt Dalby and Rein Ulijn for their advice and support during this project. I'd particularly like to thank Carol-Anne Smith whose guidance and wisdom has been essential.

My family have all been very supportive and encouraging of my work (even if they didn't always understand what I was talking about!). Especially, my sister Kate as she has even offered to read drafts of my thesis.

I am so grateful to have found such amazing friends in our DTC cohort, without whom I would have been at a loss in our first year. Ricky and Mark B have been a never-ending source of banter and Gabby is truly my partner in crime. Thanks to Mark S for being there from the beginning, Aranza for having to live with me through final year and Carolina for being shorter than me. Thanks also to the CCE girls, the "scientifically shady" Paula, Hannah, Natasha and Caroline who have shared laughs, advice, a shoulder to cry on and most importantly – hummus.

Lastly but never least I would like to say thank you to the best boyfriend and lab partner a girl could ask for. I could not have done this without him. Even though we didn't like each other at the start (that accent!) we were always there for each other. Particularly during the PhD, Jakes advice and support has been a source of comfort. He is always the first person I turn to – he is truly my rock.

### *In Memoria*

Rachel Turnbull

1927 - 2016

Mary Anderson

1926 - 2016

# Publications

## Scientific Publications

- Anderson, H. *et al.* Nanoscale surface cues and cell behaviour. in *Reference Module in Materials Science and Materials Engineering* (2017). doi:10.1016
- Roberts, J. N. *et al.* Dynamic Surfaces for the Study of Mesenchymal Stem Cell Growth through Adhesion Regulation. *ACS Nano* **10**, 6667–6679 (2016).
- Anderson, H. J., Sahoo, J. K., Ulijn, R. V. & Dalby, M. J. Mesenchymal Stem Cell Fate: Applying Biomaterials for Control of Stem Cell Behavior. *Front. Bioeng. Biotechnol.* **4**, 38 (2016).

## Published Writing

- “*Women in Science and the Impact in Social Media*” Glasgow City of Science blog. Published December 2015<sup>1</sup>
- “*What is ...Tissue Engineering?*” Biological Sciences Reviews, Hodder Education, September 2017
- CCE blog articles available at [www.uofgcce.org](http://www.uofgcce.org)

## Grants

- Received £900 of funding through “New Initiatives” scheme to fund the equipment required to film videos for our YouTube channel.
- Received £500 from the Chancellor’s Fund to help with the cost of the research club “Wallstreet Wednesday”.

## Awards

- The College of Medical, Veterinary and Life Sciences “Young Researcher of the Month” award, March 2016.

---

<sup>1</sup> <http://www.glasgowcityofscience.com/blog/education-and-skills-development/504-women-in-science-and-the-impact-of-social-media?highlight=WyJoaWxhcniX>

## Presentations

Date	Location	Presentation
2014	<b>University of Glasgow</b> Glasgow Orthopaedic Research Initiative (GLORI), “Control of MSC Behaviour Through Materials Engineering”	Poster
2015	<b>University of Southampton</b> Tissue and Cell Engineering Society (TCES), <i>“Enzyme Responsive Technology for Mesenchymal Stem Cell Control”</i>	Poster
2016	<b>University of Glasgow</b> GLORI, <i>“Stem Cell Controllable materials for both MSC Self-Renewal and Differentiation”</i>	Talk
2016	<b>University of Glasgow</b> British Orthopaedic Research Society 2016, <i>“Stem Cell Controllable Materials for Both Self-Renewal and Differentiation”</i>	Poster
2017	<b>Sant Feliu</b> Biointerfaces, The Federation of European Biochemical Societies (FEBS) <i>“Dynamic Surfaces for MSC Self-Renewal and Differentiation”</i>	Poster

# Abbreviations

## Amino Acids

<b>Amino Acid</b>	<b>1 Letter Code</b>	<b>3 Letter Code</b>
Alanine	A	Ala
Cysteine	C	Cys
Aspartic Acid	D	Asp
Glutamic Acid	E	Glu
Phenylalanine	F	Phe
Glycine	G	Gly
Histidine	H	His
Isoleucine	I	Ile
Lysine	K	Lys
Leucine	L	Leu
Methionine	M	Met
Asparagine	N	Asn
Proline	P	Pro
Glutamine	Q	Gln
Arginine	R	Arg
Serine	S	Ser
Threonine	T	Thr
Valine	V	Val
Tryptophan	W	Trp
Tyrosine	Y	Tyr

## Terms

AFM	Atomic Force Microscopy
AKT	Protein Kinase B
ALCAM	Activated Leukocyte Adhesion Molecule
ALP	Alkaline Phosphatase
ALS	Amyotrophic Lateral Sclerosis
ANOVA	Analysis of Variance
ATP	Adenosine Triphosphate
BHK	Baby Hamster Kidney
BM	Bone Marrow
BMP	Bone Morphogenetic Protein
BMPR1	Bone Morphogenetic Receptor 1
Boc	<i>T</i> -Butyloxycarbonyl
BrdU	5-Bromo-2'-Deoxyuridine
BSA	Bovine Serum Albumin
BSP	Bone Sialoprotein
CAM	Cell Adhesion Molecule
CARG	Compound Annual Growth Rate
CBFA1	Core Binding Factor Alpha
Cdc42	Cell Division Control Protein 42
CFU-F	Colony Forming Units-Fibroblasts
CO <sub>2</sub>	Carbon Dioxide
COL 1	Collagen 1
CRISPR	Clustered Regularly Interspaced Short Palindromic Repeats
DAPI	4'6-Diamidine-2'-Phenylindole Dihydrochloride
DPAPI	4'6-Diamindino-2-Phenylindole
DC	Dendritic Cells
DCC	Dicyclohexylcarbodiimide
dH <sub>2</sub> O	Deionised Water
DIC	N,N'-Diisopropylcarbodiimide (Dic)
DMEM	Dulbecco's Modified Eagle's Medium
DMF	N,N-Dimethylformamide
DMP1	Dentin Matrix Protein 1

DMSO	Dimethyl Sulfoxide
DNA	Deoxyribonucleic acid
DPN	Dip Pen Nanolithography
EB	Embryoid Body
EBL	Electron Beam Lithography
ECM	Extracellular Matrix
EHIC	Ethyl (Hydroxyamino) Cyanoacetate
ELISA	Enzyme-Linked Immunosorbent Assay
ERK 1/2	Extracellular Related Kinase 1/2
ERM	Enzyme Responsive Material
ESC	Embryonic Stem Cell
FA	Focal Adhesion
FAK	Focal Adhesion Kinase
FBS	Foetal Bovine Serum
FC	Focal Complex
FDA	Food and Drug Administration
FGF-2	Fibroblast Growth Factor 2
Fmoc	9h-Fluoren-9-Ylmethoxycarbonyl
GAPDH	Glyceraldehyde 3-phosphate dehydrogenase
GF	Growth Factor
GFAP	Glial Fibrillary Acidic Protein
GOPTS	3-Glycidyoxypropyl Trimethoxysilane
GSK3	Glycogen Synthase Kinase-3
GTP	Guanosine Triphosphate
GTPase	(Hydrolysis of) Guanine Triphosphate
GVHD	Graft Versus Host Disease
H <sub>2</sub> O <sub>2</sub>	Hydrogen Peroxide
H <sub>2</sub> SO <sub>4</sub>	Sulfuric Acid
HA	Hydroxyapatite
HEFA	Human Fertilisation and Embryology Authority
HEPES	2-Hydroxyethyl-1-Piperazine-Ethanesulphonic Acid
Hif-1 $\alpha$	Hypoxia Inducible Factor-1- $\alpha$
HMDB	Human Metabolomic Database
HPLC	High Performance Liquid Chromatography
HSC	Hematopoietic Stem Cell

HUVEC	Human Umbilical Vein Endothelial Cells
ICW	In-Cell Western
IF	Intermediate Filament
IFN	Interferons
IgG	Immunoglobulin G
IL	Interleukin
IPA	Ingenuity Pathway Analysis
iPSCs	Induced Pluripotent Stem Cells
IVF	In Vitro Fertilisation
JNK	C-Jun N-Terminal Kinase
KEGG	Kyoto Encyclopaedia Genes and Genome
LIFI-11	Lactoferrin-Derived Antimicrobial Peptide
LIF	Leukaemia Inhibitory Factor
LINC	Linker of Nucleoskeleton And Cytoskeleton
LMIG	Liquid Metal Ion Gun
m / z	Mass-To-Charge-Ratio
MAPK	Mitogen Activated Protein Kinase
MAPKK	Mitogen Activated Protein Kinase Kinase
MAPKKK	Mitogen Activated Protein Kinase Kinase Kinase
MAR	Matrix Attachment Regions
MEF	Murine Embryonic Fibroblast
MHC	Major Histocompatibility
MI	Myocardial Infarction
miRNA	Micro RNA
MLCK	Myosin Light Chain Kinase
MMP	Matrix Metalloproteinase
MRSA	Methicillin Resistant <i>Staphylococcus Aureus</i>
MSC	Mesenchymal Stem Cell
MT-MMP	Membrane Bound Matrix Metalloprotease
mTOR	Mammalian Target of Rapamycin
MTT	(3-(4,5-Dimethylthiazol-2-Yl)-2,5-Diphenyltetrazolium Bromide
NaCl	Sodium Chloride
NHS	National Health Service
NIH	National Institute of Health
NK	Natural Killer

OCN	Osteocalcin
OD	Optical Density
ONS	Office of National Statistics
OPN	Osteopontin
OtBu	O- <i>Tert.</i> Butyl
p-value	Probability Value
P70 S6K	Ribosomal Protein S6 Kinase Beta-1
PAAm	Polyacrylamide
PARP	Poly ADP-Ribose
Pbf	Pentamethyldihydrobenzofuran-5-Sulfonyl
PBS	Phosphate Buffered Saline
PC 1 / 2	Principal Component 1 / 2
PCA	Principal Component Analysis
PCR	Polymerase Chain Reaction
PDMS	Polydimethylsiloxane
PEA	Poly (Ethyl Acrylate)
PEG	Poly (Ethylene Glycol)
PEG <sub>26</sub> -NH <sub>2</sub>	PEG <sub>26</sub> Diamine
PEGDA	Poly (Ethylene Glycol) Diacrylate
PI3K	Phosphoinositide 3-Kinase
PIPAAm	Poly (N-Iso- Polyacrylamide)
PKC	Protein Kinase C
PLA	Poly(lactic Acid)
PPAR $\gamma$	Peroxisome Proliferator-Activated Receptor Gamma
qRT-PCR	Quantitative Real-Time Polymerase Chain Reaction
Rack 1	Receptor of Activated Protein Kinase C 1
RGD	Arg-Gly-Asp
RGE	Arg-Gly-Glu
RhoA	Ras Homologue Gene Family Member A
RNA	Ribonucleic Acid
ROCK	Rho-Associated Protein Kinase
ROI	Regions of Interest
RUNX2	Runt-Related Transcription Factor
SD	Standard Deviation
SDS	Sodium Dodecyl Sulfate

SHH	Sonic Hedgehog
Si <sup>+</sup>	Silane
SIBLING	Small Integrin Binding Ligand N-Linked Glycoproteins
Smad	Small Mothers Against Decapentaplegic
SMAdh	Super Mature Adhesions
Sox 9	Sry-Related High Mobility Group Box 9
SPPS	Solid Phase Peptide Synthesis
tBU	T-Butyl
TE	Tissue Engineering
TFA	Trifluoroacetic Acid
TGF β	Transforming Growth Factor β
TIMP	Tissue Inhibitor of Matrix Metalloprotease
TLR	Toll Like Receptor
TNF	Tumour Necrosis Factor
ToF-SIMS	Time of Flight Mass Spectrometry
UK	United Kingdom
USD	United States Dollar
WCA	Water Contact Angle

## Measurements

cm	Centimetre
kDa	Kilodaltons
mg/ml	Milligram per millilitre
ml	Millilitre
mm	Millimetre
ng/ml	Nanogram per millilitre
nm	Nanometre
μl	microliter
μm	Micrometre
μmol	micromole

## List of Tables

<b>Number</b>	<b>Title</b>	<b>Page</b>
2.1	Supplier Information	42
2.2	Schematic of Fmoc Protected Amino Acids For SPPS	45
2.3	Sequence of Controls	46
2.4	Position of Each Spot on Abcam Antibody Array	49
3.1	Matrix Metalloprotease Families, Substrate Preference and Molecular Weights	53
3.2	Supplier Information	60
3.3	Expected M/Z Ration of Each Amino Acid Used In SPPS	63
3.4	Consensus Sequences for Selected MMPs	74
3.5	Quantification of WCA for Pre-Treatments	76
3.6	Quantification of WCA for Amino Acids	83
4.1	Supplier Information	93
4.2	Immunohistochemistry Antibodies	95
4.3	% BrdU Nuclei of Total Cells	111
5.1	Supplier Information	125
5.2	Antibodies Used for ICW	126
5.3	Primers Used for qRT-PCR	127

## List of Figures

<b>Figure</b>	<b>Title</b>	<b>Page</b>
1.1	Stem Cell Lineage	3
1.2	Number of Publications per Year For MSCs and Its Derivatives	8
1.3	The Bone and the Bone Marrow Niche	9
1.4	Downstream Effects of Integrin Binding	14
1.5	Population Data for Persons Aged 90 Years and Over	17
1.6	The “Triangle” of Materials Engineering	20
1.7	The Debate on Porosity of Hydrogel Stiffness and Effects on MSC Differentiation	25
1.8	Limitations of Light Responsive Hydrogels <i>in vivo</i>	26
1.9	Schematic of Surface Remodelled by Cell Secreted MMPs	30
1.10	Schematic of SPPS Method	32
1.11	Cell Response to Fmoc/PEG-A↓ARGD Surface	36
2.1	Pre-Treatment of a Glass Coverslip and First Amino Acid Addition	41
3.1	Range of Substrates for MMP Activity	49
3.2	Conserved Structure for the Secreted MMPs	52
3.3	MMP-2 Active Site	53
3.4	Activation of MMPs	54
3.5	Schematic of Equipment for Fluorescent Spectroscopy Analysis of Glass Coverslips	58
3.6	WCA Measurement Parameters	59
3.7	Zymography, 1 Week	62
3.8	Gelatinase Expression Over Six Weeks as Determined by ELISA	62
3.9	MMP Profile of MSC Supernatant	63
3.10	Gelatinase Consensus Sequence	68
3.11	Scissile Bond Preference	69
3.12	Preference of Other MMPs for the Sequence GPAG↓LRGD (P4-P4')	70
3.13	Progression of SPPS for Sequence PEG-GPAG↓LRGD	71
3.14	Water Contact Angle of Pre-Treated Glass Coverslip Prior to Amino Acid Addition	72
3.15	ToF-SIMS Images for SPPS Build-Up	74
3.16	ToF-SIMS Analysis of Amino Acid Addition	75

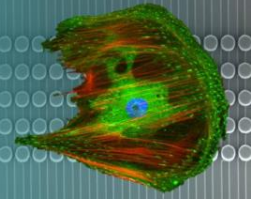
3.17	Quantified Normalised Ion Intensity per Substrate and Potential Contamination by Other Factors.	76
3.18	Fluorescent Spectroscopy of Amino Acid Addition	77
3.19	Water Contact Analysis of Amino Acid Addition	78
3.20	Cleavage by MMP-2 on Sequence PEG-GPAG↓LRGD	80
3.21	PEG Remaining After Gelatinase Treatment	81
3.22	Supernatant Treatment of DIGE-D	82
4.1	Viability of Fmoc-A↓ARGD Surface	88
4.2	Live/Dead Staining of Control Surfaces	95
4.3	Tubulin Expression After 24 Hours	97
4.4	Vimentin Staining at 24 Hours	99
4.5	Quantification of Vimentin Staining	100
4.6	Viability at 1 Week	101
4.7	Vinculin Expression at 24 Hours	103
4.8	Vinculin Quantification, 24-Hour Culture	104
4.9	Total Number of Adhesions	105
4.10	Percentage Adhesions per Cell	106
4.11	BrdU Staining	108
4.12	Quantification of BrdU Positive Cells	109
4.13	Quantification of Cell Area and Number, 1 Week	110
4.14	Gelatinase Response Per Surface Over 3 Weeks	111
4.15	Gelatin Zymography at Week 3	112
4.16	Gelatinase Expression as Determined by Membrane Analysis	112
4.17	Presence of Other MMPs and TIMP Families	114
4.18	MMP and TIMP Expression	115
5.1	Hypothetical Model of Cell Response to Surface	121
5.2	Intracellular Signalling for Osteogenic Differentiation	122
5.3	Stro-1 Expression Over 4 Weeks	128
5.4	RUNX2 Expression After 24 Hours and 7 Days	129
5.5	PCA Plot For DIGE-D And DIGE-E at Week 3	130
5.6	PCA Plots per Metabolite Group	131
5.7	4-Week ICW of Bone Markers	133
5.8	Von Kossa Staining at 4 Weeks	133
5.9	6-Week ICW of Bone Markers	134

5.10	Osteogenic Markers at 4 and 6 Weeks	135
5.11	Von Kossa Staining at 6 Weeks	136
5.12	Phenotype Determined by qRT-PCR	137

## Author's Declaration

I declare that, except where explicit reference is made to the contribution of others, that this thesis is the result of my own work and has not been submitted for any other degree at the University of Glasgow or any other institution.

Hilary Jane Anderson



# 1. Introduction: Mesenchymal Stem Cells and Tissue Engineering

The aim of tissue engineering (TE) is to create off-the-shelf tissues and organs to replace those that have become diseased or damaged. If successful, this would alleviate the limitations of current therapeutics but also to aid the crisis in organ donation. The stem cell field is central to this work and mesenchymal stem cells (MSCs) have the potential to be at the forefront of this technology. However, the expansion of MSCs *in vitro* is still inadequate due to untargeted differentiation of the cells. In the past 20 years, there have been many materials strategies applied to MSC culture, namely topography, chemistry and stiffness. However, a growing trend in MSC culture is to utilise stimuli responsive biomaterials such as light, enzyme, temperature and even electrical stimuli to manipulate the material properties at will. This work aims to continue this theme by utilising cell secreted enzymes to remodel the cell-material interface for MSC differentiation. In this chapter, we will explore the nature of stem cells, the use of static and stimuli responsive technologies for stem cell culture particularly for the differentiation of MSCs along an osteoblastic lineage.

## 1.1 Stem Cells

A stem cell is characterised as having the ability to self-replicate and form other cell types. The first observation of these types of cells were derived from experiments by Till and McCulloch (Till & McCulloch 1961). Looking at the effects of radiation on the body they noted that when bone marrow cells were injected into irradiated mice, it resulted in nodules on the spleen that were proportional to the number of cells injected (Till & McCulloch 1961). The mass was the product of proliferating colonial cells and there had to be a precursor cell that could generate daughter cells (Till & McCulloch 1961). This observation paved the way for future work on precursor cells and the identification of pure stem cells (Friedenstein 1976). Embryonic stem cells were then identified from mouse embryos in 1981 (Evans & Kaufman 1981). Evans and Kaufman established a culture of cell lines from mouse blastocysts that had normal morphology and karyotype, which grew rapidly and could form teratocarcinomas when injected into a mouse model (Evans & Kaufman 1981). Teratocarcinoma is the generation of tumour like cells that contain differentiated cells of all lineages in one cell mass (Evans & Kaufman 1981). Another breakthrough emerged in 1998 when the first human embryonic stem cells were identified (Thomson 1998). In the last few decades, there have been many discoveries in stem cell biology including the identification of multiple stem cell niches and the molecular mechanisms involved in their regulation (Ehninger & Trumpp 2011). Since the discovery of stem cells, their potential use in healthcare was immediately obvious. However, the use

of stem cells has been somewhat controversial particularly in the case of embryonic stem cells.

### 1.1.1 Embryonic Stem Cells (ESCs)

ESCs are derived from the inner cell mass of the preimplantation embryo and are characterised as cells that can form cells of all three germ layers (endoderm, mesoderm and ectoderm, Figure 1.1) (Stojkovic et al. 2004). From these cell types, differentiated cells can be obtained. Embryos are grown to blastocyst stage, then the inner cell mass is isolated and removed for culturing (Stojkovic et al. 2004). For human embryos, the inner cell mass is usually derived from fertilised gametes donated from clinical procedures such as in vitro fertilisation (IVF) or abortions (although guidelines vary per country) (Dhar & Hsi-En Ho 2009). Those that were accredited for discovery of these cells used tissue from both procedures (Thomson 1998).

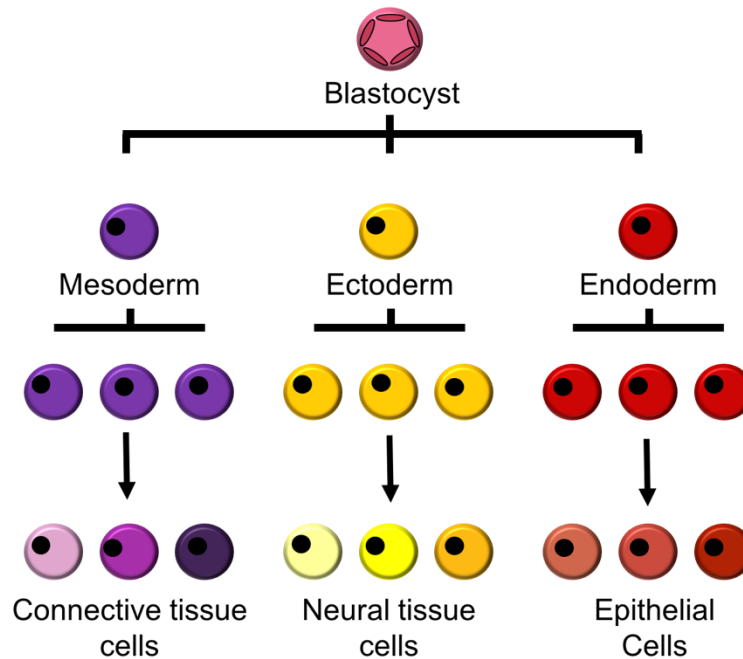


**Figure 1.1 - Stem Cell Lineage.** Embryonic stem cells are isolated from the inner cell mass of the blastocyst. These cells are described as pluripotent and can form every cell in the body. These cells then specialise and become responsible for generation of cells of each tissue layer (endoderm, mesoderm and ectoderm). The cells that form these layers are known as multipotent and can form the terminally differentiated cells of that tissue.

ESCs have a specific set of requirements for *in vitro* culture for example, the cytokine leukaemia inhibitory factor (LIF) and a feeder layer, (mitotically inactivated murine embryonic fibroblast, MEF) are typically used (Odorico et al. 2001). Differentiation occurs when they are removed from the layer and where they differentiate into embryoid

bodies (EB) (Odorico et al. 2001). ESCs express a high level of telomerase activity, characteristic of immortal cells and suggests that their replicative capacity is greater than that of somatic cells (Thomson 1998). ESCs express few major histocompatibility complex (MHC) class I molecules. This increases with specialisation and therefore differentiation results in the presence of more MHC markers (Olivier et al. 2004). Presentation of these markers creates an immune response when implanted into a patient (Vogel 2002) and so to overcome this, the patient would need to be on extremely high doses of immunosuppressant's (Odorico et al. 2001). There is a further risk in utilising these cells in that injection of ESCs to immunodeficient mice does not induce organogenesis, rather teratoma formation (Till & McCulloch 1961).

The use of ESCs have great potential for TE purposes as they have the capacity for differentiation to clinically relevant cells from a single cell source. The process of donation of human embryos is carefully considered, permitted only with informed consent and handled under the appropriate ethical guidelines (Dhar & Hsi-En Ho 2009). In the UK, the use of ESCs for research is governed by the Human Fertilisation and Embryology Act (HEFA), which requires stringent measures on consent and research is only permitted where significant knowledge on development or disease can be obtained (Dhar & Hsi-En Ho 2009). Due to the nature of the cell type and the unanswered question of embryo "consciousness" there is a lot of debate surrounding the use of these cells which in the past has been influenced even at the political level (in 2001 the Bush administration limited federal funding for ESC research <sup>2</sup>). To use these cells in the clinic, tissue typing could be employed or as was suggested in 1998 to genetically engineer the cells to combat immune rejection (Thomson 1998). Technologies such as CRISPR (Clustered Regularly Interspaced Short Palindromic Repeats) could be utilised to do this (Zhang et al. 2014).

### 1.1.2 Induced Pluripotent Stem Cells (iPSCs)

In 2006, Shinya Yamanaka created an alternative to the destruction of embryos by taking somatic cells and reprogramming their behaviour using 4 key genes: Oct3/4, Sox2, c-Myc and Klf4 (Takahashi & Yamanaka 2006). The genes were inserted into MEF cells using a retroviral transduction. The cells, when inserted into nude mice formed teratomas, with cells that had differentiated into tissues of all three germ layers (Takahashi & Yamanaka 2006). The somatic cells took on a pluripotent role which they then demonstrated was

---

<sup>2</sup> <https://www.newscientist.com/article/dn24970-stem-cell-timeline-the-history-of-a-medical-sensation/>

sufficient to aid embryonic development as they were injected into mouse blastocysts from which pups were born (Takahashi & Yamanaka 2006). In the next year, this was achieved using the same factors but moving from mouse cells to adult human fibroblasts (Takahashi et al. 2007). This was a landmark finding and the potential of this technology for healthcare was quickly recognised earning Yamanaka the 2012 Nobel Prize for medicine.

The advantage is that this method generates patient specific cells, cells that could be used to alleviate the effects of degenerative diseases. A group from Harvard applied the technique in a bid to help elderly amyotrophic lateral sclerosis (ALS) sufferers (Dimos et al. 2008). ALS is a condition which affects neurons in the spine leading to paralysis over time. One way to treat the condition is by using healthy motor neurons, so the group aimed to reprogram fibroblasts from the skin of an 82-year-old patient to produce motor neurons and glia (Dimos et al. 2008). The cells were reprogrammed with various factors via retroviral transfection and resulting cells had active cell cycle and normal karyotype. They were then induced to differentiate into neuronal cells using an agonist of sonic hedgehog (SHH) signalling and retinoic acid that resulted in increased expression of the neuronal marker  $\beta$ -tubulin IIIb (Dimos et al. 2008). The result was encouraging considering the age and phenotype of the patient.

However, subsequent work on age related iPSCs showed that reprogramming efficiency decreased with increasing age of the patient as the cells exhibited shorter telomere lengths and increased doubling time indicating cell senescence (Trokovic et al. 2015). In this case, age related disorders may not be effectively treated by autologous iPSCs (Trokovic et al. 2015). Further, it has been demonstrated that iPSCs retain DNA methylation signatures from the terminally differentiated cell they were obtained from and therefore have a bias for that phenotype (Kim et al. 2010). There are also risks associated with their use due to the factors involved in the reprogramming phase (Lai et al. 2011). For example, miRNA could be utilised to modify the cells however, this is untargeted and could disrupt the regulation of the host cell (Lai et al. 2011).

### 1.1.3 Adult Stem Cells

Although cells such as the ESCs and iPSCs have more flexibility as they are pluripotent cells, their application to TE, at present, is limited. This is due to the potential tumorigenic potential of the cells, safety concerns (from both transfection agents and non-human feeder layers), the potential immune response of the host and the ethical issues associated with

their use (Alvarez et al. 2012). Researchers are turning to adult stem cells to overcome these issues. Adult stem cells are located in specific areas in the body known as niches (Ehninger & Trumpp 2011). While these stem cells are limited in terms of lineage, they are equally as capable of forming a large populations of cells through their proliferative potential (Beyer Nardi & Da Silva Meirelles 2006). One such subset of adult stem cells that are particularly relevant for therapeutic use are the mesenchymal stem cells (MSCs). Although MSCs are derived primarily from the bone marrow niche, other sites have been located; adipose, skeletal muscle, teeth and umbilical cord (Baksh et al. 2004). However, there is little phenotypic variation between the cells from these various sources (Kolf et al. 2007). This study exclusively utilises MSCs obtained from the bone marrow niche.

### 1.1.3.1 Mesenchymal Stem Cells

MSCs were first described in 1968 by Friedenstein *et al.* where they were noted to be precursors for osteogenic cells (Friedenstein et al. 1968). In culture, MSCs were described as colony-forming unit fibroblasts (CFU-F), skeletal like cells with the capacity to form colonies (Friedenstein et al. 1968). Since this initial documentation, there has been further characterisation to define the true properties of MSCs. Firstly, they must be adherent cells that are positive in the expression of specific markers (of which there are many that are attributed including Stro-1, CD13, CD73, CD106 amongst others) (Jackson et al. 2007), notably cells negative for Stro-1 do not form CFU-Fs (Kolf et al. 2007). For MSCs, the expression of these markers does not change with trypsinisation (Pittenger 1999). The cells also form skeletal cell types; osteo-, chondro- or adipocytes (Salem & Thiemermann 2010). There is also an argument that MSCs can also form other derivatives such as muscle and neural cells (Gilbert et al. 2010; Yim et al. 2007).

The use of MSCs for TE purposes has potential for several reasons. Firstly, the ability to obtain bone marrow from a patient is a well-studied and practised procedure consisting of aspiration from the iliac crest (Ringe et al. 2002). In addition, bone is the second most transplanted tissue after blood (Shegarfi & Reikeras 2009), therefore as MSCs are precursor cells, it would be desirable to have a source of fast growing cells that bone could be derived from. They also have potential for TE due to their immunoregulatory ability (Aggarwal & Pittenger 2005). MSCs have been shown to have little expression of MHC Class I and lack MHC Class II molecules that contribute to immunogenicity (Kode et al. 2009). Moreover, MSCs can suppress the T cell response using toll like receptors (TLR), specifically TLR-3 ligation to TLR-4 (Liotta et al. 2008). MSCs have the ability to alter

cytokine secretion from natural killer cells (NK) and dendritic cells (DC) namely, reducing the expression of pro-inflammatory cytokines tumour necrosis factor (TNF- $\alpha$ ), interferon-gamma (IFN- $\gamma$ ), and interleukins (IL-1, -2 and -12) which are typically characteristics of the pathophysiology of Graft-versus-host disease (GVHD) (Aggarwal & Pittenger 2005). The reduction of these markers changes the immune response to a more anti-inflammatory phenotype and therefore may provide a mechanism for tolerance in response to transplanted tissue (Aggarwal & Pittenger 2005). This innate response of MSCs is prevalent *in vivo* as MSCs have been found to target immune cells to aid the healing of the left ventricle after myocardial infarction (MI) when injected intravenously (Luger et al. 2017). Using mouse models, Luger *et al.* found that MSCs engrafted to the heart after MI, specifically to the injured site and decreased the number of NK cells and neutrophils therefore improving ventricle function (Luger et al. 2017). For TE, these properties have the potential to reduce the risk of GVHD if used as an allogenic source of cells, improving the chances of success of the transplant (Becker & Hummelen 2007), this is not the case with ESCs or iPSCs.

These qualities have resulted in a sharp increase in the number of publications concerning MSCs and its derivatives in the last decade (Figure 1.2). In 2016, the total number of academic papers published regarding MSCs reached just over 5,500, a vast increase since the 1990's (326 papers published in 1999). This is also true for the differentiated cell types generating yearly publications in the thousands, a steady trend in the last 10 years which is set to continue in the future. This interest is due to increasing patient populations, increased approval for clinical trials and a demand for regenerative medicine. These factors have created a global stem cell market that is worth billions of dollars (USD) and is expected to increase to \$12.3bn in 2021 at a compound annual growth rate (CARG) of 13.1 % (Evers 2016). Of this market, it is estimated that MSCs occupy 23 % (Kode et al. 2009). However, there are still some barriers to the stem cell market namely ethical approval and cost. Future bioengineering strategies must be cost effective to ensure clinical use. Yet with an ageing population and strain on current health care systems it is necessary to investigate stem cell technologies in the hope of providing novel therapies.

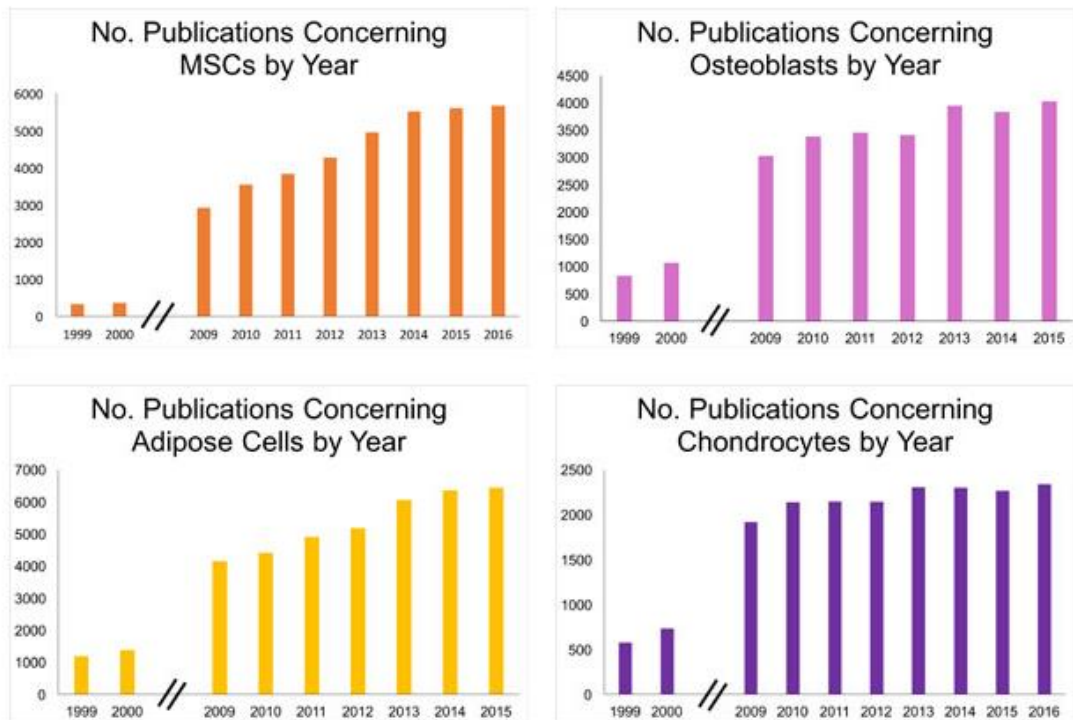


**Figure 1.2 - Number of Publications Per Year for MSCs and Its Derivatives.** In the last two decades, the number of publications for MSCs and its differentiated cells has dramatically increased. In the late 1990's publications for each cell type consisted of less than 1000 papers per year. The number of publications increased in early 2000s and has steadily increased over time (2009-2016), particularly in the case of MSCs and adipose cells. The increasing amount of research has influenced the increasing value of the stem cell market and highlights the potential of this cell type. Graphs generated from a Web of Science search for the number of publications that stated MSCs, osteoblasts, adipose cells and chondrocytes in the title for the years stated.

## 1.2 The Niche

All stem cells are located in defined specialised areas in the body called niches (Scadden 2006). The niche functions to save stem cell populations from depletion but also limits excessive proliferation (Scadden 2006). The stem cell population remains in quiescence until there is a need for specialised cells. Stem cells are then activated to form progenitor cells (through transit amplification) then by specialisation, a population of terminally differentiated cells is created (Watt & Hogan 2000). The niche is more than a holding site for the stem cells as it encompasses supporting cells and extracellular matrix (ECM) which regulate cell behaviour (Hartmann 2006; Ehninger & Trumpp 2011). Adhesion to the ECM is critical for this interaction, which is carried out by integrin proteins (section 1.4).

The bone marrow MSC niche is located in the inner cavity of bone (Clarke 2008). Anatomically, bone is surrounded by an outer membrane called the periosteum, consisting

of blood vessels and nerve endings (Clarke 2008). Bone can be subdivided to cortical (the outer layer that provides strength) and cancellous bone (referred to as “spongy” and exists as a network of trabeculae to resist external forces) (Figure 1.3). The cancellous bone is lined by the endosteum, which contains blood vessels and osteoprogenitor cells (Clarke 2008). The medullary cavity within the cancellous bone is the location of the bone marrow. Bone is a hard material due to the mineralisation of the ECM proteins (with calcium, magnesium and phosphate) but not brittle due to the flexible properties of collagen (Clarke 2008).

Bone is dynamic in nature and consists of four cell types (osteoprogenitor cells, osteoblasts, osteocytes and osteoclasts) that are in continual regulation. Osteoprogenitor cells produce osteoblasts, the cells that are responsible for the secretion of the bone matrix (Clarke 2008). Osteocytes are mature bone cells derived from osteoblasts that reside in the lacuna in a dormant state and osteoclasts are large multi-nucleated cells that resorb the bone matrix (Roodman 1996). The bone tissue is dynamic, the interplay of these cell types ensures a balance between bone formation and resorption, changes to this balance leads to the development of skeletal disorders such as osteoporosis (Boskey & Coleman 2010).

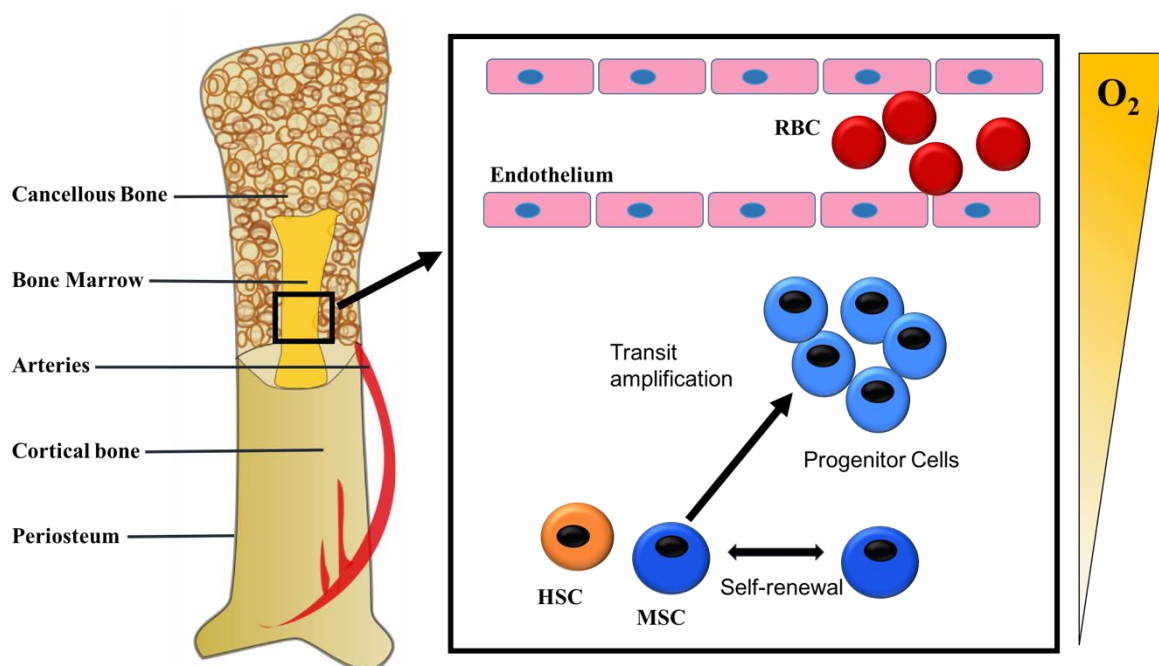


**Figure 1.3 - The Bone and the Bone Marrow Niche.** The bone marrow is located within the inner mass of the bone. Bone itself is composed of cancellous and cortical bone that are encased within the periosteum. The bone marrow is the home of not only mesenchymal stem cells (MSCs) but also the hematopoietic stem cells (HSCs). Through a myriad of factors, the stem cells are kept in regulation between self-renewal and differentiation. Differentiating cells participate in transit amplification whereby the number of progenitor cells increase in number prior to terminal differentiation. The niche is also subjected to an oxygen gradient.

The bone marrow consists of multiple cell types, however MSCs only represent 0.01-0.001% of the bone marrow cell population (Salem & Thiemermann 2010). That said, with expansion, these small numbers of MSCs can generate 50 million cells by passage 2 from 10 mL aspirates from adult donors (age 19-57 years old) (Pittenger 1999). The bone marrow niche is the location of two types of progenitor cells as MSCs occupy the same niche as that of the hematopoietic stem cells (HSCs), the progenitor cell for the blood and immune system (Figure 1.3). The niche is also subjected to an oxygen concentration gradient, while it is highly vascularised the cells display a hypoxic phenotype (expression of hypoxia inducible factor-1- $\alpha$ , Hif-1 $\alpha$ ), this is thought to play a role in maintenance of quiescence (Spencer et al. 2014) (Figure 1.3). The interplay of multiple cell types, the ECM and the oxygen gradient dynamically regulate stem cell behaviour.

### 1.3 The Extracellular Matrix

The ECM consists of many different protein types, including collagen for strength and elasticity, glycoproteins (e.g. fibronectin) and proteoglycans (e.g. hyaluronan) that together form the basement membrane (Mouw et al. 2014). As cells are anchorage dependent, the ECM is adherent and therefore necessary for cell survival, without which cells would die via anoikis (cell homelessness) (Chen et al. 1997). Shown experimentally by Chen *et al.* who utilised microcontact printing to create ECM areas of various sizes, they found that the greater the area presented to the cell (>20  $\mu\text{m}$ ), the greater the chance of survival and further, an increase in DNA synthesis and cell spreading (Chen et al. 1997). Areas below this critical threshold induced apoptosis due to limited cell spreading (Chen et al. 1997).

Within the sequence of ECM proteins, there are certain amino acid cell-adhesion motifs that are particularly directive to cells for example IKLLI, IKVAV and PDSGR for laminin and DGEA and GFOGER for collagen (Weber et al. 2007). A particularly well studied amino acid adhesion sequence is the Arginine-Glycine-Aspartic Acid (RGD) motif found in for example, fibronectin. These motifs are not always exposed in the secreted form of the protein, so are described as cryptic sites (Davis et al. 2000). The motifs can be uncovered in relation to a conformational change via matricryptins for example, by ECM remodelling or cell attachment which alter the presentation of motifs (Davis et al. 2000). These sites can work in concert, e.g. the RGD and PHSRN (the synergy sequence) promote improved cell attachment and cell spreading (Benoit & Anseth 2005). It is accepted that short peptide sequences, such as RGD, can be sufficient to direct cell behaviour making them useful for materials applications (Bellis 2011). Another consideration of utilising

peptide motifs is the recognition by specific integrin combinations. *In vivo*, distinct pairings of  $\alpha$  and  $\beta$  subtypes recognise different ECM ligands e.g.  $\alpha_1\beta_1$  binds to collagen whereas  $\alpha_v\beta_6$  recognises fibronectin in osteoblast-like cells (Shekaran & García 2011). The combination of integrins expressed has an effect on cell behaviour. For example, it is known that  $\alpha_5\beta_1$  is important for osteogenic differentiation and loss of the  $\alpha_5\beta_1$  interaction with fibronectin results in osteoblast apoptosis. In comparison, although  $\alpha_v\beta_3$  can support adhesion, it also inhibits differentiation of osteoprogenitors (Shekaran & García 2011). It has therefore been proposed that bioactive materials could target specific integrins ( $\alpha_5\beta_1$ ) whilst preventing other combinations ( $\alpha_v\beta_3$ ), and thus enhance cellular behaviour and phenotype (Shekaran & García 2011). Care should be taken however, when replicating peptide motifs *in vitro*, as peptide conformation has an effect on receptor interactions. It is known that cyclic RGD targets  $\alpha_v\beta_3$  integrins while linear RGD is less selective and can have an effect on multiple integrin receptors and therefore could alter cellular outcome (Mas-Moruno et al. 2016; Bellis 2011).

As cell shape is defined by the ECM and shape infers function (Lutolf & Blau 2009), modification of the ECM is fundamental to differentiation, development and regeneration of cells and tissues (Mannello et al. 2006). However, it is this same dynamic property that also renders the ECM subject to changes in age, disease and injury resulting in altered composition and changes in stiffness (Lutolf & Blau 2009). It has been shown that cancer cells cultured on stiff matrices invade the basement membrane unlike those cultured on compliant surfaces. Therefore tumour microenvironment is sufficient to support malignancy (Wei et al. 2015; Paszek et al. 2005).

In the context of TE, many materials have drawn on inspiration from the natural ECM. This is true for all cell types and not just that of the MSCs. For example, Ott *et al.* has utilised bioreactors to engineer a heart (Ott et al. 2008). In an animal study, they showed that seeding decellularised hearts with cardiac or endothelial cells and placing them in bioreactors that could simulate the pressure and flow of a beating heart, performed better in terms of viability, contractility and electrical signalling (Ott et al. 2008). Therefore, there are extracellular factors that play a role in cell fate.

## 1.4 Cell Adhesion

Cell adhesion is an important function for adherent cells, without which they would apoptose (Chen et al. 1997). Furthermore, adhesion is essential for cellular behaviours

(e.g. migration), maintenance of cell shape and the communication of external stimuli to the nucleus. Adhesion is modulated by a group of cell adhesion molecules (CAMs) which include cadherins and integrins (Albelda & Buck 1990), for this section, the focus will be on integrins. Integrins are transmembrane receptors that exist as dimers, with one alpha and one beta subunit (Albelda & Buck 1990). There are multiple variations of each subunit and can be expressed in different combinations on the cell surface (Hersel et al. 2003). These combinations have different preferences for ligands presented by the ECM, for example  $\alpha_5\beta_1$  integrin binds to the RGD motif of fibronectin (Humphries et al. 2006). Adhesion to the ECM is not a passive process, it induces intracellular signalling cascades and overall change in cell behaviour. Due to the multiple possible combinations of integrin subunits and the ever-changing presentation of ECM motifs, this results in a myriad of cell behaviours (Giancotti & Ruoslahti 1999). The extracellular part of the integrin ligates to adherent motifs in the ECM. The resultant adhesion can be classified by size, adhesions  $<2 \mu\text{m}$  long are known as focal complexes (or transient adhesions), these short-lived adhesions are involved in migration (Biggs et al. 2009). Adhesions  $2\text{-}5 \mu\text{m}$  long are known as focal adhesions (FA) and sizes  $>5 \mu\text{m}$  long are referred to as super mature adhesions (Biggs et al. 2009). This classification system is a progression of the “dot” and “dash” system originally described by Bershadsky (Bershadsky et al. 1985).

The binding of integrins occurs via a conformational change. Prior to binding, the integrins are tightly folded however, in the presence of an ECM ligand, they unravel and extend exposing the binding site of the  $\beta$  chain to talin (Tadokoro 2003). The unbending of the tail results in a high affinity adhesion to the ECM (Wehrle-Haller 2012). Integrin binding and successful adhesion formation depends on ligand clustering which is limited to a certain threshold. This was demonstrated by Arnold *et al.* who tethered RGD coated gold nanodots, measuring  $<8 \text{ nm}$  across for the attachment of single integrins that were spaced at 28, 58, 73 and 85 nm. Cell adhesion was most effective on substrates spaced at  $\leq 58 \text{ nm}$ , with a greater number of cells adhering (Arnold et al. 2004). Cavalcanti-Adam, continued this work also using RGD coated gold nanoparticles at 58 or 108 nm (Cavalcanti-adam et al. 2007). At 58 nm as expected, cell adherence and spreading occurred after 3 hours. In comparison, the 108 nm spacing did not facilitate integrin clustering (Cavalcanti-adam et al. 2007). Cell motility on the 108 nm pattern was erratic and adhesions that did form underwent a rapid turnover (Cavalcanti-adam et al. 2007). Furthermore, Geiger *et al.* show that increasing ligand distance is inversely proportional to projected cell size, cell size being maximal when ligand spacing is minimal (Geiger et al.

2009). In terms of cell morphology, increased spacing (58-70 nm) resulted in elongation of cells and increased migration (Geiger et al. 2009). For persistent cell spreading, at least four ligand bound heterodimers are required to maintain the adhesion (Schvartzman et al. 2011).

The intracellular component of the integrin is involved in the recruitment of various secondary proteins to the integrin site (together known as focal contact), without which an adhesion cannot be sustained (Mitra et al. 2005). These proteins are usually associated with adhesions between 1-5  $\mu\text{m}$  in size. These proteins include vinculin, FAK (focal adhesion kinase), talin and the cytoskeletal proteins (Figure 1.4). Each protein involved in the focal contact has an independent role in the formation and maintenance of the adhesion. Talin wedges between the tails of each  $\alpha$  and  $\beta$  subunit, the open conformation results in exposure of vinculin binding sites (del Rio et al. 2009). This early interaction is critical, cells that do not express talin have unstable cell spreading and lack FAs (Geiger et al. 2009). Vinculin binding results in the stability of the adhesion and an increase in focal adhesion size (Humphries et al. 2007). FAK is thought to act as a mechanosensor by revealing binding sites and promoting Src kinase signalling (Wehrle-Haller 2012).

The focal contacts connect integrins to actinomyosin in a structure which has been described as the molecular clutch (coined by Mitchison and Kirschner, 1988) that is said to be engaged when the integrins bind to actinomyosin (Sun et al. 2016). The presence of talin also increases the rate of actin polymerisation (Medda et al. 2014). Signalling events then occur including the phosphorylation of FAK and activation of guanosine triphosphatases (GTPases) through which kinase and phosphatase pathways are activated resulting in changes to cell behaviour downstream. One such change is the regulation of cell morphology through GTPases: cdc42 (cell division control protein 42), Rho (Ras homologue gene family member A) and Rac create filopodia, stress fibres and lamellipodia respectively. This process does not only involve different GTPases but also different  $\beta$  subunits particularly, the  $\beta 3$  subunit must activate to begin clustering at the tip (Wehrle-Haller 2012). The change in morphology provides the cellular apparatus for either migration or adhesion.

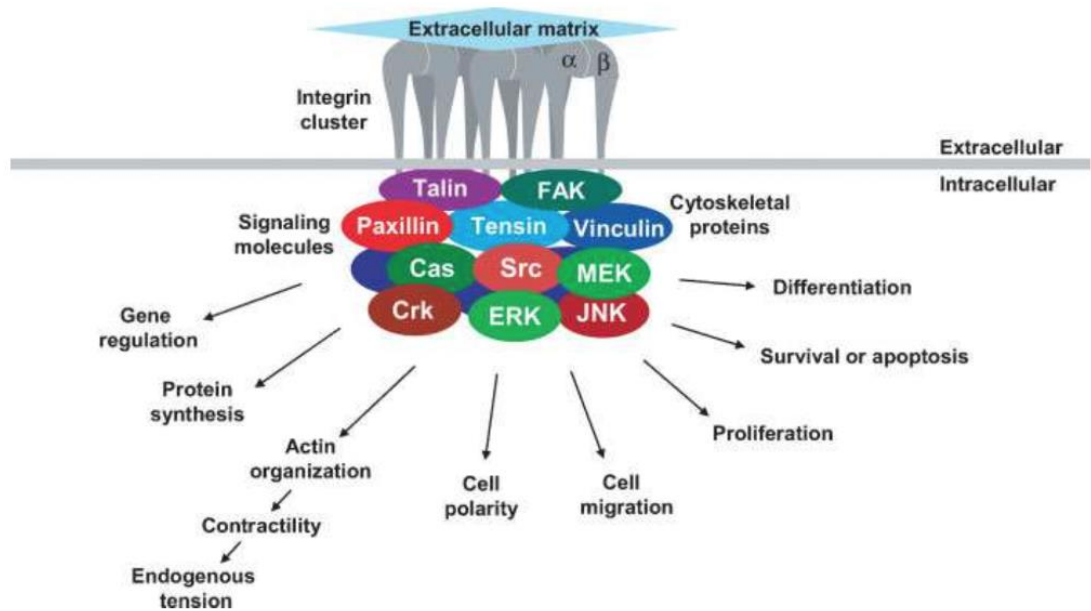


**Figure 1.4 - Downstream Effects of Integrin Binding.** Integrin binding to the ECM results in recruitment of other integrin dimers and a clustering of the integrins at the site. On the intracellular side the integrins signal various protein molecules including FAK and vinculin. Through kinase and phosphatase pathways, downstream effects are organised leading to a diverse range of cell behaviours including differentiation and protein synthesis. Figure Taken from (Berrier & Yamada 2007).

After adhesion to the ECM is established, the downstream effects are achieved by activation of genes in the nucleus as the external information is relayed by the cytoskeletal apparatus. “Tensegrity” was proposed by Ingber *et al.* to describe the method by which mechanical stimuli are transduced by cytoskeletal components to drive intracellular tension (Ingber 1993). Tensegrity is also required to maintain cell shape and resist deformation (McGarry & Prendergast 2004). Further, the mechanical stimulus can be related to the nucleus in the process of mechanotransduction where adhesion results in gene and protein level changes that alter cell behaviour (DuFort *et al.* 2011).

Direct mechanotransduction refers to the effects of the cytoskeleton, the action of the ECM having a direct effect on nuclear deformation (i.e. the pulling of cells to a substrate) (Dalby 2005). Microtubules and intermediate filaments relay this mechanical stimulus through the plasma membrane to the nuclei via the LINC complex (linker of nucleoskeleton and cytoskeleton) proteins (Crisp *et al.* 2006). The telomeres of the chromosomes are then lined to the nucleoskeletal lamins at matrix attachment regions (MARs) and mechanical changes at the adhesions sites can potentially have a direct impact on chromatin organisation (first identified in 1987 by Cockerill and Garrad (Cockerill & Garrard 1986). McNamara *et al.* utilised topography as a mechanical stimulus to demonstrate this and

found that providing tensile cues altered chromosome position and changes in gene expression (McNamara et al. 2012).

Indirect mechanotransduction is undertaken by secondary signalling molecules in a biochemical cascade induced by the occupation of integrins for example, proteins such as expression FAK and mitogen-activated kinase (MAPK) (as shown in Figure 1.4) (BurrIDGE & Chrzanowska-Wodnicka 1996). The signalling cascade results in altered gene expression (Berrier & Yamada 2007).

Tension relayed by integrins, is indicative of MSC differentiation to the osteogenic lineage. In terms of MSC differentiation to the osteogenic phenotype, it is generally observed that adhesions are large and potentially stabilised by RACK1 (receptor of activated protein kinase C 1) causing high intracellular tension (Buensuceso et al. 2001; Balaban et al. 2001; Curtis et al. 2001). Tension, through activation of RhoA and ROCKII (Rho-associated protein kinase) stimulates osteogenesis. Treatment with inhibitors that disrupt actin (e.g. blebbistatin or cytochalasin) reduces RUNX2 (runt-related transcription factor) activity (Arnsdorf et al. 2009). This introduces the idea that cell tensegrity/strain has a role in differentiation. Ward *et al.* have shown 3-5 % tensile strain on collagen I stimulates osteogenesis (Ward et al. 2007). The mechanical strain caused an increase in mineralisation and downregulated adipogenesis and chondrogenesis (Ward et al. 2007). Understanding stem cell behaviour and the mechanisms that drive differentiation is critical for future use in therapeutics. The generation of bone cells from stem cells could be applied in future skeletal therapeutics, for which there is currently an unmet need.

## 1.5 Bone Tissue Engineering

Bone is the only tissue that after repair there is no scar and the bone regenerates itself to its original capacity (McKibbin 1978). This system is only effective below a certain threshold known as the critical bone defect where beyond this size (2 mm), the bone will be unable to bridge the gap between the ends of the fragmented bone (Brydone et al. 2010). For fractures <2 mm, osteoblasts from the periosteum produce woven bone which forms a callus surrounding the dead tissue that is the fractured bone (Brydone et al. 2010; McKibbin 1978). Lamellar bone is produced via bone substitution and endochondral ossification (Brydone et al. 2010). Osteoclasts move across the fracture site followed by osteoblasts which produce more bone (Brydone et al. 2010; McKibbin 1978). For defects larger than this size caused by trauma, tumours, infections and prosthesis, there must be a

method of bridging the gap and promote of healing of bone by osseointegration to restore functionality of the skeleton (Olivier et al. 2004). Therefore, the differentiation of bone from stem cells could provide a method to bridge the gap if coupled with an appropriate material.

This is particularly relevant to the current demographic of an ageing population where we expect an increase in the rate of age related skeletal issues in the next 20 years. A 2016 study for the office for national statistics (ONS) states that 17.8 % of the UK population is aged 65 and over, an increase of 21 % from 2005, and 2.3 % of the population is aged 85 and over, an increase of 31 % since 2005 <sup>3</sup>. The number of centenarians has also risen by 65 % in the same period (Figure 1.5). There has been a steady increase in ageing population (90 years and above) from 201,195 people in 1986 to 571,245 people in 2016 (although this is representative of a small proportion of the population, Figure 1.5) <sup>4</sup>. The increase is accounted for by the decreasing mortality rates due to improvement in standard of living, nutrition and reduction in smoking. The lag in 2008 is a result of the low birth rate prior to World War I, which recovered in the 1920s. This is not just a UK trend, a recent study looked at 35 industrialised countries and analysed the projected life expectancy in the year 2030 (Kontis et al. 2017). It was calculated that in 2030 life expectancy will increase for all 35 countries. For example, they predict average life expectancy of women in South Korea would reach 90 years which was previously thought to be unobtainable (Kontis et al. 2017). The data was taken from statistics databases namely age-specific mortality rate, therefore this highlights that there is a world-wide aging population (Kontis et al. 2017). This impacts all aspects of social care globally and there will need to be a change in policy to account for geriatric care and the consequences of the ageing population (Oreffo et al. 2005).

---

<sup>3</sup><https://www.ons.gov.uk/peoplepopulationandcommunity/populationandmigration/populationestimates/bulletins/annualmidyearpopulationestimates/mid2015>

<sup>4</sup>

<https://www.ons.gov.uk/peoplepopulationandcommunity/birthsdeathsandmarriages/ageing/bulletins/estimatesoftheveryoldincludingcentenarians/2002to2016#the-oldest-old-are-getting-older>

## People Aged 90 and Over

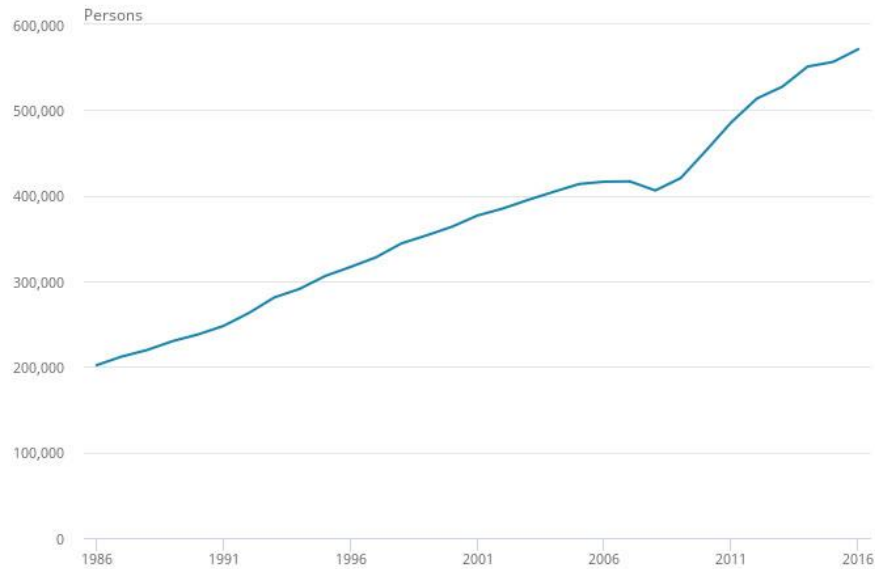


**Figure 1.5 - Population Data for Persons Aged 90 Years and Over.** Graph replicated from the ONS and shows the number of people aged 90 and over. There has been an increasing trend since 1986 and the 2016 value stands at 571,245 people. The value decreased slightly in 2008 and was attributed to the decreased birth rate prior to World War I. Overall the trend is increasing and demonstrates an increasing ageing population.

One such consequence of an ageing population is the incidence of skeletal diseases such as osteoporosis (incidence increases with age). 230,000 osteoporotic fractures occur per year and most joint replacement surgeries occur in patients over 65 years<sup>5</sup>. A group from The Netherlands state the cost of treatment for osteoporotic fractures to their country was € 200 million (2010). This accounts for 32 % of all fractures in The Netherlands where 55 % of fractures were of the hip (Lötters et al. 2016). They estimated that the costs for osteoporosis related fractures would increase by 50 % from 2010 to 2030 due to increasing incidence (40 % from 2010-2030) (Lötters et al. 2016).

Currently, bone grafts, ceramics or metal implants are utilised to repair critical defect fractures (Brydone et al. 2010). However, with allogeneic bone donations there is a risk of immune rejection (Brydone et al. 2010). Therefore, autologous bone replacements would be most effective but as each bone is specialised, rearrangement would need to ensure that the skeleton was not further compromised, which is impossible in the case of multiple fractures (Brydone et al. 2010). In addition, revision surgery is painful, costly, the sites that bone can be taken from are limited and there is a risk of comorbidity.

---

<sup>5</sup> [www.ageuk.org.uk](http://www.ageuk.org.uk)

Materials approaches have therefore been applied including the use of ceramics. Calcium phosphate ceramics including hydroxyapatite (HAP), tricalcium phosphate (TCP), amorphous calcium phosphates (ACPs) and biphasic calcium phosphates (BCPs) have been widely used (Samavedi et al. 2013). There is variation of cell response (osteointductivity and osteoconductivity) for each ceramic due to differences in surface roughness, solubility, porosity and chemistry (Samavedi et al. 2013). Moreover, ceramics can degrade over time, leading to loosening of the joint (Sumner 2015; Samavedi et al. 2013). Furthermore, ions released from the ceramics can change local pH that affects cell viability (Sumner 2015; Samavedi et al. 2013).

Metal implants are usually synthesised from titanium (McNamara et al. 2011). For joint replacement surgeries particularly that of the hip, titanium implants are mechanically sound however, there are concerns with wear, corrosion and leaching of metal leading to osteolysis and resorption of remaining bone over time (Sansone et al. 2013). Another concern of utilising metal implants is the stress shielding effect. Stress shielding refers to reduction in bone density due to removal of typical stress from the bone to the implant because of the implants high elastic modulus (Yamako et al. 2017; Sumner 2015). The loss of bone can have consequences for the long-term performance of the joint through loosening and instability, which can lead to fracture and subsequent revision surgery (Yamako et al. 2017; Sumner 2015). Brydone *et al.* state that the revision rate stands at  $11.94 \pm 2.53$  % for selected developed countries which means patients are undergoing multiple surgeries (Brydone et al. 2010). This invasive surgery effects quality of life especially for older patients (Oreffo et al. 2005) and increases the risk of hospital acquired infections such as methicillin resistant *staphylococcus aureus* (MRSA) (Struelens 1998).

The biocompatibility of current therapeutics is no longer sufficient to repair bone grafts, there is a need for bioactive materials i.e. one that encourages a response *in vivo* and can stimulate regeneration in tissues (Hench & Polak 2002). One suggestion to overcome such limitations is the use of polymer scaffolds that can be used to bridge critical bone defects, that are resorbable and porous to encourage osseointegration (Hench & Polak 2002). Bioresorbable polymers such as polycaprolactone are ideal because of their resorbable properties, porosity that can be controlled during fabrication and the batch to batch reproducibility (Koh & Atala 2004). The polymers can be used in combination to allow for differing resorption rates and partial infiltration of the scaffold by osteoblasts. Porosity is vital for the invasion (and attachment) of cells and vasculature to sustain the implant and removal of waste products (Hing 2005).

Whichever material is chosen, it will need to be seeded with a vast amount of high quality osteoprogenitor cells, a potential source of these cells would be MSCs. Traditional tissue culture plastic although biocompatible, is sub optimal for stem cell culture due to the lack of directionality and the risk of spontaneous differentiation (Hench & Polak 2002). *In vivo*, the niche is maintained by an ever-changing relay of regulatory signals (Watt & Hogan 2000). On glass, there is no maintenance of phenotype and therefore spontaneous differentiation can occur. This is where materials engineering could help by mimicking aspects of the niche and what this thesis aims to explore.

## 1.6 Materials for MSC TE

For TE to be successful, we need to have better control of cell behaviour *in vitro* to prevent off target effects. One such method for controlling cell behaviour is the use of materials, where control is gained through the cell-material interface. Manipulation of stem cell behaviour through materials allows us to direct cell behaviour *in vitro*. To be therapeutically useful, a pure population of stem cells must be available in large quantities, that can be differentiated into the target cell (Koh & Atala 2004). Material engineering gives us the opportunity to communicate to the cells the behaviour that we require, such as differentiation to bone cells. This field is becoming increasingly collaborative and therefore increasingly novel technologies evolve. The first consideration for any materials strategy is to be biocompatible and meet safety requirements, many available materials are FDA (Food and Drug Administration) approved (Koh & Atala 2004).

The use of materials has evolved over time. Biomaterials approaches in the 1970s aimed to mimic the mechanical properties of the tissue they were to replace and with minimal immune response (Hench & Polak 2002). The second generation of materials aimed to be “bioactive” and included materials such as HAP that contained functional groups that elicited a cellular response (Hench & Polak 2002). Another material advance was the creation of resorbable materials such as polylactic acid (PLA), which could be replaced over time by osseointegration. These advances did not have lasting effects and a third generation of materials was implemented that aimed to manipulate the cells molecular and gene regulation in a known and reproducible manner (Hench & Polak 2002). This was the beginning of the field of TE and with advancing technology and increasing collaboration, novel methods of synthesis and therefore “smart” materials were gained. The soft lithography methods of George Whitesides' paved the way for many materials engineers. Soft lithography was an advantage to bioengineering owing to precise, scalable and cost

effective methods of cell culture (Qin et al. 2010; Kane et al. 1999). Other materials strategies include roughness, demixing, hydrogels, photolithography, microcontact printing and electrospinning to yield substrates with a variety of properties (Anselme & Biggerelle 2005; Dalby et al. 2004; M P. Lutolf et al. 2003; Wilkinson et al. 2002; Rogers et al. 1997; Zhang et al. 2005). They can be characterised depending on the material property; chemistry, topography or stiffness, in a system that can be visualised as a triangle of cell control (Anderson et al. 2016) (Figure 1.6). The main commonality between these materials is the manipulation of cell adhesions which is not only necessary for cell survival (due to anchorage dependency) but also is responsible (in the case of stem cells) for driving changes in self-renewal or differentiation (Anderson et al. 2016). There is now a new generation of materials in the field. Stimuli responsive materials aim to be dynamic in nature to allow for the presentation of ligands to control cell behaviour in a similar way to the presentation of matricryptic sites *in vivo* (Davis et al. 2000). The following section will explore materials engineering in terms of MSC cell culture and in particular, materials utilising the adhesive tripeptide Arg-Gly-Asp (RGD) for cell attachment.

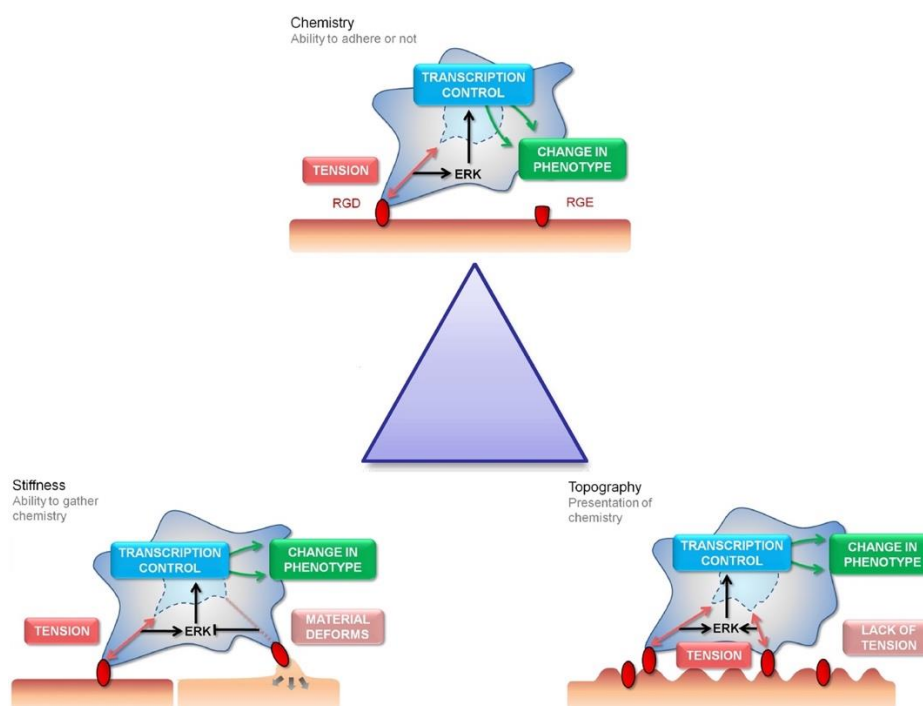


**Figure 1.6 - The “Triangle” of Materials Engineering.** The “triangle” encompasses variations in chemistry, stiffness and topography (2D), all of which manipulate MSC adhesion. The figure highlights the way in which the materials interface influences intracellular cell signalling through tension via integrins and focal adhesions (red). Reproduced from (Anderson et al. 2016).

### 1.6.1 Topography

Cellular response to substrate shape was firstly defined in 1911 by Harrison (Harrison 1911) and in 1952 Weiss and Garber coined the term “contact guidance” to describe cell

alignment to topography (Weiss & Garber 1952). However, it was not until the late 1980s that technology allowed more in-depth study of cell response to microscale. This theory was first proposed by Curtis and Wilkinson and has since been the rationale for subsequent topographical studies (Clark et al. 1987; Clark et al. 1990). The cellular response to the microscale was first tested by using baby hamster kidney (BHK) cells and a series of microchannels made from silica using photolithography (Clark et al. 1987). It was then shown that cell morphology differs due to its' contact guidance in response to changes in substrate properties; in this case, microchannel depth (Clark et al. 1987; Clark et al. 1990). Since this observation, many more publications have utilized microscale topography on a variety of cell types, all obtaining contact guidance (Britland et al. 1996; Chen et al. 1997; Engler et al. 2009; Lim et al. 2004; Teixeira et al. 2006). Microchannels are thought to be particularly appealing to nerve tissue engineering, as these materials encourage elongation of cells and indeed, were utilised by Yim *et al.* for induction of MSC differentiation in a neural lineage (Yim et al. 2007).

After the cell response to the microscale was established, nanoscale interactions were investigated. Much like the microscale, novel technologies had to be developed. Electron beam lithography (EBL) is one such technique that can produce areas of precise topographies in pre-defined geometries (Gadegaard et al. 2003). The production of these can be up scaled by injection moulding, where a negative copy is created in a nickel shim (via electroplating), this method creates a high-throughput manufacturing system, ideal for replicates for cell culture (Gadegaard et al. 2003). This technique was applied to MSC culture materials and it was found that a square geometry enabled MSCs to self-renew for up to 4 weeks, a period previously unachievable in culture (Dalby et al. 2007). Slight disorder from this configuration ( $\pm 20$  and  $\pm 50$  nm offset) facilitated osteogenic differentiation to a level comparable to traditional chemical induction (McMurray et al. 2011). EBL has undoubtedly aided precision in the nanoscale and generated materials on a scale that is therapeutically relevant ( $\text{mm}^2\text{-cm}^2$ ) however, it is time consuming (Anderson et al. 2016).

Topography has been applied on the nanoscale using other materials such as titanium, by methods such as anodising through block copolymer templating with Ps-b-P4VP to create a pillar formation rather than pits (Sjöström et al. 2009; Sjöström et al. 2013). As titanium is the current implant of choice for skeletal defects, patterning titanium with pillars could promote osseointegration (Sansone et al. 2013). McNamara and colleagues have shown that titanium pillars of 15 nm are optimal for MSC differentiation to bone (McNamara et

al. 2011). Utilising patterns such as these on implants for hip replacements, could guide MSC differentiation toward bone formation preventing loss of bone that is usually observed in response to plain titanium implants (McNamara et al. 2011).

## 1.6.2 Chemistry

Soluble chemistries, while able to induce cell behaviour have the risk of off target effects and variability. Materials engineering allows the same directive moieties to be tethered to a material and therefore creating a stable interface. The application of surface chemistry can be added using techniques like microcontact printing and dip pen nanolithography (DPN).

DPN is the process by which functional groups are applied in a specified pattern to a substrate using an atomic force microscopy (AFM) tip (nanoscale) (Ginger et al. 2004). This allows several layers of control over the chemistry, firstly there is a wide choice of functional groups that can be chosen (e.g. peptides to DNA) that can be deposited in defined patterns and tailored sizes (1-100 nm) (Salaita et al. 2007; Ginger et al. 2004). Further, the fabrication method is mild enough to be used in a biological context and has the added advantage of precision, durability and is cost effective (Curran et al. 2010). In the context of stem cell engineering, Curran *et al.* found that different functional molecules induced differential behaviours in MSCs (Curran et al. 2010). By spacing chemistries measuring 70 nm in square or hexagonal array at differing distance of pitch, they found that  $-CH_3$  groups maintained stemness whereas  $-NH_2$  groups promoted osteogenesis via increased cell adhesion (Curran et al. 2010).

Microcontact printing has provided a method to understand how cell shape regulates cell behaviour. McBeath *et al.* first correlated MSC spreading and tension as precursors to osteogenic fate (McBeath et al. 2004). Using polydimethylsiloxane (PDMS) stamps to print large square areas ( $10,000 \mu m^2$ ) they found that spreading facilitated osteogenesis by activating RhoA and the downstream effector ROCK (McBeath et al. 2004). In comparison, smaller stamps ( $1,024 \mu m$ ), where cell size was restricted, lipid secretion and the upregulation of fat markers were observed (McBeath et al. 2004). PDMS stamps can be used to pattern a wide array of geometries. In an extension to this study, Kilian *et al.* utilised PDMS stamps to create star, pentagonal and flower shape patterns to correlate cell differentiation to morphology (Kilian et al. 2010). These shapes, while comparable in area, differ in subcellular curvature creating changes in contractility of cytoskeletal

apparatus. It was found that a specific shape (star) promoted contractility (Kilian et al. 2010). This in turn resulted in differential signalling and activation of ERK1/2 (extracellular related kinase 1/2) and JNK (c-Jun N-terminal kinase) via RhoA, Rac and cdc42, resulting in terminal differentiation to osteoblasts (Kilian et al. 2010). Thus, demonstrating that geometric cues, provided by the ECM, can regulate cell fate.

Growth factors (GFs) are important molecules for cell physiology and homeostasis (Schultz & Wysocki 2009). As such, researchers have utilised GFs as a stimulus to direct cell behaviour, albeit with limited success. In some cases (clinical trials), the concentrations used for the effect have produced off target effects with dangerous consequences (Salmerón-Sánchez & Dalby 2016). Llopis-Hernández *et al.* have used materials based methods to counteract these side effects (Llopis-Hernández et al. 2016). Fibronectin contains specific regions for GF binding fragments (FNIII<sub>12-14</sub>), coating poly(ethyl acrylate) (PEA) with fibronectin exposes these domains and allows the tethering of GF, in this example bone morphogenetic protein 2 (BMP-2) (Llopis-Hernández et al. 2016). Osteogenic differentiation of MSCs was achieved via enhanced Smad (small mothers against decapentaplegic) signalling and co-localisation of the integrin  $\beta$ 1 subunit and the BMP receptor BMPRIa (Llopis-Hernández et al. 2016). The benefit of this system is that the GF are used in small doses (25 ng mL<sup>-1</sup>) in a localised area without off-target effects and has potential as a method for GF engineering in future (Llopis-Hernández et al. 2016).

### 1.6.3 Stiffness

Cell response to stiffness was popularised by Engler *et al.* in a seminal study in 2006 (Engler et al. 2006). Using hydrogels, they showed that the stiffness of a material can regulate MSC differentiation (Engler et al. 2006). By mimicking the stiffness of a certain tissue, MSCs will differentiate into the tissue native to that cell type i.e. by creating a hydrogel with elastic modulus that is like pre-mineralised bone, MSCs will differentiate down an osteogenic lineage (Engler et al. 2006). This study has caused a rippling effect seen on many levels. Not only was it a novel idea for MSC growth but it also changed what was understood about MSC lineage specification. Engler *et al.* created a hydrogel mimicking the elastic modulus of the brain and claimed that MSCs differentiate in a neural lineage (Engler et al. 2006). This was the first example of a neural link in potential MSC phenotypes.

Khetan's 2013 study uses hydrogels to confirm spreading and morphology is linked to cell fate decisions via traction in a 3D environment (Khetan et al. 2013). They employed phototunable hydrogels that were degradable when exposed to light. After irradiation, the cells were then able to remodel the matrix and when seeded with MSCs, encouraged cell spreading and osteogenesis. Cells that were restricted by undegradable matrix differentiate to adipogenic lineage (Khetan et al. 2013).

The stiffness engineering sector is controversial due to a debate on the mechanism of cellular response to material stiffness. Trappmann *et al.* argue that it is the hydrogels pore size that is the defining factor in the cellular response to gels (Trappmann et al. 2012). They created two different polymer hydrogels (PDMS and polyacrylamide, PAAm) on the same range of stiffness' as identified by Engler (Trappmann et al. 2012). The expected result was only produced when culturing on PAAm i.e. soft surfaces elicited adipogenesis whereas hard surfaces resulted in osteogenesis correlating to the results in Engler's work from 2006 (Figure 1.7 A) (Trappmann et al. 2012; Engler et al. 2006). Comparatively there was no trend with PDMS substrates (Figure 1.7 A) (Trappmann et al. 2012). They argued that although the bulk stiffness properties were similar, the pore size was different, therefore providing differing anchoring points to the ECM. The pore could be thought of as topography, and it was this feature that the cells are responding to, rather than the bulk stiffness (Trappmann et al. 2012). This theory was challenged by Wen *et al.* who created hydrogels of differing pore size but comparable bulk stiffness (Wen et al. 2014). On soft gels, adipogenesis was observed regardless of pore size, likewise for stiff gels that showed osteogenesis independent of pore size (Wen et al. 2014) (Figure 1.7 B). Based on current data showing that bulk stiffness effects phenotype in 2D surfaces and the additional 3D work by Engler *et al.*, it is more likely that the conclusions drawn by Wen *et al.* are closer to the truth. However, further work is required to robustly support the conclusions drawn by Wen *et al.* For instance, if they had repeated their experiments in hydrogels of different materials in addition to the polyacrylamide gels they could have effectively rule out porosity.

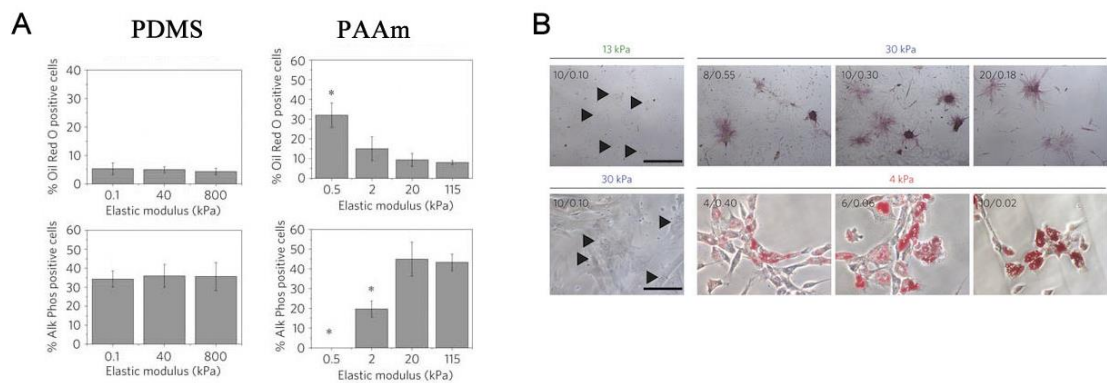


**Figure 1.7 – The Debate on Porosity of Hydrogel Stiffness and Effects on MSC Differentiation.** A) Trappman *et al.* created hydrogels of stiffness defined by Engler *et al.* 2006 in two different polymers, PDMS and PAAm. The PAAm polymer followed the same trend as described by Engler – osteogenesis on stiff and adipogenesis on soft surfaces. The PDMS did not follow any trend and it was thought that pore size of the hydrogels effected tensegrity. B) Wen *et al.* created soft and stiff hydrogels and various pore sizes for each. They found that each stiffness acted as expected and that pore size was independent to phenotype. Adapted from (Anderson et al. 2016)

## 1.7 Stimuli Responsive Materials

These previous examples, while having been invaluable to understanding MSC behaviour, provide one biological cue. Now there are materials to regulate stem cell behaviour on multiple levels using stimuli. Stimuli responsive materials dynamically alter a material property in a bid to mimic the niche by regulating cell behaviour *in situ*. Stimuli can come in many forms, the most notable are light, temperature and enzyme directive technologies.

### 1.7.1 Light

Due to the ease of control and reproducibility, light continues to be a well-used stimulus. In a two-dimensional system, a photoactive moiety is easily manipulated to change the material property. In an early example, Wirkner *et al.* have used light to degrade photoliable benzylic hydrogen caging groups that block RGD (Wirkner, Alonso, et al. 2011). Once stimulated by light, the RGD is exposed and HUVECs (human umbilical vein endothelial cells) adhere to the material (Wirkner, Alonso, et al. 2011). In a follow up study, they utilised the technology to pattern specific regions of a substrate and controlling HUVEC attachment (Wirkner, Weis, et al. 2011). This system would be beneficial for co-culture purposes to mimic tissues of specific architecture. However, using this method, once photo-activated, the effect is one way. Liu *et al.* developed a reversible system utilising azobenzene to switch from permissive to restrictive adhesion on demand,

depending on the conformation of azobenzene (trans-cis or cis-trans at 340-380 or 450-490nm respectively) (Liu et al. 2009).

Similar technology can also be applied in three dimensions. Mosiewicz *et al.* have used light to uncage an enzyme responsive sequence within a hydrogel to create an on demand stimuli responsive system for cell invasion (Mosiewicz et al. 2013). In this manner MSC adhesion can be spatiotemporally controlled in three dimensions. This could later be applied to developmental biology where spatiotemporal signalling could be tested e.g. morphogen effects on pluripotent stem cells (Mosiewicz et al. 2013). Lee *et al.* took this idea a stage further and utilised caged RGD on poly (ethylene glycol) diacrylate (PEGDA) hydrogels in an *in vivo* system (Lee et al. 2015). This was implanted in a mouse model and exposed to UV light at 350 – 365 nm (Figure 1.8A) (Lee et al. 2015). Increased cell number and cell spreading was observed with transdermal activation and subsequent availability of RGD. However, cell attachment decreases by 50 % 500  $\mu\text{m}$  from light exposure (Figure 1.8B) (Lee et al. 2015). It would be difficult to scale this up or utilise *in vivo* as light does not penetrate skin.

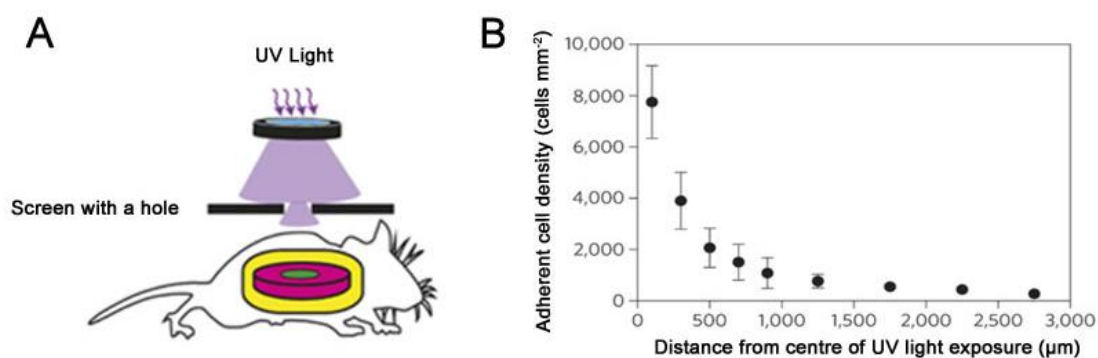


**Figure 1.8 - Limitations of Light Responsive Hydrogels *in vivo*.** A) Transdermal activation of hydrogel via photomask. B) Adherent cell density versus distance of irradiation. Adherent cells decrease dramatically with increasing distance from light source. Images adapted from (Lee et al. 2015)

Perhaps the best use of light is in conjunction with hydrogel stiffness and is used as a stimulus for either permissive or restrictive adhesion. It is thought that cells cultured at a defined stiffness prior to implantation, have a “mechanical memory” and therefore pre-treatment maintains phenotype *in vivo* (Yang et al. 2014). This was tested *in situ* by using light responsive hydrogels. Irradiation at 365 nm for 360 s changes hydrogel properties from stiff (10 kPa) to soft (2 kPa) (Yang et al. 2014). MSCs that had ten days’ pre-treatment on the stiff hydrogel, retained the osteogenic phenotype, even when the hydrogel was photoinduced to have soft properties, unlike those that had been pre-treated for less time.

Perhaps the use of light as a stimulus is more useful to *in vitro* cell culture systems where cells could be removed from culture-ware without the need for trypsinisation or for coating materials used in healthcare to prevent bacterial colonisation before use, rather than a use for *in vivo* TE due to the limitations shown in Figure 1.8B.

## 1.7.2 Temperature

There have been many examples in the literature utilising temperature responsive materials. Each have utilised various polymers and differing degrees of complexity to aid cell adherence. Lutz *et al.* created copolymers of polyethylene glycol (PEG) and methacrylate that form temperature sensitive layers (Lutz 2008). When heated (37 °C) the polymer acts as a medium for cellular adhesion (Lutz 2008). In contrast, cooling the surfaces to room temperature (25 °C) cells were repelled (Lutz 2008). This process changes conformation of the polymer but does not damage the surface and therefore generates a reversible platform for cell manipulation (Lutz 2008). The optimal application for such a material would be a clinical setting where it could be used to coat an implant which would not support the growth of any bacteria or other cell types at room temperature prior to implantation, prohibiting infection post-surgery. This technique is not sufficient for future enabling technology as it does not direct cell behaviour. An improvement on this method is presented by Yamato *et al.* who have patterned the temperature sensitive polymer poly (N-isopropylacrylamide) (PIPAAm) onto a material using electron beam irradiation (Yamato, Kwon, et al. 2001). This was employed to create a co-culture of hepatocytes and endothelial cells (Yamato, Kwon, et al. 2001). Firstly, a monolayer of hepatocytes was established then the temperature was reduced preventing adhesion of hepatocytes on the areas patterned with PIPAAm. The dish is then seeded with epithelial cells (Yamato, Kwon, et al. 2001). Co-culturing was effective as it maintained albumin secretion of the hepatocytes (the standard functional assay for hepatocyte growth in culture) (Yamato, Kwon, et al. 2001). Furthermore, by mimicking dynamic nature of cell interactions provides a better quality cell population over traditional culture particularly in the case of hepatocyte cell culture where it is difficult to maintain hepatocyte functionality *in vitro* (Schuetz et al. 1988). Temperature has also been utilised in combination with topography to create vertical micropillars that were temperature-sensitive with regard to their permissiveness for adhesion. Notably, changes in temperature gave rise to alterations in micropillars angles, which subsequently resulted in a non-adhesive conformation (Reddy et al. 2007). Using shape memory thermoplastic elastomers that altered

topography by adjusting transition temperature, adhesion could be controlled on demand (Reddy et al. 2007). Although this application is intended as a sticky material, it would also be desirable to have a similar system for cell-surface interactions for the dynamic attachment and release of cells from a material.

These techniques, while more dynamic than the 2D surfaces, do not fully encapsulate biomimicry. Changes in light and temperature are rare *in vivo*, rather cells use enzymes to alter their environment. Although temperature responsive materials *in vitro* are practical, they are unsuitable for *in vivo* use due to their limitations as a biological stimulus (de las Heras Alarcón et al. 2005).

### 1.7.3 Enzyme Responsive

Enzymes can be employed in a materials context in several ways. They can be utilised as the stimuli for self-assembly (surface build up) or as a means of modifying the pre-existing surface. This section will focus solely on the use of enzymes as a modifier. As a stimulus, enzymes are beneficial because they are natural, specific and as they are a diverse group of proteins, there are many to select from depending on the desired application (Bugg 2001). Therefore, for *in vivo* use, they could be a more appropriate as a stimulus, as they are more natural to a biological system. It is accepted that enzymes are exquisitely selective and can discern not only between proteins but also between enantiomers of the same protein with proteolysis occurring at a specific site on a peptide chain (Bugg 2001). Before synthesis of the material can occur, there are certain design aspects to consider. Firstly, a suitable enzyme must be identified for the application then selectivity and specificity of the peptide recognition sequence must be evaluated (this process can encompass both literary studies and bioinformatics). Putting these elements together yields a material that is specifically cleaved to create a conformational change (Wang et al. 2010). It is thought that this could be amenable to several different applications such as cell culture, therapeutics and diagnostics.

The identified hallmarks of a cancer cell are increased neovascularisation and metastasis (Hanahan & Weinberg 2000). The matrix metalloproteases (MMPs) are upregulated by cancer cells to promote this effect, for example glioblastoma cells show an increase in MMP-2 and MMP-9 expression. Tauro and Gemeinhart in 2005 utilised a hydrogel loaded with the cancer inhibitor cisplatin, that was selectively released due to the presence of the target enzyme at the tumour site (Tauro & Gemeinhart 2005). Therefore, in terms of therapeutics, enzyme responsive peptides within hydrogels offer another advantage in that

they can be loaded with drugs. In comparison, Lutolf *et al.* utilised MMP targetable hydrogels as a scaffold for cell invasion, to bridge a critical bone defect. Here they loaded an MMP cleavable hydrogel with BMP-2 and implanted it into a critical bone defect in mouse models and showed that this system encourages osseointegration (M P. Lutolf et al. 2003). It is also possible to miniaturise hydrogels to create hydrogel beads. Thornton *et al.* utilised this to incorporate an enzyme responsive sequence that releases a charged moiety that induces a reduction in bead swelling and pore size (Thornton et al. 2005). Prior to this cut off, the bead can absorb macromolecules from fluids and therefore could be used to remove harmful macromolecules from tissue fluids (Thornton et al. 2005). These examples offer an *in vivo* method for therapeutic benefit, but it is also possible to utilise them as *in vitro* reporters. In one application, amino acids were tethered to glass beads that were capped with a fluorescent reporter. After incubation with different enzymes, the selectivity of that enzyme could be determined by identifying the presence or absence of the fluorescent marker. This creates a high-throughput method for enzyme selectivity and could be applied to both healthcare and bioengineering (Doezé et al. 2004)

There are some factors to be taken into consideration when designing an enzyme responsive technology particularly when designing a two-dimensional surface. Enzymes are active in hydrated environments such as biological systems but kinetically different in enzyme responsive materials (ERMs) (Ulijn 2006).

## 1.8 Project Objectives

It is our aim for this project to overcome limitations to traditional stem cell tissue culture by utilising an enzyme modifiable surface for MSC differentiation. We aim to utilise the MMPs secreted by MSCs to modify a material that will result in control of MSC behaviour. This varies from other technologies available as it is under cellular control and there is potential for two behavioural cues to be delivered to the stem cells (stem cell self-renewal and differentiation).

As discussed above, effective materials engineering aims to mimic the cellular regulation that the ECM provides, this is particularly true for stimuli responsive materials where multiple roles are envisaged. The surface that we propose to explore incorporates an ERM element but adds a level of complexity in that the stimuli comes from the enzymes that the cells themselves secrete (MMPs). Figure 1.9 shows the schematic of the proposed surface. By creating a surface chemistry (of peptide chains tethered to a glass coverslip)

that is amenable to these MMPs, we hope to control cell adhesion and ultimately cell fate. The RGD sequence is hidden beneath an enzyme recognition sequence and both are capped with a blocking group, PEG. In response to MMPs, the recognition site is cleaved revealing the cell adhesive peptide RGD allowing cell binding via integrins. This in turn will stimulate intracellular tension that is capable of initiating cell differentiation along the osteogenic lineage (RGD shown previously to be permissible to osteogenic differentiation, Section 1.6). The blocking group was designed to be permissive to MSC self-renewal. In this manner, we hope to develop a system for mesenchymal cell culture that offers a non-invasive method for both stem cell self-renewal and differentiation that is under cellular control.

The surface is created by grafting peptides in a defined sequence onto a glass coverslip using solid phase peptide synthesis (SPPS). SPPS is a versatile technique that allows addition of amino acids to a solid substrate in a configuration determined by the user. We are therefore unrestricted in the length and composition of the desired sequence and we can tailor the chemistry to mimic the peptide sequence that is cleaved by MMPs. MMPs are naturally secreted by cells primarily to remodel their ECM. It has also been suggested that they have other functions within the body including development and wound healing (McQuibban et al. 2001). By providing a chemistry that is cleavable, we expect the ERM to be remodelled *in situ* by the cell population (this rationale has been previously employed in hydrogels (M P. Lutolf et al. 2003; Wade et al. 2015; Shekaran et al. 2014; Tauro & Gemeinhart 2005).

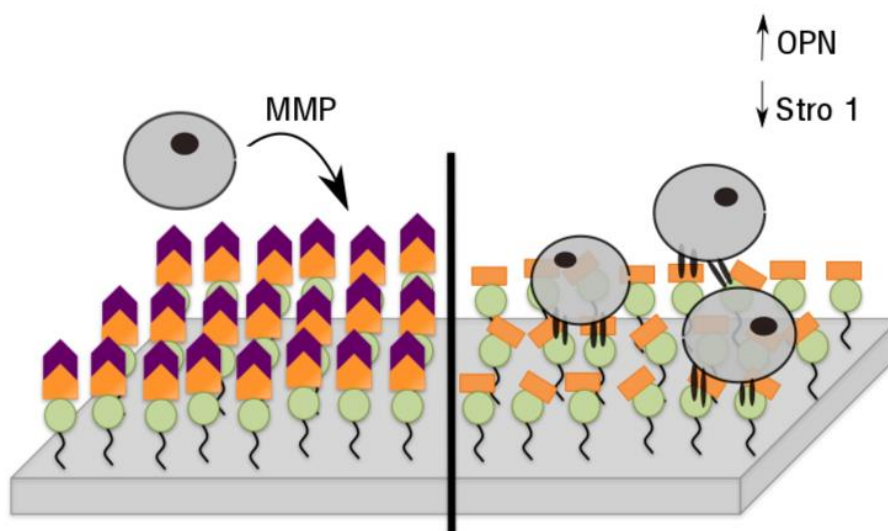


**Figure 1.9 – Schematic of Surface Remodelled by Cell Secreted MMPs.** MSC *in situ* secrete MMPs that will cleave the PEG blocking group (purple) and the recognition site (orange) to reveal RGD (green).

Binding to RGD is hypothesised to result in osteogenic lineage specialisation via increasing intracellular tension.

There is a need for new materials for MSC growth as traditional culture ware cannot provide directional cues and other materials strategies contain static or inappropriate stimuli for mammalian cell culture (Hench & Polak 2002). Our system differs from other ERMs as it is designed to be controlled by a cell population, not in response to an enzyme added by the user. Moreover, the surface is designed to provide two behavioural cues; stem cell self-renewal (in response to intermediate tension as the blocking group prevents direct binding to RGD) and differentiation (revealing of RGD). In this manner, the system is reminiscent of the bone marrow niche as there is regulation of both growth, as stem cells repopulate and targeted differentiation. In addition, the presentation of motifs (created by SPPS peptides) is like that of the dynamic presentation of cryptic sites from ECM proteins. This is unlike other technologies that are static in nature (such as topography) and is more complex than other ERMs which have only demonstrated one cell phenotype.

### 1.8.1 Solid Phase Peptide Synthesis (SPPS)

SPPS was developed in the 1960's as a method to synthesize long polypeptide chains *in vitro* that were unobtainable by other methods (Merrifield 1963). Once completed, the chains were removed from the support allowing further experimentation. Merrifield's technique was revolutionary, improving the field of peptide chemistry for which he was awarded the Nobel Prize in Chemistry in 1984.

Figure 1.10 shows the SPPS methodology. The technique works by grafting amino acids from an insoluble solid support via a linker, typically one that has a free amine group that the C-terminal of the first amino acid can bind to by a condensation reaction creating a covalent bond (Merrifield 1963; Mitchell et al. 1978). The amino acids used in the technique are protected on the N-terminal by a protecting group to prevent multiple amino acids binding to the chain and binding to each other. Side chains are also protected to prevent amino acid addition from the side group (Palomo 2014). Coupling of amino acids is performed in the presence of a catalyst (Fields & Noble 1990). Prior to chain elongation, the blocking group is removed to allow addition of the carboxyl group of the next amino acid to the free amino group of the amino acid added previously. The coupling and deprotection stages are repeated in the required pre-determined sequence until the required chain length is achieved. The sequence can then be maintained on the resin to

create a 2D surface chemistry or cleaved from the substrate to be used in other applications (Merrifield 1963).

The resin (material from which amino acids are grafted from) must have a free amino to allow coupling of the first amino acid (Merrifield 1963). If the resin does not have a free amine, a linker must be provided. One requirement for the resin is that it must withstand the continual flow of solvents at low pressure (during washing steps for *in situ* SPPS) and must be insoluble in the solvents which are utilised in the washing steps (Fields & Noble 1990). Peptides that are maintained on the resin should have linkers that are also insoluble in the solvent that is used to remove side chain protecting groups (Fields & Noble 1990).

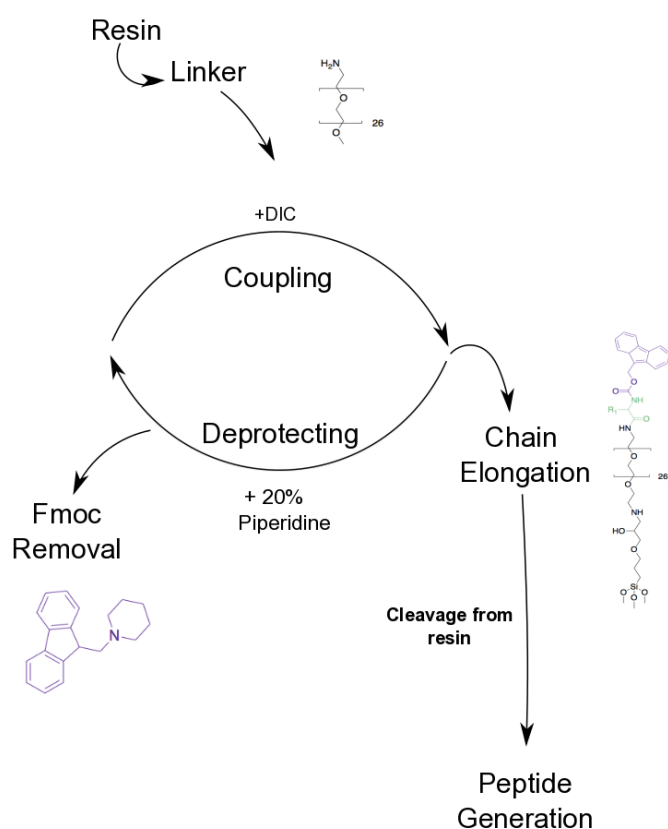


**Figure 1.10 – Schematic of SPPS Method.** Amino acids are coupled to an insoluble resin via a linker to provide a free amide group (in this case, PEG diamine). Amino acids are protected on the N-terminal by a group such as Fmoc (purple). Prior to the next amino acid addition, the Fmoc group must be removed (deprotected), in this example this is done by a base, piperidine. Coupling and deprotecting are repeated until sequence is completed (chain elongation). The chain is either maintained or cleaved from the resin.

The amino acids that are employed in SPPS are capped on the N-terminal by a variety of different N-terminal protecting groups such as *tert*-butoxycarbonyl (Boc) and fluoren-9-ylmethoxycarbonyl (Fmoc). The choice of protecting group will depend on the

application however, the use of Fmoc is favourable as it can be cleaved under mild conditions (Carpino & Han 1972). Fmoc chemistry was introduced in the 1970's and while Fmoc chemistry is advantageous to SPPS, the utilisation of both allows efficiency for chemical synthesis of a range of different compounds (Fields & Noble 1990). This study was carried out exclusively using Fmoc protected amino acids and therefore this section will focus specifically on Fmoc SPPS. As stated, the carboxyl terminus of the free amino acid is added to the amino linker of the resin via condensation reaction (removal of water). Efficiency is paramount to ensure homogenous peptide products. For efficiency, the reaction occurs in the presence of a catalyst, typically, a carbodiimide (Palomo 2014). Dicyclohexylcarbodiimide (DCC) was initially used however this was changed to diisopropylcarbodiimide (DIC) as it forms soluble urea by products that can be easily removed in washing solvents (Palomo 2014). Coupling and deprotection are repeated until the full and final sequence is obtained.

The removal of the protecting group is necessary to allow addition of the next amino acid. Fmoc is base labile and removal of the Fmoc group is therefore completed by the addition of a basic solvent for example piperidine. Side group protection is also necessary for those amino acids that contain amine groups which prevents the addition of amino acids to side groups and allows chain elongation from the N-terminal in an expected manner. Further, as Fmoc deprotection is base labile, acid labile side chain protecting groups are favourable to withstand deprotection stages. Asp side chains are typically protected by t-butyl (tBu) which meets requirements for Fmoc chemistry (Behrendt et al. 2016) Arg side chains are of particular consideration due to the trifunctional guanidine side chain which can be easily acylated (facilitate binding by NH<sub>2</sub>) (Behrendt et al. 2016). One or two of these chains have to be protected for Fmoc SPPS with for example, Pbf (Pentamethyl-2,3-dihydrobenzofuran-5-sulfonyl) (Palomo 2014). Side chain protecting groups are removed once the sequence is complete, if the chain is to be removed from the resin, the side groups and linker should be soluble in the same solvent. There are many advantages to this technique for example, each addition and deprotection stage takes place in the same vessel. This is described as continuous SPPS where coupling, filtration and washing of by-products can be performed easily (Merrifield 1963). The reagents can be used in excess to force the reaction to completion and give high yields (Erickson & Merrifield 1976). In addition, peptides can be synthesised with high purity making it attractive to use (Cherkupally et al. 2014).

## 1.8.2 SPPS for Cell-Surface Interactions

The challenge for the application of this system in a biological context is the biocompatibility aspect for both cell survival and biological analysis. Resin choice is important in this case as for microscopic techniques, transparent materials must be applied. The choice of glass as a resin is possible as it can be coated in silane which allows addition of a free amine group for amino acid addition (Piehler et al. 2000; Mosse et al. 2009). The surface was synthesised as described in Todd *et al.*; prior to amino acid addition, the coverslip is cleaned to remove organic material then silanised using (3-Glycidyloxypropyl) trimethoxysilane (GOPTS) creating a monolayer of epoxide groups for a PEG diamine to covalently bind to (Todd et al. 2009; Piehler et al. 2000). The PEG diamine provides a free amine group for the addition of the first amino acid while also preventing non-specific protein adsorption due to its anti-fouling property.

The additional benefit for bioengineering is that peptides can be added in any sequence desired, this allows biomimicry of ECM peptide motifs. As peptide motifs are instrumental for cell behaviour *in vivo* (Section 1.3) (Davis et al. 2000), this provides a method of communication with cells in a directive manner. This is achievable as it is known that short motifs are sufficient for directing behaviour without requiring the whole protein sequence (Bellis 2011). SPPS was originally applied as a method to artificially create peptides *in vitro*. Upon completion of SPPS, the peptide was cleaved from the resin and used for further analysis, independent of the resin it was grafted from (Merrifield 1963). However, resins can be biofunctionalised with peptides by maintaining the sequence on the resin after completion (Mosse et al. 2009). This creates a 2D monolayer of peptide motif that allows directive behaviour of the cells cultured on the peptides as is the case in this thesis.

SPPS has been used previously for cell culture. In 2012 Zelzer *et al.* applied it to create a ERM that changed chemical composition in response to cell secreted enzymes (Zelzer, McNamara, et al. 2012). They created adhesive phosphorylated surface chemistries that were dephosphorylated in response to alkaline phosphatase (ALP) addition or secretion by cells seeded on the surface (Zelzer, McNamara, et al. 2012). Although, the results showed that the material did not increase osteogenesis, it did provide an early indication that cell-surface interactions could be dynamically manipulated by the cells themselves (Zelzer, McNamara, et al. 2012). SPPS can also be used to present divalent peptides motifs. This is based on the concept of synergistic motifs that exist in ECM proteins for example, the

RGD and PHSRN motifs of fibronectin, which have been shown to enhance cell adhesion (Gartner & Bennett 1985) . Using SPPS, spacing between the motifs as found in fibronectin, could be mimicked and in addition, a branched chain could be created to allow accessibility to motifs by cells (Mas-Moruno et al. 2014). Saos-2 (osteosarcoma) cells were shown to attach and proliferate (Mas-Moruno et al. 2014). In 2017, this concept was modified to substitute the PHSRN sequence for the lactoferrin derived antimicrobial sequence LFI-11. The aim of this platform was to create an implant (for dentistry and orthopaedics) that can be adhesive to osteoblast like cells but prevent bacterial contamination that often results in failure of implants (Hoyos-Nogués et al. 2017). The platform enhanced osteoblast spreading and increased mineralisation in comparison to other controls (Hoyos-Nogués et al. 2017). The presence of the LFI-11 peptide was also shown to inhibit bacterial adhesion for both *S. sanguinis* and *S. aureus* by 83 % and 91 % respectively (Hoyos-Nogués et al. 2017).

Roberts *et al.* also incorporated SPPS to make an ERM (Roberts et al. 2016). Here they created a sequence that contained an enzyme modifiable component that can be targeted by the enzyme elastase (Roberts et al. 2016). Cleavage of the sequence by elastase reveals the cell adhesive peptide RGD (Figure 1.11A). This was based on the chemistry presented by Todd *et al.* where the surface modification of glass by SPPS and response of cells (osteoblasts) were analysed (Todd et al. 2009). Prior to this study, the enzyme efficiency of various enzymes (elastase, chymotrypsin and thermolysin) and recognition sequences were determined (Zourob et al. 2006). Elastase was selected, the peptide sequence was modified to reflect elastase preference (A↓A) and then RGD was incorporated (Todd et al. 2009). A peptide responsive sequence was created (Fmoc-A↓ARGD) which was not treated by piperidine after terminal amino acid was added so the N-terminal protecting group (Fmoc) therefore remained to conceal the sequence (Todd et al. 2009). By masking RGD with the Fmoc group, cell adhesion could be triggered on demand. Applying this to cell culture, they showed that seeding osteoblasts on an uncleaved surface (Fmoc-A↓ARGD) prevented cell adhesion resulting in rounded cells. In comparison with the addition of elastase (-ARGD), the osteoblasts adhered to the surface and exhibited increased cell spreading comparable to that of the RGD control. 90 % of cells were spread by 5 days on cleaved surfaces compared to the capped (5 %) or the non-adhesive, RGE control (4 %) (Todd et al. 2009) (Figure 1.11B).

This work was continued by Roberts *et al.* who applied the platform to MSC culture (Roberts et al. 2016). They also demonstrated that cleavage of the blocking group promoted cell adhesion and increased cell spreading which promoted differentiation (Roberts et al. 2016). The cells became osteoblastic in morphology and positively expressed osteocalcin by day 21 at a similar abundance to the positive control, RGD (Figure 1.11 C) (Roberts et al. 2016). The maintenance of Fmoc on the RGD prevents adhesion and therefore differentiation, as minimal osteocalcin staining was observed (Roberts et al. 2016).

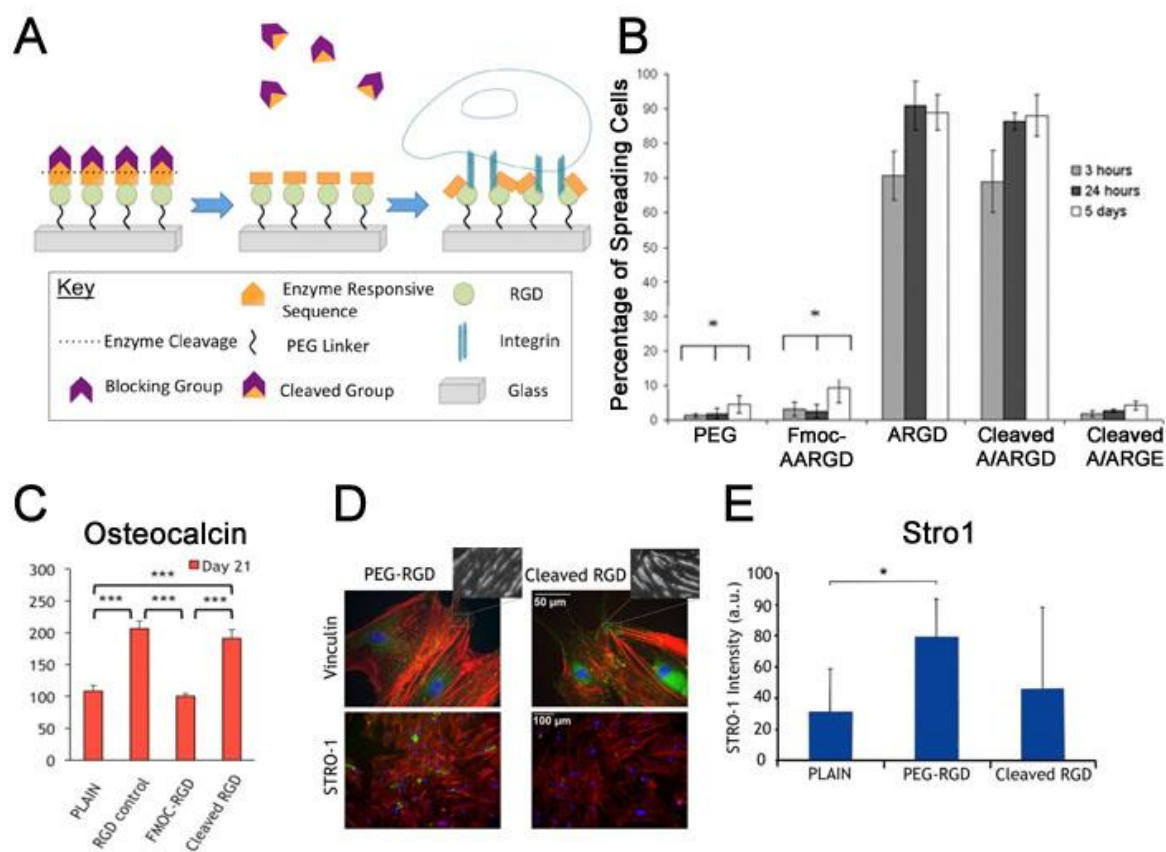


**Figure 1.11 - Cell Response to Fmoc/PEG-A↓ARGD Surface.** A) A platform for cell culture was synthesised by SPPS as in (Todd et al. 2009). Maintaining a blocking group on peptides prevents cell adhesion to the RGD group prior to enzyme addition. After the enzyme is added, the sequence is cleaved, allowing adhesion to RGD via integrin binding and stimulating MSC differentiation. Replicated from Anderson *et al.* 2017 (Anderson et al. 2017). B) After cleavage, cell spreading is increased similar to the positive control (uncapped ARGD), approximately 100 % for both. Replicated from (Todd et al. 2009). C) The experiment was repeated by Roberts *et al.* 2016 using MSCs and increasing the culture period to 21 days. After 21 days, osteocalcin expression increased on the cleaved surface and was significantly different to that of the untreated (Fmoc-D) and glass control. Replicated from Roberts *et al.* 2016. D) Roberts *et al.* also demonstrated a more biocompatible blocking group, PEG. Immunofluorescent images show increased adhesions observed by day 5 on cleaved surface and an increase of Stro-1 on uncleaved surfaces by day 21. Therefore, maintenance of PEG increases stemness and removal induces differentiation by binding to RGD. Red = actin, blue = nucleus, green = Stro-1 or vinculin. E) Images quantified for D (Stro-1). C-E Replicated from (Roberts et al. 2016). \*P<0.05, \*\*P<0.01 \*\*\*P<0.001 as determined by ANOVA.

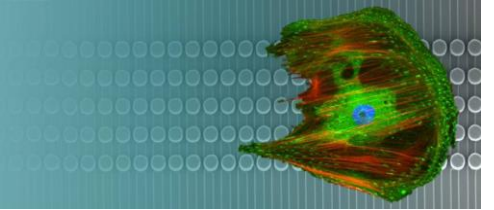
However, it was thought that the Fmoc was susceptible to fouling by cell secreted proteins and so the capping group was replaced by PEG chains that are anti-fouling and more biocompatible (PEG- A↓ARGD) (MRes project published in (Roberts et al. 2016)). It is thought that the anti-fouling nature of PEG is due to the hydrophilicity, high mobility and steric hindrance (Dong et al. 2011). This effect was increased with increasing chain length of PEG, as demonstrated by Dong *et al.* 2011 who tested a range of chain lengths on bacterial culture and found that adherence decreased with increasing chain length (Dong et al. 2011). In this study, another advantage of the change in blocking group was that it was thought to promote MSC self-renewal in comparison to the switched surface (Figure 1.11D) and when quantified, is significantly different to that of the plain glass control (Figure 1.11E) (Roberts et al. 2016). Further, cleavage of PEG resulted in increased cell adhesion (Figure 1.11D), which suggests cell differentiation via mechanotransduction (Roberts et al. 2016). These studies formed the rationale for the MMP responsive surface where PEG was maintained to promote self-renewal. In addition, focal adhesion formation was also expected in response to RGD and therefore osteogenic differentiation was anticipated.

## 1.9 Conclusion

MSCs are a worthwhile stem cell to invest research resources into for TE due to their immunogenic properties and ease of access from multiple sources. Materials engineering therefore has the capacity to overcome traditional limitations for stem cell culture by creating the directionality needed for stem cell maintenance or differentiation without the need for soluble chemistries or animal feeder layers that will limit the progression of stem cell applications in the clinic. Methods to do this include manipulation of surface characteristics such as of topography, surface chemistry or stiffness, which although have controlled MSC behaviour *in vitro* are static technologies. The next generation of materials engineering includes a dynamic feature, by applying a stimulus to modify an aspect of the surface. It is our belief that stimuli responsive strategies hold the most promise due to their versatility but also relevance to a biological context. However, future materials strategies could combine methods that dynamically replicate the niche and improve stem cell culture. Here we propose to utilise meaningful biological motifs tethered to a glass coverslip using SPPS to control MSC behaviour to provide a cell expansion strategy by mimicking the *in vivo* bone marrow niche.

## 1.10 Project Aims

- a) Understand the MMP profile of MSCs
- b) Design a peptide surface to be targeted by the MMP secreted by MSCs
- c) Synthesise the surface utilising SPPS incorporating the sequence favourable for cleavage by MMPs and the cell adhesive peptide RGD.
- d) Understand the mechanism of action by enzymes on the surface
- e) Analyse the phenotype of MSCs on the surface over time



## 2. General Methods

This chapter outlines all protocols used within this study. Surface modification was carried out using solid phase peptide synthesis (SPPS). Standard cell culture techniques are also described as well as techniques for biochemical analysis.

## 2.1 Supplier Information

**Table 2.1 – Supplier Information.** Reagents used in Chapter 2.

<b>Technique</b>	<b>Materials</b>	<b>Supplier</b>
SPPS	13mm Glass Coverslips	VWR, USA
	(3-Glycidyloxypropyl) Trimethoxysilane (GOPTS)	Sigma Aldrich, UK
	PEG <sub>26</sub> -NH <sub>2</sub> (Poly (ethylene glycol)) Diamine	Polypure, Norway
	Fmoc-Protected Amino Acids	Sigma Aldrich, UK
	N,N-Dimethylformamide (DMF)	Sigma Aldrich, UK
	Ethyl (Hydroxyamino) Cyanoacetate (EHIC)	Sigma Aldrich, UK
	N,N'-Diisopropylcarbodiimide (DIC)	Sigma Aldrich, UK
	Piperidine	Sigma Aldrich, UK
	(O-Methyl-O'-Succinyl Polyethylene Glycol 2'000) (PEG)	Sigma Aldrich, UK
	Trifluoroacetic Acid (TFA)	Sigma Aldrich, UK
Cell Culture	Dulbecco's Modified Eagles Media (DMEM)	Sigma Aldrich, UK
	Foetal Bovine Serum (FBS)	Sigma Aldrich, UK
	Penicillin / Streptomycin	Sigma Aldrich, UK
	Non-Essential Amino Acid	Invitrogen, UK
	Sodium Pyruvate	Sigma Aldrich, UK
	Trypsin	Sigma Aldrich, UK
Buffers	Phosphate Buffered Saline (PBS)	Sigma Aldrich, UK
	Bovine Serum Albumin (BSA)	Sigma Aldrich, UK
	Tween-20	Sigma Aldrich, UK
	2-Hydroxylethyl-1-Piperazine-Ethanesulphonic Acid (HEPES)	Sigma Aldrich, UK
Zymography	Gelatin / Casein Gels	BioRad, USA
	Running Buffer	BioRad, USA

	Zymogram Sample Buffer	BioRad, USA
	Precision Plus Protein <sup>TM</sup> Dual Colour Standards	BioRad, USA
	Renature Buffer	BioRad, USA
	Development Buffer	BioRad, USA
ELISA	MMP-9 ELISA	Invitrogen, UK
	MMP-2 ELISA	Life Technologies, UK
Array	MMP Antibody Array	Abcam, UK

## 2.2 Surface Modification

Surfaces were synthesised using SPPS as in (Todd et al. 2009). Glass coverslips were sonicated in acetone, ethanol, methanol, deionised water (dH<sub>2</sub>O) for 10 min each then allowed to dry. The coverslips were acid cleaned in piranha solution: 3:7 solution of hydrogen peroxide (H<sub>2</sub>O<sub>2</sub>) and concentrated sulfuric acid (H<sub>2</sub>SO<sub>4</sub>) for 1 hour. Coverslips were then rinsed in deionised water (dH<sub>2</sub>O) until the solution was neutralised, and coverslips were rinsed individually in 3x dH<sub>2</sub>O before drying with nitrogen (Figure 2.1i). As per Piehler *et al.* surfaces were silanized by immersing the coverslips in GOPTS at 37 °C for 1 hour followed by washing 3x in acetone and drying overnight at 75 °C (Figure 2.1ii) (Piehler et al. 2000). PEG<sub>26</sub>-NH<sub>2</sub> was melted onto surface at 75 °C for 48 hours to create an amine-functionalised monolayer, excess PEG<sub>26</sub>-NH<sub>2</sub> was removed by washing the surfaces in 3x dH<sub>2</sub>O (Figure 2.1iii). To build up the peptide chain, the first Fmoc protected amino acid (20 mM) was coupled to PEG<sub>26</sub> diamine in a solution of EHICA (0.4 mmol) and DIC (0.4 mmol) per 10 mL of anhydrous DMF. Samples were treated for 2 hours under agitation. Samples were then rinsed in DMF, ethanol, methanol and DMF for 10 min under agitation (Figure 2.1iv). For the addition of subsequent amino acids, the Fmoc protecting group (of the bound amino acid) was removed using piperidine (20 % in DMF) for 2 hours under agitation then washed in DMF, ethanol, methanol and DMF for 10 min (Figure 2.1v). The next Fmoc protected amino acid was added and last two steps were repeated until the sequence was complete (N-terminal and side chain protected amino acids shown in Table 2.2). The sequences of controls synthesised are shown in Table 2.3.

The Fmoc protecting group was removed from the final peptide then PEG (O-methyl-O'-succinyl polyethylene glycol 2'000) was added to the terminal amino acid prior to removal of side chains. The side chain protecting groups on the aspartic acid (O-*tert.* Butyl, OtBu)

and the arginine (pentamethyldihydrobenzofuran-5-sulfonyl, Pbf) were removed with a 90 % solution of aqueous TFA for 4 hours. Samples were then washed and stored in a desiccator until ready for use.

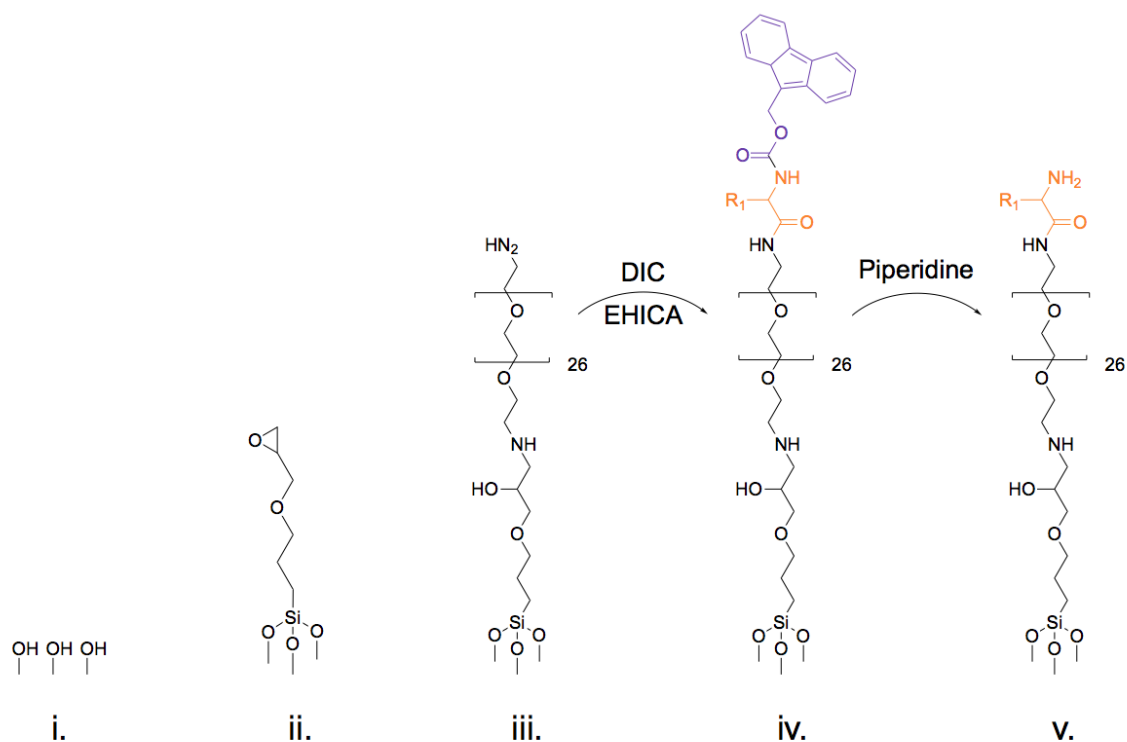
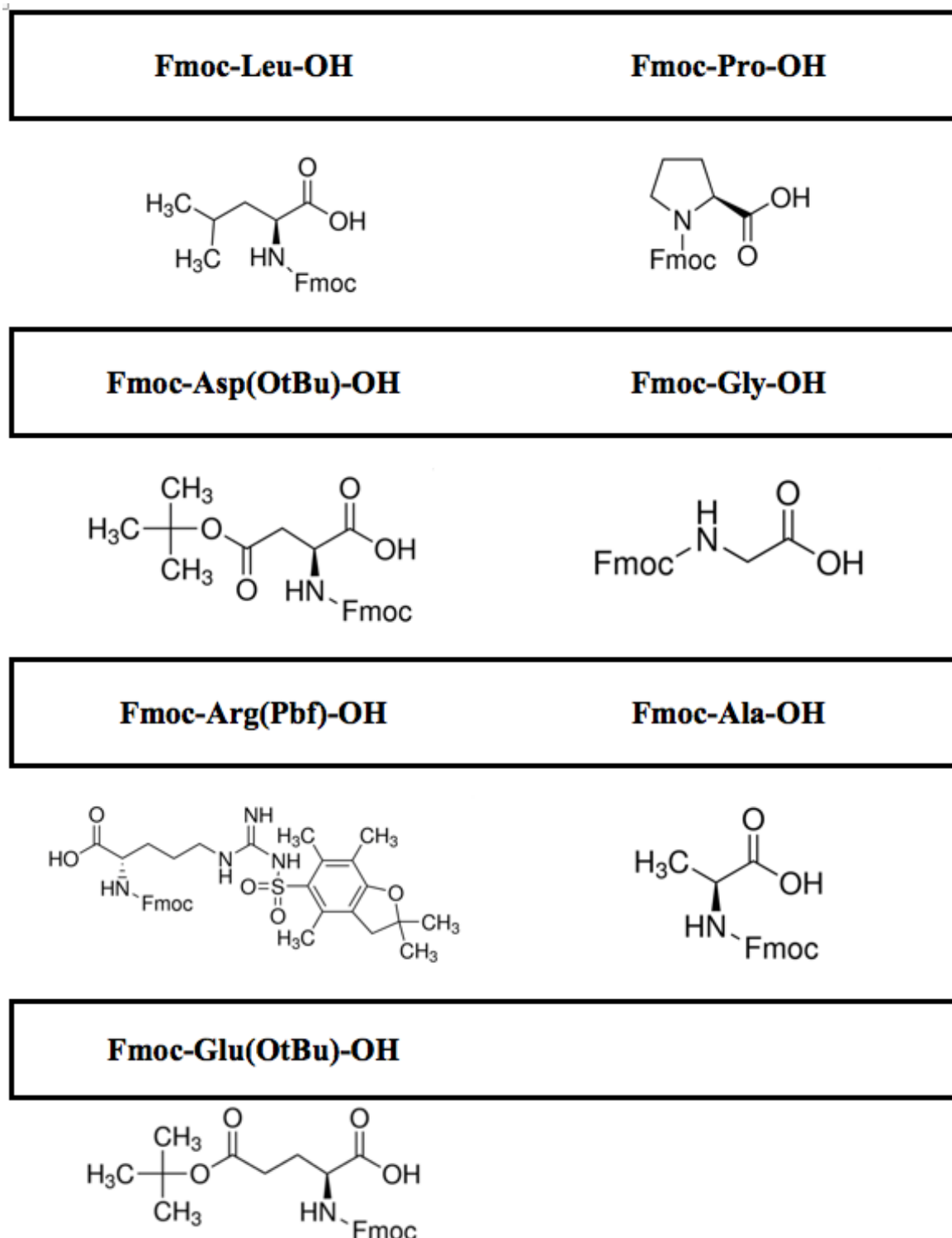


**Figure 2.1 - Pre-treatment of a glass coverslip and first amino acid addition.** i) Hydroxylation of glass via piranha solution. ii) Salinization of surface by GOPTS. iii) PEG<sub>26</sub> diamine addition. iv) First amino acid addition in presence of EHIC and DIC. v) Removal of Fmoc in solution of 20 % piperidine. Re-drawn from (Zelzer, Scurr, et al. 2012) black = surface chemistry prior to amino acid addition, orange = amino acid and side group (R<sub>1</sub>), purple = Fmoc protecting group.

**Table 2.2 - Schematic of Fmoc Protected Amino Acids for SPPS.** The chemical structure of each amino acid used in the formation of the oligopeptide sequence. All amino acids are Fmoc protected and in the case of Arg side chains are protected with Pbf and Asp and Glu side chains are protected by OtBu respectively. Images taken from Sigma Aldrich website <sup>6</sup>.



<sup>6</sup> <http://www.sigmaaldrich.com/united-kingdom.html>

**Table 2.3 - Sequence of Controls.** Adhesive controls contain RGD, non-adhesive contain RGE. For both adhesive and non-adhesive, uncleavable and pre-cleaved surfaces were synthesized.

Adhesion	Category	Amino Acid Sequence	Abbreviation
-	Glass	-	-
Adhesive	Uncleavable	PEG-RGD	-
	Pre-cleaved	LRGD	-
	Enzyme Responsive	PEG-GPAG↓LRDG	DIGE-D
Non-adhesive	Uncleavable	PEG-RGE	-
	Pre-cleaved	LRGE	-
	Enzyme Responsive	PEG-GPAG↓LRGE	DIGE-E

## 2.3 Buffers

### 2.3.1 Phosphate Buffered Saline (PBS)

PBS solutions are made in house, one tablet is diluted in 250 mL distilled water then autoclaved at 200 °C for 20 min.

### 2.3.2 Fixative

Fixative constituted 10 % formaldehyde in PBS. Generally, 10 mL formaldehyde was added to 90 mL PBS with 2 g of sucrose. Solution was stored at 4 °C prior to use.

### 2.3.3 Permeability (Perm) Buffer

Perm buffer consisted of 10.3 g sucrose, 0.292 g NaCl, 0.06 g MgCl<sub>2</sub> and 0.476 g HEPES in 100 mL. This solution was adjusted to 7.2 pH then 0.5 mL Triton X was added. Perm buffer was stored at 4 °C prior to use.

### 2.3.4 PBS/BSA

2 g of BSA was dissolved in 100 mL PBS. Solution was stored at 4 °C prior to immediate use or stored at -20 °C for long term storage.

### 2.3.5 Tween

Tween-20 was made to a solution of 0.1 % in PBS. Generally, 100 µl of Tween-20 in 100 mL PBS was stored at 4 °C prior to use.

## 2.4 Mesenchymal Stem Cell Culture

### 2.4.1 Cell Culture

MSCs were either donated from the University of Southampton with thanks to Professor Richard Oreffo (Stro-1 positive cells were selected from bone marrow by magnetic separation as in (Gronthos & Zannettino 2008)) or obtained from PromoCell (GmbH, Germany). Cells were cultured in T75 flasks prior to use (passage between P1 and P4 as stated) using DMEM supplemented with 5 mL non-essential amino acid, 50 mL FBS, 10 mL penicillin / streptomycin and 5 mL sodium pyruvate. Flasks were incubated at 37 °C in 5 % CO<sub>2</sub>. Cells were cultured to approximately 80-90 % confluence prior to cell seeding (media changes performed twice weekly). For seeding, cells were rinsed in HEPES saline, then incubated with 5 mL trypsin (37 °C in 5 % CO<sub>2</sub>) for 5 min. 5 mL culture media was added to halt the action of the trypsin, the resulting cell suspension was transferred into 15 mL falcon tube and centrifuged for 4 min at 1400 g to sediment cells. The trypsin/media supernatant was decanted, and cells resuspend in media. Cells were either seeded into another flask or used for experimental set up (Section 2.4.2).

### 2.4.2 Experimental Set Up

Prior to cell seeding, functionalised coverslips were incubated in 70 % ethanol for 10 minutes. Coverslips were then allowed to dry then were placed in a 24 well plate. Cells were treated as in Section 2.4.1. After centrifuging, cells were counted using a haemocytometer then seeded at 1,000 cells / cm<sup>2</sup> in 1 mL culture media. Coverslips were incubated for the time stated with media changes performed twice weekly. To maintain presence of cell secreted MMPs, 500 µl cell supernatant was removed from the well and topped up with a fresh 500 µl. This was done to maintain the existing cell secreted proteins within the well.

## 2.5 MMP Analysis

### 2.5.1 Zymography

Supernatant was collected from cell culture on functionalised coverslips stored at -80 °C prior to zymogram analysis. Supernatant was then mixed 1:1 with zymogram sample buffer (loading buffer) and 20 µl was loaded into each well of precast gelatin and casein gels. Precision Plus Protein <sup>TM</sup> Dual Colour Standards were used as molecular standards

(10 $\mu$ l loaded per gel). The gels were run at 200 V in running buffer (10 % Tris/Glycine/SDS running buffer diluted PBS) for 60 min in Criterion<sup>TM</sup> gel system until the bands reached the bottom. Gels were soaked in zymogram renature buffer (10 % renature buffer in PBS) using gentle agitation for 45 min with buffer changes at 15 and 30 min. The gels were then incubated in zymogram development buffer (10 % development buffer in PBS) overnight at 37 °C. Afterwards, gels were stained in 0.5 % (w/v) Coomassie Brilliant Blue R-250 in 4 % methanol, 10 % acetic acid at room temperature for 60 min with gentle agitation. The Coomassie Blue solution was replaced with destain solution (4 % methanol and 10 % acetic acid in PBS), which was replaced with 3 changes every 15 min (at room temperature) until bands were visible. Gels were imaged using a fusion Fx, Vilber Lourmat and bands were quantified using Fiji software (ImageJ derivative, free download from NIH)<sup>7</sup>.

### 2.5.2 Enzyme-Linked Immunosorbent Assay (ELISA)

MMP-2 and MMP-9 ELISAs were carried out as per the manufacturers instruction. For each ELISA, samples of DMEM were included as controls and cell supernatant was diluted 1/10 with standard diluent. For MMP-2 ELISA, an additional positive control was also included of 0.1 mg/ml MMP-2 spiked serum free media (components of serum free media include; 500 mL DMEM, 5 mL non-essential amino acid, 10 mL antibiotic, 5 mL sodium pyruvate). ELISA plates were read at 450 nm using Clariostar microplate reader (BMG Labtech, Germany). Standard curves were also performed with known concentrations of MMP and line of best fit applied. Concentrations of samples were determined utilising the equation of the line ( $y = mx + c$ ), where simultaneous equations were generated from two sets of coordinates from the line of best fit to solve the gradient (m) and the y intercept (c). From this, the optical density (OD) value of the sample was substituted for y and the equation was rearranged and solved for x.

### 2.5.3 Human MMP Antibody Array

Cells were cultured on control surfaces in DMEM for three weeks after which the cell supernatant was pooled (n=3) and stored at -80 °C until further use. The experiment was carried out as outlined in the manufacturers instruction, where 1 mL of undiluted pooled sample was added to the membrane and incubated overnight. The protein of interest is captured by antibody array chips (“spots”), biotin-conjugated antibodies and then labelled

---

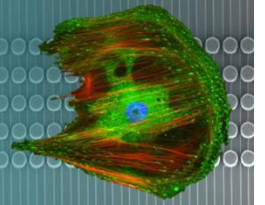
<sup>7</sup> <http://imagej.net/Fiji/Downloads>

streptavidin which are then detected (Table 2.4). The membranes were analysed with an Azure c500 Infrared Western Blot Imaging System and analysed using Fiji software (ImageJ derivative, free download from NIH)<sup>8</sup>. Pixel density was calculated for each spot then averaged.

**Table 2.4 – Position of Each Spot on Abcam Antibody Array.** Spots included both negative (neg) and positive (pos) controls along with 10 target MMPs and TIMPs (tissue inhibitors of matrix metalloproteases). All of which were spotted twice onto the array.

	<b>A</b>	<b>B</b>	<b>C</b>	<b>D</b>	<b>E</b>	<b>F</b>	<b>G</b>	<b>H</b>
<b>1</b>	pos	pos	neg	neg	MMP-1	MMP-2	MMP-3	MMP-8
<b>2</b>	pos	pos	neg	neg	MMP-1	MMP-2	MMP-3	MMP-8
<b>3</b>	MMP-9	MMP-10	MMP-13	TIMP-1	TIMP-2	TIMP-4	Neg	pos
<b>4</b>	MMP-9	MMP-10	MMP-13	TIMP-1	TIMP-2	TIMP-4	Neg	pos

<sup>8</sup> <http://imagej.net/Fiji/Downloads>



### 3. Design and Synthesis of Enzyme Responsive Dynamic Surfaces

We have discussed in Chapter 1 the limits of traditional cell culture and as stated, we aim to improve this by utilising an ERM. In response to an enzyme, the material is altered to reveal the cell adhesive peptide RGD, designed to enhance cell binding via integrins. The target enzymes for the alteration of this surface are the MMPs. MMPs primarily remodel the ECM and are involved in processes such as migration (Birkedal-Hansen et al. 1993). It is our aim that the material is controlled by these enzymes from the cell supernatant i.e. the MMPs required to remodel the ERM are secreted by the cells themselves. In this chapter, we will look at the MMP profile of MSCs and the design of the surface. We will also describe in this section the synthesis of the surface using SPPS, the characterisation of the surface and the conditions in which the surface can be remodelled.

## 3.1 Introduction

Here we aim to create peptide motifs including the RGD sequence and an enzyme responsive sequence that are to be hidden beneath a low adhesion moiety (PEG) (Figure 1.9). This material aims to control MSC behaviour in response to MMP activity *in vitro*. This work differs from previous examples (where enzymes were added by the user to activate the system) as it aims to create a dynamic material that is not only enzyme responsive, but under cellular control in two dimensions. There are earlier examples of peptides remodelling utilised in 3 dimensions and incorporated into hydrogels (Matthias P. Lutolf et al. 2003; Wade et al. 2015; Shekaran et al. 2014). However, our system is designed to be a cell expansion system for multiple uses rather than a culture system for direct implementation.

The surface is functionalised by SPPS to create a monolayer of peptides that can be cleaved by the cells. SPPS has been applied to cell culture in the past by our group along with collaborators (Roberts et al., 2016; Todd et al., 2009; Zelzer et al., 2012) and through this means, we have demonstrated effective adhesion regulation to control MSC phenotype using peptides (Roberts et al. 2016). In this chapter, we will analyse the MMP profile of MSCs, define the sequence that is likely to be targeted by the MMPs and discuss the synthesis and characterisation of the resulting material.

### 3.1.1 MMPs

The MMPs are a group of calcium dependant, zinc containing proteases that cleave the ECM. There are 23 MMPs that are classed as a family due to structural homology and functional relation. They can be subdivided by preferential action to certain ECM

substrates e.g. MMP-9 and MMP-2 are called gelatinases and act on gelatin, elastin and collagen (IV, V) (Snoek-van Beurden & Von den Hoff 2005). Other families include collagenases and stromelysins (Nagase & Woessner Jr. 1999). These MMPs are secreted by the cell as zymogens then activated by external factors (Birkedal-Hansen et al. 1993). There is also a subset of MMPs that are membrane bound (Egeblad & Werb 2002) (Table 3.1).

The primary function of the MMPs is ECM remodelling, this allows cell migration and aids in processes such as wound healing (Vu 2000). In addition to this it is also thought that MMPs may have a regulatory role through action on signalling molecules (McQuibban et al. 2001). It was thanks to the proteomic era that other substrates were identified, these substrates are collectively known as the “degradome” of MMPs (Morrison et al. 2009). This work led to novel substrates being identified that highlight the range of roles that MMPs could be involved in (receptors, mobility and angiogenesis Figure 3.1B). Surprisingly, what was thought to be their primary function (ECM regulation, Figure 3.1A) identified as 42 % prior to the degradomics testing, fell to 15 % with application of proteomic identification (Figure 3.1B) (Morrison et al. 2009). It is necessary to look at the degradome as enzymes are often implicated in disease through dysregulation. For MMPs, dysregulation can contribute to inflammatory disorders and cancer (Egeblad & Werb 2002).

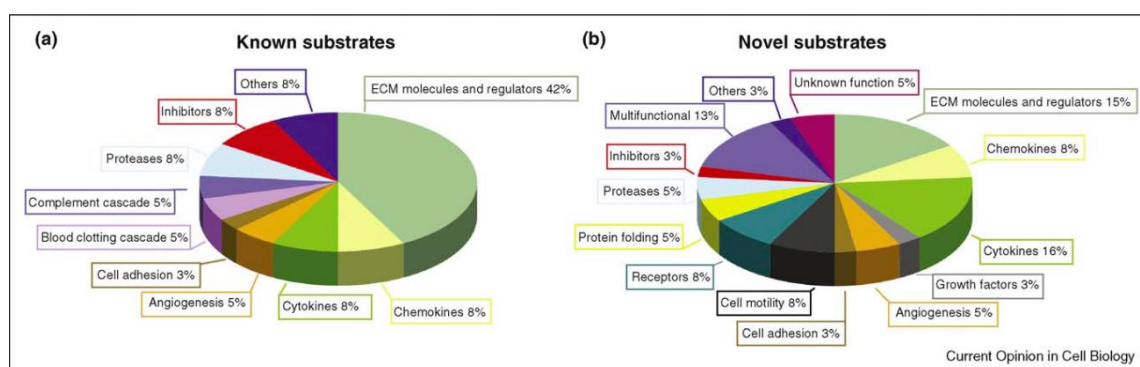


**Figure 3.1 - Range of Substrates for MMP Activity.** A) non-proteomically identified substrates for MMPs, 42 % of consists of ECM related proteins. B) Novel substrates identified by proteomics suggest that MMP have a wider range of function than initially understood (ECM regulation reduced to 15 %). Adapted from (Morrison et al. 2009)

**Table 3.1 – Matrix Metalloprotease Families, Substrate Preference and Molecular Weights.** Information was taken from (Nagase & Woessner Jr. 1999; Egeblad & Werb 2002; Birkedal-Hansen et al. 1993; Visse & Nagase 2003).

Family	Name	Substrates	Molecular Weight (M <sub>w</sub> )	
			Inactive	Active
Membrane Bound	MT-MMP1	collagen (I, II, III), aggrecan, gelatin, fibronectin, tenascin, vitronectin, laminin, entactin, perlecan	-	66,000
	MT-MMP2	fibronectin, tenascin, entactin, laminin, aggrecan, perlecan	-	72,000
	MT-MMP3	collagen I	-	64,000
	MT-MMP4	gelatin	-	58,000
Stromelysins	MMP-3	collagens (III, IV, V, VII, IX, X, XI), gelatin, elastin, fibronectin, vitronectin, laminin,	60,000	55,000
	MMP-10	collagen (III, IV, V) gelatin, elastin, fibronectin, vitronectin, aggrecan	60,000	55,000
	MMP-11	gelatin, fibronectin, collagen IV, laminin	55,000	45,000
Collagenase	MMP-1	collagens (I, II, III, VI, VIII, X, XI), gelatin, fibronectin, vitronectin, laminin, entactin	57,000	52,000
	MMP-8	collagen (I, II, III), aggrecan	75,000	65,000
	MMP-13	collagens (I, II, III, IV, VI, XI, X), gelatin, fibronectin, perlecan, aggrecan	65,000	55,000
Gelatinase	MMP-2	collagens (I, II, III, IV, V, VII, X, XI), gelatin, fibronectin, elastin, vitronectin, laminin, myelin	72,000	62,000
	MMP-9	collagen (IV, V, XI, XIV), gelatin, elastin, vitronectin, laminin, aggrecan,	92,000	82,000
Matrilysin	MMP-7	collagen (I, IV), gelatin, elastin, fibronectin, vitronectin, laminin, entactin, aggrecan	28,000	19,000

Although there are several MMP families, redundancy does occur with multiple MMPs acting on overlapping substrates, this could be due to the catalytic cleft similarity (Sternlicht & Werb 2009; Kridel et al. 2001). Turk *et al.* show experimentally that although redundancy is possible, it is not necessarily efficient (Turk et al. 2001). The consensus sequence for each MMP was synthesised, then incubated with other MMPs to

determine efficiency of cleavage using Michaelis-Menten equation,  $K_{cat}/K_M$  ( $M^{-1}S^{-1}$ ) (Turk et al. 2001). It was found that while cleavage of non-consensus sequences was possible by multiple MMPs, efficiency of cleavage increases with action of that MMP on its own consensus sequence (Turk et al. 2001).

### 3.1.2 MMP Protein Structure

The protein structure for the secreted MMPs demonstrates conserved structural homology (Birkedal-Hansen et al. 1993). MMPs consist of specific domains; signal peptide, pro-peptide, catalytic and hemopexin domain (Figure 3.2) (Kessenbrock et al. 2010). The signal peptide directs the enzyme to the secretion pathways namely, the endoplasmic reticulum (Egeblad & Werb 2002). As they are secreted as zymogens, activation occurs due to a structural change by removal of the pro-peptide (Vandooren et al. 2013). There are three  $\alpha$ -helices joined together by loops between the pro-peptide and catalytic site (Morgunova et al. 1999). Action on these loops is responsible for the activation of the zymogen (Morgunova et al. 1999). The catalytic domain contains a zinc ion which complexes with the pro-domain to maintain latency, specifically through action of cysteine group with zinc (Figure 3.2, Section 3.1.3) (Kessenbrock et al. 2015). The catalytic and hemopexin domains are separated by a hinge region that varies in length per MMP. The hemopexin region at the C-terminal domain is responsible for the specificity of substrate binding (Birkedal-Hansen et al. 1993; Sternlicht & Werb 2001) but also acts as site for inhibitors to bind to (Sternlicht & Werb 2001). The tertiary structure of the hemopexin domain consists of a 4-bladed  $\beta$ -propeller fold that is stabilised by a disulphide bond between blades I and IV (Egeblad & Werb 2002). The overall structure for most MMPs is consistent with Figure 3.2, but there are some exceptions. The matrilysins lack the hemopexin domain and the gelatinases have an additional feature of a fibronectin domain which are thought to aid binding to collagen (Snoek-van Beurden & Von den Hoff 2005; Nagase & Fields 1996; Kridel et al. 2001).

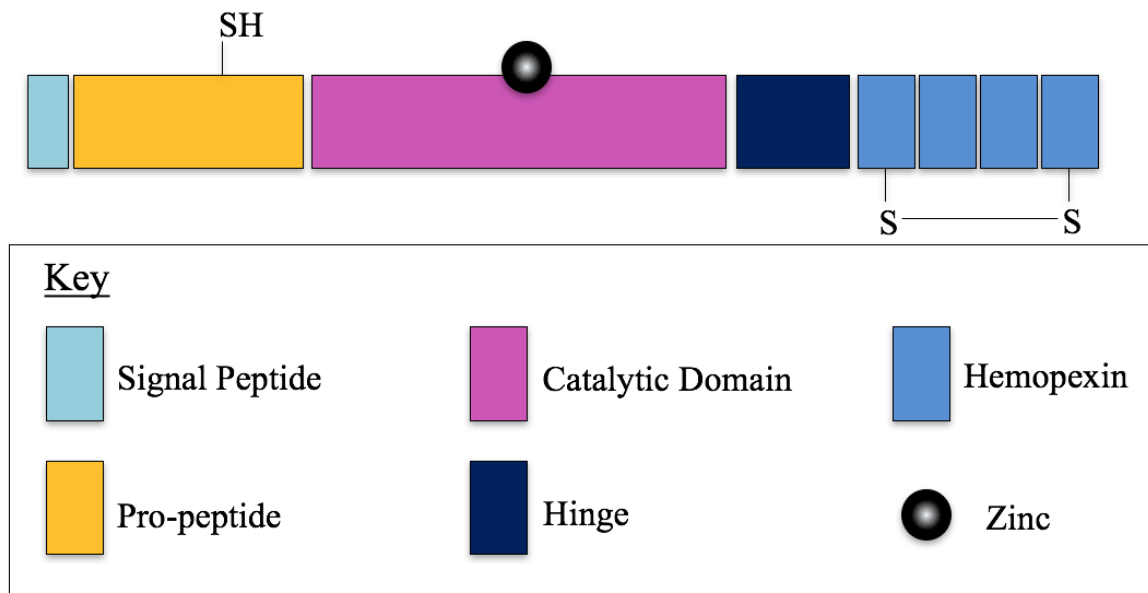


**Figure 3.2 - Conserved Structure for the Secreted MMPs.** The overall protein structure for the MMPs is conserved. Prior to activation, the pro-peptide is cleaved, altering the interaction of the sulfhydryl group (-SH) from the “cysteine switch” of the pro-peptide and the zinc ion that is associated with the catalytic domain. Activation results in the removal of the pro-peptide. The tail of the MMP contains a hemopexin region that is thought to be important for substrate specificity. The last repeats of the hemopexin domain are linked by a disulphide bond. Image adapted from (Visse & Nagase 2003; Egeblad & Werb 2002; Vandooren et al. 2013).

### 3.1.3 Activation

Latency is maintained by specific interactions of conserved sequences in both the pro-peptide and catalytic domain with the zinc ion (Visse & Nagase 2003). Figure 3.3A shows the location of these sequences within the MMP-2 enzyme. The pro-domain sequence PRCG(V/N)PD is conserved specifically, the cysteine residue is imperative for the interaction of the pro-peptide with the zinc ion, this interaction is described as the “cysteine switch” (Kessenbrock et al. 2010; Nelson et al. 2000; Nagase & Woessner Jr. 1999). Disruption of the switch results in activation of the MMP via removal of the pro-peptide (loss of around 10,000 Daltons) (Birkedal-Hansen et al. 1993; Woessner Jr. 1991). The cysteine switch is located in the loop regions between the  $\alpha$ -helices of the pro-domain, specifically between helix 1 & 2 in a region that is described as the bait region (Visse & Nagase 2003). In addition to this, the catalytic site also contains the conserved sequence HEXGHXXGXXH where the His centre around the zinc ion in the catalytic cleft (Visse & Nagase 2003) (Figure 3.3B). The catalytic site also contains a conserved Met which forms a structure known as the “Met-turn” which has been shown experimentally to be imperative to protein structure and therefore stability (Tallant et al. 2010; Nagase & Woessner Jr. 1999). Activation of the membrane bound MMPs (MT-MMP) is through a

different mechanism. They contain a specific motif, the furin site, which allows activation by furin-like serine proteases (Egeblad & Werb 2002).

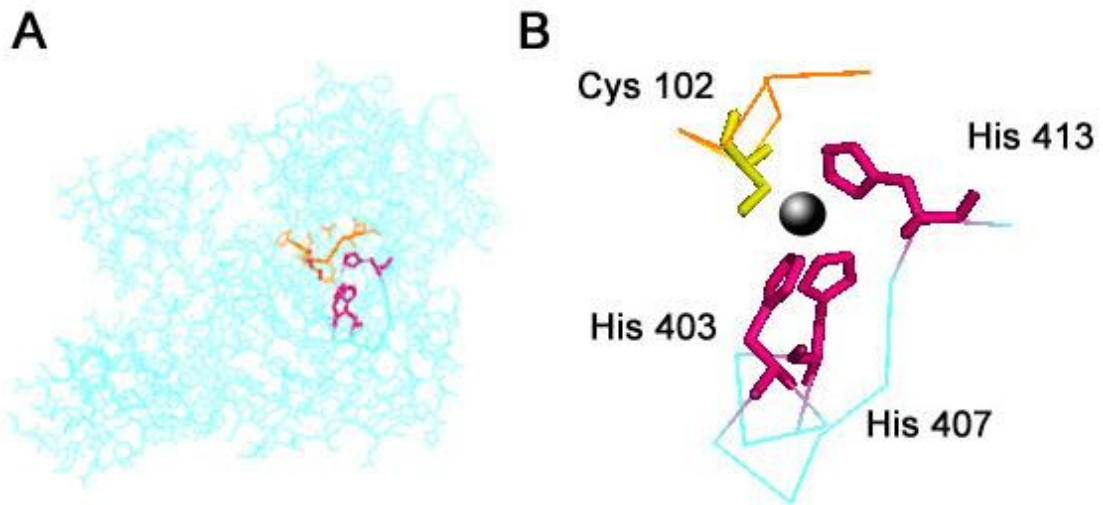


**Figure 3.3 – MMP-2 Active Site.** A) Mature MMP-2 peptide (blue) showing position of the conserved His in the catalytic site (pink) with cysteine switch (yellow) in conserved pro-domain (orange). B) His 403, 407, 413 complexes with the zinc ion (black) in the catalytic cleft. Latency is maintained by the proximity of Cys 102 of the cysteine switch with the zinc ion. Images made on Pymol software.

Regardless of the mechanism of activation, the cysteine switch must be disrupted and the pro-peptide removed for the enzyme to be activated (Nagase & Woessner Jr. 1999). Activation can be induced by growth factors, cytokines, chaotropic agents, reactive oxygens, low pH and heat treatments (Visse & Nagase 2003). The process is described as stepwise, the above factors contribute to the cleavage of the bait region in the pro-domain. However, the final step of activation is mediated by a mature MMP (Figure 3.4A) (Vartak & Gemeinhart 2007). For MMP-2, this is particularly well studied as it takes place on the cell surface via MT-MMPs (Visse & Nagase 2003). Another unique feature of this interaction is the involvement of the tissue inhibitor of matrix metalloprotease 2 (TIMP-2). MT1-MMP binds firstly to TIMP-2 then a free MT1-MMP is bound by proMMP-2 which complexes with TIMP-2 via the hemopexin domain (Worley et al. 2003). After activation, MMP-2 dissociates from the complex as an active enzyme (Figure 3.4B). This was demonstrated experimentally by Sato 1994, who engineered a membrane bound MT-MMP in lung carcinoma cells which was found to activate the MMP-2 and MMP-9 zymogens and result in invasion of cancer cells (Sato et al. 1994).

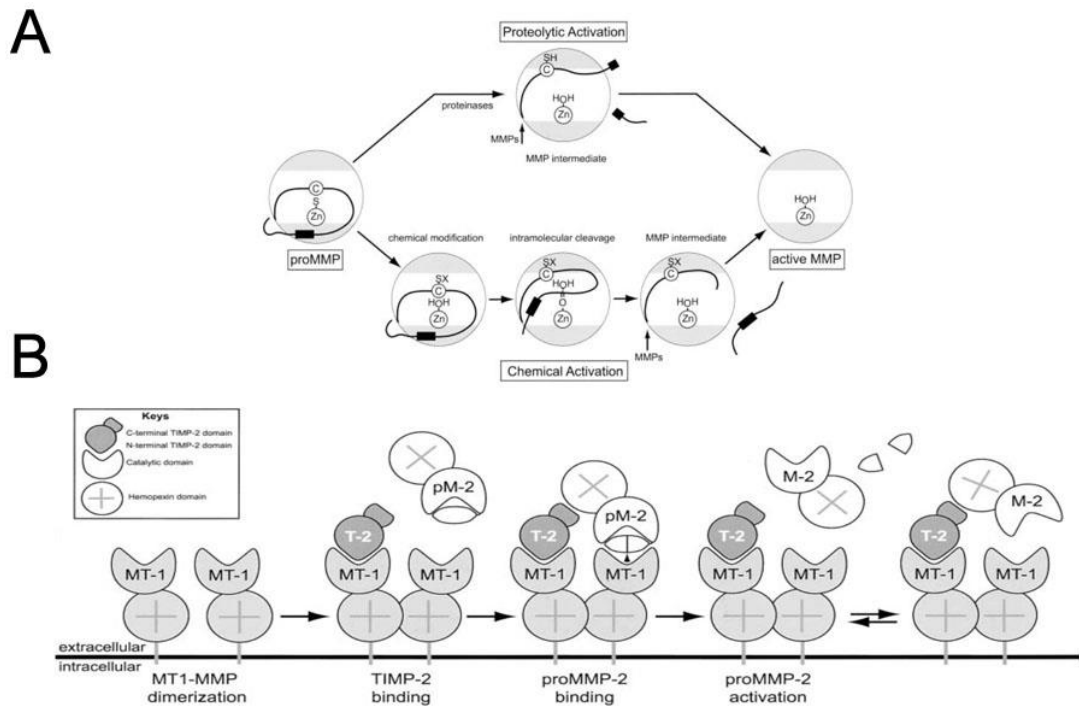


**Figure 3.4 - Activation of MMPs.** A) Stepwise activation, inactive zymogens are activated by either proteolytic or non-proteolytic methods. The catalytic site (white) contains the zinc ion. The pro-peptide (black line) is cleaved at the bait region (black box). Activation is by physical separation of the zinc ion from sulfhydryl group of the cysteine switch or chemical modification of the sulfhydryl group B) proMMP-2 is activated by MT1-MMP and TIMP2. MT-MMP1 and TIMP-2 bind on cell surface and proMMP-2 binds to TIMP-2 via hemopexin domain. MMP-2 dissociates from cell surface after activation. Both images from (Visse & Nagase 2003).

### 3.1.4 Regulation

MMPs are regulated by TIMPs of which 4 have been identified and display homologous structures (TIMP-1, -2, -3, -4) (Bigg et al. 2001; Troeberg et al. 2002). The TIMP N-terminal domain is responsible for the inhibition of the MMPs, specifically at Cys1-Pro5 sequence (Visse & Nagase 2003; Bode et al. 1999). The TIMP wedges into the active site of the MMP reversibly and with high affinity like a substrate/product interaction (Woessner Jr. 1991; Bode et al. 1999). Loss of balance of this response contributes to diseases such as rheumatoid and osteoarthritis and cardiovascular disease. TIMPs are tissue specific and act locally (Mannello 2006). Activation of MMP does not correlate with activity of MMP as they can be bound by the TIMP molecules. However, as described above (Figure 3.4) the activation of MMP-2 via MT1-MMP is mediated by TIMP-2 and occurs in a concentration dependent manner. Insufficient concentrations of TIMP means the pro-enzyme is not brought to the cell surface and high concentrations are inhibitory (Bigg et al. 2001).

### 3.1.5 MSCs and MMPs

MMP-2 and MMP-9 are found in the connective tissue cells and cells of the bone marrow (Morgunova et al. 1999). The type II fibronectin domains that are unique to the gelatinases allow them to bind gelatin, collagen and lamin (Lozito & Tuan 2011). MMP-2 is the consistently cited MMP secreted by MSCs (Morgunova et al. 1999).

#### 3.1.5.1 Migration

It is accepted that MMPs are required for ECM degradation. But in the case of MSCs (also true for cancer cells) it is required for migration (and invasion) through basement membranes (Steingen et al. 2008). MMP-2 is important for MSC homing through bone marrow (Steingen et al. 2008; Becker & Hummelen 2007). Cell surface adhesion molecules are thought to play a role in anchoring MMPs to the site of matrix destruction (Yu & Stamenkovic 1999). For example, CD44 complexes with MMP-9 in TA3 mammary carcinoma cells and increases the invasiveness of the tumour (Yu & Stamenkovic 1999). It is also thought that the SIBLING proteins (Small Integrin-Binding Ligand N-linked Glycoproteins) such as bone sialoprotein (BSP), osteopontin (OPN) and dentin matrix protein 1 (DMP1) have a MMP binding partner of MMP-2, MMP-3 and MMP-9 respectively (Karadag & Fisher 2006). Karadag *et al.* have shown that there is a localisation of MMP-2 to  $\alpha_v\beta_3$  integrin via BSP that in turn enhances the migration of bone marrow stromal cells (Karadag et al. 2004). As BSP contains RGD domains, it is thought that the binding to the integrin is mediated through the RGD (effect not seen when RGD deleted from BSP) (Karadag et al. 2004). This in turn has a downstream effect resulting in activation of MT-MMP-1 (known to be an activator of MMP-2, as in Figure 3.4) (Karadag et al. 2004).

#### 3.1.5.2 Differentiation

There is overlapping expression of secreted MMPs by stem cells however, this is due to differential protein secretion rather than indicators of lineage specification (Almalki & Agrawal 2016). In a review of MMP secretion by MSCs, Almalki *et al.* show that there are a range of MMP responses associated with MSC differentiation (but also with processes such as angiogenesis and proliferation) (Almalki & Agrawal 2016). Almalki *et al.* discuss that increases in MMP-2 & -13 and decreases in MMP-11 and TIMP-1 are a signature of adipogenic differentiation (Almalki & Agrawal 2016). Further, increases in MMP-2, -9, -13 & -14 indicate chondrogenic differentiation. In comparison, osteogenic

differentiation is thought to be as a result of increasing MMP-3, -13, -14 and TIMP-2 (Almalki & Agrawal 2016).

MMP-13 has a role in both adipogenesis and osteogenesis. MMP-13 expression is high in adipose tissue (Shih & Ajuwon 2015). In a mouse model of obesity, it was shown that inhibition of MMP-13 in this tissue suppressed adipose mass and adipocyte differentiation (Shih & Ajuwon 2015). Comparatively, Ozeki *et al.* have demonstrated that in response to inorganic phosphates, MMP-13 secretion increases over time and further siRNA against MMP-13 abolishes expression of osteogenic proteins in adipose derived MSCs (Ozeki *et al.* 2016). Taken together, the increasing expression of MMP-13 is a characteristic of both adipogenesis and osteogenesis. From this example, it is obvious that expression of MMPs in MSCs does not infer phenotype – the presence of MMP-13 in supernatant is not indicative of a specific phenotype and therefore cannot be a marker of lineage specification.

In this chapter, we confirm that MMP-2 is preferentially secreted by MSCs. From this data, we designed a peptide sequence that mimics the consensus sequence (preferential sequence cleaved by an enzyme). The synthesis of the sequence by SPPS was completed effectively and is responsive to MMP concentrations in the cell supernatant.

## 3.2 Methods

### 3.2.1 Supplier Information

**Table 3.2 – Supplier Information.** List of reagents used in Chapter 3.

<b>Technique</b>	<b>Materials</b>	<b>Supplier</b>
Supernatant Treatment	Recombinant MMP-2	Sigma-Aldrich, USA
	Recombinant MMP-9	Sigma-Aldrich, USA

### 3.2.2 SPSS

Materials were synthesised as described in Chapter 2, Section 2.2. For this chapter, DIGE-D surfaces were specifically synthesised and compared to glass controls as stated. Samples were then washed and stored in a desiccator until use. Prior to use, surfaces were washed in 70 % ethanol for 10 minutes then air dried.

### 3.2.3 Zymography

Supernatant from Stro-1 MSCs grown on glass coverslips was saved at day 7 in triplicate and stored at -80 °C prior to use. Casein and gelatin were run as in Section 2.5.1, Chapter 2. Zymograms were imaged on a Syngene PXI gel doc system and bands were quantified using Fiji software.

### 3.2.4 6-Week Supernatant Analysis

Cells were cultured on glass coverslips for 6 weeks in triplicate. Media was saved at a weekly time points and stored at -80 °C. Supernatant was diluted 1/10 in diluting buffer and ELISA performed as stated in Chapter 2, Section 2.5.2.

### 3.2.5 MMP Antibody Array

Supernatant from Stro-1 cells grown on glass coverslips were saved at 3 weeks in triplicate. Supernatant was added to a Human MMP Antibody Array (Abcam) and carried out in as described in Section 2.5.3, Chapter 2.

### 3.2.6 Fluorescent Spectroscopy

Coverslips were saved after Fmoc protected amino acid addition and after deprotection by piperidine to indicate all stages of SPSS. Coverslips were dried and mounted onto a microscope slide and fluorescence spectra recorded using a JASCO FP-6500

spectrophotometer. This technique was specifically developed for SPPS coverslips by Zelzer *et al.* 2012 and uses a custom-made sample holder (Figure 3.5 A) (Zelzer *et al.*, 2012). Coverslips were angled 30° from the incident light to minimize the amount of reflected excitation light on the detector (schematic Figure 3.5B). Samples were exposed to an emission spectra = 270 nm and excitation spectra = 320 nm with a slit width of 20 nm (light source and detector). The position of a coverslip in the holder is shown in Figure 3.5C. Analysis was performed on 3 datasets with 2 images per dataset (n=6 per set). A spectrum was generated where Fmoc peak can be observed at 320nm (Figure 3.5D).

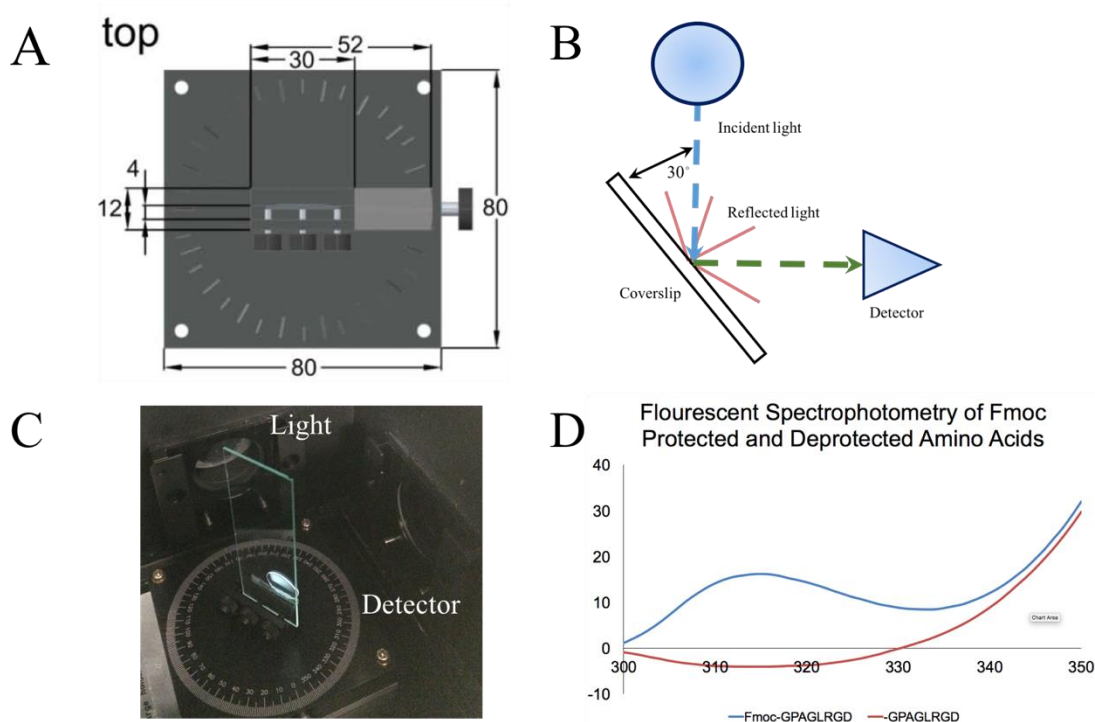


**Figure 3.5 – Schematic of Equipment for Fluorescent Spectroscopy Analysis of Glass Coverslips.** Images A and B were adapted from (Zelzer *et al.*, 2012). A) Top and bottom of the coverslip holder for the fluorescence spectroscopy, values = dimensions in mm. B) Schematic of light path from source to detector. C) Position of coverslip in the holder. D) Spectra showing peak at 350 nm in the presence of Fmoc (blue) and after the Fmoc is removed by piperidine (red).

### 3.2.7 Water Contact Angle (WCA)

Coverslips were saved after Fmoc protected amino acid addition and after deprotection by piperidine to indicate all stages of SPPS. WCA measurements were carried out using the sessile drop technique (3  $\mu$ l droplets, spotted 5 times per coverslip and angle calculated per droplet, Figure 3.6). Standard error was calculated using 50 images per dataset with 15 datasets taken across 3 substrates (n=450 images per set). The angle was calculated using a Theta optical tensiometer (Biolin Scientific, Stockholm

Sweden).

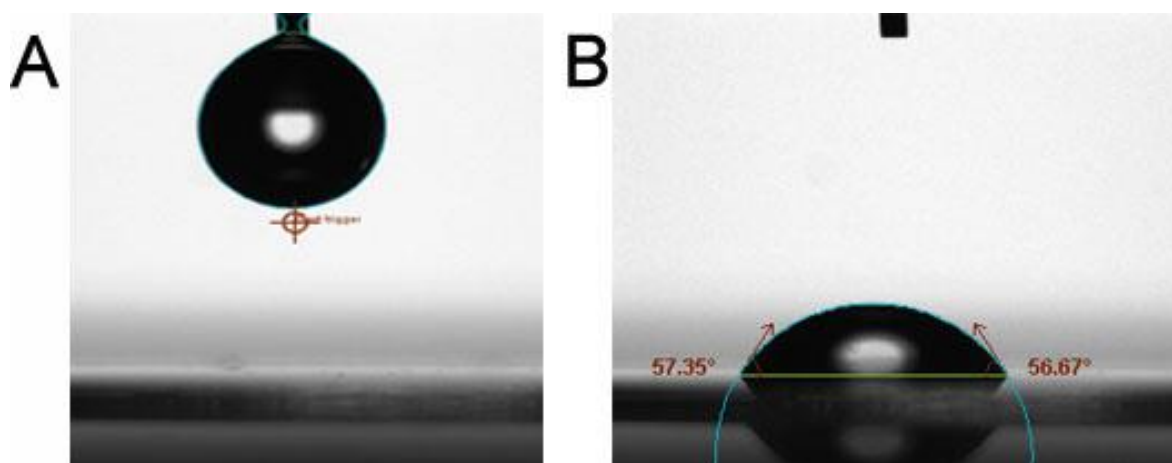


**Figure 3.6 –WCA Measurement Parameters.** A) WCA to drop. B) software measuring angles of the droplet on the surface.

### 3.2.8 ToF-SIMS for Sequence Analysis

Time of flight secondary ion mass spectrometry (ToF-SIMS) was carried out in collaboration with Dr Mischa Zelzer at the University of Nottingham. DIGE-D samples were synthesised and sent for analysis. ToF-SIMS was carried out using an ION-TOF ToF-SIMS IV instrument (Münster, Germany), equipped with a bi liquid metal ion gun (LMIG). The primary ion beam was directed at the sample under an angle of  $45^\circ$  in relation to the normal (beam spot of  $1\text{-}2\ \mu\text{m}$  in the high-current bunched mode);  $25\ \text{keV}\ \text{Bi}^{3+}$  primary ions were used in all measurements. Charging of the sample is compensated with the low-energetic electrons of the flood gun. Ion images were recorded in the high current bunched mode, which allows for higher mass resolution. Large scale ( $3\ \text{mm} \times 3\ \text{mm}$ ;  $304 \times 304$  pixels) and small scale ( $380\ \mu\text{m} \times 380\ \mu\text{m}$ ,  $256 \times 256$  pixels) images were obtained in positive polarity for each sample (1 shot per pixel). Positive ion mass spectra were calibrated with  $m/z$  15 ( $\text{CH}_3^+$ ), 29 ( $\text{C}_2\text{H}_5^+$ ), 41 ( $\text{C}_3\text{H}_5^+$ ) 67 ( $\text{C}_5\text{H}_7^+$ ) and 91 ( $\text{C}_7\text{H}_7^+$ ). A peak search was performed to identify ions indicative for amino acids according to data previously reported in the literature (Table 3.3) (Wagner & Castner 2001). Contamination was determined by identifying PDMS particles, at  $m/z$  ratios 73, 147 and 221. For semi-quantitative comparison of ion intensities, the large-scale images were divided into four regions of interest (ROIs) of  $1.5\ \text{mm} \times 1.5\ \text{mm}$  from which intensities of ions of interest were generated. Spectra used for peak shape comparison were extracted from the small-scale images.

**Table 3.3 – Expected m/z Ratio of Each Amino Acid used in SPPS.** Table shows each amino acid and the associated mass to charge ration (m/z) as determined by (Wagner & Castner 2001).

Amino Acid		Fragment	
Name	Code	m/z	Molecular Structure
Alanine	A	44	$C_2H_6N^+$
Arginine	R	43	$CH_3N_2^+$
Aspartic acid	D	88	$C_3H_6NO_2^+$
Glycine	G	30	$CH_4N^+$
Leucine	L	86	$C_5H_{12}N^+$
Proline	P	68	$C_4H_6N^+$

### 3.2.9 MMP treatment of DIGE-D coverslips

MMP-2 and MMP-9 (20 ng/ml and 0.25 ng/ml respectively) were spiked into serum free media at defined concentrations. Coverslips were incubated for 3 weeks (5 % CO<sub>2</sub> and 37 °C) then analysed by ToF-SIMS.

### 3.2.10 Supernatant Treatment for ToF-SIMS

Supernatant was saved at week 2 from cells cultured on glass surfaces. Supernatant was added to fresh DIGE-D surface and incubated for 24 hours (5 % CO<sub>2</sub> and 37 °C). Surfaces were washed in dH<sub>2</sub>O x3 then sent for ToF-SIMS analysis.

## 3.3 Results

### 3.3.1 MSC secretion of MMP

To utilise MMP as a cell secreted enzyme for materials engineering, we firstly analysed the MMP profile of MSCs in culture on glass coverslips. Using zymography we determined the presence of MMPs in cell supernatant at 7 days. Zymography is a gel-based assay that allows visualisation of MMPs from cell supernatant based on the enzymes substrate preference. Gelatin gels for example, are amenable to digestion by the gelatinases (MMP-2 and MMP-9) whereas casein gels are applied for the detection of MMP-1, -7, -12, -13. If MMPs are present, they will digest proteins the gel is synthesised from. Bands can be identified after staining with Coomassie Blue, where the background gels are stained blue and white bands highlight where digestion has occurred (Leber & Balkwill 1997). The presence of different MMP species can be implied from molecular weight.

At 7 days, no bands were observed on the casein gels and therefore we could discount the presence of those MMPs (Figure 3.7A). However, bands were identified at approximately 80 kDa and 60 kDa indicating the presence of active MMP-9 and MMP-2 respectively (Figure 3.7B). The gelatin gel also revealed presence of MMP in the media control, that may be a result of the presence of serum proteins (however, only 1 media sample was tested). The bands were quantified using Fiji software which showed that supernatant concentrations of MMP-9 were significantly less than the supernatant concentration of MMP-2, suggesting that although both MMPs were secreted the cells were actively secreting more MMP-2 after 1 week (Figure 3.7C).

We then looked at the long-term expression of the gelatinases in MSC supernatant (6-weeks). The concentration of cell secreted MMP (from cells seeded on glass coverslips) was analysed by ELISA. Figure 3.8A shows that there was a consistent concentration of MMP-2 for the period tested (10 ng/ml), it was also double that of the media control (5 ng/ml). However, this was not a significant increase. MMP-9 secretion was also analysed, it was found that MMP-9 concentration for the supernatant was reduced in comparison to MMP-2 (0.4 ng/ml compared to 10 ng/ml week 1) and comparable to that of the media control. However, MMP-9 expression did increase from week 4 onward and was significantly different to that of weeks 1-3 (Figure 3.8A). Collectively, this provides the concentration of the gelatinases in the supernatant

(Figure 3.8) and the relative activity of secreted MMP-2 in comparison to MMP-9  
(Figure 3.7C).

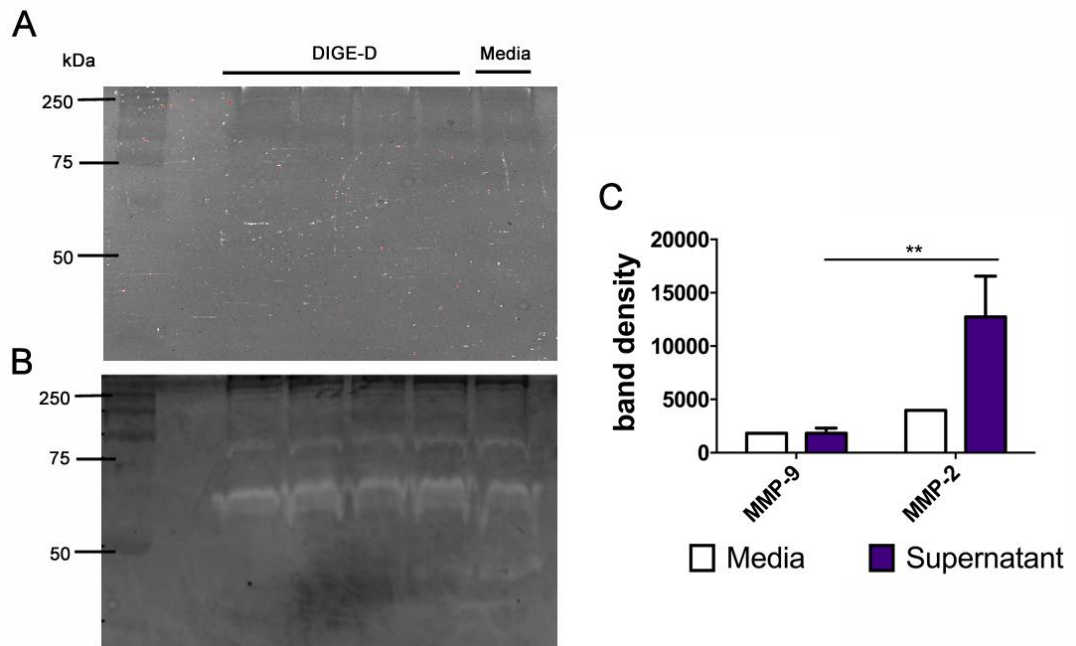


**Figure 3.7 – Zymography, 1 Week.** Supernatant from cells grown on glass in comparison to cell media at 7 days on A) Casein and B) Gelatin. Ladder shown on LHS of gel, numbers in kDa. A) MMPs were not observed on casein gels. B) Bands clearly visible on gelatin gel at 60 and 80 kDa indicating presence of MMP-2 and MMP-9 respectively. There is some MMP found in the media. C) Quantification of gelatin gel from B) indicating presence of active MMP-2 in the cell supernatant was significantly different than that found in the media. Graph shows mean  $\pm$  SD, n=4 for supernatant, n=1 for media, statistics calculated by ANOVA (\*\* p< 0.01).

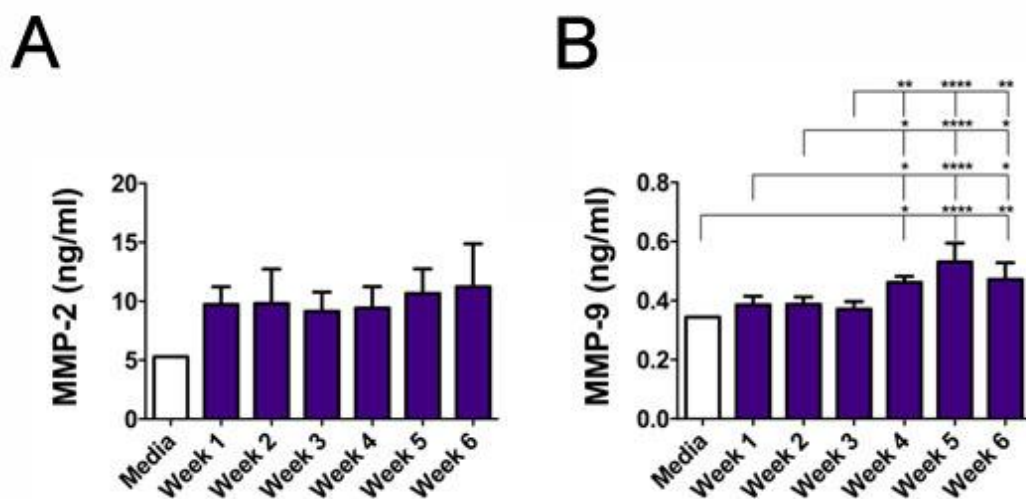


**Figure 3.8 - Gelatinase Expression Over Six Weeks as Determined by ELISA.** A) MMP-2 B) MMP-9 concentration of cell supernatant collected over 6-week culture on glass coverslips in comparison to plain DMEM media. A) MMP-2 concentration remained consistent over the period tested, approximately 11 ng/ml. B) MMP-9 concentration increased after week 3 to approximately 0.5 ng/ml (note difference in scale between both y axis). Graph shows mean  $\pm$  SD, n=3 for all controls, \* p < 0.05, \*\* p < 0.01, \*\*\*\* p < 0.0001 by ANOVA.

These results were confirmed using an antibody array against multiple MMPs to determine the full MMP profile of MSCs at 3 weeks. This technique works by spotting antibodies against specific MMPs onto an array and depending on the density, is an indicator of the relative amount of MMP. Figure 3.9 shows that MMP-2 is the most abundant MMP in the cell supernatant and is expressed at statistically significantly higher levels than the other MMPs ( $p < 0.0001$ ). MMP-9 expression was not detected which was unexpected due to the observed bands in the zymogram (Figure 3.7B) and from the ELISA data (Figure 3.8). However, concentration of MMP-9 was evaluated to be 0.4 ng/ml at 3 weeks (Figure 3.8) and is perhaps too low for detection by array. MMP-1 and MMP-3 were also detected, which suggests there is an increase in these MMPs over time as this was not observed on the casein gel at day 7 (Figure 3.7A).

These results confirm that MMP-2 is the prominent MMP that MSCs secrete. As a stimulus to activate the ERMs, it is more likely for MMP-2 to be effective due to the increased concentration of that MMP in the cell supernatant. This suggests that there is an increased likelihood of action by MMP-2 on any experimental surface design over other MMP family members. In addition, these results are consistent with the literature, where it is stated that MMP-2 is the prominent MMP expressed by MSCs (Morgunova et al. 1999).

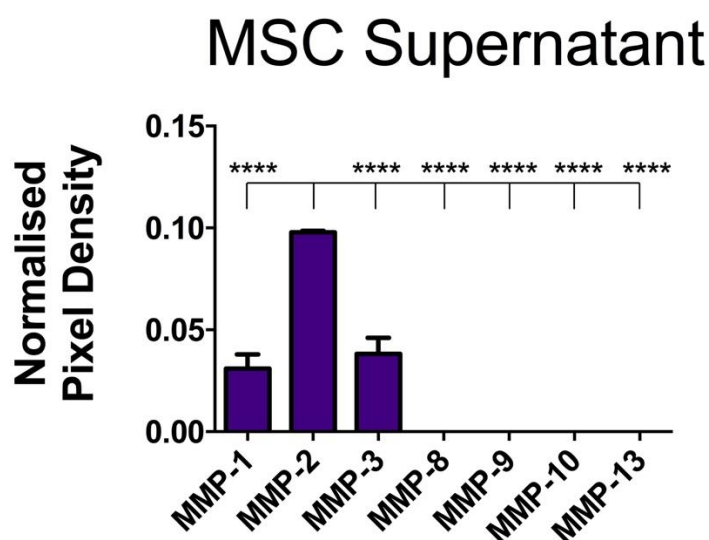


**Figure 3.9 – MMP Profile of MSC Supernatant.** Media was collected after 3 weeks of culture and MMP concentration determined using membrane analysis. Data shows that MMP-2 concentration is greater than that of the other MMPs. MMP-1 and MMP-3 were also detected albeit at a lower level. MMP-8, -9, -10 & -13 were not detected in the supernatant. Graph shows mean  $\pm$  SD,  $n=3$ , where \*\*\*\*  $p < 0.0001$  by ANOVA.

### 3.3.2 MMP Substrate Preference

The results of the previous section demonstrate that there was a greater concentration of MSC-derived MMP-2 in comparison to MMP-9. Thus, MMP-2 was considered the best candidate for surface cleavage. From this data, we progressed to define MMP-2 substrate preferences prior to synthesis of the surface. For this section, it is important to note that peptide sequences are labelled according to Schechter and Berger nomenclature. This refers to N-terminal residues which are labelled as P1, P2, P3 (non-prime) and residues that are located on C-terminal are labelled P1', P2', P3' (prime) (Schechter & Berger 1967). N-terminal and C-terminal residues are separated by the point of cleavage known as the scissile bond (Schechter & Berger 1967).

Discovery and accumulation of data from cleavage sites is becoming more high-throughput thanks to the -omics and bioinformatics era. Subsequently there is an omics field devoted to the cleavage products of proteases known as *degradomics*. This field aims not only to profile the individual proteases to determine substrate preference but also to identify the activity of these proteases *in vivo* (López-Otín & Overall 2002). One such example of this is the use of peptide libraries. Peptide libraries allow high-throughput analysis of peptide sequences and from this, patterns in preference can be highlighted (Turk et al. 2001; Vartak & Gemeinhart 2007; Seltzer et al. 1990)

Peptide libraries have been instrumental to determining MMP sequence preference. Each MMP has slight variations in preference for each position, for example, where MMP-1, MMP-2 and MMP-9 prefer Ala, Gly or Ser at P3', MMP-3 and MMP-7 prefer Met at the same position (Turk et al. 2001). For most MMPs it is thought that there is consensus for Pro at position P3, P2 is generally hydrophobic (Turk et al. 2001) and P1 is generally a small residue (Vartak & Gemeinhart 2007). Pro at position P3 is significant because of the interactions of the substrate with the enzyme, particularly the hydrophobic pocket of the enzyme active site and therefore Pro is the most kinetically favourable amino acid at P3 (Kridel et al. 2001). Recognition of sequence also depends on the complementarity of active site to the sequence in the substrate (Turk et al. 2001). Further, use of peptide libraries suggested that peptide length was important to sequence recognition. Huang *et al.* showed that increasing lengths of peptides lead to more specific cleavage at a faster rate (Huang et al. 2013). Similarly, Schilling *et al.* suggested that for MMP-2 selectivity, the subsite interactions are as important as the consensus motif (Schilling & Overall 2008). Therefore, residues surrounding the

scissile bond are equally as important in terms of enzyme kinetics. Degradation encompasses the characteristics of adjacent residues to the cleavage site and not P1↓P1' alone.

Collating the information from enzyme/peptide interactions into databases allows ease of access and wealth of knowledge for researchers in multiple fields (Rawlings 2009). For example, for healthcare, databases could include the degradome of diseased tissue to be compared to normal tissues with the view of finding drug targets based on degradomic profile (López-Otín & Overall 2002). In a bioengineering context, biomimicry of significant peptide sequences can be accessed easily to be included in materials applications.

One such protease database is the MEROPS<sup>9</sup> database that collates data from publications on various protease families to give an overview of all aspects of the protease of interest (Rawlings 2009). One advantage of this website is that it also collates data from *in vitro* studies as well as *in vivo* studies, whereas other databases for example CutDB only provides information from those peptides that are physiologically relevant (Rawlings 2009). MEROPS has gathered data from PubMed and accumulated the number of times an amino acid has been cited at each position along the scissile bond (although from this number, the context in which the MMP has been cited (i.e., active or inactive) is not known). From this, a heat map can be generated to provide a visual representation of this information. We looked specifically at the gelatinase sequence preference as shown in Figure 3.10. As noted in Section 3.3.1, MMP-2 is the predominant MMP that MSCs secrete. However, we designed the peptide motif with the aim of it being targetable to both gelatinases as it is known that there is overlap in substrate preference. This is also advantageous as while MMP-2 is mostly found in self-renewing cells and MMP-9 is involved in osteogenesis (Morgunova et al. 1999; Vu 2000).

The amino acids in Figure 3.10 have been arranged in order of properties starting with non-polar then polar, acidic and basic (Rawlings 2009). Those positions that are highly cited are more likely to be acted on by that MMP (and are coloured red in Figure 3.10). The bottom of the heat map shows the most cited peptide for each position P4-P4'. Comparing both MMP-2 and MMP-9 it is shown that there are slight differences

---

<sup>9</sup> <https://www.ebi.ac.uk/merops/>

between the gelatinase's sequence preference which could account for gelatinase redundancy. There is a similar trend for both gelatinases in that there is a favourability for non-polar amino acids at most positions along the scissile bond and in particular P2' position (Turk et al. 2001). There is also a consensus for Pro at P3 as consistent with Kridel's work (Kridel et al. 2001). What is also clear is that there is a greater number of citations for MMP-2 than MMP-9.

The citations for amino acids involved in the cleavage site are the dominant amino acids cited. There is a preference for small amino acids at position P1 and Leu at P1' for both MMP-2 and -9. It has been shown previously that MMPs cleave before a hydrophobic side chain particularly Leu, Ile, Met, Phe or Tyr (Visse & Nagase 2003). For MMP-2 this is apparent as hydrophilic amino acids are avoided, fewer than 150 citations for polar amino acids at P1' in comparison to Leu which is cited 1387 times.

To make the sequence amenable to osteogenic differentiation, RGD was substituted into P2'-P4' (as RGD has shown to help drive regulation of the osteogenic phenotype as described in Chapter 1). As shown in the Figure 3.10, Gly is maintained at position P3' for both consensus sequences. However, Asp and Arg are acidic and basic amino acids respectively. For MMP-2 a P4' A→D substitution could be tolerated (331 vs 278 citations respectively) however, P2' V→R may be less well tolerated (444 vs 99 citations respectively). It is similar for MMP-9 with P2' A→R (41 vs 34 citations respectively) and P4'A→D (49 vs 24 citations respectively). There is obviously a preference for certain amino acids at defined positions, however non-consensus sequences can also be cleaved although this would not be expected to be as efficient (Turk et al. 2001). Maintaining Pro at P3, small amino acids at P1 and Leu at P1' should be sufficient to drive cleavage. It might have been more accurate to use the full consensus sequence rather than substituting RGD at the prime side. However, due to the time taken to add one amino acid (24 hours) the RGD peptide was substituted in rather than adding to the prime side (8 amino acids rather than 11 for the consensus and RGD). Had the synthesis been automated, these sequences could have been compared to analyse the most efficient sequence for MMP cleavage.

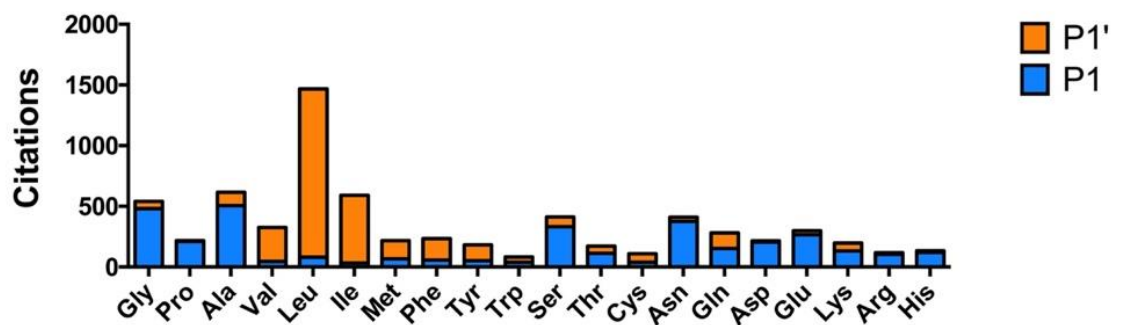
As cleavage occurs between position P1↓P1', effective mimicry of enzyme consensus sequences is imperative for efficient kinetics. We compared the number of citations exclusively for every amino acid at position P1 and P1' to determine the most likely to

be acted on (Figure 3.11). Non-polar amino acids were favoured for both enzymes at P1' with Leu as the most cited (1387 and 102 citations for MMP-2 and MMP-9 respectively). P1 for MMP-2 was more ambiguous, with approximately 500 citations for each Gly and Ala (481 and 506 respectively). However, these amino acids are small non-polar and therefore have similar properties. In the case of MMP-9 there is a clearer distinction for P1 (120 for Gly and 44 for Ala, Figure 3.11). We are confident therefore that gelatinase cleavage of a sequence occurs with a small amino acid at P1 and Leu at P1'. P1' has direct effects on enzyme kinetics as determined by Seltzer *et al.* Using synthetic peptides substituted various amino acids at P1' in the sequence Pro-Leu-Gly-↓X-Leu-Glu, they found that substitution of Leu for X (P1') enhanced cleavage efficiency by increasing the cleavage rate (80  $\mu\text{mol}/\text{mg}/\text{h}$  in comparison to Ala at 22  $\mu\text{mol}/\text{mg}/\text{h}$ ) (Seltzer et al. 1990). Maintaining Leu at this position for our sequence, gives confidence not only for peptide recognition, but also in terms of efficiency (Seltzer et al. 1990). To be amenable to both gelatinases, and substituting cell adhesive motif (RGD), we selected the sequence Gly-Pro-Ala-Gly-Leu-Arg-Gly-Asp.

		Matrix Metalloproteinase 2								Matrix Metalloproteinase 9									
		Amino Acid	P4	P3	P2	P1	P1'	P2'	P3'	P4'	Amino Acid	P4	P3	P2	P1	P1'	P2'	P3'	P4'
Non-Polar	Gly	252	120	429	481	60	125	589	289	Gly	119	19	38	120	14	31	129	41	
	Pro	196	767	70	210	8	15	29	236	Pro	15	148	37	21	10	11	8	48	
	Ala	253	368	642	506	110	235	537	331	Ala	31	52	54	47	33	41	57	49	
	Val	199	447	129	45	280	444	274	272	Val	27	29	18	21	38	25	21	19	
	Leu	258	364	178	81	1387	390	112	297	Leu	31	23	26	13	102	26	18	37	
	Ile	159	288	70	33	557	351	81	168	Ile	13	13	9	4	30	14	10	9	
	Met	82	100	44	67	150	97	47	59	Met	4	1	5	4	13	6	1	5	
	Phe	128	81	48	58	176	142	100	126	Phe	12	8	16	12	15	16	9	13	
	Trp	11	16	9	39	44	42	25	23	Trp	0	0	0	1	2	4	2	1	
Polar	Tyr	97	51	48	53	130	91	61	53	Tyr	2	3	13	10	15	6	4	6	
	Ser	178	116	483	333	79	228	485	235	Ser	19	20	27	18	20	16	31	15	
	Thr	145	93	85	112	61	252	221	161	Thr	9	10	11	13	6	31	18	13	
	Cys	37	42	51	39	70	24	11	40	Cys	1	1	4	2	0	3	4	2	
	Asn	88	67	130	376	35	120	167	138	Asn	10	4	3	17	3	9	5	11	
Acidic	Gln	166	79	226	152	129	220	128	149	Gln	12	6	20	8	21	31	9	8	
	Asp	148	12	87	206	9	25	161	278	Asp	7	4	3	7	5	8	10	24	
	Glu	166	41	161	266	33	121	146	241	Glu	9	5	16	15	8	14	11	23	
Basic	Lys	169	54	179	132	66	309	171	190	Lys	14	7	24	17	21	28	9	18	
	Arg	138	26	191	104	13	99	26	38	Arg	14	5	35	7	6	34	7	12	
	His	92	80	52	120	14	81	42	76	His	8	6	5	10	2	11	4	3	
<b>Most Cited Peptide</b>		<b>Gly</b>	<b>Pro</b>	<b>Ala</b>	<b>Ala</b>	<b>Leu</b>	<b>Val</b>	<b>Gly</b>	<b>Ala</b>	<b>Most Cited Peptide</b>	<b>Gly</b>	<b>Pro</b>	<b>Ala</b>	<b>Gly</b>	<b>Leu</b>	<b>Ala</b>	<b>Gly</b>	<b>Ala</b>	

**Figure 3.10 – Gelatinase Consensus Sequence.** MEROPS database collates the publication information available per MMP which has been replicated in this table. The number in each box refers to the number of citations for amino acids at each position along the scissile bond. For those amino acids that have a greater number of citations (red), there can be confidence that the MMP will act on that sequence when arranged at that site. For both gelatinases, there is a consensus on the non-prime side and at the cleavage site, P2' is the only position where there is variation in the consensus sequence between MMP-2 and MMP-9 (Val and Ala respectively). The cell adhesive peptide (RGD) is substituted in the prime side of the scissile bond. Number of citations were coloured on a scale from red (many citations) to green (few or no citations).

## A Scissile Bond Preference for MMP-2



## B Scissile Bond Preference for MMP-9

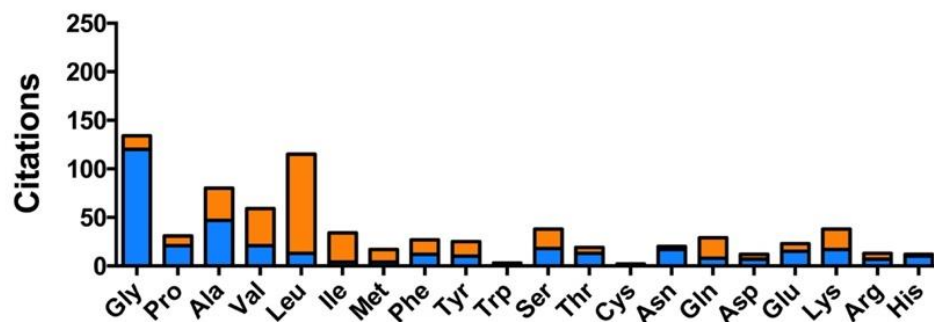


**Figure 3.11 - Scissile Bond Preference.** For all amino acids for position P1 and P1' for both MMP-2 and MMP-9, it is apparent there is a preference for Leu at the prime side. The P1 position for both MMP-2 and MMP-9 is occupied by small amino acids. For MMP-9 it is clearly defined (Gly) in comparison, MMP-2 has similar preference for small amino acids at P1 (Ala or Gly).

We also analysed the consensus sequence for other MMPs (Figure 3.12). Plotting the preference (number of citations) for each of the amino acids in the sequence, we compared the number of citations at each position for the MMPs identified. Figure 3.12 reveals that MMP-2 has the most citations as expected. MMP-9 has the next highest citations, particularly on the non-prime side of the sequence and P1', this should be expected due to the redundancy of the gelatinase family. However, the data available for the other MMPs shows that there are less than 100 citations per amino acid at each position. It is apparent from position P2' that there are less citations for Arg at this position for MMP-2 and is cited equivalent number of times with that of other MMPs. However, from Figure 3.8, only MMP-1 & -3 were identified and not expressed at the same concentration as MMP-2 in MSC supernatant and therefore it is more likely that MMP-2 is responsible for cleavage.

## Number of Citations at P4-P4' for Sequence GPAG↓LRGD for Selected MMPs

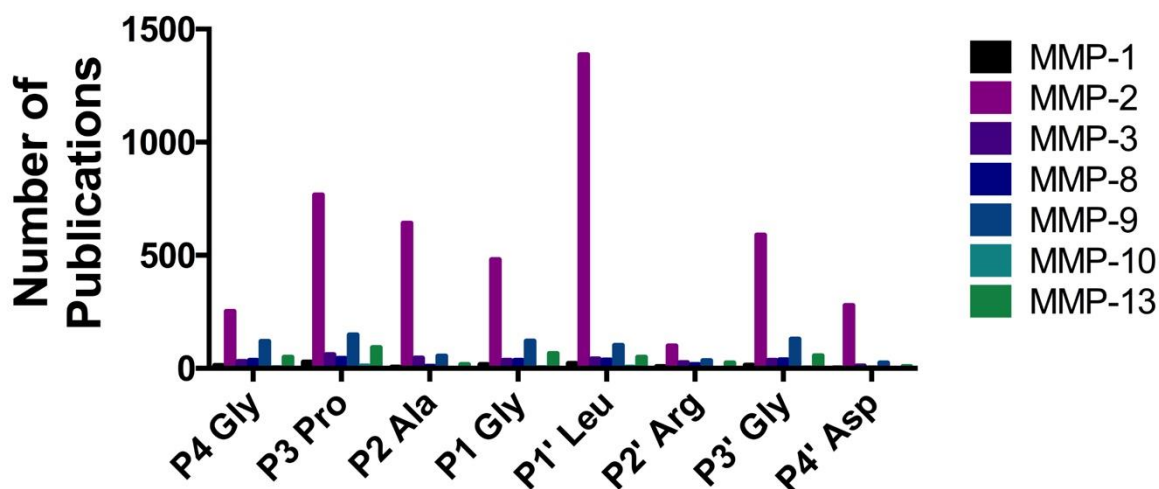


**Figure 3.12 -Preference of Other MMPs for the Sequence GPAG↓LRGD (P4-P4').** Several MMPs were identified from the supernatant of MSCs. Looking at the number of citations for each amino acid for the selected sequence GPAG↓LRGD we see that MMP-2 is favorable for all positions. Therefore, we have confidence that MMP-2 will act on the selected sequence alone.

Table 3.4 shows the most highly cited amino acids along the scissile bond for selected MMPs. The data was collected from the MEROPS database and analysed as in Figure 3.10. From this data, it is obvious that there are similar preferences for certain positions regardless of MMP family. These include Gly at P4, Pro at P3, small hydrophobic at P1 and Leu at P1'. There is a use of polar amino acids in MMP-8 and MMP-10 consensus sequence which may prevent cleavage of the selected sequence by these MMPs. There is also a preference for Arg at the P2' position, however, these MMPs are not expressed by MSCs and therefore will not contribute to surface cleavage.

**Table 3.4 – Consensus Sequences for Selected MMPs.** Preferred amino acids at P4-P4' for MMPs-1,3,8,10 & 13, taken from MEROPS database.

MMP	Scissile Bond							
	P4	P3	P2	P1	P1'	P2'	P3'	P4'
MMP-1	G	P	L/Q/E	A	L	K/R	G	A
MMP-3	G	P	A	G	L	R	G	P
MMP-8	G	P	S	G	L	R	G	L
MMP-10	G	P	A/G	G	L	S	T	A/G

<b>MMP-13</b>	G	P	P/L	G	L	R	G	P
---------------	---	---	-----	---	---	---	---	---

### 3.3.3 Design and Synthesis of the Surface

With identification of a consensus sequence for the gelatinases, synthesis was then carried out. Figure 3.13 shows the successive coupling of each amino acids from Fmoc-D to full PEG-GPAG↓LRGD sequence which we have shortened to DIGE-D for digestible adhesive peptide, -D indicating RGD. Deprotection and coupling are repeated for all amino acids in the sequence which are then capped with a PEG group after deprotection of the last amino acid (Fmoc-Gly). The sequence is synthesised bottom up from P4'-P4 which is then capped with PEG. Cleavage is hypothesised to occur between prime (green) and non-prime (orange) amino acids.

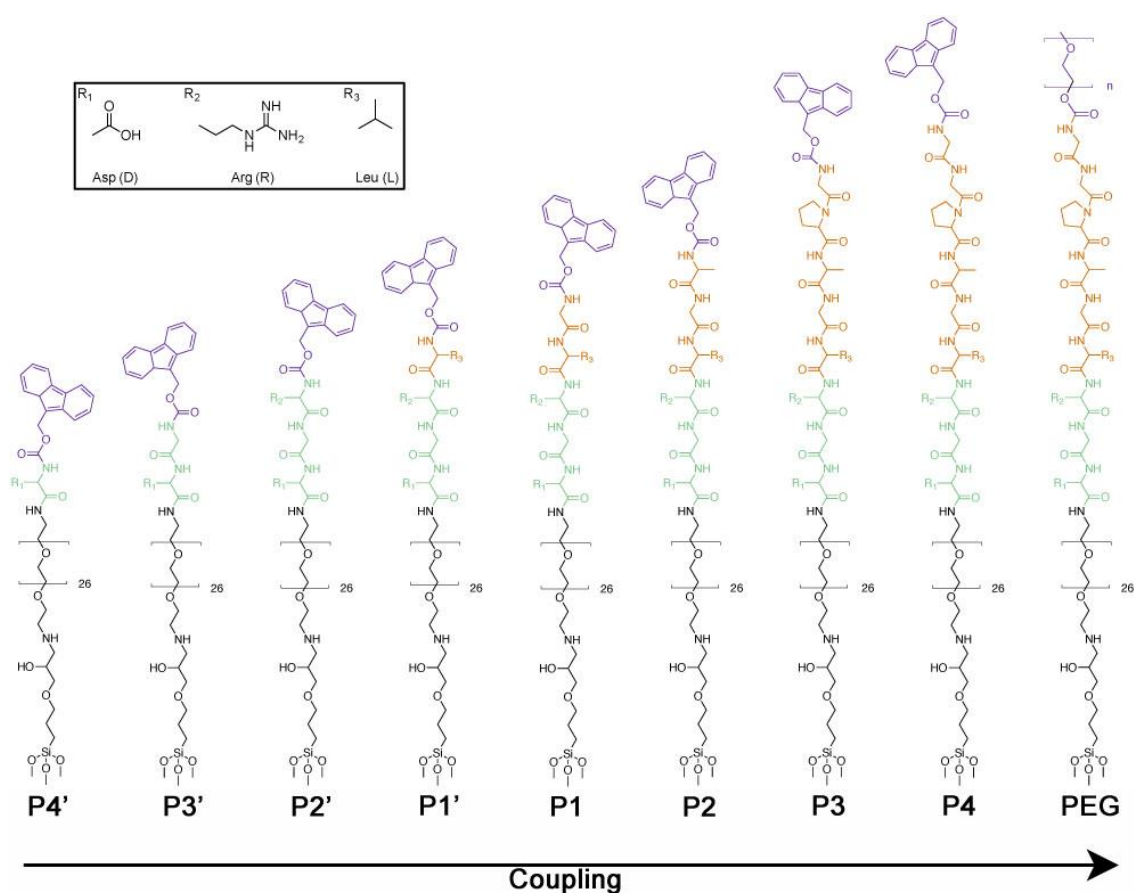


**Figure 3.13 - Progression of SPPS for Sequence PEG-GPAG↓LRGD.** Amino acids are added to the pre-treated surface (silane and PEGylation, black) from non-prime side, bottom up starting with Fmoc-Asp (P4'). Green = prime amino acids, orange = non-prime amino acid, purple = protecting (Fmoc) or blocking (PEG) group. Side chains for Asp, Arg and Leu are shown in the box.

### 3.3.4 Surface Characterisation

#### 3.3.4.1 Pre-treatment

Prior to amino acid addition, there are certain pre-treatment stages required to provide a free amine for the first amino acid to bind to (as described in Chapter 1, Section 1.8.1).

This includes cleaning (piranha solution), silanization (to create a flexible linker) and PEGylation (to provide a free amine), each of which can be tracked using WCA measurement (Figure 3.14) (Zelzer et al., 2012). Cleaning the surface by both solvent cleaning and acid cleaning increases the hydrophilicity of the surface. Coating with silane also increases the hydrophobicity due to the covalent attachment of epoxide groups (from  $40.4 \pm 4.4$  to  $39.7 \pm 3.3$ , Table 3.5). PEG is known to be hydrophilic, with an WCA of  $39.7 \pm 3.3$  (Table 3.5) being recorded suggesting that the PEG diamine has efficiently bound to the surface and the pre-treatment stages have primed the surface ready for amino acid addition.

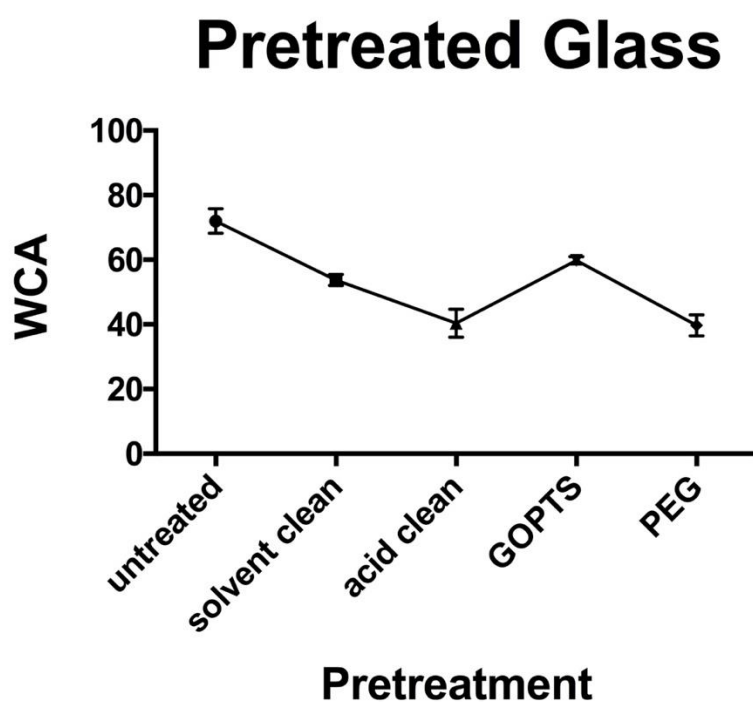


**Figure 3.14 - Water Contact Angle of Pre-Treated Glass Coverslip Prior to Amino Acid Addition.** There are various pre-treatment stages to create a free amine for a condensation reaction with carboxylic tail of the first amino acid. After washing, contact angle increases with silane addition then decreases with PEG monolayer. Pre-treatment is complete as PEG is in place for amino acid addition. Graph shows mean  $\pm$  SD, 50 images per dataset with 15 datasets taken across 3 substrates (n=450 images per set).

**Table 3.5 - Quantification of WCA for Pre-Treatments.** WCA measurements of untreated glass, cleaned glass, silane and PEG diamine treatment. Values correspond with Figure 3.14; standard error was calculated using 50 images per dataset with 15 datasets taken across 3 substrates (n=450 images per set).

Sample	Average
Untreated Glass	72.0 $\pm$ 3.8
Solvent Clean	53.7 $\pm$ 1.7

Acid Clean	40.4 ± 4.4
GOPTS	59.8 ± 1.1
PEG <sub>26</sub> diamine	39.7 ± 3.3

Due to the robustness of the technique, no further characterisation was carried out. The coating of coverslips with silane was originally published by Piehler *et al.* who demonstrated homogeneous coating utilising GOPTS that could be functionalised with PEG (Piehler *et al.* 2000). This resultant PEG layers was found to be of a higher density that was better ordered than using other amino-functionalised silanes (Piehler *et al.* 2000).

### 3.3.4.2 Amino Acid Addition

Amino acid addition was analysed firstly using ToF-SIMS. ToF-SIMS is used to analyse material surface properties by scanning the surface with a primary ion beam which causes the emissions of secondary ions that are then analysed (Hagenhoff 2000). A time of flight ioniser is used to measure the mass to charge ratio ( $m/z$ ) of the emitted ions. This is more advantageous than techniques such as WCA (which only monitors a change in surface properties) as it can distinguish between different proteins based on molecular structure (Wagner & Castner 2001).

Measurements can also generate images of the surface from the ion spectrum (Figure 3.15). We can use the emitted secondary ions to determine the abundance of specific compounds on the surface, the lighter the image the more abundant that compound is. Silicone is an indicator of untreated glass which was abundant as expected on the glass control, indicating little or no contamination of the substrate. The abundance of silicone decreased with the completion of the full-length sequence (DIGE-D). This suggests that the glass coverslip had been treated effectively by the SPPS procedure. PEG was not identified on the glass control but increases after treatment, suggesting SPPS had been carried out as expected and capped with PEG. The total ion column is the sum of all ion intensities and was used to demonstrate uniform signal intensity over the whole sample. This was slightly heterogeneous for the glass control, indicating some scratching on the surface. However, after modification the surface is a more homogeneous layer. Normalised ion intensity was quantified for both PEG and silane ( $m/z = 45$ ,  $m/z = 28$ , Figures 3.15B & C respectively). This shows that the surface had been modified and that PEG blocking group is in place.

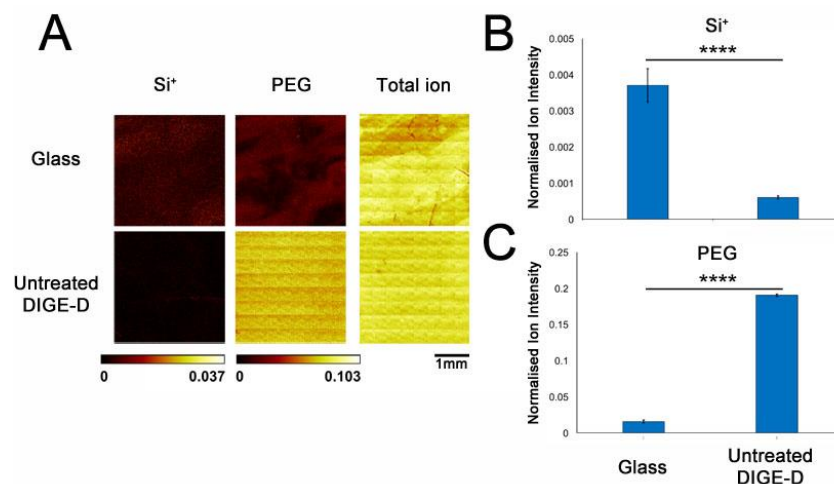


**Figure 3.15 - ToF-SIMS Images for SPPS Build-Up.** A) ToF-SIMS images and average ion intensities of surface B) before and C) after modification. The ion images were normalised to the total ion intensity. Images show a reduction in silane and increase in PEG after SPPS indicating completion of sequence. PEG was measured at  $m/z = 45$  and glass ( $\text{Si}^+$ ) measured at  $m/z = 28$ . B & C were quantified as normalised ion intensity and confirmed the abundance of silane for untreated and PEG for treated surface, \*\*\*\* $p < 0.0001$  as determined by t-test, graphs show  $\pm$ SD,  $n=4$ .

We can also look for individual mass to charge ratios of the expected amino acids (Table 3.4). Unfortunately, there was some contamination observed on untreated glass sample, specifically, Pro and Ala fragments. We would expect an increase of signal intensities on the peptide surface in comparison to glass. Indeed, peaks were observed at all expected  $m/z$  ratios for the DIGE-D samples (Figure 3.16A). Figure 3.16 B shows the same information but as an image where the last frame in Figure 3.16B compares the ion intensity of the complete peptide. There was an increase of full peptide surface for DIGE-D in comparison to glass demonstrating that although there was some contamination of the glass sample, peptides characterised on DIGE-D were more abundant (Figure 3.16B). The results are consistent with Figure 3.15, as the presence of PEG could also be viewed ( $m/z = 45$ ) for DIGE-D sample alone, confirming no PEG was observed on the untreated sample.

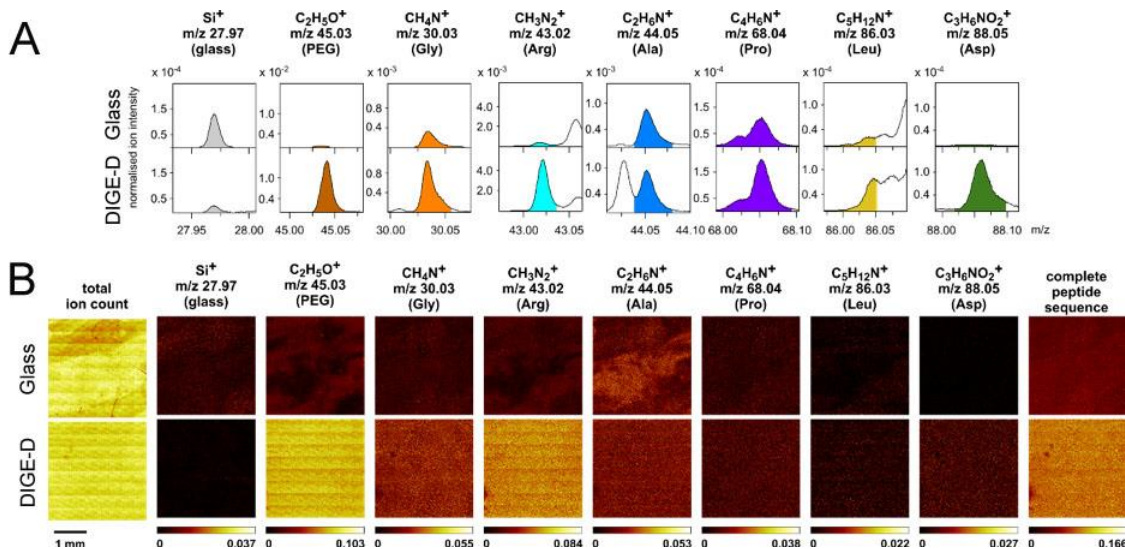


**Figure 3.16 – ToF-SIMS Analysis of Amino Acid Addition.** A) The spectra were normalised to the total ion intensity and plotted on the same scale. Signal intensities show expected amino acids on the DIGE-D surface, reduction of silane and presence of PEG. B) ToF-SIMS images of surface showing abundance of complete peptide sequence for DIGE-D samples.

The intensities of each amino acid were plotted for both glass and DIGE-D samples (Figure 3.17A). It is important to note that some amino acids in this sequence have weak ion intensities specifically, Pro and Leu (Figure 3.17A). Stronger intensities appear as a result of some amino acids producing a higher amount of stable secondary ions than others. These generate higher signals and are better indicators of the presence of the sequence (Hagenhoff 2000). The remaining amino acids, Arg, Gly, Ala and Asp were present on the surface at a higher intensity than that of glass ( $p < 0.0001$ ,  $p < 0.0001$ ,  $p < 0.01$  and  $p < 0.01$  respectively). The lack of PDMS signal on the treated surface suggests that there was no contamination of the substrate during synthesis (Figure 3.17B). If contamination had been observed, then signal may be compromised for the expected amino acids. As this is not the case, we can determine that we are indeed witnessing a true weakness of signal.

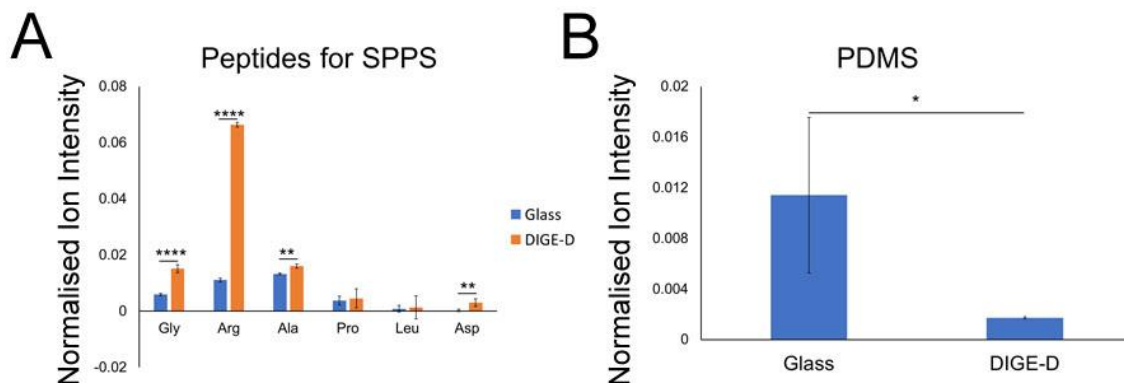


**Figure 3.17 – Quantified Normalised Ion Intensity per Substrate and Potential Contamination by Other Factors.** A) Ion intensity was calculated per amino acid at defined m/z ratios and normalised to total ion intensity then plotted on the same scale. Results show signal intensities for Gly, Arg, Asp and Ala but highlight weakness in signal for Pro and Leu. Statistics calculated by ANOVA, statistics shown for differences in normalised ion intensity for that amino acid on glass in comparison to the DIGE-D sample. \*\*\*\*p<0.0001 and \*\*p<0.01. B) Contamination by PDMS was not observed on DIGE-D surface, indicating efficient synthesis \*p<0.05, determined by t-test, graphs show  $\pm$ SD, n=4.

Due to the weakness in signal as a result of the poor ionisation of some amino acids in the sequence, the technique was complemented with fluorescence spectroscopy (Figure 3.18) and WCA measurements (Figure 3.19). An advantage of Fmoc protection is that Fmoc itself is fluorescent (Behrendt et al. 2016). Using fluorescence spectroscopy specifically designed by Zelzer *et al.* for analysis of 2D coverslips, we can track progression of coupling and deprotection via the presence or absence of the Fmoc on the coverslip at each stage of SPPS process (Zelzer et al., 2012). A specific holder for coverslips had been previously produced enabling the light path (excitation at 270 nm) to hit the coverslip at an angle, allowing detection of reflected light (emission 320 nm) (Figure 3.5) (Zelzer et al., 2012). The resulting peak on the spectra at 320 nm indicates the presence of Fmoc, which is removed after the deprotection stage. To evaluate the progression of SPPS, coverslips were removed from the batch 24 hours after amino acid addition and immediately after treatment with piperidine to demonstrate both Fmoc protection and deprotection stages (Figure 3.18). It was found that surfaces containing Fmoc emitted a spectrum at 320 nm suggesting that the Fmoc protected amino acids were coupled to the surface as expected. In comparison to those that had been treated with piperidine (to remove Fmoc), no peak was observed at 320 nm nor was any fluorescence signal detected suggesting effective removal of Fmoc in the deprotecting stage. This was tracked during the whole SPPS process for every amino acid in the sequence and implies that Fmoc amino acids were added. Although the data is not quantitative, the technique was reproducible between coverslips (n=3)

and provides an indication that effective SPPS build up has occurred. As for the final blocking group, PEG is not fluorescent and therefore the cap could not be confirmed using this technique.

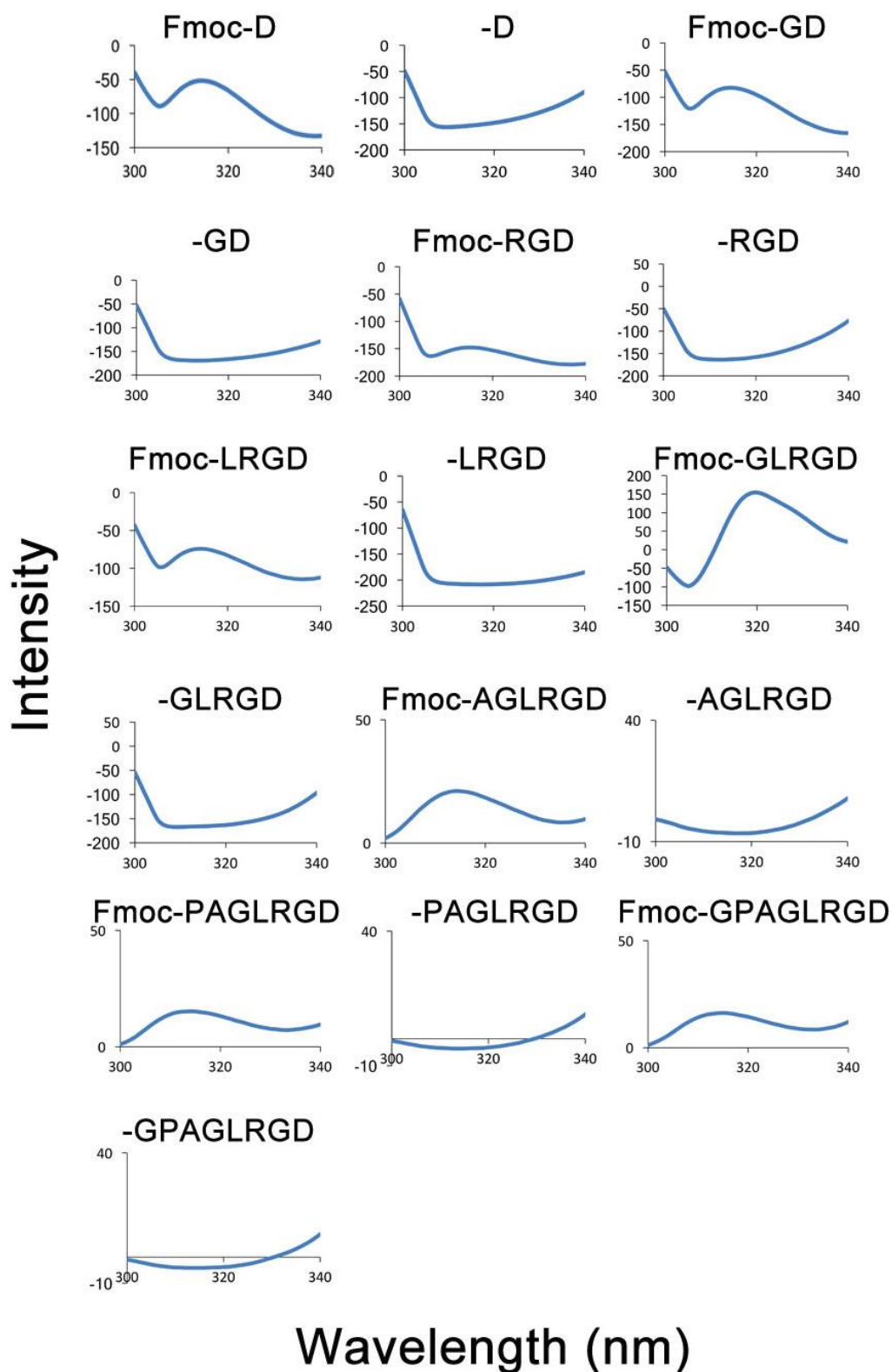


**Figure 3.18 - Fluorescent Spectroscopy of Amino Acid Addition.** Stepwise construction of peptide chain from Fmoc-D to -GPAG↓LRGD. Figures show emission spectra at 320 nm when excited at 270

nm. No peak was observed after each deprotection step suggesting effective deprotection of the amino acid.

WCA measurement was also used as Fmoc protected amino acids have slightly higher hydrophobic signature than their deprotected counterparts (Rawsterne et al. 2006). Coverslips were analysed before and after piperidine treatment to observe amino acid protection and deprotection stages. For all Fmoc protected amino acids, a more hydrophobic angle was observed ( $>50^\circ$ ) (Figure 3.19). When the piperidine is applied, we observed a significant reduction of WCA for unprotected amino acids in comparison to their protected counterpart ( $p < 0.0001$ , Table 3.6). This suggests that Fmoc protection and deprotection occurred and SPPS progressed as expected. The protecting side chains may also affect the WCA result. After addition of Arg (where the side chain is protected by Pbf to prevent acylation), angle measurement increases for subsequent coupling and deprotection stages ( $50.9^\circ \pm 2.6$  to  $65.0^\circ \pm 3.7$  with Arg addition). PEG is hydrophilic and therefore has a characteristically low contact angle value. Using this method, we can also observe the presence of the PEG capping group at a lower WCA in comparison to uncapped sequence ( $51.5^\circ \pm 1.6$  vs  $42^\circ \pm 1.5$ ).

## WCA for protected and deprotected amino acids

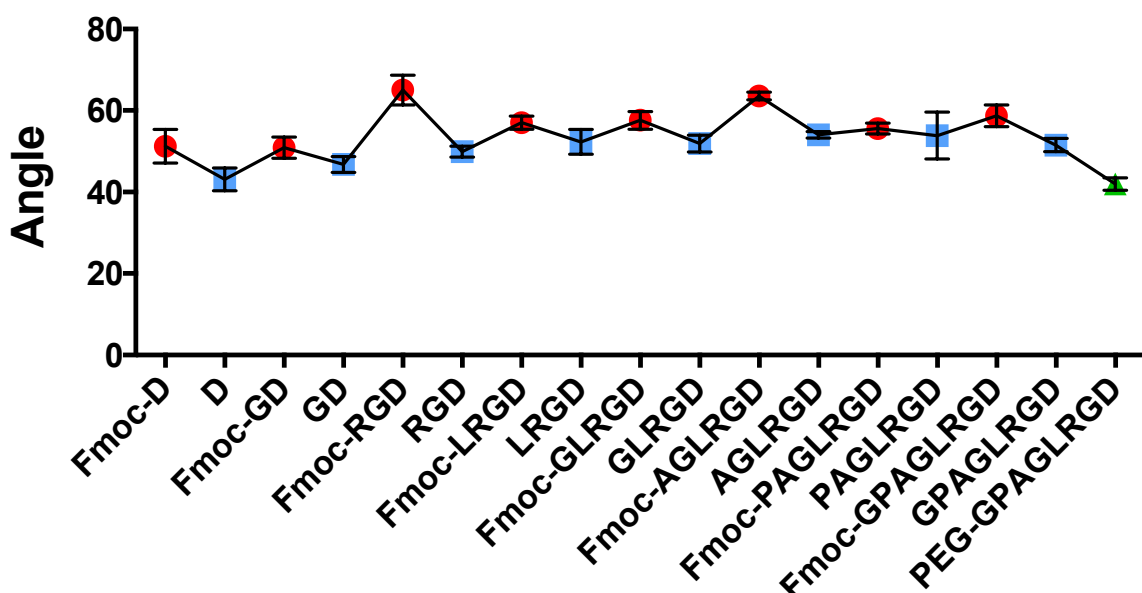


**Figure 3.19 - Water Contact Analysis of Amino Acid Addition.** Increase of WCA occurs after Fmoc coupling (red) this is reduced with removal of Fmoc in deprotection stages (blue). As PEG is a hydrophilic molecule we would expect a low angle, and the final sequence PEG-GPAGLRGD (green) exhibits such a value ( $42^\circ \pm 1.5$ ). This data suggests SPPS was completed as expected.

**Table 3.6 - Quantification of WCA for Amino Acids.** WCA measurements of each stage of SPPS (addition and deprotection). Values correspond with Figure 3.19; standard error was calculated using 50 images per dataset with 15 datasets taken across 3 substrates (n=450 images per set). Statistics calculated by ANOVA and stated for comparison of Fmoc protected and unprotected amino acids only, \*\*\*\*p<0.0001.

Fmoc Protection		Fmoc Deprotection		P value
Sequence	Angle	Sequence	Angle	
Fmoc-D	51.3 ± 4.1	D	43.1 ± 2.8	****
Fmoc-GD	50.9 ± 2.6	GD	46.8 ± 1.9	****
Fmoc-RGD	65.0 ± 3.7	RGD	49.9 ± 1.3	****
Fmoc-LRGD	57.0 ± 1.6	LRGD	52.3 ± 3.0	****
Fmoc-GLRGD	57.6 ± 2.2	GLRGD	51.9 ± 2.1	****
Fmoc-AGLRGD	63.6 ± 0.9	AGLRGD	54.0 ± 0.8	****
Fmoc-PAGLRGD	55.6 ± 1.3	PAGLRGD	53.8 ± 5.8	****
Fmoc-GPAGLRGD	58.7 ± 2.7	GPAGLRGD	51.5 ± 1.6	****
		PEG-GPAGLRGD	42.0 ± 1.5	-

### 3.3.4.3 DIGE-D Cleavage

Based on results from fluorescence, ToF-SIMS and WCA, we were satisfied that the surface had been made to completion with amino acid addition occurring as expected. With the surface complete, we performed *in vitro* experiments to determine surface cleavage. DIGE-D coverslips were incubated with defined concentrations of MMP in serum free media. The concentrations were chosen to reflect MSC gelatinase supernatant concentration in response to DIGE surface (as determined by ELISA in Figure 4.14). From the MEROPS data, we designed the sequence with the hypothesis that cleavage occurs between G and L in the sequence GPAG↓LRGD (Figure 3.20A). Using ToF-SIMS we evaluated the ion intensities for the full-length peptide (sum of ion intensity of all amino acids in the sequence GPAG↓LRGD). As expected, the untreated DIGE-D has an abundance of the full-length peptide which is reduced upon treatment by the gelatinases (p<0.0001, Figure 3.20B). This indicates that the MMPs are reducing the presence of the full-length fragment, indicating cleavage. There was a further reduction in the abundance of full length peptide when treated by MMP-9 in comparison to MMP-2 (p<0.01, Figure 3.20B). This was unexpected due to the small concentration and activity of MMP-9 observed in Figure 3.7 & 3.8 in comparison to MMP-2, this indicates MMP-9 is more potent than MMP-2, which was unexpected. We

were unable to accurately determine cleavage at G↓L due to the weak ionisation of the amino acids of the remaining fragment.

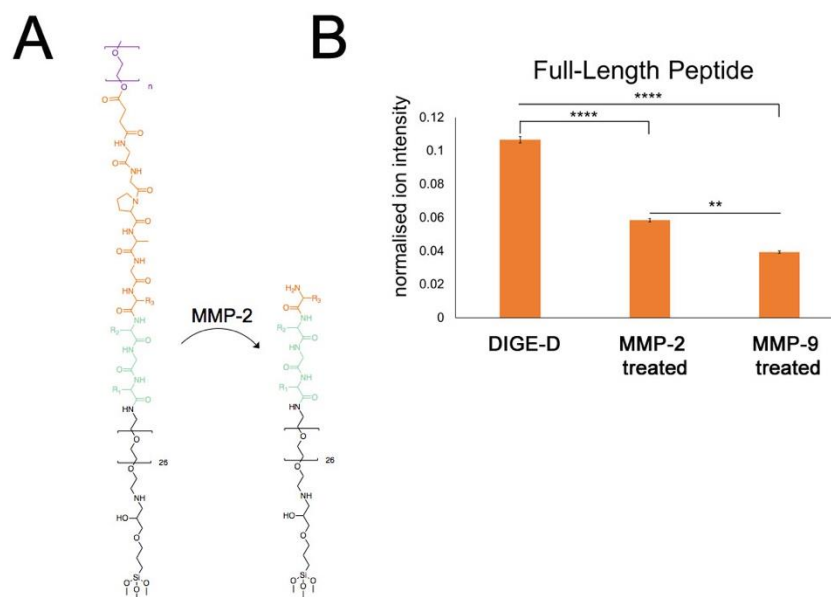


**Figure 3.20 – Cleavage by MMP-2 on Sequence PEG-GPAG↓LRGD.** A) It is hypothesised that cleavage of the sequence will occur between G↓L as determined by MEROPS. The sequence LRGD is thought to remain on the glass coverslip after PEG-GPAG↓ removal. The schematic indicates the chemical composition of the surface before and after MMP cleavage. Purple = PEG cap, orange = GPAG fragment removed after cleavage, green = LRGD remaining fragment, black = pre-treated surface. B) Normalised total ion intensity of GPAG↓LRGD amino acids before and after treatment with gelatinases. DIGE-D coverslips were treated with 20 ng/ml MMP-2 and 0.25 ng/ml MMP-9 as in cell supernatant concentration for three weeks. Statistics calculated by ANOVA where \*\*\*\* $p < 0.0001$  and \*\* $p < 0.001$ , graphs show  $\pm$ SD,  $n=4$ .

Cleavage was also analysed by observing the abundance of the PEG cap. The image in Figure 3.21A shows that there is an abundance of PEG for the untreated sample. This is reduced after treatment with the gelatinases. The image of total ion intensity is also displayed (Figure 3.21A). This indicates that surface is uniform before and after treatment by MMPs. This was then displayed graphically, showing peaks for PEG which was reduced when treated with gelatinases. PEG was quantified (from the ion intensity of PEG per sample) in comparison to the untreated surface to determine % removal of PEG. Figure 3.21B indicates that the PEG blocking group was reduced by both gelatinases at approximately 80 % removal for MMP-2 and 85 % removal for MMP-9. This figure again highlights a difference in MMP-2 efficiency in comparison to MMP-9 ( $p < 0.01$ ). To evaluate the effects of unspecific loss of peptides, this data was also expressed as a ratio which was calculated from total ion intensity of both PEG and the full peptide sequence (Figure 3.21C). This highlights that as PEG is removed,

the presence of peptide sequence material increases, indicating that removal of PEG by enzyme or unspecific loss of peptide chain still results in increased expression of peptides on the surface ( $p < 0.0001$ ). The data presented in Figures 3.15 – 3.21 suggests that the cell secreted concentration of MMP was sufficient to cleave the surface although MMP-9 is potentially a better candidate for cleavage of the sequence than MMP-2.

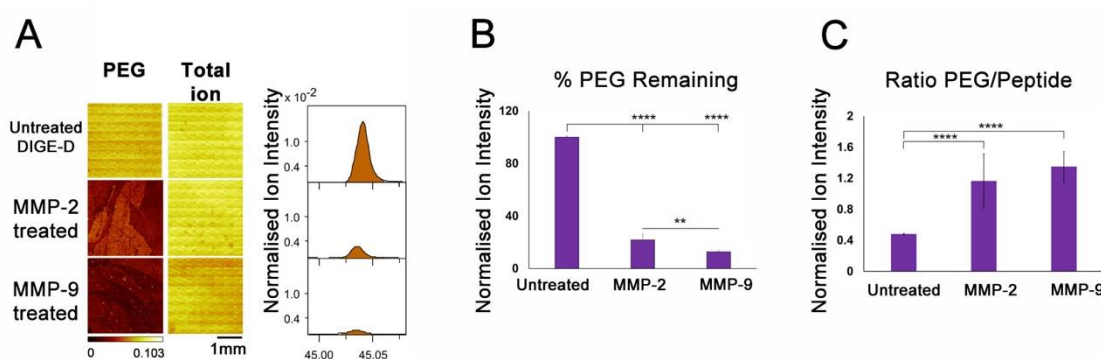


**Figure 3.21 - PEG Remaining After Gelatinase Treatment.** All samples refer to cleavage by 20 ng/ml MMP-2 and 0.25 ng/ml MMP-9. A) Images of DIGE-D surface before and after treatment with gelatinases. PEG column indicates there is an abundance of PEG on the untreated sample which is reduced in response to MMP treatment. B) Quantification of PEG total ion intensity expressed as a percentage of total ion intensity present on untreated surface. Graph indicates reduction by ~80% for both gelatinases. C) Ratio of PEG vs peptide intensity increases after treatment suggesting there is less PEG and more peptide on the surface. Reduction in PEG expression suggests cleavage occurs. Statistics calculated by ANOVA for both graphs, \*\*\*\* $p < 0.0001$  and \*\* $p < 0.01$ , graphs show  $\pm$ SD,  $n=4$ .

### 3.3.4.4 Surface Response to Supernatant

We also used ToF-SIMS to determine the effects of cell supernatant deposition on the surface (Figure 3.22). The total ion column indicates the generation of uniform sequence for Glass, PEG<sub>26</sub> diamine and untreated coverslips. Supernatant from glass coverslips was saved at week 2 then added to fresh DIGE-D surface. When treated with supernatant, it is clear that there was a heterogeneous surface with deposition of surface proteins that have accumulated on the surface. PEG<sub>26</sub> diamine was not found on untreated glass coverslips (in line with previous experiments) but increases with PEGylation and addition of PEG blocking group. With the addition of cell supernatant, we can see a reduction in PEG, this suggests cleavage of the surface by enzymes in the media. However more experiments would need to be conducted to confirm which MMP found in the supernatant is acting on the sequence.

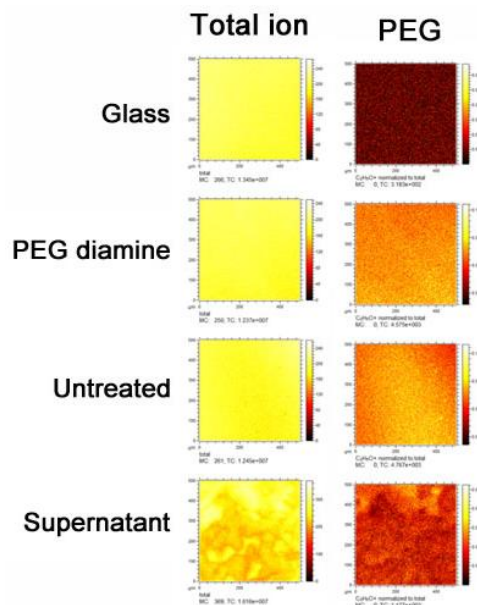


**Figure 3.22 – Supernatant Treatment of DIGE-D.** Prior to supernatant addition, a homogenous surface is observed for all stages of SPPS; untreated glass, PEGylation and untreated DIGE-D. Presence of PEG is observed in abundance for PEGylated and untreated samples as expected. Supernatant was saved from MSCs cultured on glass coverslips for 2 weeks, then added to fresh DIGE-D coverslip and incubated for 24 hours. PEG is reduced in response to cell supernatant suggesting supernatant is sufficient to reduce surface bound PEG.

### 3.4 Discussion

We have previously shown, along with our collaborators, that peptide motifs as presented to cells by SPPS have been sufficient to control and direct cell behaviour (Roberts et al., 2016; Todd et al., 2009; Zelzer et al., 2012). As described in Chapter 1, Figure 1.9 we aimed to create a surface that was amenable to cell secreted MMPs.

We have confirmed that MMP-2 is the MMP preferentially secreted by MSCs. Using zymography, ELISA and antibody arrays, MMP-2 is the most consistently expressed MMP at the highest concentration (Figure 3.7-3.9). MMP-1 & -2 were also identified at three weeks using antibody arrays (Figure 3.9) and MMP-9 concentration increased at week 4 (Figure 3.8). However, the expression of these MMPs was significantly lower than the expression of MMP-2 ( $p < 0.0001$  and  $p < 0.001$  respectively). This data led us to believe that MMP-2 would be the enzyme responsible for cleavage of the sequence. However, due to the redundancy of the gelatinases and the increase in MMP production at week 4 (Figure 3.8), we designed the sequence to be amenable to both MMP-2 and MMP-9. Therefore, the sequence that was selected was PEG-GPAG↓LRGD, which mimics the position of Pro at P3, scissile bond to be between G↓L and use of small hydrophobic amino acids (Figure 3.10-3.11). RGD was

substituted into the prime side of the sequence. The sequence was abbreviated to DIGE-D to denote digestible peptide. Due to the time taken to synthesise the sequences, we were unable to test sequences that did and did not substitute RGD to the prime side (GPAG↓LRGD in comparison to GPAGL↓V/AGARGD) to better understand efficiency of cleavage by the gelatinases (Section 3.3.2). This was a limitation and if synthesis had been of higher throughput, multiple sequences could have been compared to find the most efficient and specific sequence.

As stated above, manual synthesis was time consuming. Synthesis of materials manually took 1 month. This was a limitation and it would have been better to automate synthesis however; this technique was not available to us. In addition, there may have been areas where synthesis could have been improved, for example, when coating coverslips in PEG diamine. This procedure was again done by manually spreading molten PEG over the surface of the coverslip. This does not guarantee a homogeneous surface and due to human error, there could be areas in PEG distribution. This could have created local areas where there was no coating by peptides which will have an effect on cell behaviour and potentially create an unsynchronised population of cells. In hindsight it would have been better to confirm coating efficiency utilising the ninhydrin test (Pires et al. 2014). The test is a simple colour change that indicates the presence of free amines (solution is blue in presence of free amine). This could also have been utilised at the coupling stage to confirm that all free amines were bound and that the correct combination of peptides were added. Based on the result of the test, coupling could have been repeated until there was no free amine available. By not ensuring efficiency, there is a risk that deletion peptides, peptides with the wrong sequences or areas with no peptide could be found on the surface, which may have an affect the biological result.

We utilised several techniques to confirm the presence of peptides. Using WCA and fluorescent spectroscopy we can track the presence of the Fmoc moiety in terms of its hydrophobicity and fluorescent properties. The addition of Fmoc protected amino acids results in the presence of a peak of 320 nm when excited by 270 nm as shown in Figure 3.19. Presence of Fmoc is also categorised by a larger WCA and is therefore hydrophobic (Figure 3.19). Analysing successive rounds of SPPS using WCA and fluorescent spectroscopy allows tracking of coupling and deprotection stages in real time. There is a limitation to using fluorescent spectroscopy and WCA measurement. Fluorescence only shows the presence or absence of Fmoc and although is an indicator

of SPPS, it is not quantitative. Similarly, WCA is only a measurement of the hydrophobicity of the surface and can be caused by other properties such as topography. Both techniques comment on the change of surface but not the chemical modification.

Utilising ToF-SIMS has the advantage of looking at surface properties including chemical composition. The chemical signature of all reagents was identifiable by m/z ratios. We observe the reduction of silane signal ( $\text{Si}^+$ ) indicating the presence of peptides and the increase of PEG suggesting the blocking group is in place (Figure 3.15-3.17). Figure 3.16 shows the presence of all expected amino acids are observed on the surface indicating successful synthesis. Taken together, (with knowledge of the limitations of each strategy) this data strongly suggests that SPPS has been completed and synthesised as expected and all amino acids are in place. ToF-SIMS is qualitative and can be used to comment on the chemical composition, but in this case, is a challenge due to the weakness in ion intensities of selected amino acids. We also tried to confirm the presence of peptides by high-performance liquid chromatography (HPLC), but it was thought that the concentration of peptide was too low. We also utilised Raman spectroscopy to identify the presence of peptides on 2D surface as described by Sahoo *et al.* however, we could not replicate the results (Sahoo *et al.* 2016).

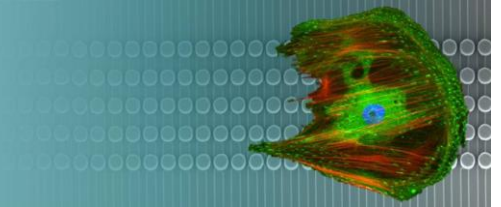
Using recombinant MMP, we can conclude that cleavage of the surface is occurring as monitored by ToF-SIMS where we see approximately an 80 % reduction of PEG with the addition of each gelatinase (Figure 3.21). It was observed there was further cleavage when treated by MMP-9 than MMP-2 suggesting MMP-9 may be more efficient (Figure 3.20-3.21). This was an unexpected observation, which has several potential interpretations. Namely, MMP-9 (0.25 ng/ml) is more potent than MMP-2 (20 ng/ml) or MMP-2 was added in excess and its activity compared to MMP-9 cannot be inferred. The amino acid sequence selected was permissive for both gelatinases and therefore action by both MMPs is not unexpected. Thus, potency of the respective enzymes requires further investigation. To achieve this would require an exhaustive dose response curve which was unachievable during this PhD, as it would have comprised more months of synthesis and expense in utilising TOF for analysis.

Finally, this experiment was also carried out using cell supernatant showing a decreasing abundance of PEG in response to cell secreted enzymes (Figure 3.22). It

would have been prudent to block expression of MMP-2 and MMP-9 in culture either utilising small molecule inhibitors or siRNA to confirm these enzymes were responsible for cleavage alone.

### 3.5 Conclusions

Based on initial results of increasing concentrations of MMP-2, a gelatinase responsive surface was designed using bioinformatics data and synthesised using SPPS. Although we have shown there is more abundance of MMP-2 expressed by MSCs, cleavage data suggests it is not necessarily more efficient than cleavage by MMP-9. More experiments will have to be conducted to understand MMP potency in response to DIGE-D surfaces.



## 4. Biocompatibility

This chapter aims to determine the initial cell response to the surface chemistry in terms of biocompatibility. We also created other surface chemistries including those with the non-adhesive peptide (RGE) incorporated as controls. We utilised live/dead staining, alamar blue and methylthiazolyldiphenyl tetrazolium (MTT) assay to determine cell viability in response to the peptides. The surface chemistry (particularly RGE controls) did seem to affect cell behaviour initially however, this became less apparent with increasing time in culture. Further, we analysed cell adhesion and the presence of ‘super-mature’ adhesions, which were increased on RGD controls comparison to RGE; confirming that RGE is non-adhesive to cells and RGD is manipulating cell adhesion. MMP secretion was also determined and MMP-2 was found to increase on DIGE surfaces after 3 weeks in culture. These factors provide initial data that suggests the cells are responding favourably to the surface chemistry in that they are surviving, adhering and responding to the enzyme sequence with an increase in MMP-2 secretion.

## 4.1 Introduction

As discussed in Chapter 1, the presence of peptide motifs incorporated into a material are sufficient to direct cell behaviour. The use of RGD has shown great successes in directing behaviour of MSC differentiation (Kilian & Mrksich 2012). The method of SPPS to graft RGD to the surface has also been proven to be effective (Todd et al. 2009; Zelzer, McNamara, et al. 2012; Roberts et al. 2016).

The previously designed enzyme responsive peptide surface (as described in Chapter 1, Figure 1.11) was user controlled and contained an Fmoc cap group (Fmoc-A↓ARGD). Biocompatibility of MSCs cultured on Fmoc-A↓ARGD was demonstrated by Roberts *et al.* using both live/dead staining and MTT assay (Roberts et al. 2016). In addition to the enzyme remodelled surface (Fmoc-A↓ARGD) a non-adhesive capped surface was also synthesized (Fmoc-A↓ARGE) and pre-cleaved ARGD and ARGE controls. It was shown that the surface chemistry did not negatively affect the survival of cells on the surface (Roberts et al. 2016). With exception of PEG<sub>18</sub> diamine and RGE controls, survival was observed on all other controls (Roberts et al. 2016). PEG is known to be anti-fouling and non-adhesive therefore cell adhesion to PEG is not expected (Dong et al. 2011). The results of the live/dead stain carried out in the Roberts paper is shown below (Figure 4.1) (Roberts et al. 2016). Figure 4.1A shows the non-adhesive properties of RGE which resulted in fewer cells binding as would be expected on this surface; those that did attach however, survived. The results also highlighted that Fmoc did not negatively affect cell

survival and therefore the blocking group was biocompatible (Figure 4.1A). The trigger for cell adhesion in this example is via elastase addition which acts on the dialanine sequence (A↓A). As determined by MTT, the addition of elastase did not affect cell viability and there is no difference in cell metabolism with the addition of elastase (Figure 4.1B) (Roberts et al. 2016).

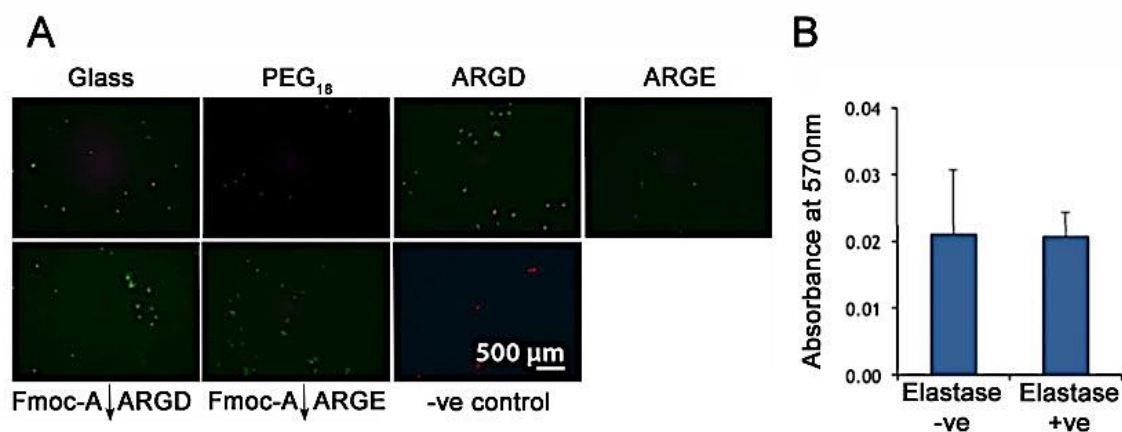


**Figure 4.1 – Viability of Fmoc-A↓ARGD Surface.** A) Live/dead staining on cells grown on different control surface chemistries. RGE control and PEG<sub>18</sub> diamine limit cell adhesion and therefore fewer cells are observed on these surfaces. The RGD controls promote adhesion and viability. There is little difference between Fmoc-RGD and Fmoc-RGE suggesting that Fmoc itself is biocompatible however, the presence of RGD enhances the effect. Green = live cells, red = dead cells. B) MTT assay of cells on switched surfaces (treated with elastase) in comparison to unswitched surfaces (no elastase added). There is no detrimental effect of elastase on the cell culture. Both images replicated from (Roberts et al. 2016).

At longer time points (>4 weeks) it was thought that Fmoc became coated with ECM proteins therefore reducing the efficacy of the surface (Roberts et al. 2016). The blocking group was substituted from Fmoc to PEG to reduce this effect allowing the peptides to direct behaviour rather than ECM proteins (Roberts et al. 2016). We have thus maintained the use of PEG as the blocking group for the MMP modifiable surface (PEG-GPAG↓LRGD). We hypothesise that this surface is both biocompatible and adhesive in a similar manner to that shown in Figure 4.1. In addition to this, we have synthesised an uncleavable and pre-cleaved control (PEG-RGD and LRGD respectively). These sequences were repeated substituting Asp for Glu creating the non-adhesive RGE control (full list of sequences in Table 2.3, Chapter 2). RGE is low adhesion as determined by Chen *et al.* who demonstrated that by mutating Asp for Glu in vitronectin, the mutant protein was found to be non-adhesive due to reduced interaction of integrin binding to the protein (Chen et al. 2009). The β3 integrin is central in the recognition of the YGRGDSP sequence of vitronectin with specific interactions between the integrin and the receptor

(Chen et al. 2009). This is lost in the mutant protein and integrin binding is not achieved (Chen et al. 2009).

The uncleavable sequence was synthesized by removing the enzyme target sequence and the RGD/E peptide was capped with the PEG blocking group (PEG-RGD/E). This was synthesised to evaluate the cell interaction with PEG and determine changes in MSC self-renewal as originally observed in Roberts *et al.* Figure 1.11 (Roberts et al. 2016). A pre-cleaved positive control was also synthesised (LRGD/E) to mimic the action of MMP and removal of the PEG and prime side of the sequence.

In this section, we tested the viability of the controls used in this study using a variety of techniques; alamar blue, MTT and live/dead assays. In addition, proliferation analysis and adhesion studies were also performed to confirm the adhesiveness of RGD and RGE peptides. And finally, the MMP profile of the MSCs in response to the manipulation of surface chemistries.

## 4.2 Methods

### 4.2.1 Suppliers Information

**Table 4.1 – Supplier Information.** List of reagents used in Chapter 4.

Technique	Reagent	Supplier
Viability	Live/dead kit	Invitrogen, Molecular Probes, UK
	Calcein	Invitrogen, Molecular Probes, UK
	Ethidium homodimer-1	Invitrogen, Molecular Probes, UK
	MTT powder	Sigma Aldrich, UK
	Dimethyl Sulfoxide (DMSO)	Sigma Aldrich, UK
	Alamar Blue	BioRad, UK
Immunohistochemistry	Primary antibodies	Sigma –Aldrich, USA
	Biotinylated secondary antibodies	Vector Laboratories, USA
	Tween-20	Invitrogen, USA
	Phalloidin conjugated rhodamine	Invitrogen, USA
	Fluorescein streptavidin	Vector Laboratories, USA
	DAPI	Vector Laboratories, USA
Proliferation	BrdU Kit	GE Healthcare, USA

### 4.2.1 Cell Seeding

Prior to seeding with MSCs, surfaces were ethanol sterilised for 10 minutes then air dried in the fume hood. Coverslips were then seeded at a density of 1,000 cells/cm<sup>2</sup> in DMEM and incubated at 37 °C, 5 % CO<sub>2</sub> for times as stated.

### 4.2.2 Viability

*Live/dead* - P2 MSCs (PromoCell GmbH, Germany) were seeded on all controls and incubated for 24 hours under standard conditions (37 °C, 5 % CO<sub>2</sub>). Cells were stained using 1 µl of calcein and 1 µl ethidium homodimer-1, which was added to 1 mL of cell culture media (DMEM). 100 µl of solution was added to controls for 30 min (37 °C, 5 % CO<sub>2</sub>). The coverslips were then inverted and placed on microscope slide. Slides were then

imaged using Zeiss Axiophot fluorescence microscope with an Evolution QEi digital monochromatic CCD camera and Q-capture imaging software.

*MTT* - P3 MSCs (Stro-1 selected, University of Southampton) were cultured for 1 week. Samples were rinsed in 1x PBS. A 5 mg/mL solution of MTT powder in 1 x PBS was added to the samples 1:10 in DMEM. The well plate was placed on shaking plate for 5 min then incubated under standard conditions (37 °C, 5 % CO<sub>2</sub>) for 5 hours. The media was removed, and the cells were washed twice in cold PBS. 200 µl of DMSO was added, then the cells were shaken for 5 min. The solution was transferred to a new 96 well plate and analysed using a Clariostar microplate reader (BMG Labtech, Germany). % viability was calculated using the following equation;

$$\% \text{ viability} = \left( \frac{\text{sample}}{\text{positive control}} \right) \times 100$$

*Alamar Blue* – P3 MSCs (Stro-1 selected, University of Southampton) were cultured for 1 week under standard conditions. Alamar blue solution was mixed 1:10 in DMEM then 600 µl was added to each coverslip then incubated for 6 hours (30 °C, 5 % CO<sub>2</sub>). 3 x 200µl of solution (supernatant) was transferred to a 96 well plate and analysed using a Thermo-Scientific, Multiskan FC. Absorbance was analysed at  $\lambda_1 = 570$  nm and  $\lambda_2 = 600$  nm. % reduction was calculated using the following equation;

$$\% \text{ Reduced} = \frac{(\epsilon_{OX})_{\lambda_2} A_{\lambda_1} - (\epsilon_{OX})_{\lambda_1} A_{\lambda_2}}{(\epsilon_{RED})_{\lambda_1} A'_{\lambda_2} - (\epsilon_{RED})_{\lambda_2} A'_{\lambda_1}} \times 100$$

Where;

$(\epsilon_{OX})_{\lambda_2} = 11,7216$	$A_{\lambda_1}$ = absorbance, test well
$(\epsilon_{OX})_{\lambda_1} = 80,586$	$A_{\lambda_2}$ = absorbance, test well
$(\epsilon_{RED})_{\lambda_1} = 155,677$	$A'_{\lambda_1}$ = absorbance, control
$(\epsilon_{RED})_{\lambda_2} = 14,652$	$A'_{\lambda_2}$ = absorbance, control

### 4.2.3 Immunohistochemistry

P2 MSCs (PromoCell GmbH, Germany) were seeded on controls for 24 hours then fixed. The cell culture media was removed from the wells and coverslips were rinsed in 1x PBS. Cells were then fixed with fixative for 15 min at 37 °C followed by perm buffer at 4 °C for 5 min. Cells were then blocked in a solution of PBS/BSA for 5 min at 37 °C. Primary antibodies were added at 1/150 in PBS/BSA (see Table 4.2) at 37 °C for 1 hour then

washed 3x in Tween-20. The biotinylated secondary antibodies and phalloidin conjugated rhodamine (F-actin staining) were added at a 1/150 dilution at 37 °C for 1 hour then washed 3x in Tween-20. Fluorescein streptavidin was added (1/100) at 4 °C for 30 min followed by a final washing step 1x in Tween-20. Coverslips were mounted on microscope slides using Vectashield-DAPI mounting medium. Images taken using a Zeiss Axiophot fluorescence microscope with an Evolution QEi digital monochromatic CCD camera and Q-capture imaging software.

**Table 4.2 – Immunohistochemistry Antibodies.** Samples were stained using tertiary staining method.

Primary antibodies		Secondary Antibody	Tertiary Antibodies
Marker	Raised in		
$\beta$ -tubulin	Mouse monoclonal IgG	Biotinylated anti-mouse,	Fluorescein Streptavidin
Vinculin			
Vimentin	Goat monoclonal IgG	Biotinylated anti-goat,	

#### 4.2.4 Proliferation

P3 MSCs (Stro-1 selected, University of Southampton) were cultured for 1 week under standard conditions. A solution of 1mM 5-bromo-2-deoxyuridine (BrdU) in DMEM was made then 600  $\mu$ l was added to each coverslip and incubated for 6 hours. Cells were washed in 1x PBS then fixed at 37 °C for 15 min. Cells were permeabilised for 5 min at 4 °C then washed in 1% PBS/BSA for 10 min at 37 °C. Mouse monoclonal anti-BrdU (1/100 in nuclease solution, prepared as per manufacturer's instruction at 37 °C for 2.5 hours. Samples were rinsed in Tween-20 then 1 x 5 min wash in Tween-20. A dilution of 1/100 biotinylated anti-mouse IgG in PBS/BSA was added at 37 °C for 1 hour after which the coverslips were washed 3x Tween-20 for 5 min. A dilution of 1/100 fluorescein streptavidin and 1/150 rhodamine-phalloidin was added to coverslips in PBS/BSA for 37 °C for 1 hour. Then 1/100 fluorescein streptavidin was added in PBS/BSA to coverslips which were incubated at 4 °C for 30 min then washed using Tween-20 1 x 5min. Coverslips were mounted onto slides with DAPI mounting media and imaged using a Zeiss Axiophot fluorescence microscope with an Evolution QEi digital monochromatic CCD camera and Q-capture imaging software.

#### 4.2.5 MMP Profile

*Zymography* – Supernatant was collected at 3 weeks from DIGE-D, DIGE-E and glass surfaces (n=3). Zymogram was carried out as described in Section 2.5.1, Chapter 2.

*ELISA* – Supernatant was collected at 3 weeks from DIGE-D, DIGE-E and glass surfaces (n=3) and compared to DMEM control. Array was carried out as described in Section 2.5.2, Chapter 2.

*MMP Antibody Array* – Supernatant was collected at 3 weeks from DIGE-D, DIGE-E and glass surface (n=3) in comparison to DMEM control. Array was carried out as described in Section 2.5.3, Chapter 2.

## 4.3 Results

### 4.3.1 Cell Viability

After several publications using SPSS to create substrates for cell growth (Todd et al. 2007; Roberts et al. 2016; Zelzer, McNamara, et al. 2012), we are confident that cell survival is maintained on these surfaces. To demonstrate this for the MMP responsive sequences, viability was tested using live/dead staining, tubulin staining, MTT and alamar blue between 24 hours and 7 days.

We initially analysed cell survival using live/dead staining after 24-hour exposure to the surface chemistries. Cells survived on all surfaces however, the most striking result of this experiment was the difference in the number of cells observed on the RGD surface in comparison to RGE controls, indicating a direct correlation between cell adhesion and cell survival. Figure 4.2A shows cells seeded on glass controls that exhibit minimal cell death (no red staining observed) and further, numerous cells that were observed that had adhered, but were small and fibroblastic in morphology. The presence of the PEG blocking group did not affect cell survival (Figure 4.2B and 4.2C) or cell number (Figure 4.2H), as determined via both image analysis and quantification. In comparison to glass however, PRG-RGE was significantly different ( $p < 0.05$ ) whereas PEG-RGD was not. This could be due to proximity of the cells to the peptides; an observation previous documented in (Roberts et al. 2016). RGD and RGE had observable differential effects on cell adhesion, as is apparent when comparing Figure 4.2D (LRGD) and Figure 4.2E (LRGE), where less cells are on the LRGE surface. Those cells that did adhere survived but were poorly spread. Figure 4.2H confirms this, and also provides support that there was a significant difference between LRGD and LRGE controls ( $p < 0.0001$ ), suggesting that the peptides were directing cellular behaviour. The images appear to suggest that there were fewer cells on DIGE-E in comparison to DIGE-D (Figure 4.2F-G). However, when quantified, there was no difference in cell number between controls, although DIGE-E may be behaving similarly to LRGE and was statistically significant in comparison to glass (Figure 4.2H). Furthermore, from the images there may be a difference in cell morphology (cells have an elongated phenotype on DIGE-E, Figure 4.2G in comparison to DIGE-D, Figure 4.2F). Suggesting that PEG cap is not affecting cell number between controls, although there may be a response to the peptide underneath the cap. Collectively, the RGE controls were different to that of the glass control in terms of cell number ( $p < 0.05$ ,  $p < 0.0001$  and  $p < 0.001$  respectively for PEG-RGE, LRGE and DIGE-E, Figure 4.2H). It was expected that PEG-RGE and DIGE-E would behave more similarly and although they are not

statistically different from each other, DIGE-E has more of a negative effect on cell survival in comparison to glass ( $p < 0.05$  and  $p < 0.01$  respectively). This could be due to increasing chain length of peptide and limited adhesion from RGE. This is consistent with prior expectations, as it was hypothesised that there would be limited cell attachment. The presence of RGD was comparable to glass suggesting that at this time point, survival is not enhanced by the presence of RGD. Furthermore, the presence of PEG does not seem to affect cell survival for RGD controls, as they are comparable with glass and each other. Taken together, there is a cellular awareness of peptides beneath the PEG cap.

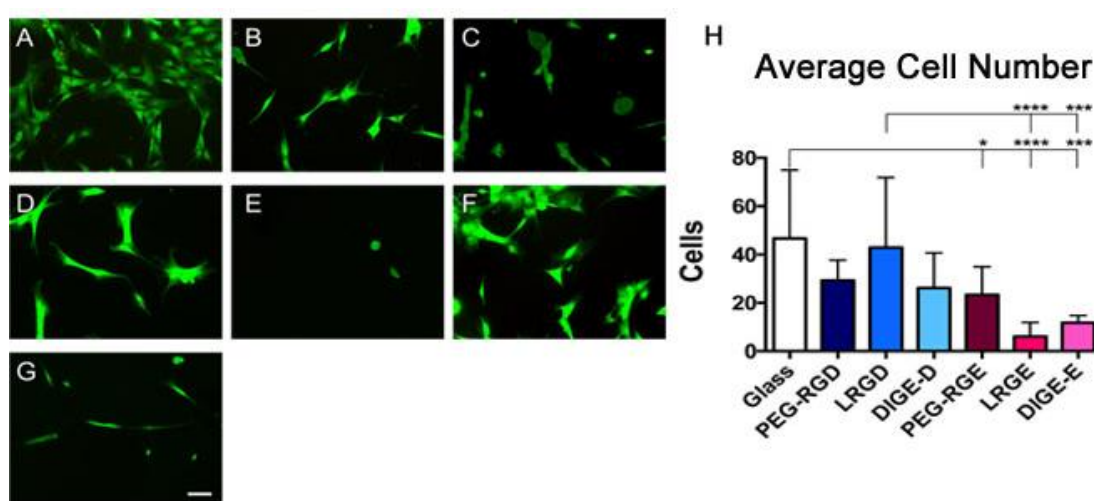


**Figure 4.2 – Live/dead Staining of Control Surfaces.** Cell survival was analysed using live/dead staining after 24 hours. Cell survival differed per surface. A) Glass B) PEG-RGD C) PEG-RGE D) LRGD E) LRGE F) DIGE-D G) DIGE-E. The glass coverslip supports adherence of cells in higher quantities than the other controls. The RGD coverslips are more adhesive and cells were subject to increased spreading in comparison to RGE controls, and although cells stained positive for survival, there is fewer present to analyse. This suggests there is a difference in adherence of cells on the RGE coverslips. Scale bar = 100 $\mu$ m green = live, red = dead. H) Cell number from images A-G were quantified. RGE controls have significantly less cells per surface in comparison to glass confirming RGE is non-adhesive to cells. Graph shows mean  $\pm$  SD, n=15, statistics determined by ANOVA \* $p < 0.05$  \*\*\* $p < 0.001$  \*\*\*\* $p < 0.0001$ .

To assess the metabolic activity of the cells, we looked at tubulin staining after 24 hours on all controls. Tubulin gives an indirect measure of cell metabolism as microtubules are associated with vesicles and motor proteins as a means of transport of metabolites (Caviston & Holzbaur 2006). The increased expression of tubulin would indicate a more metabolically active cell, one that is utilising energy and transporting metabolites intracellularly.

We observed increased tubulin expression on the glass control indicating metabolically active cells (Figure 4.3A). There is a similar expression of tubulin for cells grown on RGD controls (PEG-RGD, LRGD and DIGE-D, Figures 4.3 B – D). Filopodial formation was also observed on RGD controls although this was most prominent on LRGD (Figure 4.3C) suggesting that when PEG is removed, adhesion is enhanced. Tubulin was expressed throughout these cells in dense bundles, and even expressed to the ends of the filopodia (Figure 4.3C). In comparison, for the RGE controls (PEG-RGE, LRGE and DIGE-E, Figure 4.3 E - G), we noticed limited tubulin organisation and reduced cell spreading particularly for PEG-RGE and LRGE (Figure 4.3 E & G). No filopodia were observed on RGE controls, although the representative pictures allude to more cells present on DIGE-E (Figure 4.3G) in comparison to PEG-RGE (Figure 4.3E), which was not expected due to the results from Figure 4.2H. Future quantification studies are required to follow up this observation. Taken together these results suggest that cells on the RGD controls were more metabolically active at this time point and further, promote filopodial formation.

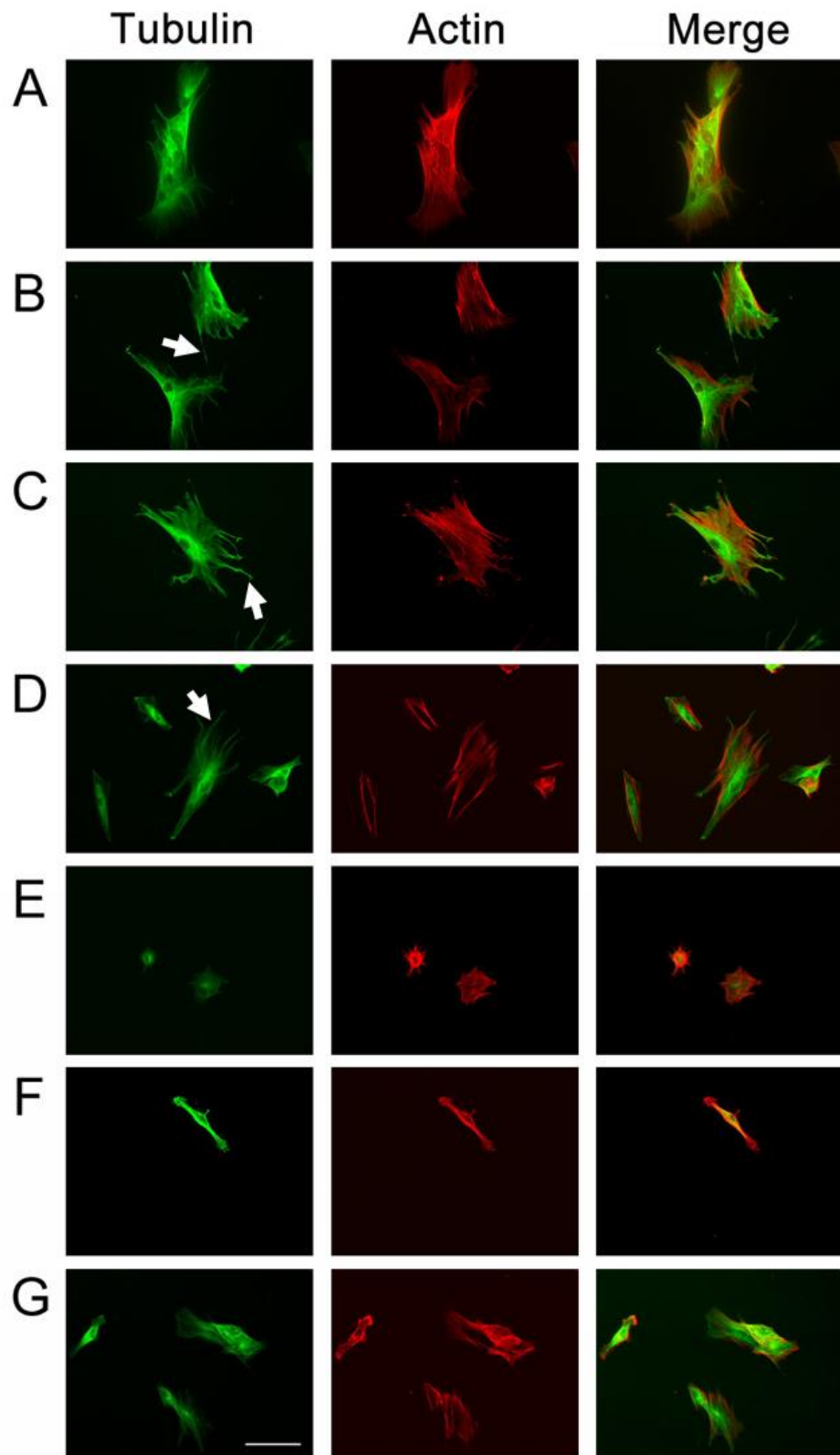


**Figure 4.3 – Tubulin Expression After 24 Hours.** A) Glass B) PEG-RGD C) LRGD D) DIGE-D E) PEG-RGE F) LRGE G) DIGE-E. Cells were stained for tubulin 24 hours after seeding. There are clear differences in morphology after 24 hours in response to surface chemistry. Those cells cultured on RGD surfaces show noticeable tubulin expression and increased spreading with filopodia formation (white arrow). Cells cultured on RGE are less spread and show less tubulin expression. Green = tubulin, red = actin, scale bar = 100 $\mu$ m.

Vimentin staining was also used as a marker of cell integrity. Vimentin is an intermediate filament (IF) and a component of the cytoskeleton, IFs also included desmin, keratin and glial fibrillary acidic protein (GFAP). IFs are so named due to their intermediary diameter size in comparison to other cytoskeletal components (10 nm) and along with the myosin and actin filaments are responsible for the cell cytoskeletal function (Fuchs & Weber 1994). Of the IF proteins, vimentin is widely expressed in mesenchymal cell types. IFs in general associate with membranes including that of the nucleus via interactions with laminin (Fuchs & Weber 1994). In addition, vimentin organises cell organelles and membrane associated proteins by acting as a scaffold. Through this mechanism, vimentin also has a role in adhesion through regulation of integrins that associate with IFs (Ivaska et al. 2007). It is thought that the phosphorylation of vimentin is dynamically regulated depending on cell functions including differentiation (Ivaska et al. 2007).

Vimentin was well organised in the control cells (glass) as expected, cell spreading was also observed (Figure 4.4A). The result was similar for the adhesive PEG-RGD and LRGD controls particularly around the nucleus of the cells where dense vimentin staining was observed (Figure 4.4B&C). This indicates cell integrity on these surfaces in response to the RGD motif. The staining on DIGE-D surface was more pronounced with uniform expression of vimentin throughout the cell. The results from the adhesive controls show adequate cell binding and in turn, increased cell spreading (Figure 4.4D). PEG-RGE also showed well defined staining, in comparison, limited vimentin was observed for LRGE surfaces and there were differences in cell morphology (Figure 4.4E&F). This result indicates that the PEG is providing better adhesion for the cells on the RGE surfaces compared to LRGE alone (Figure 4.4G). However, vimentin was observed on all surfaces suggesting that the presence of peptides do not negatively affect cell structure and IFs are expressed uniformly throughout the cell.

Cell area was quantified in Figure 4.5 which confirms lack of cell spreading for LRGE, which had significantly lower cell area in comparison to all other controls. The capped controls behaved similarly ( $5000 \mu\text{m}^2$  each) and there was a slight increase in cell area for both LRGD and DIGE-D surfaces although this is not significant. The PEG group on the pre-cleaved and full length RGE controls seems to enhance spreading when compared to the LRGE.

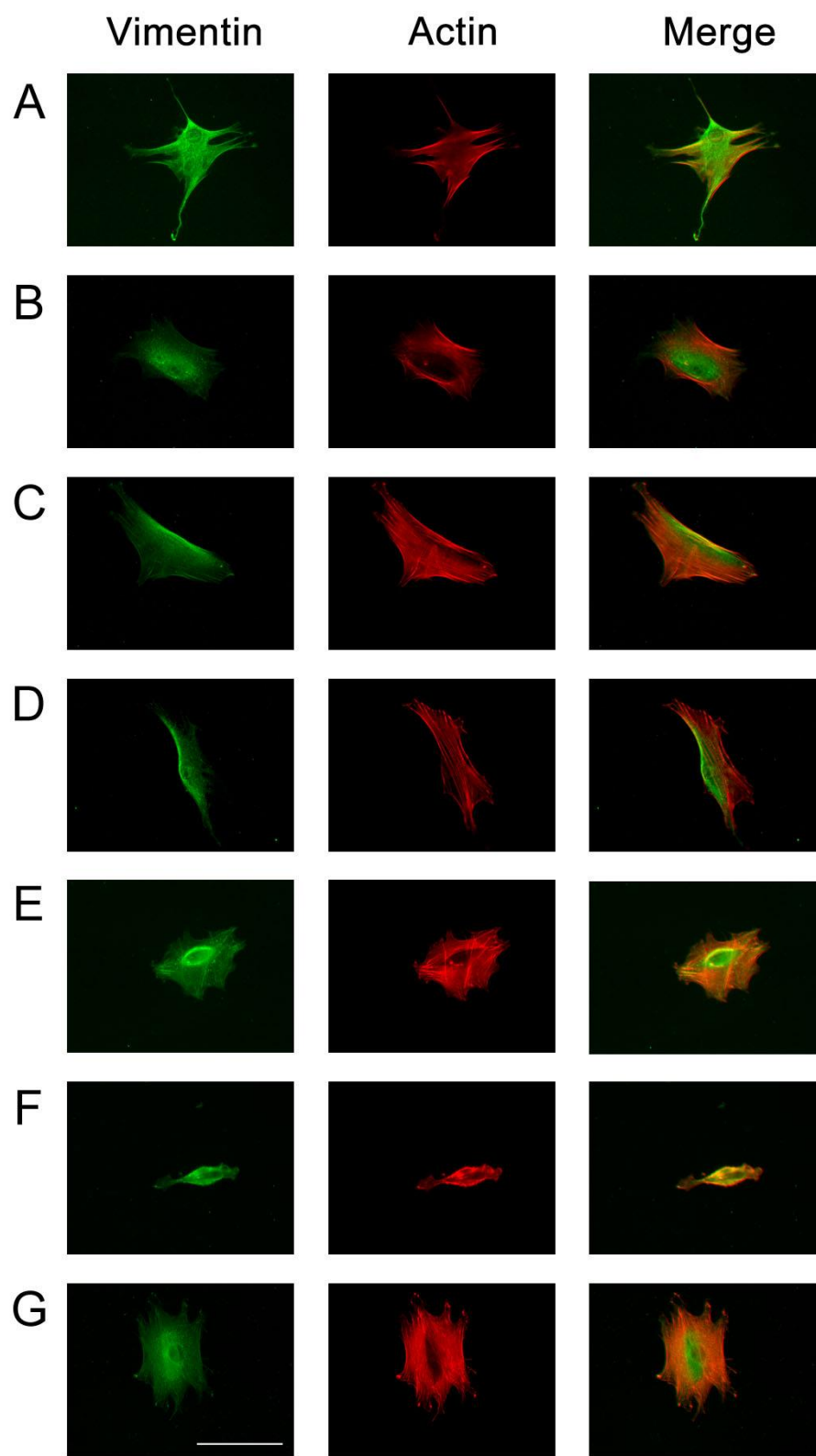


**Figure 4.4 – Vimentin Staining at 24 hours.** A) Glass B) PEG-RGD C) LRGD D) DIGE-D E) PEG-RGE F) LRGE G) DIGE-E. Image shows uniform vimentin staining across most controls. Vimentin is less well defined on the LRGE surface and this correlate to limitation in cell spreading. Scale bar = 100µm, green = vimentin, red = actin.

## Average Cell Area

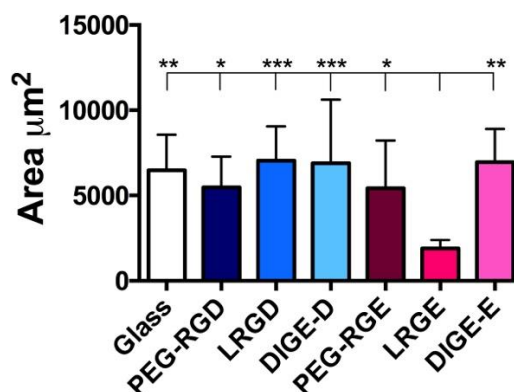


**Figure 4.5 – Quantification of Vimentin Staining.** Cell area was quantified from images above. There is a trend for increasing cell area on the DIGE-D surface. All surfaces were significantly different to that of the LRGE control which had a minimal cell area. Graph shows mean  $\pm$  SD,  $n=15$  (frames), statistics calculated using ANOVA where \* $p<0.05$ , \*\* $p<0.01$  and \*\*\* $p<0.001$ .

We increased the duration of the culture to 1 week and determined cell viability at this point using both MTT and Alamar Blue assays. MTT is used to assess cell metabolic activity by determining the activity of enzymes to reduce MTT to formazan dyes (Riss et al. 2004). The quantity of formazan is directly proportional to the number of viable cells and therefore is a quantitative assay (Mosmann 1983). Viable cells actively convert MTT to formazan creating a purple product that can be analysed using a spectrophotometer at 570 nm (Mosmann 1983). Apoptotic cells lose the ability to convert MTT and therefore no colour change is observed. The conversion of MTT is via the enzymes of the mitochondria (Riss et al. 2004). A complementary technique to this is the use of Alamar Blue. Alamar Blue is a commercial product used to test viability of cells using redox indicator; the reduction of resazurin to the resorufin product (Riss et al. 2004). Again, this results in a colour change from blue to pink analysed by a fluorometer at 560 nm excitation (Riss et al. 2004). Both techniques are high throughput techniques as they are carried out in 96 well plate format and read with plate reader (Riss et al. 2004).

We expected that cells were viable on each surface with increased time as shown in previous publications (Figure 4.1) and due to the results in Figures 4.2-4.5. The results from the MTT assay (Figure 4.6A) and the Alamar Blue assay (Figure 4.6B) are consistent with this. The data suggests that after one week in culture, the cells are surviving on all control surfaces. The results show comparable levels of cell metabolism for all surfaces (Figure 4.6), which was unexpected due to the lack of adherence on the LRGE surfaces for Figures 4.2 – 4.5, although the live/dead staining did indicate that there was survival of a

few cells on this surface (Figure 4.2). Those that did adhere, had the ability to survive, probably aided by the culture medium. The cells are cultured in 10 % serum and therefore the presence of serum proteins could influence the long-term survival of the cells on the non-adhesive surfaces. The exposure of RGD on the pre-cleaved surface did not have a synergistic effect on survival in that the results were comparable to the RGE pre-cleaved control. We can therefore conclude that after 1 week, cell survival is comparable across multiple controls as determined by two different assays.

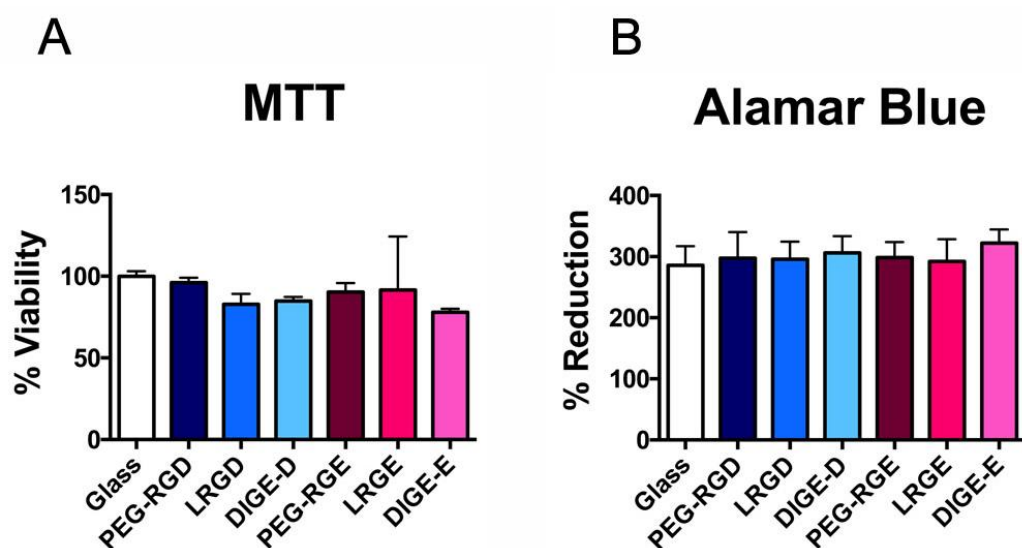


**Figure 4.6 - Viability at 1 Week.** A) MTT assay expressed as % viability in comparison to glass control B) Alamar blue expressed as the % reduction of resazurin product in comparison to glass control. Data is consistent for both methods suggesting viability of MSCs across all controls. Graph shows mean  $\pm$ SD, n=3 for both.

### 4.3.2 Cell Adhesion

Based on the morphology observed from the 24-hour experiments (filopodial expression on RGD surfaces and lack of adhesion on LRGE and DIGE-E Figure 4.1, 4.2 & 4.3), it would suggest that there are early changes in cell adhesion in response to the surface chemistries. We looked at vinculin expression after 24 hours to observe focal adhesion (FA) expression for each surface (Figure 4.7). Vinculin is a key component of FAs and is recruited by integrins to bridge to the actin cytoskeleton (Geiger et al. 2001). The length and density of vinculin adhesions serves to determine the adhesiveness of the surface and in addition is proportional to the cellular tension that results from the clustering of integrins (Wozniak et al. 2004) (Section 1.4, Chapter 1).

On the glass control, there were defined adhesions at the periphery of the cell (Figure 4.7A). Spreading on the PEG-RGD control was enhanced as there was prominent adhesions at the edge of the cell (Figure 4.7B). The PEG-RGE control (Figure 4.7C),

although much less spread than the adhesive counterpart does also express vinculin. This suggests that the surface chemistry under the PEG blocking group had an effect on cell adhesion, similar to the data presented in Figure 4.2H. The number of adhesions per cell was quantified (Figure 4.8A) where this difference was confirmed ( $p < 0.001$ ). PEG-RGD (Figure 4.7B) appears to have a larger cell area than LRGD (Figure 4.7C), although when quantified there is no difference between controls (Figure 4.8). It was thought the uncapping of peptides would enhance cell spreading however, it could be too early to see differences or there could be a risk in that the process of capping with PEG during SPPS has not been efficient and therefore has affected cell behaviour. LRGD controls are much more spread than LRGE controls (Figure 4.7D and 4.7E), with cells cultured on LRGD expressing many more adhesions than the LRGE (Figure 4.8A,  $p < 0.001$ ). The enzyme cleavable surfaces also differed in the expression of vinculin depending on the presence of adhesive RGD. The cells cultured on DIGE-D appeared to show more pronounced adhesions than the DIGE-E control (Figure 4.7F and 4.6G), however, the average number of adhesions per cell is not different between these controls nor is cell area (Figure 4.8A&B). Overall, this suggests that there are changes in adhesion in response to the surface chemistry and further, it is the presence of RGD that is driving large scale adhesions. The effects shown in Figure 4.7 are quantified in Figure 4.8.

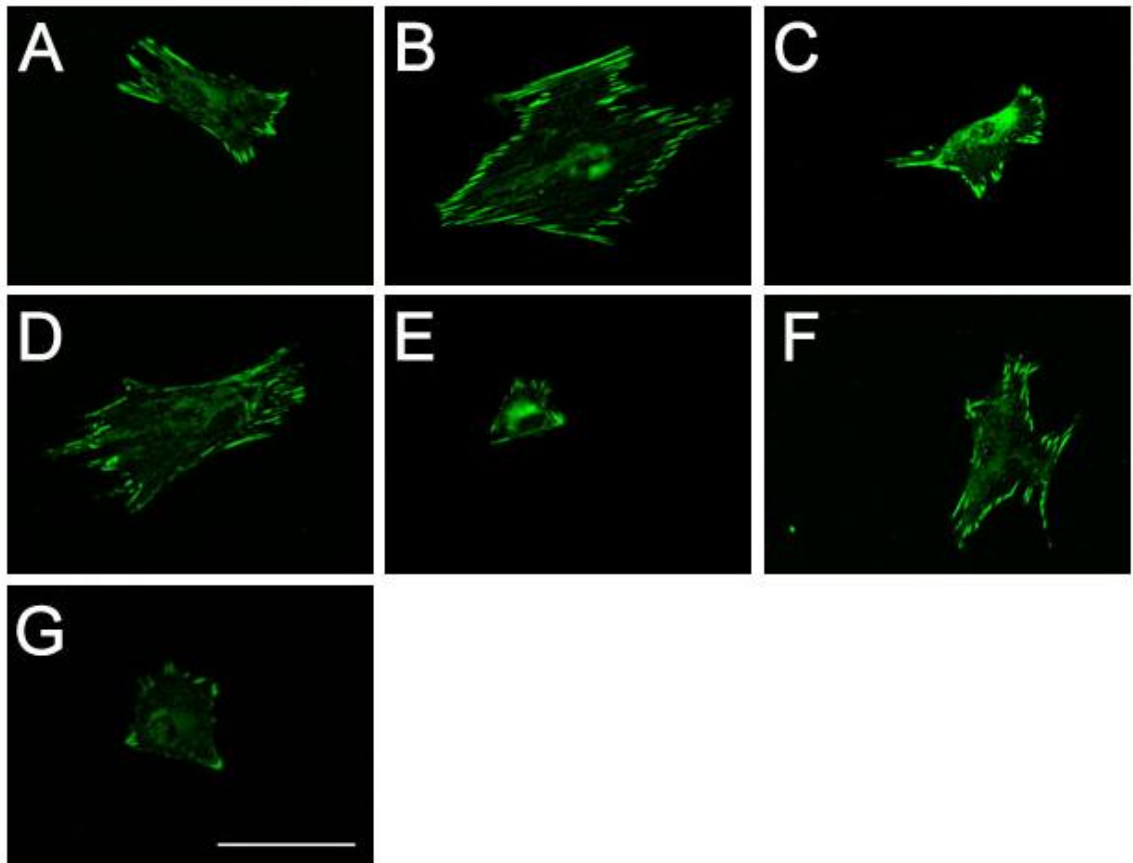


**Figure 4.7 - Vinculin Expression at 24 Hours.** A) Glass B) Peg-RGD C) Peg-RGE D) LRGD E) LRGE F) DIGE-D G) DIGE-E. Cells positively express vinculin on all surfaces. There are differences in the number of adhesions and cell spreading. Cells on RGD surfaces express many, substantial adhesions at the periphery of the cell. Those on RGE controls have a limited number of adhesions. Green = vinculin, scale bar = 100 $\mu$ m.

Overall, the PEG-RGE and LRGE controls have significantly less adhesions per cell in comparison to the glass controls (Figure 4.8A). The LRGE chemistries are less adhesive to cells than RGD, which was significantly different to the uncapped, pre-cleaved and full length RGD ( $p < 0.0001$ ,  $p < 0.01$  and  $p < 0.01$  respectively). It was unexpected that the DIGE-E control did not behave like LRGE and PEG-RGE, this could potentially be due to chain length and the increasing distance from the RGE peptide.

We quantified cell spreading ( $\mu\text{m}^2$ ) to determine if there was correlation between increasing cell spreading and increasing number of adhesions. Figure 4.8 shows that there was a similar trend for both, with PEG-RGD showing the greatest number of adhesions and the largest cell area (65 adhesions,  $\sim 8000 \mu\text{m}^2$ ) comparatively, LRGE controls contained least number of adhesions and the smallest cell area (23 adhesions,  $\sim 3000 \mu\text{m}^2$ , Figure 4.8A & B). The smallest cell area was observed on the LRGE, which is consistent with previous observations (Figure 4.5).

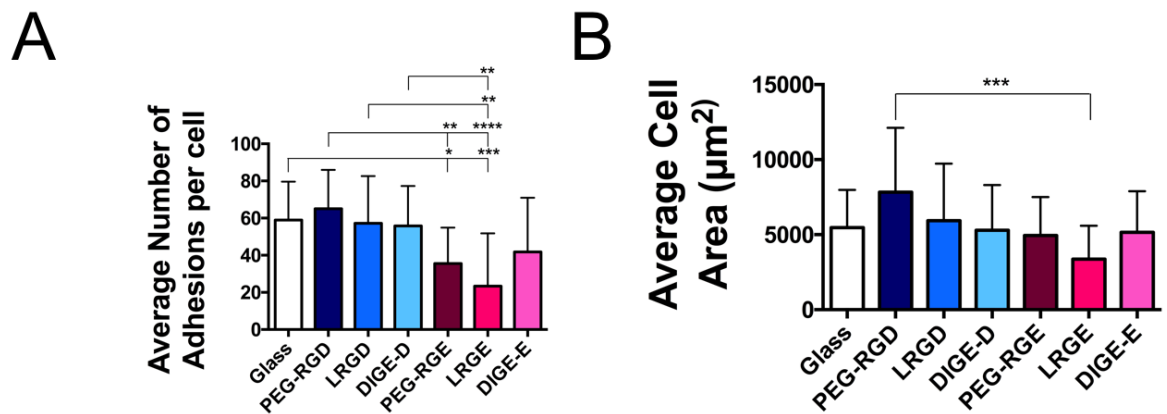


**Figure 4.8 – Vinculin Quantification, 24-Hour Culture.** Quantification from Figure 4.7 A) The average number of adhesions per cell, per control. B) Average cell area ( $\mu\text{m}^2$ ). Graph show mean  $\pm$  SD, n=15, statistics calculated by ANOVA, \*P<0.05, \*\*P<0.01, \*\*\*P<0.001 \*\*\*\*P<0.0001.

Adhesions can be classified depending on length. Differential adhesion length was originally defined by Bershadsky in 1985 and defined as “dot” and “dash” adhesions (Bershadsky et al. 1985). Since this observation, adhesions have been reclassified depending on their size with each size responsible for a different role. Focal complexes (FCs) are short transient adhesions that measure  $<2 \mu\text{m}$  in length and are usually involved in cell mobility and migration (Sun et al. 2016). FAs are greater than  $2 \mu\text{m}$  long and are stable adhesions involved in cell maturation and ECM production (Wozniak et al. 2004). Super mature adhesions (SMAdh) are very large adhesions that indicate high intracellular tension and in case of skeletal cells, encourage osteoblastic differentiation (Biggs et al. 2009).

From the results of Figure 4.7, we separated the adhesions into FCs, FAs and SMAdhs and totalled the number of adhesions across all images (Figure 4.9). For all controls, there was generally fewer FCs than FAs or SMAdhs. The number of FAs and SMAdhs for the RGD controls were comparable (approximately 400 in total for both). There was a larger difference in the number of FA and SMAdh for the glass control in comparison to RGD controls which suggests that the presence of the RGD increases the number of SMAdhs. There was a decrease in the number of SMAdhs for the non-adhesive controls. The LRGE samples had fewer adhesions for all subtypes as expected in comparison to RGD controls. This result confirms that the RGE controls are non-adhesive and for the pre-cleaved control (LRGE) this is due to the direct exposure of the cells to the peptide motif.

## Total number of adhesions

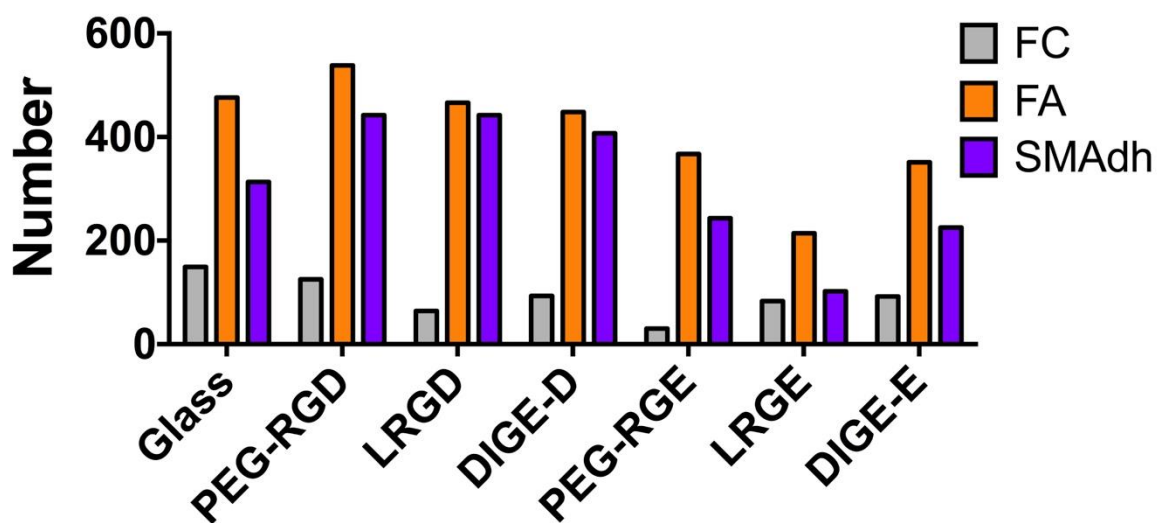


**Figure 4.9 – Total Number of Adhesions.** Distribution of adhesion length for all controls. Total number of adhesions quantified by length from all cells imaged, n=15. FA = focal adhesion (<2  $\mu\text{m}$ ), FC = focal complexes (2-5 $\mu\text{m}$ ), SMAdh = super mature adhesion (>5 $\mu\text{m}$ ). There are a greater number of SMAdh on RGD controls.

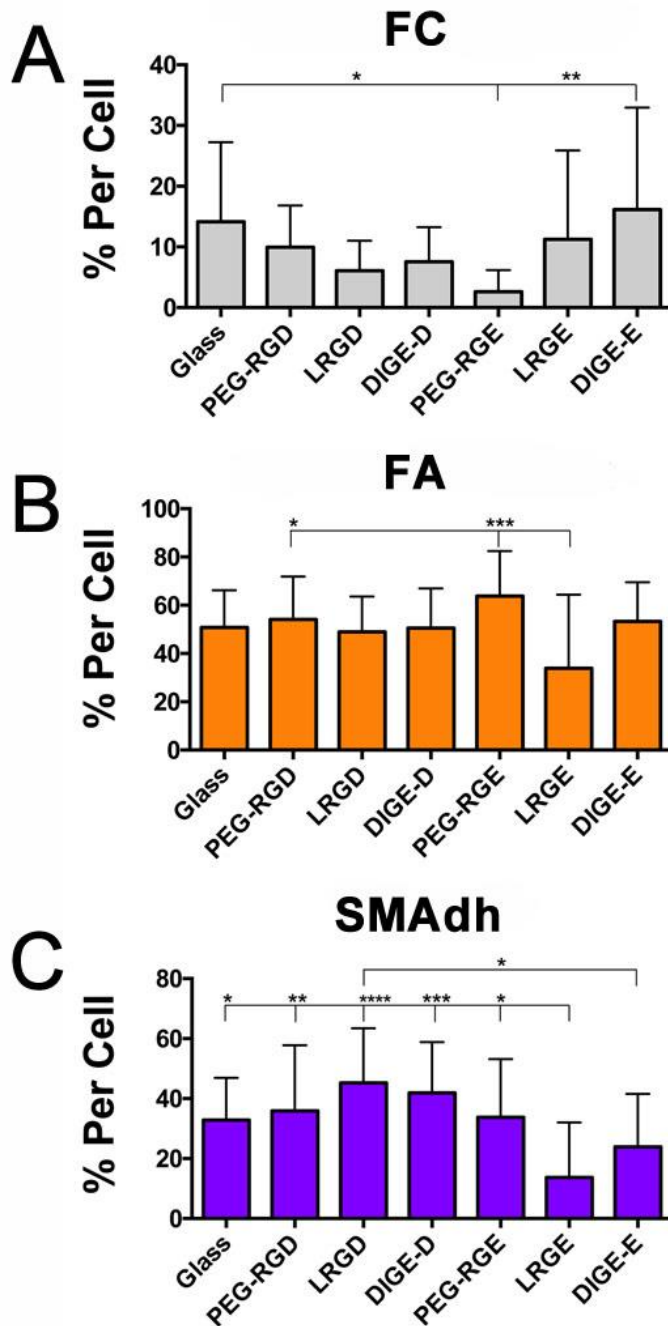


**Figure 4.10 – Percentage Adhesions Per Cell.** A) FC B) FA C) SMAdh. A) FCs are prominent on glass and RGE controls except for PEG-RGE. LRGE and DIGE-E controls have limited number of adhesions with increasing number of FCs in comparison to other controls. B) FAs are the main adhesion type of the PEG-RGE control however, FAs are the major adhesive component for all controls accounting for approximately 50 % of total cell adhesions. C) SMAdh are most prevalent on the RGD controls, specifically for the LRGD (40 % of adhesions are SMAdh). Graph shows mean  $\pm$  SD, n=15 (cells), statistics calculated by ANOVA \*P<0.05, \*\*P<0.01, \*\*\*P<0.001 \*\*\*\*P<0.0001.

This data (Figure 4.9) was then expressed as the % adhesions per cell for each adhesion length (Figure 4.10A-C). FCs account for approximately <10 % of adhesions per cell, this is slightly higher for the glass, LRGE and DIGE-E surfaces and could indicate cell motility for these controls (Sun et al. 2016) (Figure 4.10A). The percentage of FAs per cell was

greater than that of the FCs (approximately 50 % for all controls). This would be expected as the FAs are expressed in response to adherent surfaces (whether that is ECM production or peptides). The results in Figure 4.10B suggests that the cells on all surfaces are adhering, which is consistent with the previous data presented in this chapter. However, as the density and length of FAs increase as the density of adhesive moieties increase (Chen et al. 1997; Cavalcanti-adam et al. 2007). There was a decrease in FAs expressed on LRGE surfaces (approximately 30 %), consistent with the previous data in that there were a few cells that had adhered to the LRGE control. This must reflect a minimal level of adhesion as the percentage of these adhesions that have been measured as SMAdhs equalled <20 % (statistically different from the rest of the controls, Figure 4.10C) reinforcing that LRGE is not supporting increased cellular adhesion. Figure 4.10C also shows that there is a greater proportion of SMAdh per cell for the RGD control specifically, LRGD enhances this effect (approximately 50 % are SMAdhs) due to the proximity of cell to the RGD element. However, there was no difference between the RGD controls in terms of the number of SMAdhs, suggesting that the blocking group was having no effect on adhesion. This should be repeated at later time point to fully understand if this phenotype is maintained.

### 4.3.3 Proliferation

We determined cell proliferation utilising BrdU (brominated analogue of thymidine) uptake. This assay was utilised to provide insight to the ability of surface chemistry to induce cell growth and population expansion. BrdU is incorporated into cell DNA at the S phase of the cell cycle (Taupin 2008). Upon addition to the media, BrdU can replace thymidine in the cell's DNA and be stained for with an anti BrdU antibody.

After one week, proliferation was observed on all surfaces (Figure 4.11). No difference was observed between controls (Figure 4.12) and proliferating nuclei were calculated to account for between 10-20 % of the total cell number (Table 4.3). From the image in Figure 4.11D, there appeared to be more proliferating nuclei in DIGE-D than those observed in the other control samples. However, when quantified, there was found to be no difference between controls (Figure 4.12). Proliferation was also observed on RGE controls (Figure 4.11 E-F), this gives an indication that cell survival is occurring on the RGE controls over time resulting in viable cells as consistent with Figure 4.6. This study only reveals a 6-hour window in a 1-week culture. It would have perhaps been better to

conduct this experiment at 24 hours, to understand the initial response to peptides and correlate the lack of cells observed in Figure 4.1 to proliferation.

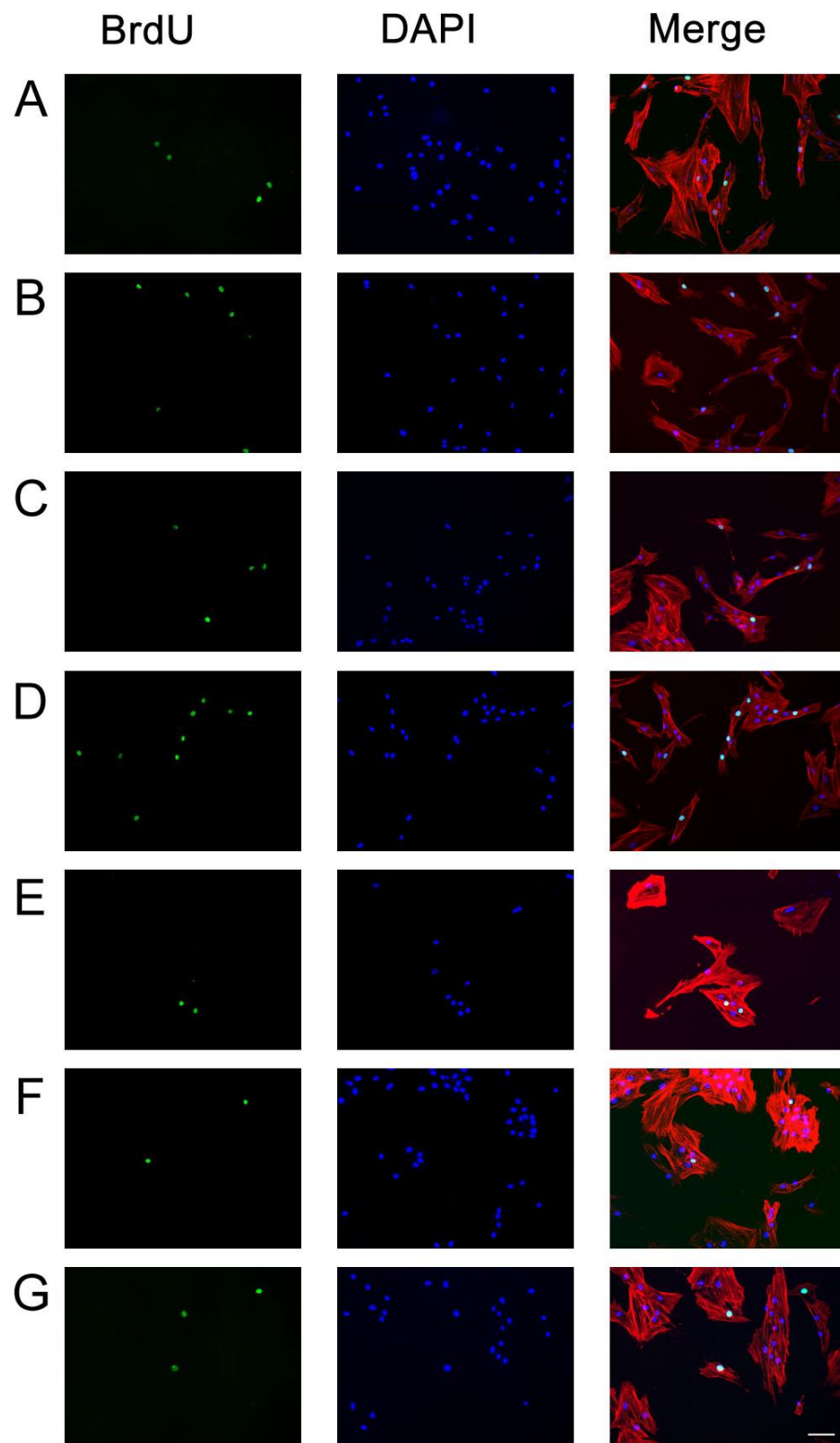


**Figure 4.11 – BrdU Staining.** Cells were cultured for 1 week then treated with BrdU for 6 hours. A) Glass B) PEG-RGD C) LRGD D) DIGE-D E) PEG-RGE F) LRGE G) DIGE-E. Proliferating nuclei (green) in comparison to total nuclei (blue). Merge, actin = red. Actin = red scale bar = 100 $\mu$ m.

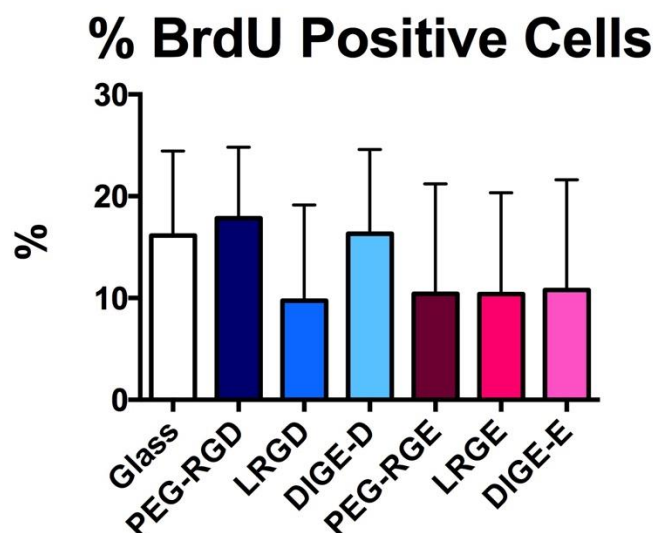


**Figure 4.12 – Quantification of BrdU Positive Cells.** Average % positive BrdU cells per frame calculated from Figure 4.11. There is no difference in % proliferation between controls. Graph shows mean  $\pm$  SD, n=15 (frames).

**Table 4.3 - % BrdU Nuclei of Total Cells.** Images from Figure 4.11 were quantified and expressed as % of the total cell population  $\pm$  SD (n=15 frames).

Surface	% positive BrdU nuclei $\pm$ SD	Surface	% positive BrdU nuclei $\pm$ SD
Glass	16.1 $\pm$ 8.3	-	-
<b>Adhesive Controls</b>		<b>Non-Adhesive Controls</b>	
PEG-RGD	17.8 $\pm$ 7.0	PEG-RGE	10.4 $\pm$ 10.8
LRGD	9.7 $\pm$ 9.3	LRGE	10.4 $\pm$ 10
DIGE-D	16.3 $\pm$ 8.3	DIGE-E	10.8 $\pm$ 10.8

We then quantified cell area and cell number from the images in Figure 4.11. Figure 4.13A shows that after 1 week, LRGD surfaces have larger cell size than that of PEG-RGD and LRGE ( $p < 0.05$  for both). There was a large standard deviation observed for cells cultured on LRGD. Perhaps this was due to poor homogenisation of the surface and there may be some areas where the coverslip has not been totally covered by peptide and therefore there was not coordinated cell behaviour. It was unexpected that LRGD was significantly different to PEG-RGD ( $p < 0.005$ ), which suggests the cells may not be responding to peptides under the blocking group as originally thought from previous work (Figure 4.7). The controls containing PEG blocking group were not different from each other, which could suggest that the PEG group itself is controlling behaviour in some way. Cell number was also quantified for Figure 4.11 and it was found that there is no difference in cell number between controls at 1-week culture (Figure 4.13). This was unexpected due

to the results seen in Figure 4.2 but suggests the cells on the LRGE and DIGE-E controls have recovered. This further supports the data presented in Figure 4.6, which highlighted cell metabolism was similar per control as cell survival is not negatively affected by 1 week.

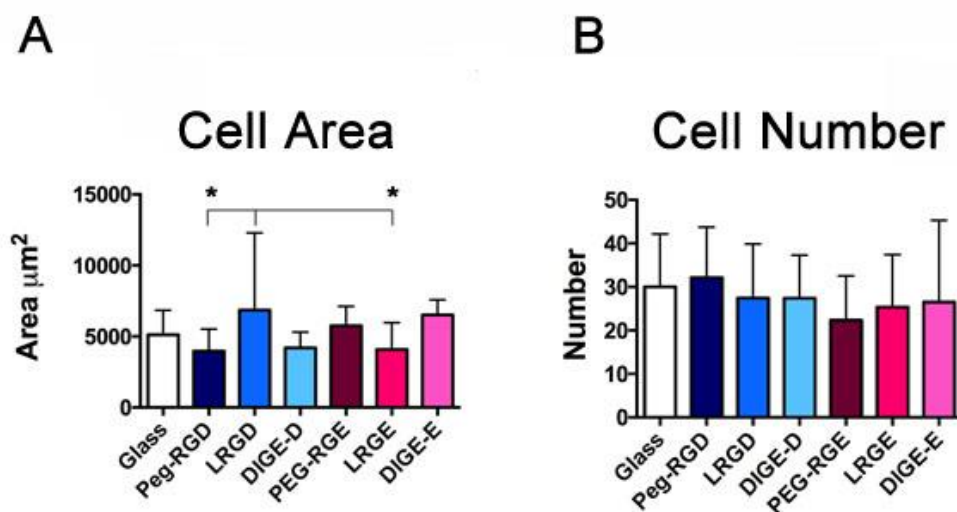


**Figure 4.13 – Quantification of Cell Area and Number, 1 week.** Images from Figure 4.11 were quantified for A) cell area and B) cell number. A) cells cultured on LRGD were significantly larger than cells cultured on PEG-RGD and LRGE. B) there was a similar number cells per frame for all controls tested. Graphs show  $\pm$  SD, n=15, statistics calculated by ANOVA where \*p<0.05.

### 4.3.4 MMP response to the surface

#### 4.3.4.1 Gelatinases

We then looked at the MMP profile in response to the surfaces. Using an ELISA, we analysed cell supernatant concentration of both gelatinases over three weeks (Figure 4.14). At week 3, there is no trend for MMP-9 expression and supernatant concentration is maintained at approximately 0.2 ng/ml. There was a slight increase for LRGE at week 2 (p< 0.05) however, this effect was not sustained to week 3.

There was a significant difference in concentration of MMP-2 for DIGE-D, LRGE and DIGE-E at week 3 in comparison to week 1 from approximately 9 ng/ml to approximately 14 ng/ml (p<0.01, p<0.01 and p<0.05 respectively). For the DIGE surfaces, this could suggest that the cells are accumulating their MMP expression in the presence of the enzyme responsive sequence. Comparing expression of both MMPs, the results show that for MMP-9, there was a 10-fold reduction of expression in comparison to MMP-2. This is consistent with Figure 3.8 (gelatinase in response to glass) suggesting that the presence of surface chemistry has maintained the relative abundance of each gelatinase. MMP-2 concentration increases at week 3 for DIGE and LRGE controls in comparison to the

concentrations observed at weeks 1 and 2 for each. Furthermore, MMP-2 concentration on DIGE controls at week 3 were significantly different to that of glass ( $p < 0.05$ ), suggesting the increase is due to the presence of peptides. This data formed the basis of the hypothesis that at this time point due to the increasing abundance of MMP-2, the concentration in culture would be sufficient for cells to cleave the surface. However, Chapter 3 demonstrated that relatively small concentrations of MMP-9 were sufficient to cleave DIGE-D surfaces. From the data presented in Figure 4.14 alone, we cannot rule out that MMP-9 is not having an effect on the surface and that abundance does not guarantee potency. It would have also been useful to have a media control to understand relative amounts of MMP from serum and if it could be contributing to cleavage.

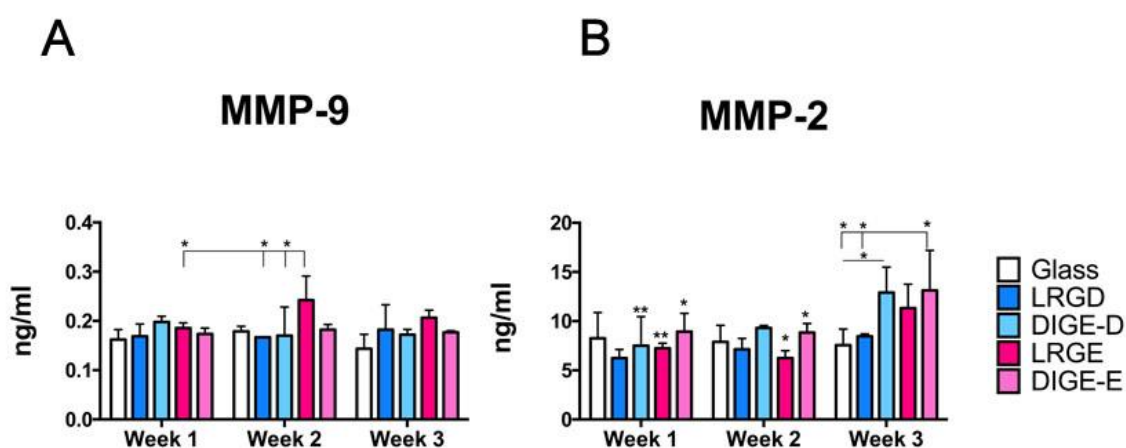


**Figure 4.14 – Gelatinase Response per Surface Over 3 Weeks.** Using ELISA, the concentration of the Gelatinases was determined over three weeks for both A) MMP-9 and B) MMP-2. A) There was consistent expression of MMP-9 for 3 weeks. There was a slight increase in MMP-9 on LRGE at week 2. B) There was a significant increase in MMP-2 expression by week 3 for cells cultured on full length surfaces and LRGE. MMP-9 concentration is 10-fold lower of that of MMP-2. Therefore MMP-2 expression is altered in response to the surface over time. Graph shows mean  $\pm$  SD,  $n=3$ , statistics calculated by ANOVA where  $*p < 0.05$  and  $**p < 0.01$ .

This was repeated for the DIGE-D and DIGE-E controls at 3 weeks using gelatin zymography (Figure 4.15). Due to the weight of the band (62 kDa for MMP-2 and 82 kDa for MMP-9) we were observing the active form of the enzyme. Again, it was apparent that for all surfaces, MMP-2 expression was greater than that of MMP-9. There was no difference in activity of MMP-2 between controls, which taken together with the results of Figure 4.14 highlights that concentration does not correlate to potency.

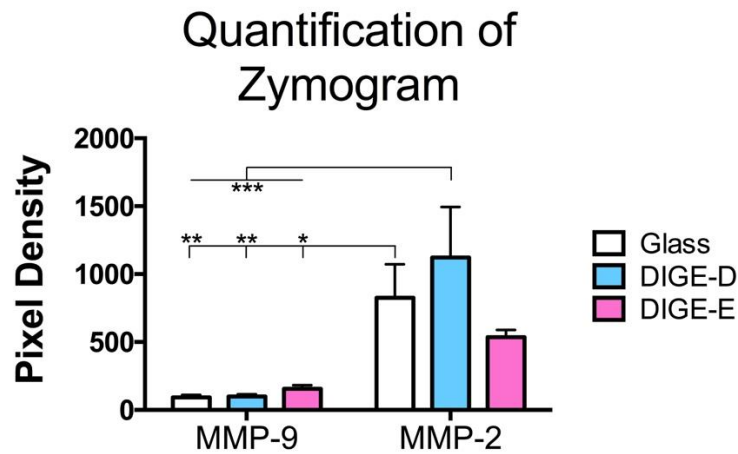


**Figure 4.15 – Gelatin Zymography at Week 3.** Supernatant was collected from Glass, DIGE-D and DIGE-E surfaces and ran on gelatin gels. MMP-9 is still expressed at very low levels in comparison to MMP-2. There was a slight increase of MMP-2 for DIGE-D controls. Graph shows mean  $\pm$  SD, n=3, statistics calculated by ANOVA where \*p < 0.05, \*\*p < 0.01 and \*\*\*p < 0.001.

This was again repeated by antibody array. Here, we specifically looked at the gelatinase expression of MSCs cultured on DIGE surfaces in comparison to plain DMEM (with serum) and cell supernatant from cells seeded on glass (Figure 4.16). The results showed that there was minimal level of MMP-9 in all supernatant tested apart from that of the glass supernatant from which MMP-9 was absent. MMP-2 appeared to be expressed in all samples at a higher level than that of MMP-9 as would be expected from the previous data (Figures 4.14 and 4.15). However, it was not found to be statistically different.

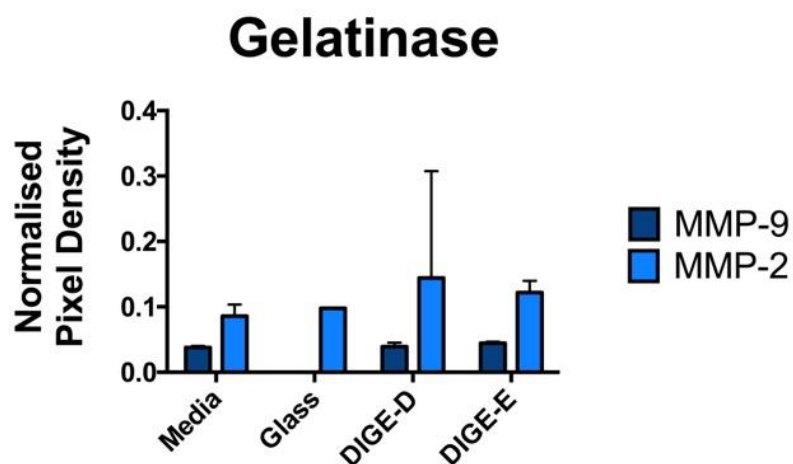


**Figure 4.16 - Gelatinase Expression as Determined by Membrane Analysis.** MMP-9 expression is at a similar level for most surfaces although there is an absence of MMP-9 detected on glass. MMP-2 was found in all samples tested. Graph  $\pm$ SD, n=2, ns as determined by ANOVA.

#### 4.3.4.2 MMP Family Members

The antibody array also provided information on other MMP families in addition to the gelatinases; stromelysins (MMP-3, -10), the collagenases (MMP-1, -8, -13) and the regulatory TIMP (TIMP-1, -2, -4) families. Firstly, for the MMP families, in comparison to the gelatinases, these were expressed at a much lower level (Figure 4.16 compared to Figure 4.17A&B). Figure 4.17A shows the results for the collagenases. No difference in MMP-1 expression was found between controls whereas MMP-8 was absent from all samples (Figure 4.17A). However, MMP-13 is specifically secreted by cells that are cultured on DIGE controls ( $p < 0.01$  and  $p < 0.05$  for DIGE-D and DIGE-E respectively), suggesting cells are actively secreting MMP-13 in these control conditions (Figure 4.17A). There was no expression of MMP-10 of the stromelysin family in either DMEM nor secreted by the cells (Figure 4.17B). For MMP-3 it was apparent that expression was inhibited by culture on DIGE-D and that it was expressed at similar concentrations for all other controls (DIGE-D statistically different from other controls, Figure 4.17B). TIMP expression was specifically observed in response to the culture of cells on substrates (there may be a slight concentration observed in DMEM for TIMP-2 and TIMP-4, Figure 4.16C). However, TIMP-1 expression is the most abundant of all TIMPs tested, TIMP-1 expression is further increased in supernatant taken from DIGE controls ( $p < 0.001$  and  $p < 0.05$  for DIGE-D and DIGE-E in comparison to glass). Wilhelm *et al.* show that in response to secretion of significant levels of TIMP-1, TIMP-1 complexes and inhibits MMP-9 (Wilhelm *et al.* 1989). This could account for the limit in MMP-9 expression observed in this and previous sections. It has been observed that for MSCs, expression of TIMP-2 in conjunction with MT1-MMP and MMP-2 are required from MSC mobilisation and invasion (Ries *et al.* 2007). If TIMP-2 is acting as an activator of MMP-2 then this could account for the increased expression of MMP-2 observed on the DIGE sequences. TIMP-2 expression was lower than that of TIMP-1 for glass, DIGE-D and DIGE-E surfaces ( $p < 0.05$ ,  $p < 0.0001$ ,  $p < 0.01$  respectively). TIMP-4 was absent from glass and expressed at a much lower concentration than TIMP-1 ( $p < 0.001$  in comparison to other control surfaces). Data published by Bigg *et al.* show that TIMP-4 specifically inactivates MMP-2 (Bigg *et al.* 2001). As shown in Figure 4.14, MMP-2 increases at week 3, this could be due to increasing TIMP-2 and decreasing TIMP-4. This experiment could be repeated with supernatant collected at weeks 1-3 to determine the interplay of TIMPs and their regulation of MMPs in MSCs in response to the surface chemistries.

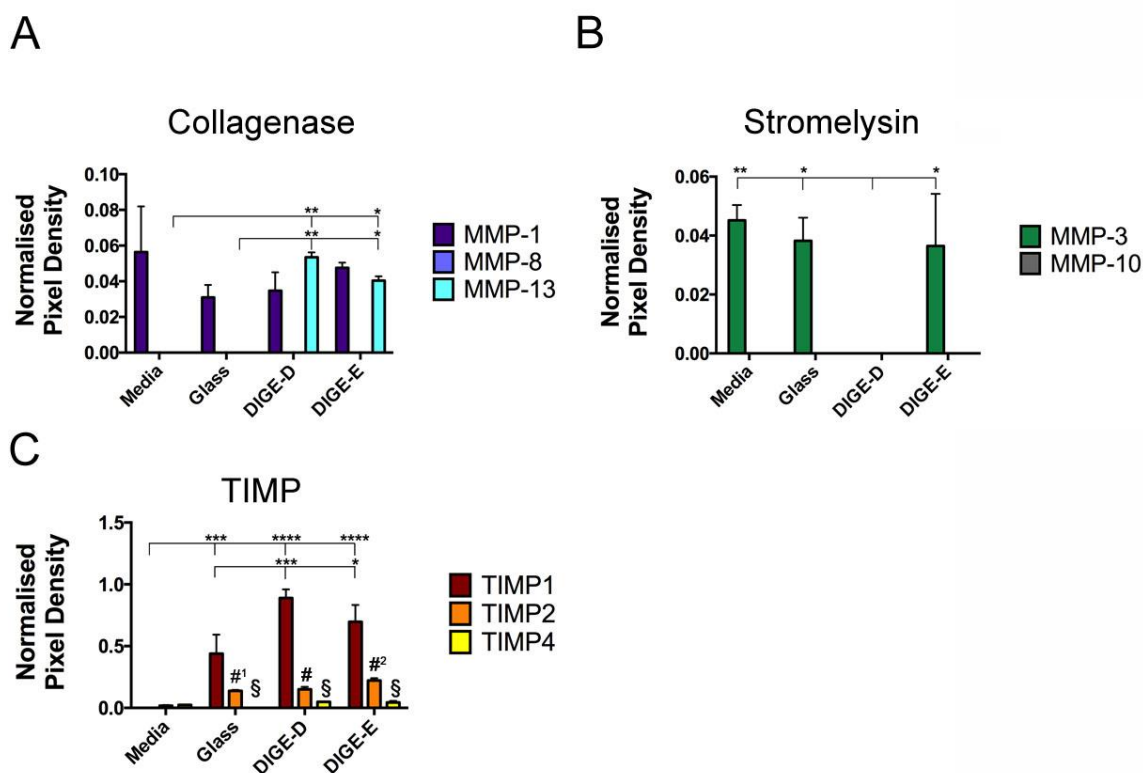


**Figure 4.17 - Presence of Other MMPs and TIMP Families.** There is differential expression of selected MMPs per surface. A) MMP-13 expression is specifically expressed on both peptide surfaces whereas MMP-8 is absent. B) MMP-10 was not found on any controls and further MMP-3 is not secreted in response to DIGE-D. C) TIMP expression is specific to cell culture. TIMP-1 may be an increasing on DIGE controls. In comparison to other controls. Graphs show  $\pm$  SD,  $n=2$  (spots per membrane), \*\*\*\* $p<0.0001$ , \*\*\* $p<0.001$ , \*\* $p<0.05$ . For # and §, statistics calculated in relation to TIMP-1 for that control. #<sup>1</sup> $p<0.05$ , #<sup>2</sup> $p<0.01$ , # and §  $p<0.0001$ .

All data obtained from the 3-week antibody array (Figures 4.16 & 4.17) was plotted on the same scale (Figure 4.18). TIMP-1 was expressed at the greatest level in comparison to other TIMPs and MMPs. This suggests that there is a regulation of MMPs by TIMPs as secreted by the cell population. TIMP-1 expression was specifically expressed in the cell supernatant demonstrating that these regulators are specifically secreted by the cells, regardless of surface chemistry. DMEM (media) contains less MMP-2 than the supernatant analysed from the controls suggesting the media itself is not contributing to cleavage.

## MMP and TIMP Expression, all surfaces

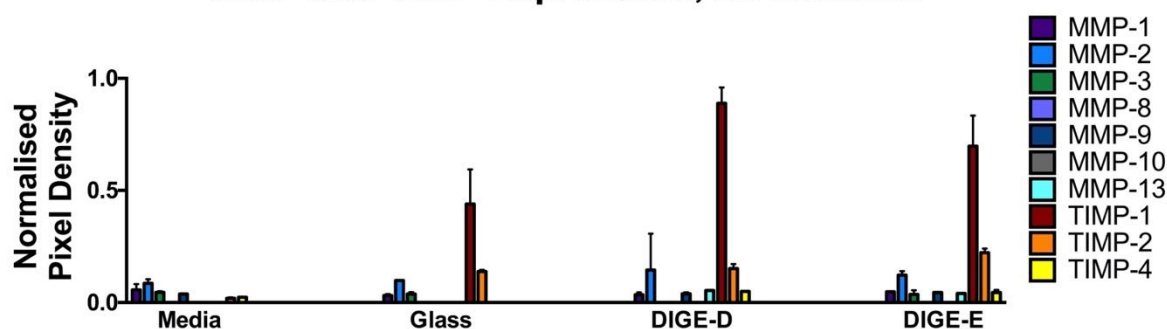


**Figure 4.18 – MMP and TIMP Expression.** The results show all MMPs and TIMPs identified by the antibody array per control. There was differential expression of MMPs depending on the surface chemistries. It was apparent that the cell supernatant contains TIMPs which are expressed at a much higher concentration than that of the MMPs. This is only a feature of the supernatant which highlights that the cells are regulating the secretion of MMPs.

## 4.4 Discussion

After the design and synthesis of the surface was deemed to be sufficient (Chapter 3), cell survival in response to surface chemistries was evaluated. Due to the previous studies of cells on similar chemistries employed by our collaborators, we expected good cell growth (Figure 4.1) (Roberts et al. 2016; Todd et al. 2009; Zelzer, McNamara, et al. 2012). The results from live/dead staining show that cells were found on all surfaces however, cell number was greatly decreased for DIGE-E and LRGE controls (Figure 4.2). This shows that the cells can react to the presence of the surface chemistries. When quantified, the data confirms that there were less cells observed on RGE controls (in comparison to glass) which indicates reduced cell attachment (Figure 4.2H).

Tubulin is a marker of cell metabolism and is actively involved with the transport of metabolites in the cell (Caviston & Holzbaaur 2006). Tubulin expression was prominent on RGD controls and in particular, LRGD (Figure 4.3). The results of this also highlighted differences in cell morphology as filopodia were observed on LRGD controls which is consistent with the literature as adhesion to RGD peptides allow for increasing spreading and a well organised cell cytoskeleton (Kilian and Mrksich, 2012). This appeared to be enhanced for LRGD in comparison to PEG capped RGD controls. Importantly, this experiment set-up should be repeated over multiple time points to track if there are any further changes to cell morphology in response to uncapped peptide. Changes in morphology are also apparent on RGE controls, with round or slightly elongated cells indicating that RGE is not supporting adhesion or spreading (Figure 4.3). However, it must be acknowledged that for the early cell studies (24-hour; Figure 4.2-4.4 & 4.7) the PEG

blocking group did seem to support cell survival even for RGE controls. There was a similar trend for vimentin staining which can also be used as a marker for cell integrity (Figure 4.4).

Cell culture time was increased to 1 week and cell survival analysed by MTT and Alamar Blue assays. The results in Figure 4.6 show consistency for both assays for all controls. After 1 week, it is apparent that all cells that had attached are metabolising on all controls. This was surprising due to the results of the 24-hour studies where it was indicated that RGE is limited in cell adhesion and survival (Figure 4.2-4.5). Figure 4.13B shows that there is a comparable number of cells on all surfaces by 1 week suggesting recovery of cells from 24 hours to 1 week. This effect could be due to the presence of serum proteins deposited on the surface which may affect the surface properties and therefore support survival of cells on RGE controls (Bellis 2011). Figure 3.22 does allude to coating by supernatant proteins and perhaps this had an impact on cell behaviour. However, the presence of the PEG should minimise this due to the anti-fouling properties of this chain length (PEG diamine  $M_w = 2,000$ ) for capped controls (Dong et al. 2011) and therefore this effect was unexpected. Perhaps different blocking groups or longer PEG chains should have been used or the percentage of serum used to culture cells should have been reduced.

Vinculin staining confirmed there is a difference in adhesion at 24 hours across each surface. Figure 4.7 suggested an increase in vinculin expression for RGD controls and increase in cell spreading specifically for PEG-RGD control. This result was quantified in Figure 4.8A which confirmed an increasing number of adhesions for the RGD controls per cell in comparison to the PEG-RGE and LRGE controls. The increase in the number of adhesions resulted in a similar trend in cell spreading as quantified in Figure 4.8B and was most pronounced for the PEG-RGD control.

Vinculin expression was then calculated as a unit of length ( $\mu\text{m}$ ), then distributed into specific size brackets to represent FCs ( $<2 \mu\text{m}$ ), FAs ( $2-5 \mu\text{m}$ ) and SMAdhs ( $>5 \mu\text{m}$ ). Results from Figure 4.9 show a limited expression of FCs, most adhesions were classed as FAs and the presence of SMAdhs was directly correlated to the presence of RGD (Figure 4.9). When separated into adhesion type and expressed as a percentage of total cell adhesions, FCs were prominent for glass controls and LRGE and DIGE-E surfaces (Figure 4.10). FAs composed the majority of cell adhesions but was slightly upregulated for the uncleavable controls. SMAdh were most prominent on RGD controls specifically in comparison to LRGE and DIGE-E. This suggests that presence of RGD is promoting

mature adhesion formation which in turn is expected increase cellular tension downstream (as explored in Chapter 5). This adhesion morphology has been observed in the past to be responsible for MSC differentiation to osteogenic phenotype (Biggs et al. 2009). Taken together, the results from Figures 4.3-4.5 & 4.7-4.8 suggest that cell adhesion correlates with cell spreading. Further, cell adhesion is differentially regulated depending on surface chemistry which, in turn, alters cell morphology in response. This could suggest that the cells are experiencing increased tension in response to the surface chemistry. And indeed, at week 1 the uncapped LRGD surface had a larger cell area (than PEG-RGE and LRGE, Figure 4.13A).

The result of the BrdU assay when quantified and analysed showed no significance between controls (Figure 4.12). This was only a 6-hour snapshot in a 1-week culture. More specifically, it would have been better to observe the first 24 hours to determine if there are changes in proliferation and the changes observed in Figure 4.2H are just the result of changes in adhesion. This experiment could be repeated at various time points to determine proliferative changes in response to surface chemistry over time (Chong et al. 2009).

We then looked at the cell secreted MMP-2 concentration over a range of weeks. Using an ELISA for MMP-2, it was determined that there was an increase at week 3 for LRGE, DIGE-D and DIGE-E sequences (Figure 4.14). This suggests that MMP-2 is actively secreted by cells at this time. The concentration of MMP-2 was much higher than MMP-9 consistent with Figure 3.8. However, we know from Chapter 3 that abundance does not necessarily mean potency and even though MMP-9 is not expressed at the same level as MMP-2, it could still be acting on the peptide. However, it was this data that contributed to the hypothesis that switching of the surface occurs at the 3-week time point.

We also found differential expression of TIMPs, stromelysins and collagenases (Figure 4.17). However, the differential regulation of MMPs is not an indicator of cell phenotype. Amalki *et al.* highlight in their review that differentiating MSCs secrete multiple MMPs and that no one MMP drives differentiation to a specific lineage (Amalki & Agrawal 2016). From the results presented in Figure 4.17, we cannot say definitively if the trends in MMP expression correlate to phenotype. It may have also been better to explore the media concentrations of MMPs to determine their effects. If it was found to have an effect, we could have lowered the concentration of serum for cell culture. Moreover, Figure 3.20 and 3.21 indicate that potency does not correlate to concentration, therefore the

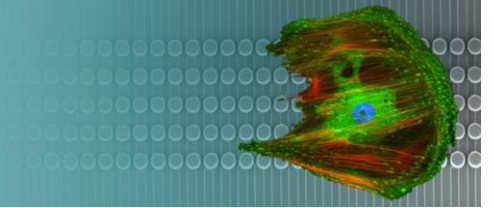
action of the identified MMPs from Figure 4.17 should have been tested on DIGE-D surfaces to rule out the effects of these MMPs on the surface.

Expression of TIMP-2 was exclusively observed in the cell supernatant which could suggest a migratory function of the seeded MSCs. However, as shown in Figure 3.4, TIMP-2 is a mode of activation for proMMP-2 in conjunction with MT1-MMP (Worley et al. 2003). Therefore, the increased secretion of this TIMP could relate to the activation of proMMP-2 via MT1-MMP although this is dependent on concentration (activation was determined to be 0.3 to 5 nM concentrations of TIMP-2 (Bigg et al. 2001)). The increased expression of TIMP-1 hints that this is a factor in the inactivation of MMP-9. These observations could explain the increase in MMP-2 and decrease in MMP-9 expression shown in Figure 4.14-4.16.

Finally, due to lack of characterisation of efficiency in the build-up of peptides by SPPS, the presence of deletion peptides or peptides with differing sequences may be present on the surface. This could affect the cell behaviour as a result. Further the MMP secretion by the cell was assumed to be a trigger for the whole coverslip. This may not be the case and the MMPs could be acting locally and therefore there may be an heterogenous display of peptides. The action of MT-MMPs was also not explored, however the action of these MMPs on the peptides could also contribute to any local effects.

## 4.5 Conclusion

The early cell studies did hint at differential behaviour in response to peptides however, cell number did recover by week 1 which was unexpected. The increase in MMP-2 was thought to be driver of cleavage due to the increase in expression at week 3 but the question of potency remains. Increasing TIMP expression may also be having a regulatory effect on the MMPs, which may affect efficiency of cleavage and also may be acting locally.



## 5. Phenotype

Having established effective synthesis of the surface (Chapter 3) and demonstrated cell viability in response to the chemistry (Chapter 4), we then determined the phenotypic changes of the MSCs. This is twofold due to the aim of this technology; to provide two behavioural cues to MSCs on one dynamic surface. In this chapter, we looked for self-renewal markers in response to the PEG cap and osteogenic markers in response to RGD. Osteogenesis was expected on RGD controls rather than RGE controls due to enhanced adhesion as demonstrated in Chapter 4. The results of Chapter 5 show a reduction of self-renewal over time on all surfaces tested. Osteogenesis was specifically observed in response to DIGE-D surface whereas cells cultured on DIGE-E surface also exhibited upregulation of other phenotypic markers, suggesting an unsynchronised cell population.

## 5.1 Introduction

This chapter aims to determine cell phenotype in response to the surface chemistries. It has been shown that the presence of similar engineered surface chemistry was not detrimental to MSCs (Roberts et al. 2016) which we have also observed for the MMP responsive surfaces. Further, there was differential adhesion and cell spreading in response to the surface chemistries (Chapter 4) which has been shown previously to be a prerequisite to osteoblastogenesis (McBeath et al. 2004). Therefore, it is our intention for this chapter to determine if the differential regulation of adhesions observed in the previous chapter, results in changes in phenotype over time.

Figure 5.1 shows the hypothesised MSC response to the surfaces. It was hypothesised that the PEG cap increases stem cell self-renewal of MSCs. This was previously demonstrated by Roberts *et al.* for the PEG-A $\downarrow$ ARGD surface (Figure 1.11) (Roberts et al. 2016). This response was thought to be due to an intermediate tension generated by MSCs; the proximity to the RGD coupled with the blocking group prevents full attachment and high intracellular tension negating osteoblastic differentiation and encouraging self-renewal (Roberts et al. 2016). Continued self-renewal of MSCs would therefore be expected until the PEG group is removed by cell secreted MMPs. From previous chapters, we observe an increase in cell secreted MMP-2 at week 3 (Chapter 4, Section 4.3.4). This was originally thought to be the enzyme responsible for cleavage and experiments were conducted prior to ToF-SIMS analysis where cell supernatant concentration of MMPs was applied to DIGE-D surfaces. Chapter 3 revealed that cell supernatant concentration of MMP-2 at week 3 was determined to be sufficient as this effect was mimicked *in vitro* and the PEG signal was reduced (Figure 3.20 – 3.22, Chapter 3). The original hypothesis was, that if in

response to increasing cell supernatant concentration of MMP-2 at week 3, the PEG cap is completely removed, then this time point is the starting point for osteogenesis due to MSC exposure to RGD and subsequent integrin binding (Figure 5.1). Generation of osteoblasts from MSCs with calcification and mineralisation was estimated to take 28 days (Stein & Lian 1993). We would therefore expect osteogenesis to occur 28 days after the 3-week time point due to the removal of PEG (Figure 5.1). However, 0.25 ng/ml MMP-9 also seemed to reduce the PEG signal (Figure 3.20 and 3.21) and therefore may also be having an effect on cell behaviour. Unfortunately, this was not fully explored, and phenotypic experiments were generated based on the original hypothesis (MMP-2 responsible and sufficient at week 3).

Increased adhesion that precedes osteogenesis is communicated to the nucleus via integrins as described Chapter 1 (mechanotransduction, Section 1.3). Based on the presence of SMAdhs observed on RGD controls (Chapter 4, Figure 4.8 & 4.9), we therefore expected that the increased adhesion would result in osteogenesis over time on this control.

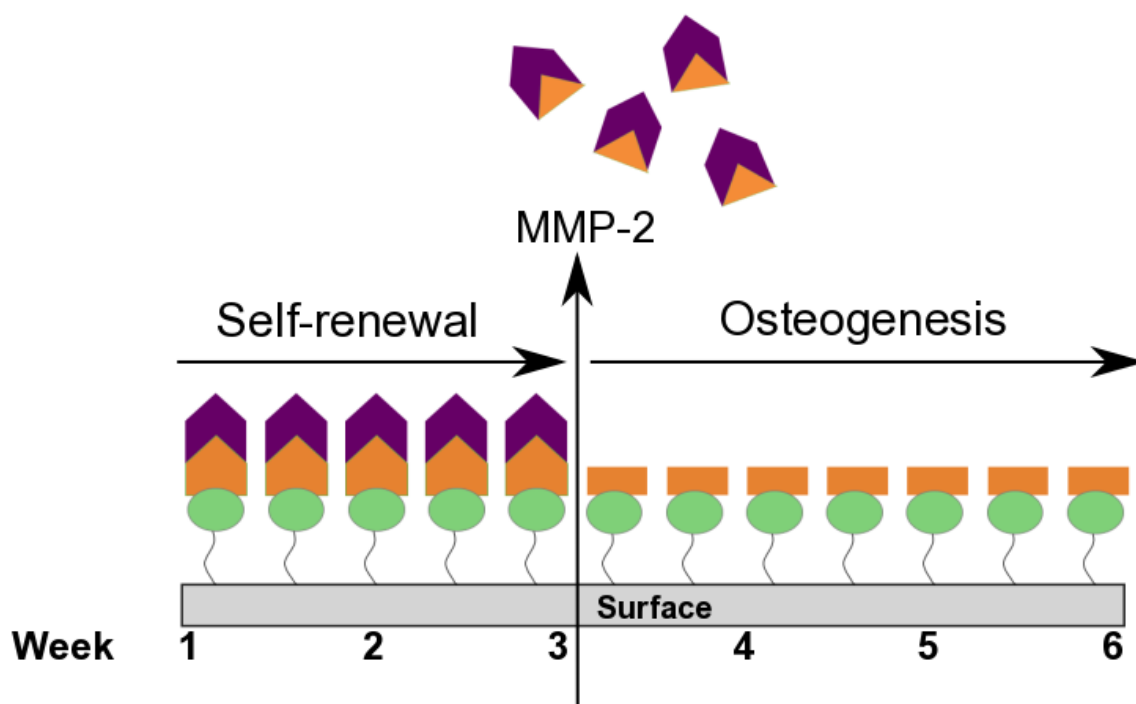


**Figure 5.1 – Hypothetical Model of Cell Response to Surface.** The presence of the PEG blocking group is proposed to stimulate self-renewal until a critical point where MMP concentration is sufficient to cleave the surface (week 3). With a sufficient concentration of MMP-2, the blocking group is removed, and differentiation can occur via cell binding to RGD. Therefore week 3 is hypothesised as the start point for osteogenesis.

### 5.1.1 Osteogenesis as a result of adhesion

As stated above, MSCs adhesions influences phenotype. Low adhesive states correlate to adipogenic phenotypes, whereas osteogenic phenotypes are as a result of increased focal adhesion formation (Engler et al. 2006; McBeath et al. 2004). With increased adhesive components available to the cell (by either ECM proteins *in vivo* or strategically placed by materials engineering *in vitro*) integrin clustering and SMAdh formation occurs (Cavalcanti-adam et al. 2007). This in turn leads to downstream changes in phenotype, namely osteogenesis (Figure 5.2). Adhesion size is also thought to influence the differentiation of MSCs, those that are elongated and stable limit cell growth and encourage differentiation (comparatively, small adhesions promote cell migration) (Biggs et al. 2009).

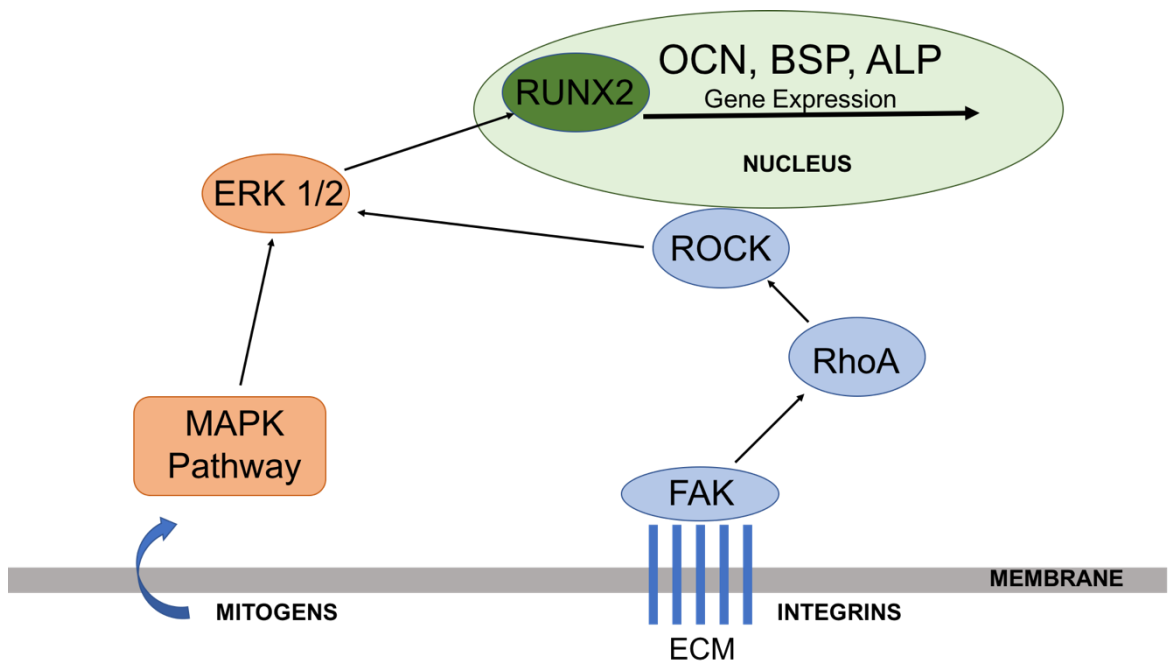


**Figure 5.2 – Intracellular Signalling for Osteogenic Differentiation.** Osteogenic gene expression is activated in response to integrin clustering and subsequent signalling via FAK to ROCK activation which influences cell contractility. This also promotes ERK signalling. ERK can also be activated by the MAPK pathway, which is initiated by soluble mitogens. ERK is a prerequisite for osteogenic differentiation as it activates the transcription factor RUNX2 that is responsible for the activation of osteogenic specific genes (redrawn from (Khatiwala et al. 2009)).

Adhesion to the surface is translated from clustering integrins to the nucleus via structural proteins (including FAK, talin and paxillin) during direct mechanotransduction (Mitra et al. 2005). The clustering of integrins and recruitment of these proteins result in changing signalling cascades that influence cell morphology and end terminal differentiation

(McBeath et al. 2004). As shown in Figure 5.2 clustering integrins activate ROCK via FAK and RhoA. McBeath *et al.* correlated the expression of ROCK to increased cell spreading (McBeath et al. 2004). Cells cultured on areas of fibronectin created by large PDMS stamps (10,000  $\mu\text{m}^2$ ) exhibited increase ROCK expression and osteogenic phenotype, even in the presence of adipogenic differentiation factors (McBeath et al. 2004). The expression of ROCK can also result in the expression of ERK signalling. ERK is a mitogen activated protein kinase (MAPK), the last effector of the MAPK pathway (activated by mitogens rather than mechanotransduction) (Khatiwala et al. 2009). ERK is responsible for the activation of the transcription factor runt-related transcription factor 2, RUNX2, (also known as core-binding factor alpha 1 (CBFA1) an activator of osteo-specific genes (osteocalcin (OCN), bone sialoprotein (BSP) and alkaline phosphatase (ALP)) (Ducy 2000). ERK deficient cells are incapable of osteogenic differentiation, with very limited mineralisation and bone marker formation demonstrating that ERK expression is a precursor to osteogenesis (Lai et al. 2001). Similarly, the inhibition of ROCK by disruption of cell shape (treatment with blebbistatin and cytochalasin) abrogated RUNX2/CBFA activation and therefore osteogenic differentiation is dependent on several downstream factors as discussed above (McBeath et al. 2004). RUNX2/CBFA is the main transcription factor for osteogenic activation. CBFA<sup>-/-</sup> mice are osteoblast deficient, lack mineralisation and have limited vascularisation of the marrow (Otto et al. 1997). Terminal osteogenesis is marked by mineralisation which is crucial for mature bone formation (Stein & Lian 1993). The bone ECM is mineralised by calcium (from hydroxyapatite) and inorganic phosphates that in turn facilitate skeletal development and contributes to the mechanical properties of bone (Staines et al. 2012; Shekaran & García 2011). The interplay of bone deposition and mineralisation is constantly regulated in conjunction with bone resorption by osteoclasts to maintain bone mass (Shekaran & García 2011).

### 5.1.2 Metabolomics

There is a wealth of genomic and proteomic information that has been generated to allude to cellular processes (Fiehn 2001). However, metabolomic analysis provides a complementary method to these techniques by providing a way to view the end process of gene expression, active cellular responses (Fiehn 2001). Metabolomics can be stratified into targeted and untargeted approach. As the name suggests, a targeted approach is applied to identify a specific metabolic pathway or a group of metabolites. In comparison, an untargeted approach refers to identification of the entirety of small molecules present in that data set. In this Chapter, we use an untargeted approach on MSCs seeded on DIGE-D

surfaces at week 3 to allude to how metabolically active cells are when cultured on different surfaces. If they are active, then this would suggest a differentiating phenotype conversely down regulation of metabolites suggest a quiescent phenotype.

### 5.1.3 Aims

The objective for this chapter was to determine cell phenotype in response to surface chemistry. Due to the observation that there was differential adhesion regulation and increasing MMP-2 secretion on DIGE-D and DIGE-E specifically (Chapter 4), we concentrated our work to encompass DIGE-D/E controls only in comparison to glass for the experiments carried out in this chapter. We initially determined self-renewal in response to the surface, then observed cell behaviour over longer term cultures

## 5.2 Methods

### 5.2.1 Supplier Information

**Table 5.1 – Supplier Information.** List of reagents used in Chapter 5.

<b>Technique</b>	<b>Reagent</b>	<b>Supplier</b>
In-cell Western	CellTag™ 700 stain	LI-COR, USA
	Goat anti-mouse	LI-COR, USA
	Stro-1 antibody	Santa Cruz, USA
	OPN antibody	Sigma –Aldrich, USA
	OCN antibody	Sigma –Aldrich, USA
	ALP antibody	Abcam, UK
qRT-PCR	RNeasy Micro Kit	Invitrogen, UK
	GAPDH antibody	Sigma-Aldrich, USA
	Superscript II reverse transcription kit	Invitrogen, UK

### 5.2.2 ICW

Supernatant was removed from the wells and samples were rinsed in PBS. Cells were then fixed for 15 min at 37 °C and permeabilised at 4 °C for 4 minutes. Perm buffer was removed and milk protein (1 % milk protein in 1x PBS) was added at 37 °C for 1.5 hours on a shaker after which, the primary antibody (1/100) in PBS/BSA was added and incubated at 37 °C for 2.5 hours. Samples were washed 5 x 5 min in tween, then the

secondary antibody (1/800) and CellTag™ (1/500) (both diluted in milk protein) were added for 1 hour at room temperature. Washing was carried out on a shaker 5 x in Tween for 5 min each at room temperature. Coverslips were removed and dried on white paper then inverted into a new 24 well plate. ICW was performed using a LI-COR Odyssey plate reader and data was analysed using Odyssey SA software. List of primary and secondary antibodies are shown in Table 5.2. Data was analysed by normalising the protein of interest over the total number of cells.

**Table 5.2 – Antibodies used for ICW.**

<b>Marker Type</b>	<b>Primary Antibodies</b>		<b>Secondary Antibody</b>	<b>Control</b>
	<b>Marker</b>	<b>Raised in</b>		
Self-renewal	Stro-1	Mouse monoclonal IgG	Goat anti-mouse IgG	CellTag™ 700 stain
Osteogenic	OPN			
	OCN			
	ALP			

### 5.2.3 von Kossa

P2 (Stro-1 selected, University of Southampton) were cultured on controls for the time stated in the text. Cells were rinsed in 1x PBS then fixed with fixative. A 5 % solution of silver nitrate in dH<sub>2</sub>O was added to samples and was placed under UV for 30 min. Samples were rinsed twice in dH<sub>2</sub>O then under running tepid water. 5 % solution of sodium thiosulphate in dH<sub>2</sub>O was added for 10 min then samples were rinsed in dH<sub>2</sub>O. Samples were then counterstained with nuclear fast red (0.1 g nuclear fast red, 5 g aluminium sulphate in 100 mL dH<sub>2</sub>O) for 10 min and rinsed in dH<sub>2</sub>O followed by rinsing in 70 % ethanol. Images were taken using a Zeiss Axiophot fluorescence camera with an Evolution QEi digital monochromatic CCD camera and Q-capture imaging software and analysed using Fiji (free download from NIH).

### 5.2.4 qRT-PCR

RNA was extracted from cells using RNeasy Micro Kit. RNA was reverse transcribed into cDNA using Superscript II reverse transcription kit. qRT-PCR was carried out using PCR 7500 machine (Applied Biosystems, UK) using relative comparative method. Glyceraldehyde 3-phosphate dehydrogenase (GAPDH) was used as reference controls (n=3). Gene expression was expressed as a fold change after normalising to GAPDH.

**Table 5.3 - Primers used for qRT-PCR.**

<b>Target</b>	<b>Primer</b>	
<b>CD63</b>	Back	5'-ATCCCACAGCCCACAGTAAC-3'
	Forward	5'-GCTGTGGGGCTGCTAACTAC-3';
<b>Sox9</b>	Back	5'-CGGCAGGTACTGGTCAAAC-3'
	Forward	5'-AGACAGCCCCCTATCGACTT-3'
<b>PPAR<math>\gamma</math></b>	Back	5'CTGCAGTAGCTGCACGTGTT-3'
	Forward	5'-TGTGAAGCCCATTGAAGACA-3'
<b>Col 1a</b>	Back	5'-AGGTGAAGCGGCTGTTGCC-3'
	Forward	5'-GCTCCGACCCTGCCGATGTG-3'

### 5.2.5 Metabolomic Analysis

Culture medium was removed from wells and the cells rinsed in chilled sterile PBS. The PBS was then removed from wells and 150  $\mu$ l chilled extraction buffer (1:3:1 Chloroform:Methanol:Water (v/v)) was added. The plate was placed on rotary shaker on ice at 4 °C for 1 hour. Extracted metabolites were placed in Eppendorf tubes and centrifuged for 3 minutes at 13000 g at 4 °C. A pooled sample (5  $\mu$ l from each sample combined) was also included for analysis. The supernatant was analysed using liquid chromatography separation with a ZIC-pHILIC 150 mm x 4.6 mm, 5  $\mu$ m column (Merck Sequant), operated by an UltiMate liquid chromatography system (Dionex, Camberly, Surrey). Mass spectrometry was performed using an Orbitrap Exactive (Thermo Fischer Scientific, Hemel Hempstead, UK) with mass range m/z 70-1400 in polarity switching mode at the Glasgow Polyomics facility (Creek et al. 2011). Metabolite identification was carried out using IDEOM analysis pipeline and analysed metaboanalyst <sup>10</sup>.

<sup>10</sup> <http://www.metaboanalyst.ca>

## 5.3 Results

### 5.3.1 Self-Renewal

It was hypothesised that the presence of the PEG blocking group in conjunction with RGD peptides would induce self-renewal response in MSCs, consistent with the work presented in Roberts *et al.* (Roberts et al. 2016). We stained the MSCs for Stro-1, a MSC surface marker of self-renewal using ICW (Lv et al. 2014). ICW is an immunohistochemical technique that shows the proportion of the marker to be investigated in terms of the whole cell population. Unfortunately, as there was no positive control, data was interpreted relative to the values obtained for other controls. We analysed Stro-1 expression over 4 weeks. We found similarity between all controls, showing a decreasing trend in Stro-1 expression over time (weeks 1 - 4) (Figure 5.3). This phenotype could be due to increasing differentiation and therefore loss of stem cell phenotype. As the glass control exhibits no behavioural cue to promote MSC differentiation in a targeted way, we could postulate that there is unspecific differentiation. This effect is maintained at week 3 on the DIGE-D surface which is comparable to that of week 2. It could also be possible that cleavage of the sequence has occurred at week 3 and that exposure of RGD is stimulating differentiation (Figure 5.1). This could explain the decrease in Stro-1 expression for DIGE-E and DIGE-D which is significantly different at week 4 (in comparison to week 1 values for both  $p < 0.0001$ ). Stro-1 expression decreases with specialisation and therefore self-renewal is not promoted on any control as Stro-1 expression decreases over time (Arpornmaeklong et al. 2009). It was expected that Stro-1 would be maintained for 21 days in response to PEG as described in Roberts *et al.* (Roberts et al. 2016). We can speculate that this is due to increasing distance from the RGD peptide as the enzyme recognition sequence is double the length tested previously. From the data presented in this Figure, we cannot say definitively that the decreasing Stro-1 expression indicates a heterogeneous population of progenitor cells. However, MSCs behave similarly between week 2 and 3 on DIGE-D suggesting a more comparative phenotype on this surface for these times.

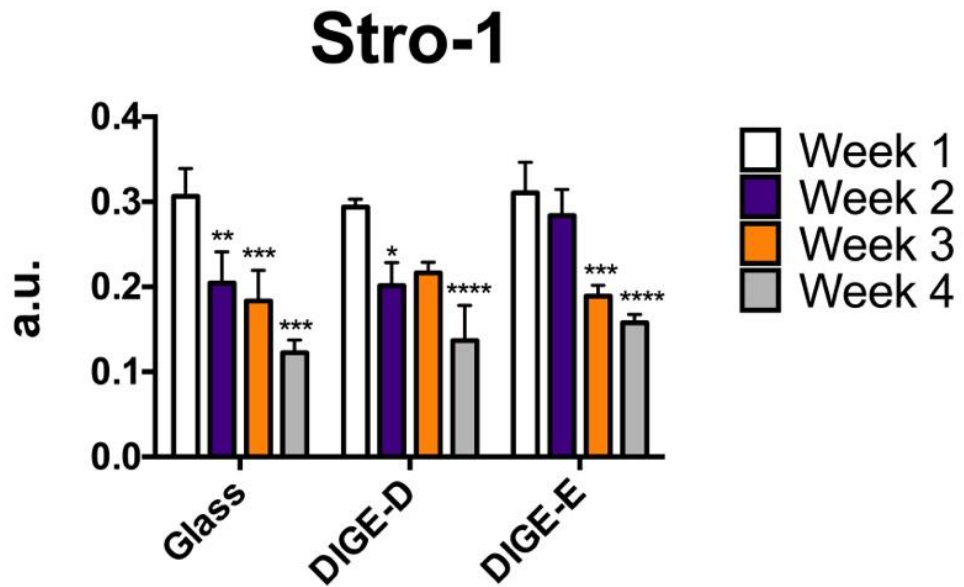


**Figure 5.3 – Stro-1 Expression Over 4 Weeks.** For all controls, Stro-1 expression decreases from week 1 – 4. Graph shows differences in comparison to week 1 for that control. Graph shows mean  $\pm$  SD,  $n=3$  where \* $p<0.05$ , \*\* $p<0.01$ , \*\*\* $p<0.001$ , \*\*\*\* $p<0.0001$ . Statistical analysis calculated by ANOVA and completed in respect to week 1.

### 5.3.2 Early Markers of Osteogenesis

To determine if the loss of Stro-1 was in response to increasing osteogenesis, we looked at the expression of RUNX2. RUNX2 expression was minimal on glass for both time points tested suggesting that glass was not promoting osteoblastic differentiation (both DIGE-D and DIGE-E were statistically different for both time points tested in comparison:  $p<0.05$  and  $p<0.01$  respectively). At day 7, there was significantly different expression of RUNX2 in response to the surface chemistries in comparison to glass. Surprisingly for DIGE-E this was more pronounced ( $p<0.05$ ) suggesting an upregulation of RUNX2 on this surface. The expression of RUNX2 at day 7 for the DIGE-D surface was more comparable to the glass control suggesting that osteogenesis at this stage was not promoted by RGD which was surprising due to the results presented in Chapter 4.

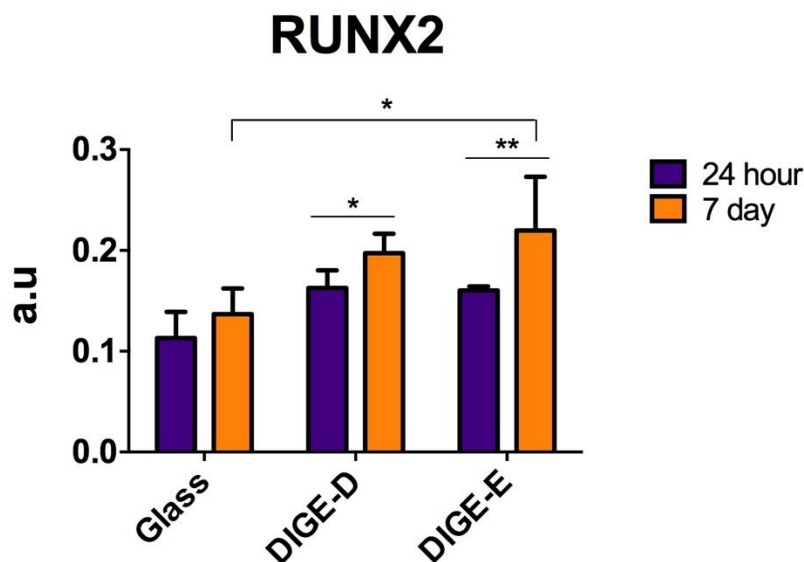


**Figure 5.4 – RUNX2 Expression After 24 Hours and 7 Days.** ICW analysis of RUNX2 expression as an initial response to the surface. There is an increasing trend for RUNX2 expression after 7 days in response to surface chemistry as expression of RUNX2 is significantly different to that of day 7 glass for both DIGE controls. Graph shows mean  $\pm$  SD,  $n=3$  where  $*p<0.05$ , statistics analysed by ANOVA and completed in respect to glass.

### 5.3.3 Metabolite Analysis, Week 3

In previous studies (Roberts et al. 2016) we utilised metabolomics to understand how active cells were i.e. does the uncapping of the PEG blocking group result in the upregulation of the metabolome indicating cellular differentiation? In those studies, we identified that there were some differences in the unswitched (blocking group in place) and switched controls (RGD exposed) (Roberts et al. 2016). This experiment was repeated for this Thesis, although it was conducted comparing DIGE-D and DIGE-E surfaces. We performed an untargeted metabolomics screen to understand the secretion of metabolites for both DIGE-D and DIGE-E controls in comparison to glass at week 3 (osteogenic time point 0, Figure 5.1). This was employed to understand how metabolically active the cells were, indicating the uncapping of PEG and subsequent cell differentiation in response to peptides. Metabolomics data was firstly analysed using MetaboAnalyst 3.0, a web based tool for metabolomic interpretation (Xia & Wishart 2011). Using MetaboAnalyst, we identified similarities between data sets when expressed as PCA plots (principal component analysis). Samples with distinct clusters indicate differences in each sample set whereas those with overlap indicate a more similar dataset (Fiehn 2001; Robinson et al. 2005). Variation is determined by principal component (PC) and is usually plotted using first and second components, PC1 and PC2 where those with the most variance first (Robinson et al. 2005). Figure

5.5 shows data for Glass (blue), DIGE-D (red) and DIGE-E (green) surfaces where there was an overlap between samples. Overall, there was similar behaviour on all surfaces and in addition there may be more variation of DIGE surfaces than glass (more spread across both axis). DIGE-E samples, display more variance on the PC1 axis that spans the most variation (73.4 %). In comparison, DIGE-D data sets were spread over PC2 axis indicating less variation between triplicates (21.9 %).

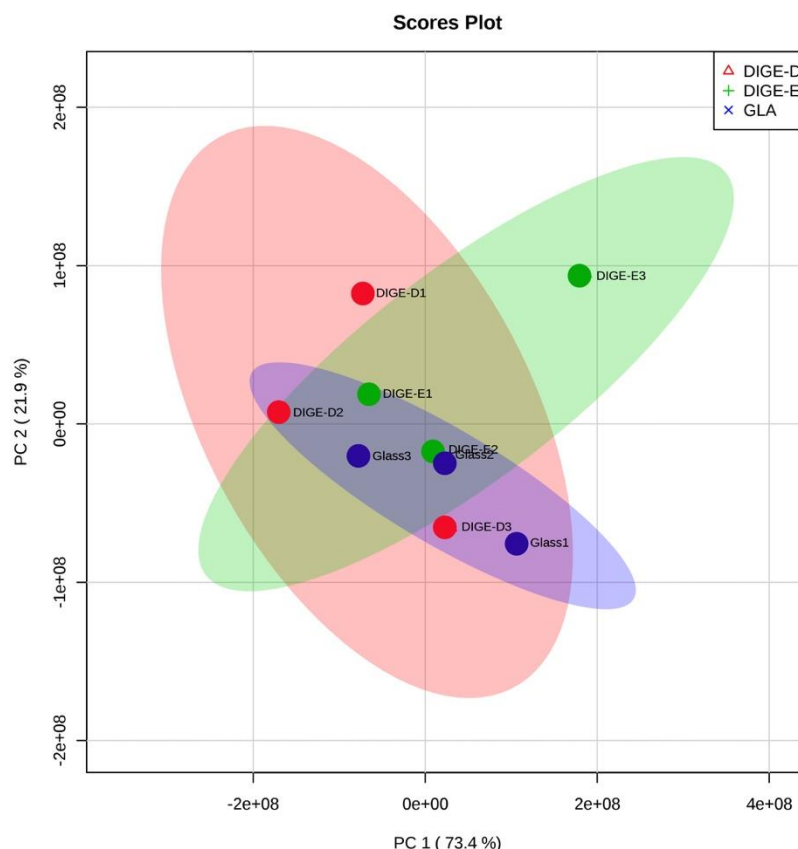


**Figure 5.5 - PCA Plot for DIGE-D and DIGE-E at Week 3.** Metabolomics data was uploaded to Metaboanalyst and a PCA plot generated. Data shows overlap in metabolite expression from cells from both samples indicating MSC phenotype at 3 weeks is similar. Data labels are coloured where red = DIGE-D, green = DIGE-E, blue = glass (n=3).

We then separated the metabolites into categories (lipids, nucleotides, carbohydrates and amino acids) then performed a PCA analysis (Figure 5.6). For lipids, there was a significant overlap for all data points from both controls, with glass controls the most tightly clustered. DIGE-D and DIGE-E were much more spread. DIGE-E showing more variation over PC1 (96.8 %) than DIGE-D where PC2 totalled just 1 %. Comparatively, glass controls exhibit more variation when looking at other metabolite types than there was for lipids. Overall, the behaviour of DIGE surface act similarly for all metabolites. DIGE-E samples appear to be more spread over PC1 and DIGE-D samples are spread over PC2. This suggests that there is less variation for DIGE-D controls than DIGE-E. For all parameters tested, there is no distinct clustering of

metabolites indicating a degree of overlap of all metabolites for both controls and variation between the triplicates tested. PCA plots reveal the similarities between data sets, not the regulation of the metabolites in those sets.

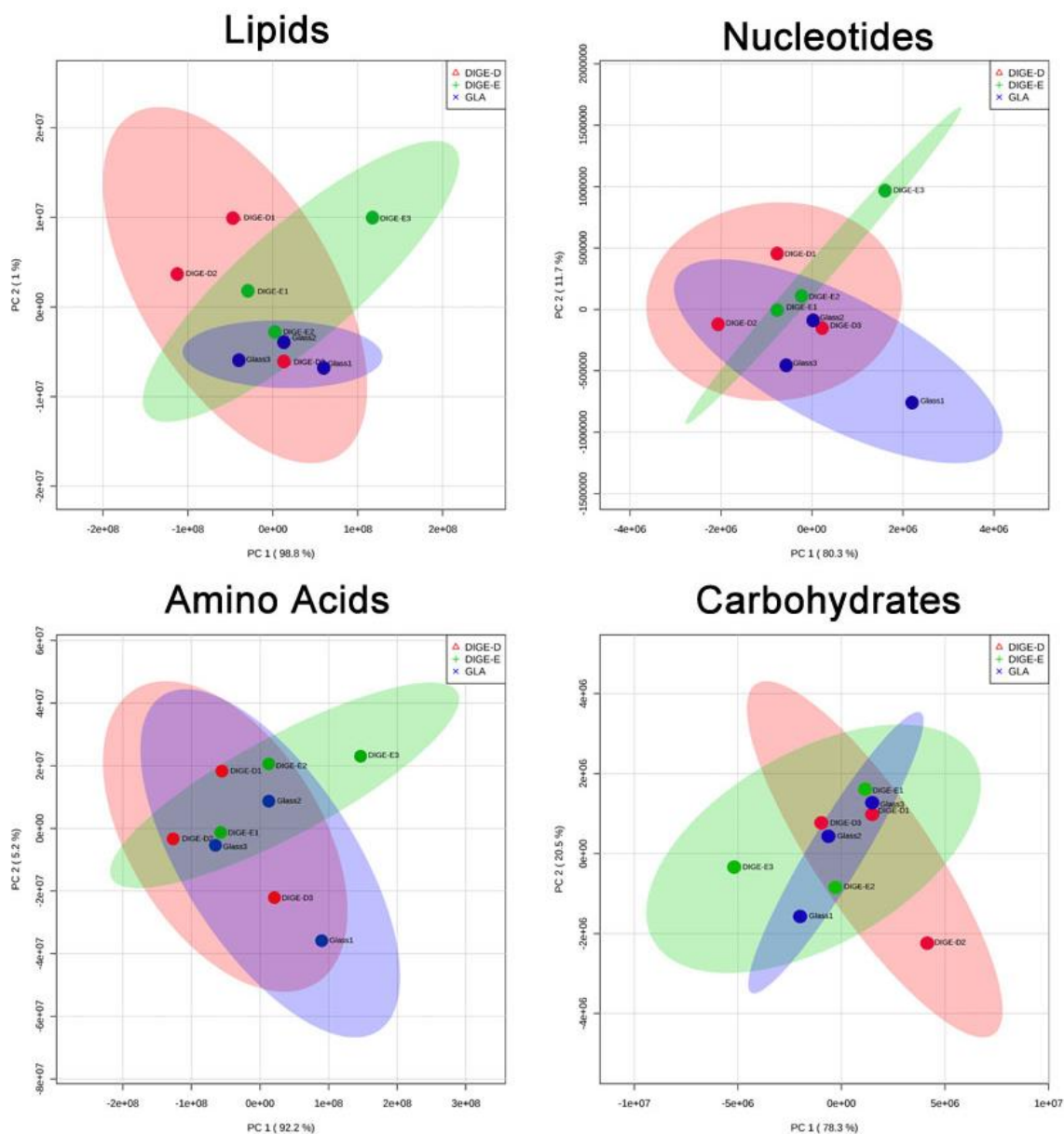


**Figure 5.6 – PCA Plots per Metabolite Group.** Data was separated into metabolite type (lipid, nucleotide, carbohydrate and amino acid) and expressed as PCA plot using MetaboAnalyst. Data shows that there is a degree of overlap for all metabolites tested, indicating similarities in expression in all metabolite subgroups. Data labels are coloured where blue = glass, green = DIGE-D and red = DIGE-E, n=3.

The metabolites were then statistically evaluated using the IDEOM file where a T Test was carried out in comparison to the glass control. Few metabolites that were identified as statistically different also had high confidence in their identification. Identification of metabolites was based on the retention time from the separation phase and the mass and intensity as calculated by the mass spectrophotometry (Sumner et al.

2007). If a metabolite has been matched to a standard, then it could be described as an authenticated metabolite and given a high confidence score on IDEOM (Sumner et al. 2007). Otherwise it is an annotated metabolite and therefore has a lower confidence score. Metabolites with a statistical difference but with low confidence scores were excluded. Applying these parameters revealed few identified metabolites with statistical significance as consistent with Figures 5.5 & 5.6.

When comparing DIGE-E to glass, 3 metabolites were identified as statistically significant; octadecanoic acid, taurine and phenylacetaldehyde, which are involved in fatty acid biosynthesis, bile acid metabolism (lipid metabolism) and phenylalanine metabolism (amino acid metabolism) respectively. Conversely comparing DIGE-D to glass reveals two metabolites that were statistically different. Both of which were classified as members of the amino acid metabolism pathway; L-Citrulline and N-Dimethyl-2-aminoethylphosphonate, which are involved in the arginine and proline pathway and the aminophosphonate metabolism pathway respectively.

It should be noted that during the execution of this experiment there was some level of extraction solvent evaporation prior to analysis. This therefore limits the reliability of the experiments and the quantification of the identified metabolites. Due to this limitation and the few metabolites that were identified, there is not enough data to comment on the peptides effects on these metabolites.

#### 5.3.4 Differentiation, Week 4 - 6

Cell culture was then extended to 6 weeks to observe phenotypic changes in response to increased MMP-2 secretion and cleavage of the surface (Section 5.5.1). To understand if the decrease in Stro-1 (Figure 5.3) correlates to increasing specialisation, we looked at osteogenic makers at 4 weeks using an ICW (Figure 5.7). We found that ALP is upregulated on all controls at week 4 and was significantly different to that of OCN and osteopontin (OPN,  $p < 0.0001$  for all controls). ALP is an early marker of osteogenesis and would be expected to be secreted before OPN and OCN in differentiating cells (Stein & Lian 1993). It was not expected that all surfaces would promote similar levels of ALP with no one surface is actively promoting ALP over the other chemistries. Furthermore, it was thought that osteogenesis had not occurred at this time point as OPN and OCN are mature markers of osteogenesis which were expressed at minimal levels. (Stein & Lian 1993)

## 4 Week

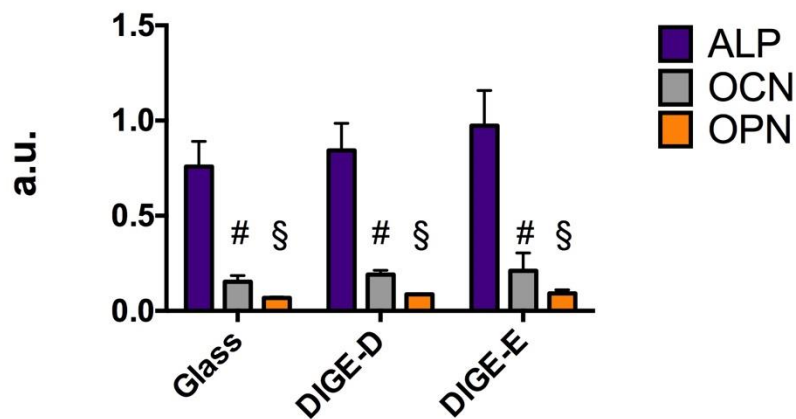


**Figure 5.7– 4-week ICW of Bone Markers.** ICW was performed for ALP, OCN and OPN. Results show there is similar expression for each marker across all controls indicating that this time point is insufficient for osteogenesis. Graph shows mean  $\pm$  SD, n=3. Statistics calculated by ANOVA, where ALP controls are statistically significant with respect to OCN = # and OPN = § (\*\*\*\* p < 0.0001 for both # and §), ns observed between controls for ALP expression.

We then analysed samples for evidence of mineralisation at 4 weeks using von Kossa staining. As stated in the introduction of this chapter, mineralisation represents terminal bone formation (Shekaran & García 2011). Mineralisation of MSCs can be observed using von Kossa staining where silver ions react with phosphate to create silver phosphate which is then degraded to silver in response to light that can be observed by microscopy (Bills et al. 1971). For von Kossa analysis, cells are treated with silver nitrate that is deposited, replacing calcium in the mineralised part of bone. It is then reduced by a strong light to be visualised as metallic silver (Bills et al. 1971). Figure 5.8 shows no mineralisation was observed on any controls at week 4 which was expected due to the results in the previous Figure (Figure 5.7).

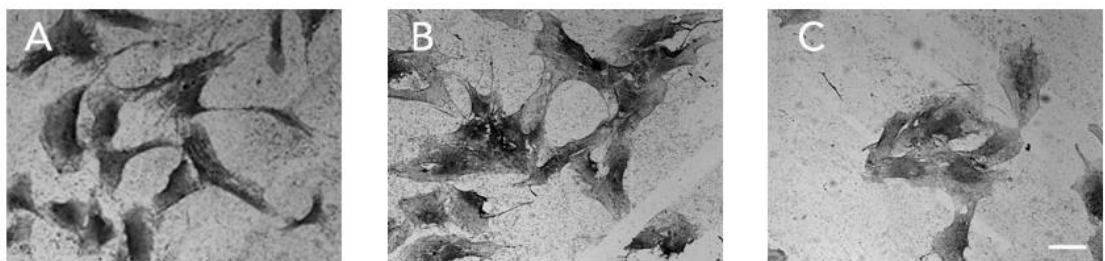


**Figure 5.8 – Von Kossa Staining at 4 Weeks.** A) Glass B) DIGE-D C) DIGE-E. There is little mineralisation observed on all controls. Scale bar = 100  $\mu$ m, n=15 (frames).

We then extended the culture time to 6 weeks and repeated the above experiments. There was a change in the presentation of osteogenic markers at 6 weeks as determined

by ICW specifically, OPN was upregulated after 6 weeks (Figure 5.9). Further, OPN secretion on DIGE-D surfaces was statistically increased in comparison to Glass and DIGE-E surfaces ( $p < 0.05$  and  $p < 0.01$ , respectively). OPN is also expressed at a much higher level than that of OCN and ALP. It is known that ALP is an early marker of osteogenesis, which is replaced with OPN and then OCN with extended culture (Stein & Lian 1993), and thus the change of markers between 4 and 6 weeks was not unexpected. Due to the markers following the expected pattern of expression, it was thought that cleavage had occurred. It was surprising that this trend was reproduced in all coverslip preparations, although OPN expression at 6 weeks did increase specifically on the DIGE-D surface. It is possible that if cultures were extended to 8 weeks, then we would have seen a further change in expression.

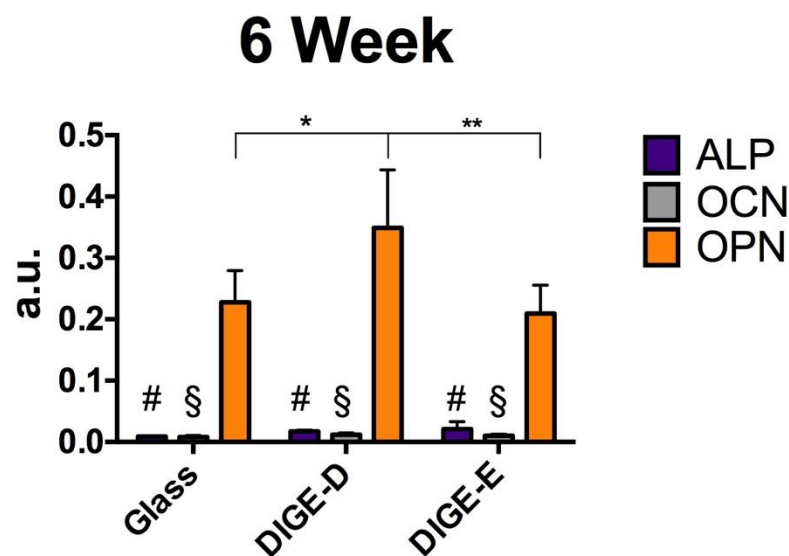


**Figure 5.9 – 6-Week ICW of Bone Markers.** ICW was performed at 6 weeks using the osteogenic markers ALP, OCN and OPN. Data shows increases in OPN staining, specifically for DIGE-D control. This suggests that the osteogenic phenotype was induced by presentation of RGD. OPN expression was statistically different to OCN and ALP. Graph shows mean  $\pm$  SD,  $n=3$ . Statistics calculated by ANOVA, where \*  $p < 0.05$  and \*\* $p < 0.01$ . Concentrations of ALP (#) and OCN (\$) were statistically different from concentration of OPN for that control # and \$ =  $p < 0.0001$ .

This was repeating using qRT-PCR at 4 & 6 weeks. OPN staining correlated with the results observed in Figure 5.9 where OPN was predominately expressed on the DIGE-D surface at 6 weeks (Figure 5.10A). OCN followed a similar trend as shown in the previous figure (Figure 5.9) and was not expressed at comparable levels to that of OPN (Figure 5.10). DIGE-D expression of OCN was comparable for both weeks tested and OCN expression was greatest at 4 weeks for the DIGE-E surface which was unexpected (Figure 5.10B).

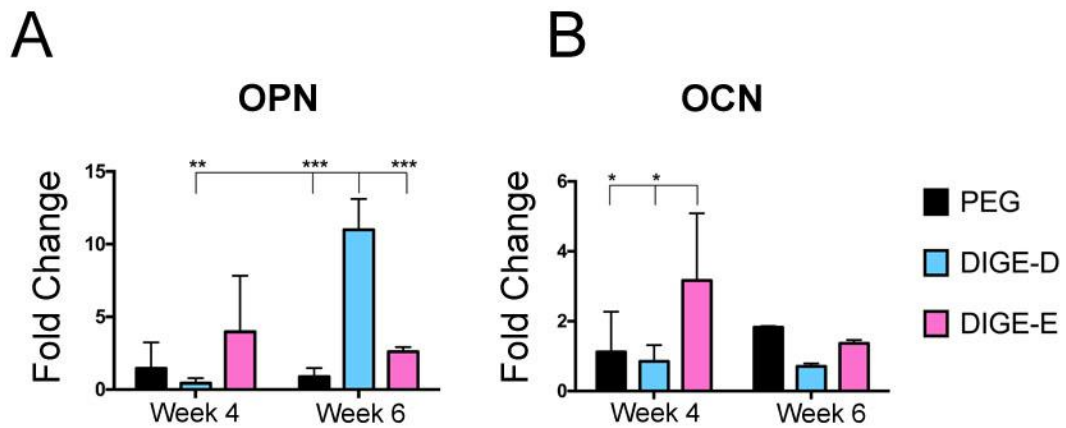


**Figure 5.10 – Osteogenic Markers at 4 and 6 Weeks.** For A) OPN and B) OCN (note difference in scale between A&B). A) OPN expression was significantly different to that of other controls at week 6. B) OCN expression was greatest on DIGE-E at week 4. Graph shows fold change in relation to glass control, mean  $\pm$  SD, n=3, statistics were calculated by ANOVA where \* p<0.05, \*\*p<0.01 and \*\*\* p < 0.001.

Due to increased OPN staining, it was thought that mineralisation of the DIGE-D sample would occur. Mineralisation was tested at 6 weeks using von Kossa staining (Figure 5.11). We observed comparable average nodule size for both glass and DIGE-D (approximately 40  $\mu\text{m}^2$ , Figure 5.11D). There was more consistency observed on DIGE-D with less variation in size observed between nodules whereas nodules observed on glass controls exhibited a large standard deviation (Figure 5.11D). The DIGE-E surface presented few areas of staining and all less than 20  $\mu\text{m}^2$ . However, even though nodule size on DIGE-E was half that of DIGE-D, this was not statistically different and therefore we cannot say that any surface is promoting osteogenesis. This result was unexpected after the increase in OPN shown at the same time point (Figure 5.9 and 5.10). After this extended culture time, with cleavage expected, this suggests that the DIGE-D peptide is not promoting the expected phenotype.

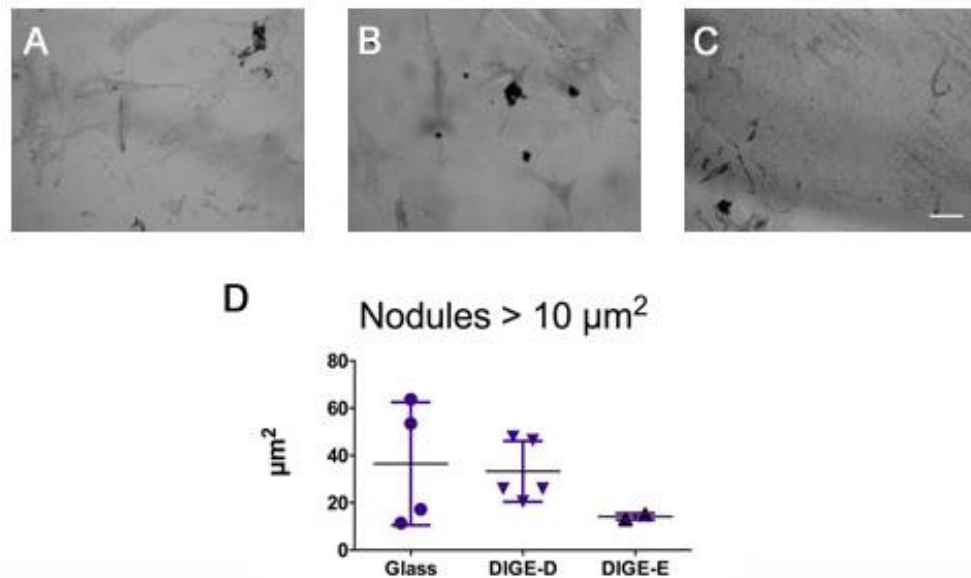


**Figure 5.11 – Von Kossa Staining at 6 Weeks.** Images of A) Glass, B) DIGE-D, C) DIGE-E stained using von Kossa. Image shows increased mineralization after 6 weeks of culture. Scale bar = 100μm. D) Results of A-C were quantified showing a limitation of mineralisation on DIGE-E controls suggesting that this is not promoting osteogenic phenotype. Glass and DIGE-D have similar average size nodules, however there is less deviation observed between nodules for DIGE-D suggesting a more synchronised population. Graph shows average  $\pm$  SD, n=15 (frames).

### 5.3.5 Spontaneous Differentiation

Using qRT-PCR, we tested the presence of differentiation and stem cell markers at weeks 4 and 6. Figure 5.12 depicts fold change in comparison to glass, PEG<sub>21</sub> diamine was also used as a control (treated glass with GOPTS then PEG diamine as per first stage of SPPS prior to amino acid addition).

All markers were upregulated in comparison to glass (Figure 5.12). Firstly we observed the Sox9 (Sry-related high mobility group box 9) marker, a cartilage specific transcription factor (Behringer et al. 1999) which is significantly upregulated at 6 weeks for MSCs cultured on the PEG surface over time ( $p < 0.05$ , Figure 5.12A). Sox9 expression was slightly greater on the DIGE-E surface than DIGE-D (3-fold compared to no change on glass). We then looked at PPAR $\gamma$  (peroxisome proliferator activated receptor gamma), an adipose related transcription factor. It was apparent from Figure 5.12B that PPAR $\gamma$  expression was greatest on the DIGE-E surface at 4 weeks. However, this phenotype was not sustained at 6 weeks indicating the 4-week time point either marks the beginning of adipogenesis or is an artefact. PPAR $\gamma$  was expressed at much lower degree for the other controls tested however, by week 6 PPAR $\gamma$  expression was negligible for all controls. Expression of Collagen I (Col I) was also evaluated as

it comprises a significant amount of the bone matrix (Brodsky & Persikov 2005). Figure 5.12C shows a greater amount of collagen expression for all surfaces at 4 weeks in comparison to 6 weeks. However, there is no increasing trend for collagen deposition over time on any surface. This is expected as determined by Stein and Lian, Col-I expression is maximal at early stage culture (7 – 14 days) and decreases over time with matrix maturation and was consistent with results from Figure 5.7 – 5.10. (Stein & Lian 1993).

Self-renewal was also tested by observing CD63 expression. CD63 expression for both PEG and DIGE-D controls was similar between the two-time points tested (Figure 5.12C). The results could suggest that PEG could support a degree of chondrogenic differentiation and DIGE-E might potentially support adipogenic differentiation however, this could also be the result of spontaneous differentiation. However, we can confirm that DIGE-D surface chemistry was not promoting differentiation towards other phenotypes (adipogenesis or chondrogenesis).

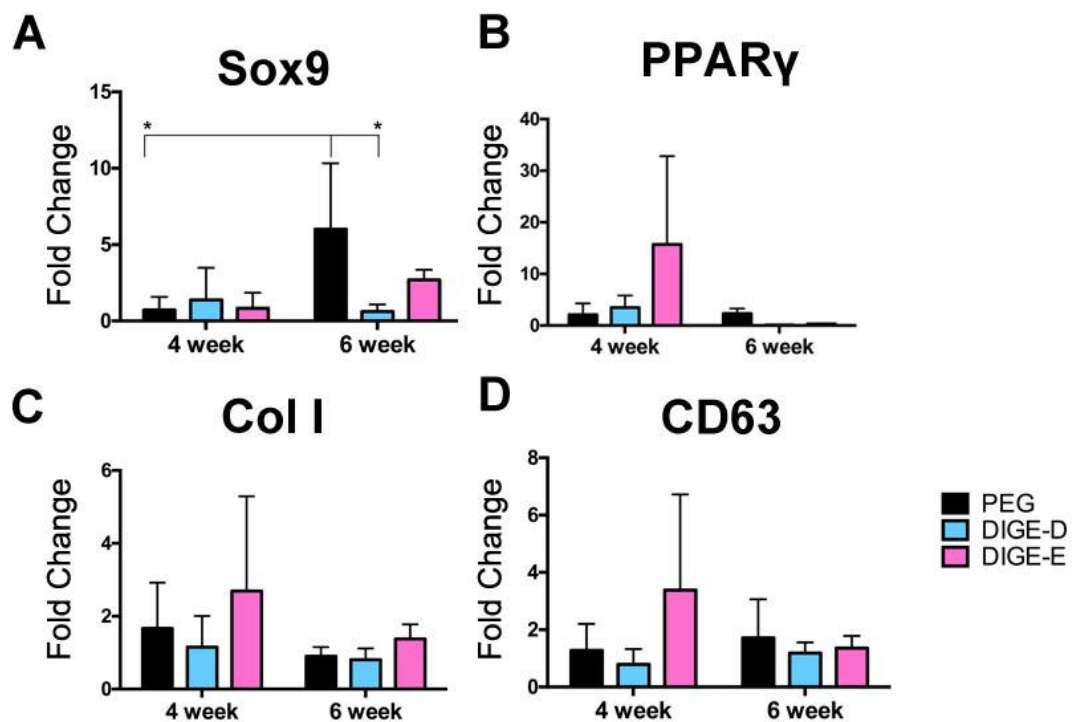


**Figure 5.12 – Phenotype Determined by qRT-PCR.** Primers against A) Sox9 B) PPAR $\gamma$  C) COL I and D) CD63 were used and analysed at 4 and 6 weeks. Graph shows mean  $\pm$  SD, n=3, fold change in relation to glass control, statistics calculated using ANOVA, where \*p<0.05.

## 5.4 Discussion

Self-renewal was expected in response to the PEG group as we had observed previously with Roberts *et al.* (Roberts et al. 2016). There was in general a decreasing abundance of Stro-1 for all controls tested over time and this demonstrates that the cell response to the peptide sequences is similar to that of glass at each week tested (Figure 5.3). As Stro-1 is lost with specialisation, this data further suggests that cells are not self-renewing. Although the presence of peptide is therefore not accelerating Stro-1 loss, it is also not enhancing it. It would have been better to repeat the experiment with a different marker of self-renewal e.g. ALCAM. The decrease in self-renewal could have also been correlated to other proliferative makers (to suggest transit amplification) or transcription factors that would indicate differentiation. This was briefly looked at using RUNX2. It was found that RUNX2 expression was not greatly increased at early time points and therefore osteogenesis at this stage cannot account for the quick loss of Stro-1 as determined by Figure 5.3.

The lack of self-renewal was unexpected due to the Results from Roberts *et al.* The result in Figure 5.3 could be due to increasing chain length from A↓A used in Roberts *et al.* to GPAG↓L used in this work and therefore increasing distance from RGD (Roberts et al. 2016). It was thought that the cells had an awareness of the RGD peptide beneath the PEG blocking group, which enabled an intermediate tension phenotype that is required for MSC self-renewal (Roberts et al. 2016). There is a chance that the increased chain length was not promoting the same effect and thus potentially drives a fibroblastic population of cells (Dalby et al. 2018).

An untargeted metabolomics screen was conducted. From the data presented in Figure 5.5 (PCA plots), we can determine that there is overlap between the samples suggesting a similarity between all controls. This suggests that there was little variation between samples and when this data was striated into metabolite categories little variation was observed between metabolite classes (Figure 5.6). This result was confirmed when looking at those metabolites that were significantly different to glass as few identified compounds were different ( $p < 0.05$ ). Due to the limitation of the experiment (evaporation of sample prior to analysis) this may not be representative of the cell metabolism and due to the expense of running the technique, the experiment was not repeated. Furthermore, if there was more time and availability of materials it would have been better to compare DIGE-D to LRGD, as this would have enable us to

understand the role of PEG in preventing access to RGD (unswitched sample in comparison to switched), and to understand metabolite regulation as an indication of a quiescent population.

Differentiation of MSCs was not predicted to occur prior to PEG cleavage. Cleavage was thought to be dependent on cell supernatant concentration of MMP-2, which is not sufficient until week 3 (Figure 5.1). Further work should be done to understand the role of MMP-9, as it was shown in Chapter 3 that cleavage is obtained at 20 ng/ml MMP-2 but also at a much lower concentration (0.25 ng/ml) of MMP-9. A method to test uncapping *in situ* would have been beneficial, although challenging to do in the presence of cells. There is also a risk that secreted MMPs are acting locally and that there is variation across the surface with only a proportion of peptides being cleaved. From the data, we are unable to definitively say when cleavage has occurred, which will affect cell phenotype as a response.

From the data presented, there was an indication that osteogenesis was beginning after 4 weeks in culture and this appeared to be consistent with the original hypothesis. From the ICW data at weeks 4&6 (Figure 5.7 and 5.9), the DIGE-D sample seemed to follow the protein expression expected of differentiating cultures (Stein & Lian 1993). Moreover, OPN expression was seen to increase on DIGE-D surface at the transcriptional level (Figure 5.10). However, when this was tested using Von Kossa staining, as an indicator of mineralisation (terminal stage of osteogenic differentiation, Figure 5.11), evaluation of areas of mineralisation revealed there was no statistically significant difference, which was surprising due to the previous data (Figure 5.7 – 5.10). This final result suggests that the DIGE-D is not promoting osteogenesis.

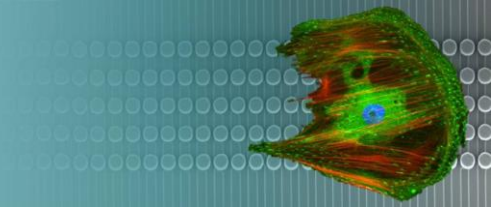
The qRT-PCR data also suggests a lack of self-renewal in the MSC populations, although over long-term culture which wouldn't be unexpected (lack of CD36 by 6 weeks, Figure 5.12D). This could be due to differentiation by this time point, possibly in response to cleavage of the PEG cap. There is potentially a role of CD63 in osteogenesis. It was suggested by Egea *et al.* that TIMP-1 co-localises with CD63 to prevent osteogenesis via the miRNA Let-7f promoting the knockdown of  $\beta$ -catenin/wnt signalling (Egea et al. 2012). From the previous chapter, it was observed that there is an increase in TIMP-1 expression at week 3 (Figure 4.17C & 4.18) and so perhaps the increase in TIMP-1 could delay osteogenesis in addition to the restriction in adhesion due to the PEG cap. However, if TIMP-1 is acting through this mechanism, and

expression remains high in cell supernatant over time, this could account for the delay of osteogenesis (Figure 5.11). To investigate this further, TIMP-1 expression should be tracked for the 4 and 6-week time points and correlated to the trend in osteogenesis. Co-localisation studies of CD63 and TIMP-1 could also be conducted.

Further, it should be noted that DIGE-D does not support differentiation towards chondrogenic (Figure 5.12A) or adipogenic (Figure 5.12B) phenotypes and therefore, spontaneous differentiation was not expected on this surface. This alludes to a more synchronised population of cells in response to DIGE-D. In comparison, various markers were observed on DIGE-E surface, this could be as a result of spontaneous differentiation. More analysis should be done to understand the interplay of all phenotype markers from week 1 to week 6. This would enable a better understanding the point at which differentiation begins and to account for the loss of Stro-1.

## 5.5 Conclusion

From the data presented in this Chapter there is a suggestion that DIGE-D is driving differentiation of MSCs in an osteoblastic lineage due to increased expression of bone makers however, this did not culminate in extensive mineralisation. Extending the culture time would perhaps enhance this data however, this presents a challenge in that there would be an increasing risk of infection. There not enough evidence of self-renewal and the results were not consistent with those presented in Robert's *et al.* (probably due to increasing chain length) (Roberts et al. 2016). Due to the increased proliferative and differentiation markers in response to DIGE-E and the lack of directive peptides, we suggest a fibroblastic population in response to this surface with increasing culture length. In comparison, the specificity of osteogenic markers alone suggests that the DIGE-D surface is directing the cell population to osteoblastic cells specifically.



## 6. Discussion

We are currently limited by the provision of adequate therapies to aid not only age-related illnesses, such as arthritis and osteoporosis, but also morbidity associated with organ donation (Ringe et al. 2002). These conditions make regenerative therapies utilising stem cells attractive. However, we are currently limited in the provision of high-quality stem cells and therefore high-quality terminal differentiated cells. We have designed a surface using SPPS that was intended to provide dual functionality as a cell culture platform. In this Chapter, we will discuss the benefits of regenerative medicine, the outcomes of the project, limitations of the system and assess further areas that could be investigated.

## 6.1 Introduction

Dynamic surface-based therapeutics are rapidly becoming the gold standard for biomaterials. These surfaces are thought to pave the way for the future of TE as they are better able to recapitulate the critical aspects of the ECM and thus drive phenotype development. The ECM is known to control cell behaviour as altering stiffness, topography and chemical composition leads to the activation of various genes and therefore control of cell behaviour. The *in vivo* ECM comprises an elaborate web of proteins, growth factors, physical and chemical cues which dictates a level of detail unmatched outside the biological world. However, materials are being designed in order to better control these aspects. Engineers and biologists are collaborating to develop more sophisticated surfaces that can change in response to a stimulus and therefore provide cells with abounding behavioural cues in an attempt to recreate the *in vivo* niche *in vitro* (Ulijn 2006).

As described in Chapter 1, current dynamic strategies involve using light, temperature, enzymes and hydrogels with tuneable stress relaxation to alter surface properties in a user defined spatiotemporal manner (Chaudhuri et al. 2016; Lee et al. 2015; Engler et al. 2006; Yamato, Utsumi, et al. 2001; Roberts et al. 2016). The most successful materials have incorporated the RGD adhesive tripeptide which has not only satisfied cell adhesion for survival, but in the case of MSCs, has driven lineage specification. This thesis continues with this theme as an ERM was synthesised and hypothesised to provide two behavioural cues in one cell culture platform; self-renewal and differentiation. The rationale was to maintain stem cell behaviour initially then, in response to enzyme expression by the MSC population, cleave the surface to allow differentiation to bone forming osteoblasts. This type of technology could be beneficial in future therapeutics as a method to produce higher

quality bone cells for skeletal defects. The method is advantageous as it mimics the natural process of stem cell maturation *in vivo*.

## 6.2 Regenerative Medicine

In the last 100 years discoveries such as the biocompatibility of plastics and isolation of stem cells (Friedenstein et al. 1968), have rapidly progressed the potential of TE organs as therapeutics. In this case, biomaterials must be adherent to allow cells to populate it otherwise the cells will die (Koh & Atala 2004; Chen et al. 1997). In addition, the advantage of stem cells is that lots of cells can be generated from a single source and could provide a method to generate sufficient numbers of cells needed to seed the organs (Koh & Atala 2004). There are many challenges to TE; safety concerns, provision of an ethical source of cells and the complexity involved in creating those organs with specialized functions and highly ordered architectures (e.g. the heart) (Prestwich et al. 2012). We aimed to aid the provision of high quality bone cells derived from stem cells thereby increasing the likelihood of meeting safety standards by providing a pure population of cells using materials engineering. Further utilising MSCs is again advantageous due to their immunoregulatory properties (Kode et al. 2009).

The implementation of bioactive materials coupled with stem cell technologies for TE could have the potential to replace a disease or damaged tissue which would have a positive effect on the patient's quality of life. There would be other economic impacts that arise from this for example; reduction in health care costs due to less frequent hospital stays and consequently, reduced prescription of drugs to relieve symptoms. This is particularly important to consider when faced with the problems of an ageing population because at present, health care provision cannot fully support this demographic. TE might provide one method to overcome some of these challenges. The work presented here could in future have an impact on this situation through the provision of bone cells from MSCs to repair skeletal defects.

The bone architecture, is complex and materials solutions should consider both the unique shape (e.g. the jaw) and mechanical properties, particularly for load bearing sites (e.g. pelvis). Shape can be created by 3D printing for example, which can tailor make scaffolds, in addition, mechanical properties are usually compensated for by utilising metals (Mironov et al. 2003; McNamara et al. 2011). Traditional metal implants include titanium structures which ultimately weaken the bone marrow over time due to stress shielding effects, contributing to the revision rate of surgeries (Brydone et al. 2010; Sumner 2015).

The provision of bioactive implants could be one such method to reduce costs to the NHS (National Health Service). Bioactive implants could reduce the number of restorative surgeries attributed to implant failure. Readmission to hospital and multiple surgeries also increase the risk of hospital acquired infections which in turn contributes to antimicrobial resistance (Struelens 1998). These factors have a detrimental effect on the general health and wellbeing of patients and particularly to geriatric patients. Surgical revisions may not be an option for some geriatric patients due to an increased risk undertaking surgeries with increasing patient age. In addition, with increasing hospital stays there is obviously a cost to the NHS. However, for older patients an extended stay (and therefore a reduction in their activity) equates to a loss of 5 % muscle mass per day according to a study commissioned by the national audit office <sup>11</sup>. The effect on the muscle contributes to loss of mobility which will ultimately put them at risk of more age-related fractures. The incorporation of bioactive implants seeded with stem cells therefore would be a better product than that of metal implants. The need for revision would decrease which then reduces hospital stays, minimising the risk of infection that ultimately would reduce NHS costs and increase patient wellbeing.

Another area of concern centres on the wait for organ donation. Currently in the UK there are 6,500 patients waiting for a donation and approximately 500 patients die while waiting for a transplant <sup>12</sup>. Creation of “off the shelf” TE bioactive implants has been thought to be one such method to alleviate this. In this way, there would be no need for donors (assuming it was materials-based scaffold rather than a decellularised cadaveric scaffold). This is another area in which stem cells could be employed. Provided there were sufficient cells available to create an allogeneic graft (phenotype maintained by materials engineering), then the wait for organs would be reduced.

My thesis aims directly at this cell supply issue to find an approach that allows MSC expansion without loss of phenotype and then differentiation to bone forming osteoblasts for use in bone therapy. The material, was designed to provide two stem cell phenotypes in one cell culture platform as a method to deliver the cells for potential therapeutics to meet the challenges that are described in this section. The outcomes of this work will be discussed in the following section.

---

<sup>11</sup> <https://www.nao.org.uk/wp-content/uploads/2015/12/Discharging-older-patients-from-hospital.pdf>

<sup>12</sup> <https://www.nhsbt.nhs.uk/what-we-do/transplantation-services/organ-donation-and-transplantation/>

## 6.3 Thesis discussion

In this study, we present a dynamic cell controllable stimuli responsive material. As presented in Chapter 1, enzymes as a stimulus are preferable for this application due to their efficacy in mild conditions (including cell culture conditions) (Bugg 2001). Further, the use of short peptides has been shown previously to be sufficient to direct cell behaviour (Roberts et al. 2016; Zelzer, McNamara, et al. 2012). Therefore, combining these 2 elements together in the same platform hypothetically provides an ideal platform for stem cell growth. The incorporation of PEG as a blocking group was also thought to be beneficial due to the biocompatibility of the polymer, particularly in comparison to Fmoc which was found to be susceptible to biofouling (Roberts et al. 2016). The removal of this blocking group by cell secreted enzymes again provided another method of autonomy. Stimuli including light, temperature and electricity (Mosiewicz et al. 2013; Yamato et al. 2002; Yeo et al. 2003) may not be as appropriate for cell culture as the stimuli is not natural *in vivo*. This system was therefore designed to have biomimetic and biocompatible parameters.

The objectives of the Thesis are presented in Section 1.10, this section will address how the results obtained have satisfied the original objectives:

- a) Understand the MMP profile of MSCs.

The MMP profile was evaluated using ELISA, zymography and membrane assay, all of which confirmed MMP-2 is the primary MMP secreted by MSCs, as consistent with previous research (Morgunova et al. 1999). Other MMPs were identified in MSC supernatant (MMP-9, MMP-3 and MMP-1, Figure 3.7-3.9) although it was originally thought that due to the increased concentration of MMP-2 in comparison to other MMPs identified, MMP-2 would be responsible for cleavage of the peptide. The concentration of MMP-2 remained consistent over many weeks when cells were cultured on glass (Figure 3.8A).

- b) Design a peptide surface to be targeted by the MMP secreted by MSCs.

Using bioinformatics methods, we identified the likely target sequence for MMP-2 although it was noted that some redundancy with MMP-9 was expected (Chapter 3, Section 3.3.1). It was thought the sequence GPAG↓LRGD was the most kinetically

favourable, as we have maintained specific amino acids at particular positions in line with the Schechter and Berger nomenclature. This includes P at P3 and G↓L at P1↓P1' for cleavage site, which have been noted to be important for MMP recognition and cleavage (Turk et al. 2001; Vartak & Gemeinhart 2007; Kridel et al. 2001). Due to the constraints of manual synthesis, multiple sequences were not tested for efficacy in response to MMP-2. Efficacy could have been improved by maintaining the prime side of the sequence and adding RGD to the consensus sequence instead of substituting it into the prime side. It should also be acknowledged that enzymes in solution act differently to those tethered and in linear conformation, and therefore other sequences could have been explored to better understand efficiency (Ulijn 2006).

- c) Synthesise the surface utilising SPPS incorporating the sequence favourable for cleavage by MMPs and the cell adhesive peptide RGD.

Manual SPPS was utilised for synthesis and characterised utilising the techniques available. This includes WCA, fluorescent spectroscopy and ToF-SIMS, which although have limitations (lack of specificity of WCA and fluorescent spectroscopy and the lack of ionization of particular amino acids during ToF-SIMS), are complementary. We determined there was sufficient evidence to conclude that the surface had been synthesized (Chapter 3, Section 3.3.4). This was expected due to the robustness of the technique (Piehler et al. 2000) and our experience of synthesis from previous studies (Roberts et al. 2016; Todd et al. 2009; Zelzer, McNamara, et al. 2012). There could have been additional steps incorporated to maintain efficiency at all stages (Ninhydrin test) and prevent the presence of deletion peptides or peptides with the wrong sequences. Manual synthesis of the sequence comprised many weeks which was limiting and will be further explored in Section 6.4.

- d) Understand the mechanism of action by enzymes on the surface

By mimicking the cell secreted concentration of MMPs, we have shown that cleavage has occurred using ToF-SIMS on DIGE-D surfaces. To conduct the ToF-SIMS experiment, cell supernatant concentration of MMPs from cells cultured on peptides sequences was utilised (Figure 4.14). When applied to the surface, there was a reduction in the presence of full length peptide suggesting cleavage (Figure 3.20 and 3.21). It was surprising that MMP-9 at a concentration of 0.25 ng/ml was as effective, if not better at cleavage than MMP-2 at a concentration of 20 ng/ml. Unfortunately, this experiment was not conducted until the end of the PhD prior to which, the hypothesis was that MMP-2 alone was

responsible for cleavage. Due to the increase in secretion of MMP-2 at week 3, this was thought to be osteogenic time point 0, where the PEG barrier to RGD peptides was presumed removed and could therefore allow differentiation. It would have been better to follow up this experiment utilising differing concentrations of MMP in a dose-dependent manner to provide a broader picture of MMP action on the surface. It was also assumed that the cell secreted concentration of MMP would be sufficient to trigger changes across the surface however, local action of MMPs could be possible. The role of MT-MMPs was also not explored and therefore local action by these enzymes also cannot be ruled out. Local areas of peptide cleavage could result in an unsynchronised population of cells, which would not be applicable to clinical use.

e) Analyse the phenotype of MSCs on the surface over time

Early time point studies revealed changes in cell spreading and adhesions between controls. This was enhanced on RGD and limited for RGE controls highlighting that RGE surfaces were indeed non-adherent (Figure 4.8). However, those cells that did attach on the RGE surfaces, survived as after 1 week in culture, survival is similar for all controls tested (Figure 4.6 & 4.13). Although there is differential cell morphology and adhesion, this did not relate to an increase in Stro-1 maintenance as expected (Figure 5.3). This should have been repeated with other stem cell markers including ALCAM. This was affected by the availability of materials and long-term cultures were prioritised. This was an oversight and it would have been easier to concentrate efforts at earlier time points (1-3 weeks) than late stage cultures (4-6 weeks). It is with regret that not enough data was generated to satisfy the question of dual functionality of the surface.

Cell differentiation was not enhanced on DIGE-D surfaces prior to 6 weeks in culture. Osteogenic differentiation was thought to be occurring due to the increase in markers such as ALP and OCN (Figure 5.7, 5.9, 5.10). However, this did not result in increased mineralisation at 6 weeks, the marker of end terminal differentiation. Furthermore, our data suggests that there are no other phenotypes observed on the DIGE-D surface (chondrogenic or adipogenic, Figure 5.12). Hypothetically, the culture period could be extended to understand if these indications could lead to mature bone cells. This would extend to 8 weeks of culture where the risk of infection increases.

Taken together, the surface is not promoting stem cell self-renewal nor enhancing differentiation in the manner that was expected. Due to the risk of an unsynchronised

population coupled with the extended culture time, this system would not be utilised for the provision of high quality bone cells from a stem cell precursor.

## 6.4 Limitations

In terms of clinical translation, this concept, in this format, may not be feasible for the provision of cells for therapeutics. If possible, the technology described in this work would be more suited to an allogeneic approach (provided it could be a cost-effective strategy) due to the duration of culture. There are indications that the MSC population is specifically directed to osteogenic phenotypes therefore the incorporation of peptides is beneficial for the provision of higher quality bone cells. For patients with fractures, the turn around with potential autologous treatments should be as short as possible to provide the cells for treatment. In this case, there is a need to create high quality bone cells quickly. For allogeneic treatments, high quality bone cells could be stored in a biobank and utilised on request. However, the time taken to generate these cells, in this case, is at least 6 weeks which is not time effective for a therapeutic turnover. In addition, increases the risk of infection of the culture. This risk would again increase when scaling up to provide for demand.

The creation of surfaces took at least one month's synthesis manually and was limited by the number of vessels and space to create the amount of controls required. Scale up would subsequently be a problem for manual SPPS, this would not be feasible for future health care strategies. An automated SPPS process could be pursued if it was to be implemented as it has the advantage of speed and further increases in reproducibility between batches.

It is argued that reversibility is preferable in a platform technology allowing cyclic applications of that technology (Xia & Jiang 2008). We understand the limitations in that this system is not reversible however, in this setting we feel that as stem cell differentiation to bone is a "one way" system. This material fits this purpose through promotion of end terminal differentiation. A reversible system would however minimize single use materials and the reduction of waste which would have a better economic impact.

The main advantage of this ERM was that the material would be responding to the demands of the cell population. However, the uniformity of the switching was not fully explored and therefore poses the risk of an unsynchronised population. It may be that the user-controlled system described in Robert *et al.* is therefore a better method to control

surface properties, thereby creating a defined ON/OFF switch that guarantees duality (Roberts et al. 2016).

## 6.5 Future work

Due to the limitations described in the previous section (namely availability of materials) there are several experiments that were not conducted. Had the system been more high-throughput, multiple stem cell markers could have been assessed for various time points. Specifically, markers of self-renewal, differentiation and proliferation should be assessed weekly for the duration of the culture (1 – 6 weeks). This would be particularly relevant at the 3-week time point to test the original hypothesis. For early stage cultures it would be prudent to look for other progenitor markers of MSCs including ALCAM and CD34 to confirm the same trend as observed for the Stro-1 data (Figure 5.3). Furthermore, additional data on the colonisation of cells on the surface (proliferation) and the phenotype of these cells over the many weeks of culture, should also be assessed.

Alternatively, to characterize phenotype in a high-throughput manner, we could spike supernatant with MMP-2 (on DIGE-D and DIGE-E surfaces in comparison to glass). Due to the length of time taken to achieve phenotypic changes there was difficulty pinpointing the exact time for early osteogenesis. By speeding up the cleavage time point and decreasing controls, we could process more samples with more time points in a high-throughput manner. Using this method, we could also provide more evidence for cleavage of the surface. Although applying this method would revert the system to the user applied stimulus that was utilised in Roberts *et al.* (Roberts et al. 2016).

The role of MMPs should be more fully characterised with different concentrations of MMPs tested to understand potency. An experiment could be designed where an Fmoc-GPAG↓LRGD surface could be synthesized, treated with different MMPs at various concentrations then the presence of Fmoc analysed using fluorescent spectroscopy. This would again allow a more high-throughput approach to the analysis of cleavage, as more samples can be run at less expense and has the added advantage that technique can be carried out in-house. Moreover, we could apply small molecule inhibitors against MMPs to confirm which MMP is required for cleavage in the cell supernatant.

Additionally, the MSC secretome could be analysed to identify another enzyme that could be secreted at higher quantities at earlier time points (Kim et al. 2013). This would involve a change of sequence to accommodate this enzyme.

The interplay of MMPs, TIMPs and phenotype could be further explored. As stated in Figure 3.4 the activation of proMMP-2 is by MT-MMP1 (Visse & Nagase 2003). MT1-MMP can complex with the  $\beta$ 1 integrin which increases secretion of MMP-2 and ALP signalling, therefore contributing to osteoblastic differentiation. It would be worthwhile tracking the expression of MT-MMP1, particularly at the 3-week time point to determine if the increase in MMP-2 could be correlated with this mode of activation. And further to determine co-localisation of MMP-2 with the  $\beta$ 1 integrin to substantiate this further (Karadag & Fisher 2006; Karadag et al. 2004).

## 6.6 Conclusion

There were numerous aims to the project. We identified the most likely peptide sequence for cleavage based on the MMP profile of MSCs. This was synthesised using a robust technique although there could be improvements to guarantee efficiency considering synthesis comprised many weeks manually. While we did observe cleavage of this sequence by MMPs, more work should have been done to understand the potency of MMPs at different concentrations. However, due to time taken for synthesis, access to ToF-SIMS and limited availability of the materials, this was not fully explored. Cellular phenotype was analysed initially as an indicator of viability then in long term culture for differentiation. While we ascertained that cell survival was adequate on the expected surfaces and that there was some upregulation of osteogenic markers, MSC self-renewal could have been better understood.

To guarantee a fully synchronised cell population at a more therapeutically relevant time point, other materials strategies should be explored.

# References

- Aggarwal, S. & Pittenger, M.F., 2005. Human mesenchymal stem cells modulate allogeneic immune cell responses. *Blood*, 105(4), pp.1815–1822.
- Albelda, S.M. & Buck, C.A., 1990. Integrins and other cell adhesion molecules. *FASEB J*, 4(11), pp.2868–2880.
- Almalki, S.G. & Agrawal, D.K., 2016. Effects of matrix metalloproteinases on the fate of mesenchymal stem cells. *Stem Cell Research & Therapy*, 7(1), p.129.
- Alvarez, C. V et al., 2012. Defining stem cell types: understanding the therapeutic potential of ESCs, ASCs, and iPS cells. *J Mol Endocrinol*, 49(2), pp.R89-111.
- Anderson, H. et al., 2017. Nanoscale Surface Cues and Cell Behaviour. In *Reference Module in Materials Science and Materials Engineering*.
- Anderson, H.J. et al., 2016. Mesenchymal Stem Cell Fate: Applying Biomaterials for Control of Stem Cell Behavior. *Frontiers in Bioengineering and Biotechnology*, 4, p.38.
- Anselme, K. & Bigerelle, M., 2005. Topography effects of pure titanium substrates on human osteoblast long-term adhesion. *Acta Biomaterialia*, 1(2), pp.211–222.
- Arnold, M. et al., 2004. Activation of Integrin Function by Nanopatterned Adhesive Interfaces. , pp.383–388.
- Arnsdorf, E.J. et al., 2009. Mechanically induced osteogenic differentiation--the role of RhoA, ROCKII and cytoskeletal dynamics. *Journal of cell science*, 122(Pt 4), pp.546–53.
- Arpornmaeklong, P. et al., 2009. Phenotypic characterization, osteoblastic differentiation, and bone regeneration capacity of human embryonic stem cell-derived mesenchymal stem cells. *Stem cells and development*, 18(7), pp.955–68.
- Baksh, D., Song, L. & Tuan, R.S., 2004. Adult mesenchymal stem cells: characterization, differentiation, and application in cell and gene therapy. *Journal of Cellular and Molecular Medicine*, 8(3), pp.301–316.
- Balaban, N.Q. et al., 2001. Force and focal adhesion assembly: a close relationship studied using elastic micropatterned substrates. *Nature cell biology*, 3(5), pp.466–72.
- Becker, a De & Hummelen, P. Van, 2007. -Expanded Human Mesenchymal Stem Cells Through Bone Marrow Endothelium Is Regulated By Matrix Metalloproteinase-2 and Tissue Inhibitor of Metalloproteinase-3. ..., pp.440–449.
- Behrendt, R., White, P. & Offer, J., 2016. Advances in Fmoc solid-phase peptide synthesis.

- Journal of Peptide Science*, 22(1), pp.4–27.
- Behringer, R.R. et al., 1999. Sox9 is required for cartilage formation. *Nature Genetics*, 22(1), pp.85–89.
- Bellis, S.L., 2011. Biomaterials Advantages of RGD peptides for directing cell association with biomaterials q. *Biomaterials*, 32(18), pp.4205–4210.
- Benoit, D.S.W. & Anseth, K.S., 2005. The effect on osteoblast function of colocalized RGD and PHSRN epitopes on PEG surfaces. , 26, pp.5209–5220.
- Berrier, A.L. & Yamada, K.M., 2007. Cell - Matrix Adhesion. *Journal of Cellular Physiology*, 213(June), pp.565–573.
- Bershadsky, A.D. et al., 1985. Focal contacts of normal and RSV-transformed quail cells. Hypothesis of the transformation-induced deficient maturation of focal contacts. *Experimental cell research*, 158(2), pp.433–44.
- Beyer Nardi, N.. & Da Silva Meirelles, L., 2006. Mesenchymal stem cells: Isolation, in vitro expansion and characterization. *Handbook of Experimental Pharmacology*, 174, pp.249–282.
- Bigg, H.F. et al., 2001. Tissue inhibitor of metalloproteinases-4 inhibits but does not support the activation of gelatinase a via efficient inhibition of membrane type 1-matrix metalloproteinase. *Cancer Research*, 61(9), pp.3610–3618.
- Biggs, M.J.P. et al., 2009. The use of nanoscale topography to modulate the dynamics of adhesion formation in primary osteoblasts and ERK/MAPK signalling in STRO-1+ enriched skeletal stem cells. *Biomaterials*, 30(28), pp.5094–103.
- Bills, C.E., Eisenberg, H. & Pallante, S.L., 1971. Complexes of organic acids with calcium phosphate: the von Kossa stain as a clue to the composition of bone mineral. *The Johns Hopkins medical journal*, 128(4), pp.194–207.
- Birkedal-Hansen, H. et al., 1993. Matrix metalloproteinases: a review. *Crit Rev Oral Biol Med*, 4(2), pp.197–250.
- Bode, W. et al., 1999. Insights into MMP-TIMP interactions. *Annals of the New York Academy of Sciences*, 878, pp.73–91.
- Boskey, A.L. & Coleman, R., 2010. Aging and bone. *Journal of dental research*, 89(12), pp.1333–48.
- Britland, S. et al., 1996. Synergistic and Hierarchical Adhesive and Topographic Guidance of BHK Cells. *Experimental Cell Research*, 228(2), pp.313–325.
- Brodsky, B. & Persikov, A. V., 2005. Molecular structure of the collagen triple helix. *Advances in Protein Chemistry*, 70, pp.301–339.
- Brydone, A.S., Meek, D. & Maclaine, S., 2010. Bone grafting, orthopaedic biomaterials, and the clinical need for bone engineering. *Proceedings of the Institution of*

- Mechanical Engineers, Part H: Journal of Engineering in Medicine*, 224(12), pp.1329–1343.
- Buensuceso, C.S. et al., 2001. The WD protein Rack1 mediates protein kinase C and integrin-dependent cell migration. *Journal of cell science*, 114(Pt 9), pp.1691–8.
- Bugg, T.D.H., 2001. Enzymes: General Properties. *eLS*.
- Burridge, K. & Chrzanowska-Wodnicka, M., 1996. Focal adhesions, contractility, and signaling. *Annu Rev Cell Dev Biol*, 12, pp.463–518.
- Carpino, L.A. & Han, G.Y., 1972. The 9-Fluorenylmethoxycarbonyl Amino-Protecting Group. *Journal of Organic Chemistry*, 37(22), pp.3404–3409.
- Cavalcanti-adam, E.A. et al., 2007. Cell Spreading and Focal Adhesion Dynamics Are Regulated by Spacing of Integrin Ligands. *Biophysical Journal*, 92(8), pp.2964–2974.
- Caviston, J.P. & Holzbaur, E.L.F., 2006. Microtubule motors at the intersection of trafficking and transport. *Trends in Cell Biology*, 16(10), pp.530–537.
- Chaudhuri, O. et al., 2016. Hydrogels with tunable stress relaxation regulate stem cell fate and activity. *Nature Materials*, 15(3), pp.326–334.
- Chen, C.-Y. et al., 2009. Effect of D to E mutation of the RGD motif in rhodostomin on its activity, structure, and dynamics: Importance of the interactions between the D residue and integrin. *Proteins: Structure, Function, and Bioinformatics*, 76(4), pp.808–821.
- Chen, C.S. et al., 1997. Geometric Control of Cell Life and Death. *Science*, 276(5317).
- Cherkupally, P. et al., 2014. Immobilized Coupling Reagents: Synthesis of Amides/Peptides. *ACS combinatorial science*.
- Chong, J.-L. et al., 2009. E2f1–3 switch from activators in progenitor cells to repressors in differentiating cells. *Nature*, 462(7275), pp.930–934.
- Clark, P. et al., 1990. Topographical control of cell behaviour: II. Multiple grooved substrata. *Development (Cambridge, England)*, 108(4), pp.635–44.
- Clark, P. et al., 1987. Topographical control of cell behaviour. I. Simple step cues. *Development (Cambridge, England)*, 99(3), pp.439–448.
- Clarke, B., 2008. Normal Bone Anatomy and Physiology. *Clinical Journal of the American Society of Nephrology*, 3(Supplement 3), pp.S131–S139.
- Cockerill, P.N. & Garrard, W.T., 1986. Chromosomal loop anchorage of the kappa immunoglobulin gene occurs next to the enhancer in a region containing topoisomerase II sites. *Cell*, 44(2), pp.273–282.
- Creek, D.J. et al., 2011. Toward global metabolomics analysis with hydrophilic interaction liquid chromatography-mass spectrometry: Improved metabolite identification by retention time prediction. *Analytical Chemistry*, 83(22), pp.8703–8710.

- Crisp, M. et al., 2006. Coupling of the nucleus and cytoplasm: Role of the LINC complex. *Journal of Cell Biology*, 172(1), pp.41–53.
- Curran, J.M. et al., 2010. Introducing dip pen nanolithography as a tool for controlling stem cell behaviour: unlocking the potential of the next generation of smart materials in regenerative medicine. *Lab on a Chip*, 10(13), pp.1662–1670.
- Curtis, A.S. et al., 2001. Substratum nanotopography and the adhesion of biological cells. Are symmetry or regularity of nanotopography important? *Biophys Chem*, 94(3), pp.275–283.
- Dalby, M.J. et al., 2007. The control of human mesenchymal cell differentiation using nanoscale symmetry and disorder. *Nat Mater*, 6(12), pp.997–1003.
- Dalby, M.J., 2005. Topographically induced direct cell mechanotransduction. *Medical Engineering & Physics*, 27(9), pp.730–742.
- Dalby, M.J., García, A.J. & Salmeron-Sanchez, M., 2018. Receptor control in mesenchymal stem cell engineering. *Nature Reviews Materials*, 3.
- Dalby, M.J., Pasqui, D. & Affrossman, S., 2004. Cell response to nano-islands produced by polymer demixing: a brief review. *IEE Proc Nanobiotechnol*, 151(2), pp.53–61.
- Davis, G.E. et al., 2000. Regulation of tissue injury responses by the exposure of matricryptic sites within extracellular matrix molecules. *The American journal of pathology*, 156(5), pp.1489–1498.
- Dhar, D. & Hsi-En Ho, J., 2009. Stem cell research policies around the world. *The Yale journal of biology and medicine*, 82(3), pp.113–5.
- Dimos, J.T. et al., 2008. Induced Pluripotent Stem Cells Generated from Patients with ALS Can Be Differentiated into Motor Neurons. *Science*, 321(5893).
- Doezé, R.H.P. et al., 2004. Profiling Primary Protease Specificity by Peptide Synthesis on a Solid Support. *Angewandte Chemie International Edition*, 43(24), pp.3138–3141.
- Dong, B. et al., 2011. Antifouling ability of polyethylene glycol of different molecular weights grafted onto polyester surfaces by cold plasma. *Polymer Bulletin*, 66(4), pp.517–528.
- Ducy, P., 2000. CBFA1: A molecular switch in osteoblast biology. *Developmental Dynamics*, 219(4), pp.461–471.
- DuFort, C.C., Paszek, M.J. & Weaver, V.M., 2011. Balancing forces: architectural control of mechanotransduction. *Nat Rev Mol Cell Biol*, 12(5), pp.308–319.
- Egea, V. et al., 2012. Tissue inhibitor of metalloproteinase-1 (TIMP-1) regulates mesenchymal stem cells through let-7f microRNA and Wnt/ -catenin signaling. *Proceedings of the National Academy of Sciences*, 109(6), pp.E309–E316.
- Egeblad, M. & Werb, Z., 2002. New functions for the matrix metalloproteinases in cancer

- progression. *Nat Rev Cancer*, 2(3), pp.161–174.
- Ehninger, A. & Trumpp, A., 2011. The bone marrow stem cell niche grows up: mesenchymal stem cells and macrophages move in. *J Exp Med*, 208(3), pp.421–428.
- Engler, A.J. et al., 2006. Matrix elasticity directs stem cell lineage specification. *Cell*, 126(4), pp.677–689.
- Engler, A.J. et al., 2009. Multiscale Modeling of Form and Function. *Science*, 324(5924), pp.208–212.
- Erickson, B.W. & Merrifield, R.B., 1976. 3 – Solid-Phase Peptide Synthesis. In *The Proteins*. pp. 255–527.
- Evans, M.J. & Kaufman, M.H., 1981. Establishment in culture of pluripotential cells from mouse embryos. *Nature*, 292(5819), pp.154–156.
- Evers, P., 2016. *The Global Market for Stem Cells*,
- Fiehn, O., 2001. Combining genomics, metabolome analysis, and biochemical modelling to understand metabolic networks. *Comparative and functional genomics*, 2(3), pp.155–68.
- Fields, G.B. & Noble, R.L., 1990. Solid phase peptide synthesis utilizing 9-fluorenylmethoxycarbonyl amino acids. *International journal of peptide and protein research*, 35(3), pp.161–214.
- Friedenstein, A.J. et al., 1968. Heterotopic of bone marrow. Analysis of precursor cells for osteogenic and hematopoietic tissues. *Transplantation*, 6(2), pp.230–247.
- Friedenstein, A.J., 1976. Precursor Cells of Mechanocytes. *International Review of Cytology*, 47(C), pp.327–359.
- Fuchs, E. & Weber, K., 1994. Intermediate Filaments: Structure, Dynamics, Function and Disease. *Annual Review of Biochemistry*, 63(1), pp.345–382.
- Gadegaard, N., Mosler, S. & Larsen, N.B., 2003. Biomimetic polymer nanostructures by injection molding. *Macromolecular Materials and Engineering*, 288(1), pp.76–83.
- Gartner, T.K. & Bennett, J.S., 1985. The tetrapeptide analogue of the cell attachment site of fibronectin inhibits platelet aggregation and fibrinogen binding to activated platelets. *The Journal of biological chemistry*, 260(22), pp.11891–4.
- Geiger, B. et al., 2001. Transmembrane extracellular matrix– cytoskeleton crosstalk. *Nature reviews. Molecular cell biology*, 2(November), pp.793–805.
- Geiger, B., Spatz, J.P. & Bershadsky, A.D., 2009. Environmental sensing through focal adhesions. *Nature reviews. Molecular cell biology*, 10(1), pp.21–33.
- Giancotti, F.G. & Ruoslahti, E., 1999. Transduction - Integrin signaling. *Science*, 285(5430), pp.1028–1032.
- Gilbert, P.M. et al., 2010. Substrate elasticity regulates skeletal muscle stem cell self-

- renewal in culture. *Science*, 329(5995), pp.1078–1081.
- Ginger, D.S., Zhang, H. & Mirkin, C.A., 2004. The evolution of dip-pen nanolithography. *Angewandte Chemie-International Edition*, 43(1), pp.30–45.
- Gronthos, S. & Zannettino, A.C.W., 2008. A Method to Isolate and Purify Human Bone Marrow Stromal Stem Cells. In *Mesenchymal Stem Cells*. Totowa, NJ: Humana Press, pp. 45–57.
- Hagenhoff, B., 2000. High Resolution Surface Analysis by TOF-SIMS. *Microchimica Acta*, 132(2), pp.259–271.
- Hanahan, D. & Weinberg, R.A., 2000. The hallmarks of cancer. *Cell*, 100(1), pp.57–70.
- Harrison, R.G., 1911. On the Stereotropism of Embryonic Cells. *Science*, 34(870), pp.279–281.
- Hartmann, C., 2006. A Wnt canon orchestrating osteoblastogenesis. *Trends Cell Biol*, 16(3), pp.151–158.
- Hench, L.L. & Polak, J.M., 2002. Third-generation biomedical materials. *Science*, 295(5557), pp.1014–1017.
- Hersel, U., Dahmen, C. & Kessler, H., 2003. RGD modified polymers: biomaterials for stimulated cell adhesion and beyond. *Biomaterials*, 24(24), pp.4385–4415.
- Hing, K.A., 2005. Bioceramic bone graft substitutes: Influence of porosity and chemistry. *International Journal of Applied Ceramic Technology*, 2(3), pp.184–199.
- Hoyos-Nogués, M. et al., 2017. Regenerating Bone via Multifunctional Coatings: The Blending of Cell Integration and Bacterial Inhibition Properties on the Surface of Biomaterials. *ACS Applied Materials & Interfaces*, 9(26), pp.21618–21630.
- Huang, Y. et al., 2013. Length-dependent proteolytic cleavage of short oligopeptides catalyzed by matrix metalloprotease-9. *Peptide Science*, 100(6), pp.790–795.
- Humphries, J.D. et al., 2007. Vinculin controls focal adhesion formation by direct interactions with talin and actin. *The Journal of cell biology*, 179(5), pp.1043–57.
- Humphries, J.D., Byron, A. & Humphries, M.J., 2006. Integrin ligands at a glance. *Journal of Cell Science*, 119(19), pp.3901–3903.
- Ingber, D., 1993. Cellular tensegrity: defining new rules of biological design that govern the cytoskeleton. *J. Cell Sci.*, 104(3), pp.613–627.
- Ivaska, J. et al., 2007. Novel functions of vimentin in cell adhesion, migration, and signaling. *Experimental Cell Research*, 313(10), pp.2050–2062.
- Jackson, L. et al., 2007. Adult mesenchymal stem cells: differentiation potential and therapeutic applications. *Journal of postgraduate medicine*, 53(2), pp.121–7.
- Kane, R.S. et al., 1999. Patterning proteins and cells using soft lithography. *Biomaterials*, 20(23–24), pp.2363–2376.

- Karadag, A. et al., 2004. Bone sialoprotein, matrix metalloproteinase 2, and alpha(v)beta3 integrin in osteotropic cancer cell invasion. *Journal of the National Cancer Institute*, 96(12), pp.956–965.
- Karadag, A. & Fisher, L.W., 2006. Bone sialoprotein enhances migration of bone marrow stromal cells through matrices by bridging MMP-2 to alpha(v)beta3-integrin. *Journal of bone and mineral research : the official journal of the American Society for Bone and Mineral Research*, 21(10), pp.1627–1636.
- Kessenbrock, K., Plaks, V. & Werb, Z., 2010. Matrix Metalloproteinases: Regulators of the Tumor Microenvironment. *Cell*, 141(1), pp.52–67.
- Kessenbrock, K., Wang, C.-Y. & Werb, Z., 2015. Matrix metalloproteinases in stem cell regulation and cancer. *Matrix Biology*, 44–46, pp.184–190.
- Khatiwala, C.B. et al., 2009. ECM Compliance Regulates Osteogenesis by Influencing MAPK Signaling Downstream of RhoA and ROCK. *Journal of Bone and Mineral Research*, 24(5), pp.886–898.
- Khetan, S. et al., 2013. Degradation-mediated cellular traction directs stem cell fate in covalently crosslinked three-dimensional hydrogels. *Nat Mater*, 12(5), pp.458–465.
- Kilian, K.A. et al., 2010. Geometric cues for directing the differentiation of mesenchymal stem cells. *Proc Natl Acad Sci U S A*, 107(11), pp.4872–4877.
- Kilian, K.A. & Mrksich, M., 2012. Directing stem cell fate by controlling the affinity and density of ligand-receptor interactions at the biomaterials interface. *Angewandte Chemie (International ed. in English)*, 51(20), pp.4891–5.
- Kim, J.-M. et al., 2013. Comparative secretome analysis of human bone marrow-derived mesenchymal stem cells during osteogenesis. *Journal of Cellular Physiology*, 228(1), pp.216–224.
- Kim, K. et al., 2010. Epigenetic memory in induced pluripotent stem cells. *Nature*, 467(7313), pp.285–90.
- Kode, J.A. et al., 2009. Mesenchymal stem cells: immunobiology and role in immunomodulation and tissue regeneration. *Cytotherapy*, 11(4), pp.377–391.
- Koh, C.J. & Atala, A., 2004. Tissue engineering, stem cells, and cloning: opportunities for regenerative medicine. *J Am Soc Nephrol*, 15(5), pp.1113–1125.
- Kolf, C.M., Cho, E. & Tuan, R.S., 2007. Mesenchymal stromal cells. Biology of adult mesenchymal stem cells: regulation of niche, self-renewal and differentiation. *Arthritis research & therapy*, 9(1), p.204.
- Kontis, V. et al., 2017. Future life expectancy in 35 industrialised countries: projections with a Bayesian model ensemble. *The Lancet*, 389(10076), pp.1323–1335.
- Kridel, S.J. et al., 2001. Substrate Hydrolysis by Matrix Metalloproteinase-9\*. *Journal of*

*Biological Chemistry*, 276(23), pp.20572–20578.

- Lai, C.F. et al., 2001. Erk is essential for growth, differentiation, integrin expression, and cell function in human osteoblastic cells. *The Journal of biological chemistry*, 276(17), pp.14443–50.
- Lai, M.I. et al., 2011. Advancements in reprogramming strategies for the generation of induced pluripotent stem cells. *Journal of assisted reproduction and genetics*, 28(4), pp.291–301.
- de las Heras Alarcón, C., Pennadam, S. & Alexander, C., 2005. Stimuli responsive polymers for biomedical applications. *Chemical Society Reviews*, 34(3), pp.276–285.
- Leber, T.M. & Balkwill, F.R., 1997. Zymography: a single-step staining method for quantitation of proteolytic activity on substrate gels. *Anal Biochem*, 249(1), pp.24–28.
- Lee, T.T. et al., 2015. Light-triggered in vivo activation of adhesive peptides regulates cell adhesion, inflammation and vascularization of biomaterials. *Nature Materials*, 14(3), pp.352–360.
- Lim, J.M. et al., 2004. Retinal pigment epithelial cell behavior is modulated by alterations in focal cell-substrate contacts. *Investigative Ophthalmology and Visual Science*, 45(11), pp.4210–4216.
- Liotta, F. et al., 2008. Toll-Like Receptors 3 and 4 Are Expressed by Human Bone Marrow-Derived Mesenchymal Stem Cells and Can Inhibit Their T-Cell Modulatory Activity by Impairing Notch Signaling. *Stem Cells*, 26(1), pp.279–289.
- Liu, D. et al., 2009. Using azobenzene-embedded self-assembled monolayers to photochemically control cell adhesion reversibly. *Angewandte Chemie - International Edition*, 48(24), pp.4406–4408.
- Llopis-Hernández, V. et al., 2016. Material-driven fibronectin assembly for high-efficiency presentation of growth factors. *Science advances*, 2(8), p.e1600188.
- López-Otín, C. & Overall, C.M., 2002. Protease degradomics: a new challenge for proteomics. *Nature reviews. Molecular cell biology*, 3(7), pp.509–519.
- Lötters, F.J.B. et al., 2016. Current and Future Incidence and Costs of Osteoporosis-Related Fractures in The Netherlands: Combining Claims Data with BMD Measurements. *Calcified Tissue International*, 98(3), pp.235–243.
- Lozito, T.P. & Tuan, R.S., 2011. Mesenchymal stem cells inhibit both endogenous and exogenous MMPs via secreted TIMPs. *Journal of Cellular Physiology*, 226(2), pp.385–396.
- Luger, D. et al., 2017. Intravenously Delivered Mesenchymal Stem Cells: Systemic Anti-Inflammatory Effects Improve Left Ventricular Dysfunction in Acute Myocardial Infarction and Ischemic Cardiomyopathy. *Circulation research*, 120(10), pp.1598–

- Lutolf, M.P. et al., 2003. Repair of bone defects using synthetic mimetics of collagenous extracellular matrices. *Nature Biotechnology*, 21(5), pp.513–518.
- Lutolf, M.P. et al., 2003. Synthetic matrix metalloproteinase-sensitive hydrogels for the conduction of tissue regeneration: engineering cell-invasion characteristics. *Proceedings of the National Academy of Sciences of the United States of America*, 100(9), pp.5413–8.
- Lutolf, M.P. & Blau, H.M., 2009. Artificial stem cell niches. *Adv Mater*, 21(32–33), pp.3255–3268.
- Lutz, J., 2008. Polymerization of oligo (ethylene glycol)(meth) acrylates: toward new generations of smart biocompatible materials. *Journal of Polymer Science Part A: Polymer Chemistry*, 46(11), pp.3459–3470.
- Lv, F.-J. et al., 2014. Concise Review: The Surface Markers and Identity of Human Mesenchymal Stem Cells. *STEM CELLS*, 32(6), pp.1408–1419.
- Mannello, F., 2006. Commentary: Multipotent Mesenchymal Stromal Cell Recruitment, Migration, and Differentiation: What Have Matrix Metalloproteinases Got to Do with It? *Stem Cells*, 24(8), pp.1904–1907.
- Mannello, F. et al., 2006. Role and function of matrix metalloproteinases in the differentiation and biological characterization of mesenchymal stem cells. *Stem Cells*, 24(3), pp.475–481.
- Mas-Moruno, C. et al., 2014. Novel peptide-based platform for the dual presentation of biologically active peptide motifs on biomaterials. In *ACS Applied Materials and Interfaces*. pp. 6525–6536.
- Mas-Moruno, C. et al., 2016.  $\alpha\beta3$ - or  $\alpha5\beta1$ -Integrin-Selective Peptidomimetics for Surface Coating. *Angewandte Chemie - International Edition*, 55(25), pp.7048–7067.
- McBeath, R. et al., 2004. Cell shape, cytoskeletal tension, and RhoA regulate stem cell lineage commitment. *Developmental cell*, 6(4), pp.483–95.
- McGarry, J.G. & Prendergast, P.J., 2004. A three-dimensional finite element model of an adherent eukaryotic cell. *European cells & materials*, 7, pp.27-33; discussion 33-34.
- McKibbin, B., 1978. The biology of fracture healing in long bones. *The Journal of bone and joint surgery. British volume*, 60–B(2), pp.150–62.
- McMurray, R.J. et al., 2011. Nanoscale surfaces for the long-term maintenance of mesenchymal stem cell phenotype and multipotency. *Nat Mater*, 10(8), pp.637–644.
- McNamara, L.E. et al., 2011. Skeletal stem cell physiology on functionally distinct titania nanopopographies. *Biomaterials*, 32(30), pp.7403–7410.
- McNamara, L.E. et al., 2012. The role of microtopography in cellular

- mechanotransduction. *Biomaterials*, 33(10), pp.2835–2847.
- McQuibban, G. a et al., 2001. Matrix metalloproteinase activity inactivates the CXC chemokine stromal cell-derived factor-1. *The Journal of biological chemistry*, 276(47), pp.43503–43508.
- Medda, R. et al., 2014. Investigation of early cell-surface interactions of human mesenchymal stem cells on nanopatterned beta-type titanium-niobium alloy surfaces. *Interface Focus*, 4(1), p.20130046.
- Merrifield, R., 1963. Solid Phase Peptide Synthesis. I. The Synthesis of. *Journal of the American Chemical Society*, 85(14), pp.2149–2154.
- Mironov, V. et al., 2003. Organ printing: Computer-aided jet-based 3D tissue engineering. *Trends in Biotechnology*, 21(4), pp.157–161.
- Mitchell, A.R. et al., 1978. A New Synthetic Route to tert-Butyloxycarbonylaminoacyl-4-(oxymethyl)phenylacetamidomethyl-resin, an Improved Support for Solid-Phase Peptide Synthesis'. *Journal of Organic Chemistry*, 43, pp.2845–2852.
- Mitra, S.K., Hanson, D. a & Schlaepfer, D.D., 2005. Focal adhesion kinase: in command and control of cell motility. *Nature reviews. Molecular cell biology*, 6(1), pp.56–68.
- Morgunova, E. et al., 1999. Structure of Human Pro-Matrix Metalloproteinase-2: Activation Mechanism Revealed. *Science*, 284(5420), pp.1667–1670.
- Morrison, C.J. et al., 2009. Matrix metalloproteinase proteomics: substrates, targets, and therapy. *Current Opinion in Cell Biology*, 21(5), pp.645–653.
- Mosiewicz, K.A. et al., 2013. In situ cell manipulation through enzymatic hydrogel photopatterning. *Nat Mater*, 12(11), pp.1071–1077.
- Mosmann, T., 1983. Rapid Colorimetric Assay for Cellular Growth and Survival: Application to Proliferation and Cytotoxicity Assays. *Journal of Immunological Methods*, 65, pp.55–63.
- Mosse, W.K. et al., 2009. Peptides grafted from solids for the control of interfacial properties. *Langmuir*, 25(3), pp.1488–1494.
- Mouw, J.K., Ou, G. & Weaver, V.M., 2014. Extracellular matrix assembly: a multiscale deconstruction. *Nature Reviews Molecular Cell Biology*, 15(12), pp.771–785.
- Nagase, H. & Fields, G.B., 1996. Human matrix metalloproteinase specificity studies using collagen sequence-based synthetic peptides. *Biopolymers*, 40(4), pp.399–416.
- Nagase, H. & Woessner Jr., J.F., 1999. Matrix metalloproteinases. *J Biol Chem*, 274(31), pp.21491–21494.
- Nelson, a R. et al., 2000. Matrix metalloproteinases: biologic activity and clinical implications. *Journal of clinical oncology : official journal of the American Society of Clinical Oncology*, 18(5), pp.1135–1149.

- Odorico, J.S., Kaufman, D.S. & Thomson, J. a, 2001. Multilineage differentiation from human embryonic stem cell lines. *Stem cells (Dayton, Ohio)*, 19(3), pp.193–204.
- Olivier, V., Faucheux, N. & Hardouin, P., 2004. Biomaterial challenges and approaches to stem cell use in bone reconstructive surgery. *Drug Discovery Today*, 9(18), pp.803–811.
- Oreffo, R.O. et al., 2005. Mesenchymal stem cells: lineage, plasticity, and skeletal therapeutic potential. *Stem Cell Rev*, 1(2), pp.169–178.
- Ott, H.C. et al., 2008. Perfusion-decellularized matrix: using nature’s platform to engineer a bioartificial heart. *Nat Med*, 14(2), pp.213–221.
- Otto, F. et al., 1997. Cbfa1, a Candidate Gene for Cleidocranial Dysplasia Syndrome, Is Essential for Osteoblast Differentiation and Bone Development. *Cell*, 89(5), pp.765–771.
- Ozeki, N. et al., 2016. Polyphosphate-induced matrix metalloproteinase-13 is required for osteoblast-like cell differentiation in human adipose tissue derived mesenchymal stem cells. *BioScience Trends*, 10(5), pp.365–371.
- Palomo, J.M., 2014. Solid-phase peptide synthesis: an overview focused on the preparation of biologically relevant peptides. *RSC Adv.*, 4(62), pp.32658–32672.
- Paszek, M.J. et al., 2005. Tensional homeostasis and the malignant phenotype. *Cancer cell*, 8(3), pp.241–54.
- Piehler, J. et al., 2000. A high-density poly(ethylene glycol) polymer brush for immobilization on glass-type surfaces. *Biosensors and Bioelectronics*, 15(9–10), pp.473–481.
- Pires, D.A.T., Bemquerer, M.P. & do Nascimento, C.J., 2014. Some Mechanistic Aspects on Fmoc Solid Phase Peptide Synthesis. *International Journal of Peptide Research and Therapeutics*, 20(1), pp.53–69.
- Pittenger, M.F., 1999. Multilineage Potential of Adult Human Mesenchymal Stem Cells. *Science*, 284(5411), pp.143–147.
- Prestwich, G.D. et al., 2012. What Is the Greatest Regulatory Challenge in the Translation of Biomaterials to the Clinic? *Science Translational Medicine*, 4(160).
- Qin, D., Xia, Y. & Whitesides, G.M., 2010. Soft lithography for micro- and nanoscale patterning. *Nature protocols*, 5(3), pp.491–502.
- Rawlings, N.D., 2009. A large and accurate collection of peptidase cleavages in the MEROPS database. *Database*, 2009.
- Rawsterne, R.E. et al., 2006. Controlling protein retention on enzyme-responsive surfaces. *Surface and Interface Analysis*, 38(11), pp.1505–1511.
- Reddy, S., Arzt, E. & Del Campo, A., 2007. Bioinspired surfaces with switchable

- adhesion. *Advanced Materials*, 19(22), pp.3833–3837.
- Ries, C. et al., 2007. MMP-2, MT1-MMP, and TIMP-2 are essential for the invasive capacity of human mesenchymal stem cells: differential regulation by inflammatory cytokines. *Blood*, 109(9), pp.4055–4063.
- Ringe, J. et al., 2002. Stem cells for regenerative medicine: advances in the engineering of tissues and organs. *Die Naturwissenschaften*, 89(8), pp.338–351.
- del Rio, A. et al., 2009. Stretching Single Talin Rod Molecules Activates Vinculin Binding. *Science*, 323(5914).
- Riss, T.L. et al., 2004. *Cell Viability Assays*, Eli Lilly & Company and the National Center for Advancing Translational Sciences.
- Roberts, J.N. et al., 2016. Dynamic Surfaces for the Study of Mesenchymal Stem Cell Growth through Adhesion Regulation. *ACS Nano*, 10(7), pp.6667–6679.
- Robinson, A.R. et al., 2005. The potential of metabolite profiling as a selection tool for genotype discrimination in *Populus*. *Journal of Experimental Botany*, 56(421), pp.2807–2819.
- Rogers, J.A., Jackman, R.J. & Whitesides, G.M., 1997. Microcontact printing and electroplating on curved substrates: Production of free-standing three-dimensional metallic microstructures. *Advanced Materials*, 9(6), p.475-.
- Roodman, G., 1996. Advances in Bone Biology: The Osteoclast. *Endocrine Reviews*, 17(4), pp.308–332.
- Sahoo, J.K. et al., 2016. Analysis of enzyme-responsive peptide surfaces by Raman spectroscopy. *Chem. Commun.*, 52(25), pp.4698–4701.
- Salaita, K., Wang, Y.H. & Mirkin, C.A., 2007. Applications of dip-pen nanolithography. *Nature Nanotechnology*, 2(3), pp.145–155.
- Salem, H.K. & Thiemermann, C., 2010. Mesenchymal stromal cells: current understanding and clinical status. *Stem cells (Dayton, Ohio)*, 28(3), pp.585–96.
- Salmerón-Sánchez, M. & Dalby, M.J., 2016. Synergistic growth factor microenvironments. *Chem. Commun.*, 52(91), pp.13327–13336.
- Samavedi, S., Whittington, A.R. & Goldstein, A.S., 2013. Calcium phosphate ceramics in bone tissue engineering: A review of properties and their influence on cell behavior. *Acta Biomaterialia*, 9(9), pp.8037–8045.
- Sansone, V., Pagani, D. & Melato, M., 2013. The effects on bone cells of metal ions released from orthopaedic implants. A review. *Clinical cases in mineral and bone metabolism: the official journal of the Italian Society of Osteoporosis, Mineral Metabolism, and Skeletal Diseases*, 10(1), pp.34–40.
- Sato, H. et al., 1994. A matrix metalloproteinase expressed on the surface of invasive

- tumour cells. *Nature*, 370(6484), pp.61–65.
- Scadden, D.T., 2006. The stem-cell niche as an entity of action. *Nature*, 441(7097), pp.1075–1079.
- Schechter, I. & Berger, a, 1967. On the size of the active site in proteases. I. Papain. *Biochemical and biophysical research communications*, 27(2), pp.157–162.
- Schilling, O. & Overall, C.M., 2008. Proteome-derived, database-searchable peptide libraries for identifying protease cleavage sites. *Nature Biotechnology*, 26(6), pp.685–694.
- Schuetz, E.G. et al., 1988. Regulation of gene expression in adult rat hepatocytes cultured on a basement membrane matrix. *Journal of Cellular Physiology*, 134(3), pp.309–323.
- Schultz, G.S. & Wysocki, A., 2009. Interactions between extracellular matrix and growth factors in wound healing. *Wound Repair and Regeneration*, 17(2), pp.153–162.
- Schwartzman, M. et al., 2011. Nanolithographic control of the spatial organization of cellular adhesion receptors at the single-molecule level. *Nano Letters*, 11(3), pp.1306–1312.
- Seltzer, J.L. et al., 1990. Cleavage specificity of human skin type IV collagenase (gelatinase): Identification of cleavage sites in type I gelatin, with confirmation using synthetic peptides. *Journal of Biological Chemistry*, 265(33), pp.20409–20413.
- Shegarfi, H. & Reikeras, O., 2009. Review Article: Bone Transplantation and Immune Response. *Journal of Orthopaedic Surgery*, 17(2), pp.206–211.
- Shekaran, A. et al., 2014. Bone regeneration using an alpha 2 beta 1 integrin-specific hydrogel as a BMP-2 delivery vehicle. *Biomaterials*, 35(21), pp.5453–5461.
- Shekaran, A. & García, A.J., 2011. Extracellular matrix-mimetic adhesive biomaterials for bone repair. *Journal of Biomedical Materials Research - Part A*, 96 A(1), pp.261–272.
- Shih, C.L.M. & Ajuwon, K.M., 2015. Inhibition of MMP-13 prevents diet-induced obesity in mice and suppresses adipogenesis in 3T3-L1 preadipocytes. *Molecular Biology Reports*, 42(7), pp.1225–1232.
- Sjöström, T. et al., 2013. 2D and 3D nanopatterning of titanium for enhancing osteoinduction of stem cells at implant surfaces. *Advanced Healthcare Materials*, 2(9), pp.1285–1293.
- Sjöström, T. et al., 2009. Fabrication of pillar-like titania nanostructures on titanium and their interactions with human skeletal stem cells. *Acta Biomaterialia*, 5(5), pp.1433–1441.
- Snoek-van Beurden, P.A. & Von den Hoff, J.W., 2005. Zymographic techniques for the

- analysis of matrix metalloproteinases and their inhibitors. *Biotechniques*, 38(1), pp.73–83.
- Spencer, J.A. et al., 2014. Direct measurement of local oxygen concentration in the bone marrow of live animals.
- Staines, K.A., MacRae, V.E. & Farquharson, C., 2012. The importance of the SIBLING family of proteins on skeletal mineralisation and bone remodelling. *Journal of Endocrinology*, 214(3), pp.241–255.
- Stein, G.S. & Lian, J.B., 1993. Molecular mechanisms mediating proliferation/differentiation interrelationships during progressive development of the osteoblast phenotype. *Endocrine Reviews*, 14(4), pp.424–442.
- Steingen, C. et al., 2008. Characterization of key mechanisms in transmigration and invasion of mesenchymal stem cells. *J Mol Cell Cardiol*, 44(6), pp.1072–1084.
- Sternlicht, M. & Werb, Z., 2009. How Matrix metalloproteinases regulate cell behavior. *Annu Rev Cell Biol*, pp.463–516.
- Sternlicht, M.D. & Werb, Z., 2001. How matrix metalloproteinases regulate cell behavior. *Annual Review of Cell and Developmental Biology*, 17, pp.463–516.
- Stojkovic, M. et al., 2004. Derivation, growth and applications of human embryonic stem cells. *Reproduction (Cambridge, England)*, 128(3), pp.259–67.
- Struelens, M.J., 1998. The epidemiology of antimicrobial resistance in hospital acquired infections: problems and possible solutions. *BMJ (Clinical research ed.)*, 317(7159), pp.652–4.
- Sumner, D.R., 2015. Long-term implant fixation and stress-shielding in total hip replacement. *Journal of Biomechanics*, 48(5), pp.797–800.
- Sumner, L.W. et al., 2007. Proposed minimum reporting standards for chemical analysis: Chemical Analysis Working Group (CAWG) Metabolomics Standards Initiative (MSI). *Metabolomics*, 3(3), pp.211–221.
- Sun, Z., Guo, S.S. & Fässler, R., 2016. Integrin-mediated mechanotransduction. *Journal of Cell Biology*, 215(4), pp.445–456.
- Tadokoro, S., 2003. Talin Binding to Integrin Tails: A Final Common Step in Integrin Activation. *Science*, 302(5642), pp.103–106.
- Takahashi, K. et al., 2007. Induction of Pluripotent Stem Cells from Adult Human Fibroblasts by Defined Factors. *Cell*, 131(5), pp.861–872.
- Takahashi, K. & Yamanaka, S., 2006. Induction of pluripotent stem cells from mouse embryonic and adult fibroblast cultures by defined factors. *Cell*, 126(4), pp.663–676.
- Tallant, C. et al., 2010. On the Relevance of the Met-turn Methionine in Metzincins \* □ S.
- Taupin, P., 2008. *Stem cells and regenerative medicine. Volume I, Adult neurogenesis and*

*neural stem cells*, Nova Biomedical Books.

- Tauro, J.R. & Gemeinhart, R.A., 2005. Matrix metalloprotease triggered delivery of cancer chemotherapeutics from hydrogel matrixes. *Bioconjug Chem*, 16(5), pp.1133–1139.
- Teixeira, A. et al., 2006. The effect of environmental factors on the response of human corneal epithelial cells to nanoscale substrate topography. *Biomaterials*, 27(21), pp.3945–3954.
- Thomson, J.A., 1998. Embryonic Stem Cell Lines Derived from Human Blastocysts. *Science*, 282(5391), pp.1145–1147.
- Thornton, P.D., McConnell, G. & Ulijn, R. V., 2005. Enzyme responsive polymer hydrogel beads.
- Till, J.E. & McCulloch, E.A., 1961. A Direct Measurement of the Radiation Sensitivity of Normal Mouse Bone Marrow Cells. *Radiation Research*, 14(2), p.213.
- Todd, S.J. et al., 2009. Enzyme-Activated RGD Ligands on Functionalized Poly(ethylene glycol) Monolayers: Surface Analysis and Cellular Response. *Langmuir*, 25(13), pp.7533–7539.
- Todd, S.J. et al., 2007. Enzyme-triggered cell attachment to hydrogel surfaces. *Soft Matter*, 3(5), p.547.
- Trappmann, B. et al., 2012. Extracellular-matrix tethering regulates stem-cell fate. *Nat Mater*, 11(7), pp.642–649.
- Troeberg, L. et al., 2002. E. coli Expression of TIMP-4 and comparative kinetic studies with TIMP-1 and TIMP-2: Insights into the interactions of TIMPS and matrix metalloproteinase 2 (Gelatinase A). *Biochemistry*, 41(50), pp.15025–15035.
- Trokovic, R. et al., 2015. Combined negative effect of donor age and time in culture on the reprogramming efficiency into induced pluripotent stem cells. *Stem Cell Research*, 15(1), pp.254–262.
- Turk, B.E. et al., 2001. Determination of protease cleavage site motifs using mixture-based oriented peptide libraries. *Nature biotechnology*, 19(July), pp.661–667.
- Ulijn, R. V., 2006. Enzyme-responsive materials: a new class of smart biomaterials. *Journal of Materials Chemistry*, 16(23), p.2217.
- Vandooren, J., Van den Steen, P.E. & Opdenakker, G., 2013. Biochemistry and molecular biology of gelatinase B or matrix metalloproteinase-9 (MMP-9): The next decade. *Critical Reviews in Biochemistry and Molecular Biology*, 48(3), pp.222–272.
- Vartak, D. & Gemeinhart, R., 2007. Matrix metalloproteases: Underutilized targets for drug delivery. *Journal of Drug Targeting*, 15(1), pp.1–20.
- Visse, R. & Nagase, H., 2003. Matrix metalloproteinases and tissue inhibitors of metalloproteinases - Structure, function, and biochemistry. *Circulation Research*,

92(8), pp.827–839.

- Vogel, G., 2002. Embryonic stem cells. Stem cells not so stealthy after all. *Science (New York, N.Y.)*, 297(5579), pp.175–7.
- Vu, T.H., 2000. Matrix metalloproteinases: effectors of development and normal physiology. *Genes & Development*, 14(17), pp.2123–2133.
- Wade, R.J. et al., 2015. Protease-degradable electrospun fibrous hydrogels. *Nature Communications*, 6.
- Wagner, M.S. & Castner, D.G., 2001. Characterization of Adsorbed Protein Films by Time-of-Flight Secondary Ion Mass Spectrometry with Principal Component Analysis. *Langmuir*, 17(30), pp.4649–4660.
- Wang, C. et al., 2010. An enzyme-responsive polymeric superamphiphile. *Angew Chem Int Ed Engl*, 49(46), pp.8612–8615.
- Ward, D.F. et al., 2007. Mechanical strain enhances extracellular matrix-induced gene focusing and promotes osteogenic differentiation of human mesenchymal stem cells through an extracellular-related kinase-dependent pathway. *Stem cells and development*, 16(3), pp.467–80.
- Watt, F.M. & Hogan, B.L.M., 2000. Out of Eden: Stem cells and their niches. *Science*, 287(5457), pp.1427–1430.
- Weber, L.M. et al., 2007. The effects of cell-matrix interactions on encapsulated beta-cell function within hydrogels functionalized with matrix-derived adhesive peptides. *Biomaterials*, 28(19), pp.3004–3011.
- Wehrle-Haller, B., 2012. Structure and function of focal adhesions. *Current Opinion in Cell Biology*, 24(1), pp.116–124.
- Wei, S.C. et al., 2015. Matrix stiffness drives epithelial–mesenchymal transition and tumour metastasis through a TWIST1–G3BP2 mechanotransduction pathway. *Nature Cell Biology*, 17(5), pp.678–688.
- Weiss, P. & Garber, B., 1952. Shape and Movement of Mesenchyme Cells as Functions of the Physical Structure of the Medium - Contributions to a Quantitative Morphology. *Proceedings of the National Academy of Sciences of the United States of America*, 38(3), pp.264–280.
- Wen, J.H. et al., 2014. Interplay of matrix stiffness and protein tethering in stem cell differentiation. *Nat Mater*, 13(10), pp.979–987.
- Wilhelm, S.M. et al., 1989. THE JOURNAL OF BIOLOGICAL CHEMISTRY SV40-transformed Human Lung Fibroblasts Secrete a 92-kDa Type IV. , 264(29), pp.17213–17221.
- Wilkinson, C.D.W. et al., 2002. The use of materials patterned on a nano- and micro-

- metric scale in cellular engineering. *Materials Science and Engineering C*, 19(1–2), pp.263–269.
- Wirkner, M., Weis, S., et al., 2011. Photoactivatable caged cyclic RGD peptide for triggering integrin binding and cell adhesion to surfaces. *Chembiochem: a European journal of chemical biology*, 12(17), pp.2623–9.
- Wirkner, M., Alonso, J.M., et al., 2011. Triggered cell release from materials using bioadhesive photocleavable linkers. *Advanced materials (Deerfield Beach, Fla.)*, 23(34), pp.3907–10.
- Woessner Jr., J.F., 1991. Matrix metalloproteinases and their inhibitors in connective tissue remodeling. *FASEB J*, 5(8), pp.2145–2154.
- Worley, J.R. et al., 2003. Sequence motifs of tissue inhibitor of metalloproteinases 2 (TIMP-2) determining progelatinase A (proMMP-2) binding and activation by membrane-type metalloproteinase 1 (MT1-MMP). *The Biochemical journal*, 372(Pt 3), pp.799–809.
- Wozniak, M.A. et al., 2004. Focal adhesion regulation of cell behavior. *Biochimica et Biophysica Acta (BBA) - Molecular Cell Research*, 1692(2), pp.103–119.
- Xia, F. & Jiang, L., 2008. Bio-inspired, smart, multiscale interfacial materials. *Advanced Materials*, 20(15), pp.2842–2858.
- Xia, J. & Wishart, D.S., 2011. Web-based inference of biological patterns, functions and pathways from metabolomic data using MetaboAnalyst. *Nature Protocols*, 6(6), pp.743–760.
- Yamako, G. et al., 2017. Improving stress shielding following total hip arthroplasty by using a femoral stem made of  $\beta$  type Ti-33.6Nb-4Sn with a Young's modulus gradation. *Journal of Biomechanics*, 63, pp.135–143.
- Yamato, M., Kwon, O.H., et al., 2001. Novel patterned cell coculture utilizing thermally responsive grafted polymer surfaces. *Journal of biomedical materials research*, 55(1), pp.137–140.
- Yamato, M. et al., 2002. Thermally responsive polymer-grafted surfaces facilitate patterned cell seeding and co-culture. *Biomaterials*, 23(2), pp.561–567.
- Yamato, M., Utsumi, M., et al., 2001. Thermo-responsive culture dishes allow the intact harvest of multilayered keratinocyte sheets without disperse by reducing temperature. *Tissue engineering*, 7(4), pp.473–480.
- Yang, C. et al., 2014. Mechanical memory and dosing influence stem cell fate. *Nat Mater*, 13(6), pp.645–652.
- Yeo, W.S., Yousaf, M.N. & Mrksich, M., 2003. Dynamic Interfaces between Cells and Surfaces: Electroactive Substrates that Sequentially Release and Attach Cells. *Journal*

- of the American Chemical Society*, 125(49), pp.14994–14995.
- Yim, E.K., Pang, S.W. & Leong, K.W., 2007. Synthetic nanostructures inducing differentiation of human mesenchymal stem cells into neuronal lineage. *Exp Cell Res*, 313(9), pp.1820–1829.
- Yu, Q. & Stamenkovic, I., 1999. Localization of matrix metalloproteinase 9 to the cell surface provides a mechanism for CD44-mediated tumor invasion. *Genes and Development*, 13(1), pp.35–48.
- Zelzer, M., Scurr, D.J., et al., 2012. Development and Validation of a Fluorescence Method to Follow the Build-up of Short Peptide Sequences on Solid 2D Surfaces. *Acs Applied Materials & Interfaces*, 4(1), pp.53–58.
- Zelzer, M., McNamara, L.E., et al., 2012. Phosphatase responsive peptide surfaces. *Journal of Materials Chemistry*, 22(24), p.12229.
- Zhang, F., Wen, Y. & Guo, X., 2014. CRISPR/Cas9 for genome editing: progress, implications and challenges. *Human Molecular Genetics*, 23(R1), pp.R40–R46.
- Zhang, Y. et al., 2005. Electrospinning of gelatin fibers and gelatin/PCL composite fibrous scaffolds. *Journal of Biomedical Materials Research - Part B Applied Biomaterials*, 72(1), pp.156–165.
- Zourob, M., Gough, J.E. & Ulijn, R.V., 2006. A Micropatterned Hydrogel Platform for Chemical Synthesis and Biological Analysis. *Advanced Materials*, 18(5), pp.655–659.